Linking Wheels for use in Quantum Information Processing

A thesis submitted to The University of Manchester for the degree of Doctor of Philosophy in the Faculty of Engineering and Physical Sciences

2010

Laura Carthy

School of Chemistry

Contents

List of Figures

List of Tables

List of Schemes

Abstract

Heterometallic Cr_7Ni-containing wheels have been identified as potential qubits for use in quantum information processing. The work described in this thesis details attempts to form a variety of multi-qubit systems for the purposes of better understanding the interactions occurring between the wheels and also forming potential 2-qubit quantum gates using redox/photo-active links.

Mono-substituted wheels of type $[Pr_2NH_2][Cr_7MF_8(O_2CCMe_3)_{15}(L)]$, where L is a carboxylate with a pendant coordinating group, have been synthesised for use as bulky ligands in coordination chemistry with metal complexes. Various carboxylates have been substituted into the wheels and the products reacted with first row transition metal complexes in order to extend the series of linked-wheel systems. Many of these novel complexes have been characterised by X-ray crystallography, and in certain cases EPR studies have been undertaken to probe the strength of interactions occurring via different bridging units.

The first well-established substituted wheel, $[Pr_2NH_2][Cr_7NiF_8(O_2CCMe_3)_{15}(O_2CPy)]$ (Py = pyridine), has also been used in reactions with second and third row transition metal centres to show its ability to act as a ligand under more harsh conditions. In addition, the disubstituted product $[Pr_2NH_2][Cr_7NiF_8(O_2CCMe_3)_{14}(O_2CPy)_2]$ has been reacted with a copper complex in order to form a polymeric structure.

Purple wheels of type $[Cr_7NiF_3(O_2CCMe_3)_{15}(EtGu)(H_2O)]$ have been linked through a variety of extended organic molecules containing a minimum of two pendent pyridyl groups. Use of a ligand containing four pyridyl groups, 2,2′:4,4′′:4′,4′′′-quaterpyridyl (qpy) produced a three-wheel-containing system, creating an interesting modification of the wheel backbone not seen before.

A series of transition metal complexes, containing qpy and its extended derivative bbpe, has been synthesised in order to form linked-wheel systems. While none of these systems has to date yielded a crystal structure, a significant amount of evidence has been collected to confirm successful formation of the desired products. UV-vis spectroscopic and electrochemical measurements show that these compounds are photo and/or redox-active, and preliminary luminescence studies indicate that the presence of the wheels quenches the emission from metal-to-ligand charge-transfer excited states.

A series of mixed-wheel systems has been synthesised by reacting four different mono-substituted green wheels with four purple wheels (Cr_7M, where M = Ni, Co, Mn or Zn). A total of fourteen novel systems has been formed, with two of the attempted reactions failing to occur. EPR studies on Cr_7Ni-Cr_7Ni linked systems show that the strongest interaction occurs when using isonicotinate as a link, with 4-pyridazinecarboxylate giving the weakest coupling. Studies have also been undertaken on Cr_7Ni-Cr_7Mn and Cr_7Ni-Cr_7Zn systems, with the former showing interactions and the latter showing none.

Initial work to link wheels together indirectly via their templates was ultimately unsuccessful, but a variety of potential linker molecules were synthesised and are described.

Declaration

I hereby declare that no portion of the work referred to in this thesis has been submitted in support of an application for another degree or qualification of this or any other university or other institute of learning.

Copyright

i. The author of this thesis (including any appendices and/or schedules to this thesis) owns any copyright in it (the "Copyright") and she has given The University of Manchester the right to use such Copyright for any administrative, promotional, educational and/or teaching purposes.

ii. Copies of this thesis, either in full or in extracts, may be made **only** in accordance with the regulations of the John Rylands University Library of Manchester. Details of these regulations may be obtained from the Librarian. This page must form part of any such copies made.

iii. The ownership of any patents, designs, trade marks and any and all other intellectual property rights except for the Copyright (the "Intellectual Property Rights") and any reproductions of copyright works, for example graphs and tables ("Reproductions"), which may be described in this thesis, may not be owned by the author and may be owned by third parties. Such Intellectual Property Rights and Reproductions cannot and must not be made available for use without the prior written permission of the owner(s) of the relevant Intellectual Property Rights and/or Reproductions.

iv. Further information on the conditions under which disclosure, publication and exploitation of this thesis, the Copyright and any Intellectual Property Rights and/or Reproductions described in it may take place is available from the Head of School of Chemistry.

Acknowledgements

There are so many people I must thank, in helping me to succeed in getting this far. First of all I must thank my principal supervisor, Dr Ben Coe, for all his support and encouragement through the past three years. Thanks also go to my secondary supervisor, Professor Richard Winpenny, for his advice on "all things wheel" and other members of staff including, Dr Mark Whiteley, Professor David Collison, Professor Eric McInnes, Dr Alan Brisdon, Dr Louise Natrajan and Dr Richard Layfield for their enthusiasm towards my work and suggestions along the way.

A massive thanks must go to Dr Grigore Timco, the "Godfather of the heterometallic wheel family". Without him sparing me so much time, many useful tips and a large amount of purple wheels I would not have achieved as many nice results. Thanks also to Dr Simon Foxon for allowing me to plunder his organic ligand cupboard in the name of linking wheels, saving me precious time in the final few months of my project.

Thanks to all Coe group members, past and present; Emma, Cat, Liz, Simon, Leila, John, Zhang, Miguel, Octavia, Yien, Martyn, Daniela, Becky, Drew, Lizzie, Lee, Rob, Valentine, Adam, Aastha and Jon, for all their help and general putting up with me and my incessant singing in labs. Thanks also to other members of the department, who have also offered me counsel when I have needed it and have made The University of Manchester Chemistry department a fun and friendly place to study, especially Kat and Sophia and the 5th and 3rd floor offices. Many thanks to the wonderful Dave, Emma and Danny for their help proof-reading various chapters.

Thanks go to the technical staff at The University of Manchester in the mass spectrometry, NMR and microanalytical labs, Katayune Presland for helping me to run the luminescence studies on my purple wheel compounds, Tom Faust for running the paramagnetic NMR of my Cr_7Co compounds and Dr Lindsay Harding of the University of Huddersfield for running the mass spectrometry of some of my linked wheel compounds. Thanks also to Dr Emma Fitzgerald for running some of the initial electrochemistry measurements.

Crystallographers who must be thanked for tackling the not so very well behaved wheel systems are Dr Robin Pritchard, Dr Chris Muryn, Dr John Fielden, Dr Liz Harper, Dr

Madeline Helliwell and finally Dr Simon Teat, for running crystals at the Synchrotron at the Lawrence Berkeley Nationaly Lab, without whom several of my crystal structures would remain unmeasured. Thanks must also go to Dr Floriana Tuna and John Machin for their EPR studies on my linked wheel systems.

For financing my PhD I must thank the EPSRC, and thanks to the RSC and GRC for grants to be able to attend the IUPAC conference in Glasgow and the GRS conference in Biddeford, New England respectively.

Last but not least a massive thanks go to all my friends and family, who have supported me through the hard times and encouraged me through the good, and without whom I am sure I would not have made it as far as I have. I could fill a further two pages with people to whom I am grateful, but you know who you are so I will refrain. I would like to say a final thanks to my parents, who have always encouraged me to fulfil my potential and who patiently sat through my final year presentation, despite not understanding chemistry, to help me develop my presentation skills and win prizes for two talks.

Abbreviations

2,2´-bpy	2,2´-bipyridyl
4,4´-bpy	4,4´-bipyridyl
4-pic	4-picoline
4-pyac	4-pyridylacrylate
4-pyd	4-pyridazine carboxylate
BOC	*tert*-butoxycarbonyl
bbpe	4,4´-bis-[(*E*)-2-(4-pyridyl)vinyl]-2,2´-bipyridyl
bpe	*E*-1,2-bis(4-pyridyl)ethylene
bph	(*E*,*E*,*E*)-1,6-bis(4-pyridyl)-1,3,5-hexatriene
bpvb	1,4-bis[*E*-2-(4-pyridyl-ethenyl]benzene
bpym	2,2´-bipyrimidine
CV	cyclic voltammetry
cyclen	1,4,7,10-tetraazacyclododecane
DCM	dichloromethane
DIC	diisopropylcarbodiimide
DMF	*N,N*-dimethylformamide
DMSO	dimethylsulfoxide
EPR	electron paramagnetic resonance
ESI-TOF	electrospray ionisation time-of-flight
ES-MS	electrospray mass spectrometry
Et	ethyl
EtGlu	*N*-ethyl-*D*-glutamine
Et_2O	diethyl ether
EtOH	ethanol
fac	facial
H-bond	hydrogen bond
hfac	hexafluoroacetylacetonate
HOBT	1-hydroxybenzotriazole
HOPG	highly oriented pyrolytic graphite
IR	infrared
ISNA	isonicotinate
λ_{max}	wavelength of maximal absorption

MALDI-MS	matrix assisted laser desorption ionisation mass spectrometry
Me	methyl
MeCN	acetonitrile
MeOH	methanol
mer	meridonal
MLCT	metal to ligand charge transfer
MS	mass spectrometry
NMR	nuclear magnetic resonance
Pr	propyl
py	pyridine
pytpy	4′-(4′′′-pyridyl)-2,2′:6′2′′-terpyridine
QIP	quantum information processing
qpy	2,2′:4,4′′:4′,4′′′-quaterpyridyl
qubit	quantum bit
SAM	self assembled monolayer
SMM	single molecule magnet
sol	solvent
SQUID	superconducting quantum interference device
STM	scanning tunnel microscopy
tacn	1,4,7-triazacyclononane
^{t}Bu	*tert*-butyl
TFA	trifluoroacetic acid
THF	tetrahydrofuran
TLC	thin layer chromatography
UV	ultraviolet
VdW	Van der Waal's forces
vis	visible
VT	variable temperature
XPS	x-ray photoemission spectroscopy

Dedicated to my granddad, William Chatfield, my first great educator.

Chapter 1 - Introduction

1.1 – OVERVIEW

Since the design of "Baby", the first computer as we know it, in Manchester in 1948[1] the field of computer technology has been continuously advancing with the speed and memory capacity of new computers improving greatly year by year. The rate of advancement is slowing however, primarily due to a limit on the miniaturisation scale of silicon chips.[2] Consequently demand has increased for the development of a new genre of computing, and since the 1970s the concept of quantum computing has been increasingly studied. Theoreticians have long been designing concepts by which quantum computing could become a reality, in a top-down approach, and more recently chemists have become involved trying to solve the problem from a bottom-up approach.

Recent theoretical studies by Loss and Meier have suggested that multi-spin clusters may be suitable for use as qubits, data storage units in quantum information processing, as long as their overall molecular spin is a stable two state system.[3,4] Consequently, heterometallic Cr_7Ni-containing wheels synthesised by the Winpenny group, which have a ground state spin of ½, show promise for this application.[5,6] As in regular computers, quantum computers require logic gates containing multiple qubits. These must be linked together through a molecule that allows a selective inter-cluster exchange enabling entanglement and thus communication between the qubits.

A range of synthetic approaches to link magnetic molecular wheels are considered here, both using the templates of these wheels and also directly through their backbones. Numerous compounds are considered as linkers, some for the purpose of observing permanent effects of communication on the wheels, and others with the aim of creating a molecular switch. Focus on switchable linkers is primarily on the use of photo- and/or redox-active molecules, such as viologens or metal-to-ligand charge-transfer (MLCT)-active transition metal complexes. These have been chosen as it is expected that they will have sufficiently long excited-state lifetimes to affect communication between the wheels.

1.2 PARAMAGNETISM

1.2.1 Electron Spin and Magnetic Fields

Species that contain unpaired electrons demonstrate a phenomenon known as paramagnetism.[7] This results in an attraction of the unpaired electrons to a magnetic field, dependent upon the field strength and temperature. Electrons have a property known as spin, with a magnetic quantum number of $M_S = \pm 1/2$. The unpaired electrons can align themselves with or against the magnetic field, with it being much more favourable to align with the field, creating an energy gap between the two spin states. The energy gap grows proportionally to the magnitude of the magnetic field. The effect of the magnetic field on the energy gap, known as the Zeeman splitting[8], is depicted in Figure 1 and quantified by Equation 1.

Equation 1: $\Delta E = g\mu_B H$

ΔE = energy gap, g = g-factor, μ_B = Bohr magneton, H = magnetic field, *S* = spin state.

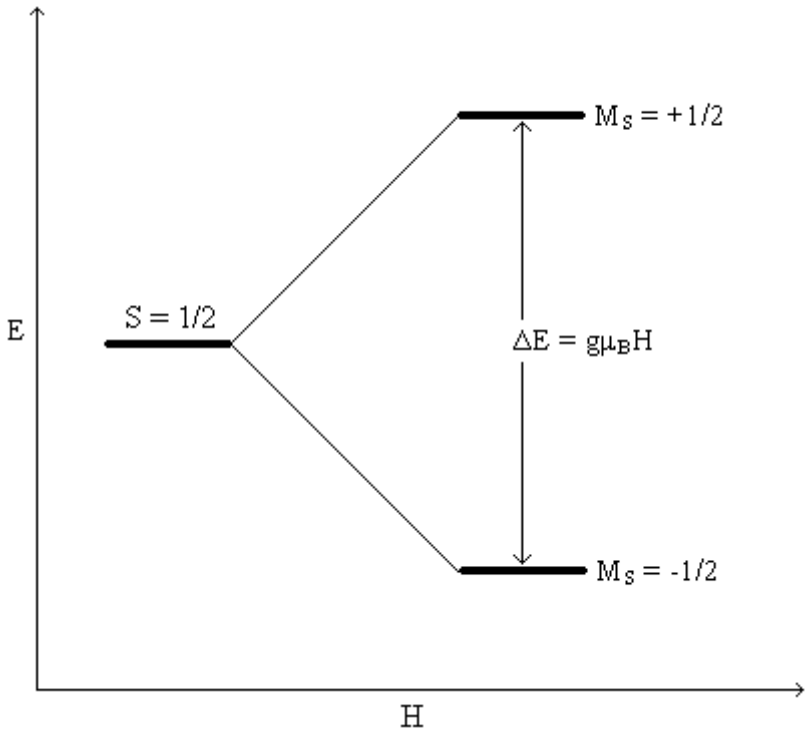

Figure 1. Influence of magnetic field on energy gap between spin states.

The state that aligns with the field is known as the ground state. If the thermal energy is less than the energy gap between the ground state and other excited states ($kT << g\mu_B H$) then the spins will populate the ground state exclusively. If, however, the thermal energy is greater than the energy gap ($kT >> g\mu_B H$) then the spins align themselves randomly.

Equation 2: $$\chi = \frac{\delta M}{\delta H}$$

The magnetic susceptibility, χ, of a substance (Equation 2) is defined as the effect that a magnetic field, H, has on the magnetisation, M. If a substance has a high magnetic polarisation then it can obtain a magnetic field itself thus becoming a magnet. It has been found in certain paramagnetic substances that the magnetic susceptibility is inversely proportional to the temperature, according to Curie's Law (Equation 3).

Equation 3: $$\chi = \frac{C}{T} \qquad \text{Where } C = \frac{N_A g^2 B^2}{4K}$$

C = Curie constant, N_A = Avogadro's constant (6.023×10^{23} mol^{-1}), g = electron g factor, B = Bohr magneton (9.27×10^{-24} $J.T^{-1}$), K = Boltzmann constant (1.38×10^{-23} $m^2kgs^{-2}k^{-1}$)

1.2.2 Coupling between Magnetic Centres

If there are multiple paramagnetic centres in proximity to one another, then coupling interactions can occur between the unpaired electrons. This can either occur directly, as in bulk metals for example, or through bridging ligands in metal complexes. The unpaired electrons can couple mutually parallel, increasing the size of the overall magnetic dipole in a ferromagnetic interaction. They can also couple antiparallel, cancelling out the dipole in an antiferromagnetic interaction (Figure 2). If the spins couple anti-ferromagnetically but the sizes of the magnetic dipoles differ then a ferrimagnetic interaction is observed, leaving the substance or molecule with an overall magnetic moment.

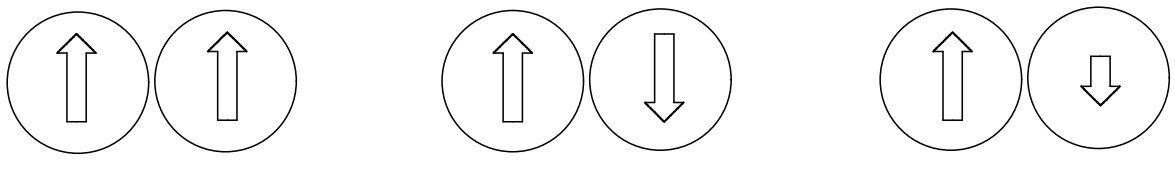

Figure 2. Representations of coupling interactions between magnetic centres.

If the magnetic coupling is enabled by a bridging ligand then an effect known as superexchange occurs.[9] The magnetic coupling between the spins can be described by the isotropic Heisenberg Hamiltonian, seen in Equation 4, where $J_{i,j}$ is the coupling constant between the spin of i, S_i, and the spin of j, S_j. If J is positive, then the coupling between the metals is ferromagnetic, and if it is negative the coupling is anti-ferromagnetic.

Equation 4:

$$\hat{\mathcal{H}}_{HB} = \sum_{i<j} J_{i,j}\mathbf{S}_i \cdot \mathbf{S}_j$$

If the metal centres in a large cluster are coupled ferromagnetically to each other it is possible to obtain clusters with extremely large ground-state spins. The largest overall spin for a single molecule recorded to date being $^{83}/_{2}$ for a Mn_{19} cluster, with 12 Mn^{III} and 7 Mn^{II} ions all being coupled together ferromagnetically.[10]

1.2.3 Single Molecule Magnetism

"Single molecule magnet" (SMM) is a term used to describe a single molecule that can demonstrate magnetic memory behaviour, as opposed to more traditional magnetism that deals with bulk materials. The SMM phenomenon was first demonstrated in 1991[11] with a Mn_{12}-containing molecule, $[Mn_{12}O_{12}(O_2CMe)_{16}(H_2O)_4]$, synthesised by Lis in 1980.[12] This cluster is comprised of eight Mn^{III} ions, each with a spin of 2, and a central cluster of four $S = {}^{3}/_{2}$ Mn^{IV} ions. The Mn^{III} and Mn^{IV} clusters are anti-ferromagnetically coupled to each other giving the cluster an overall ground-state spin of 10 (Figure 3).

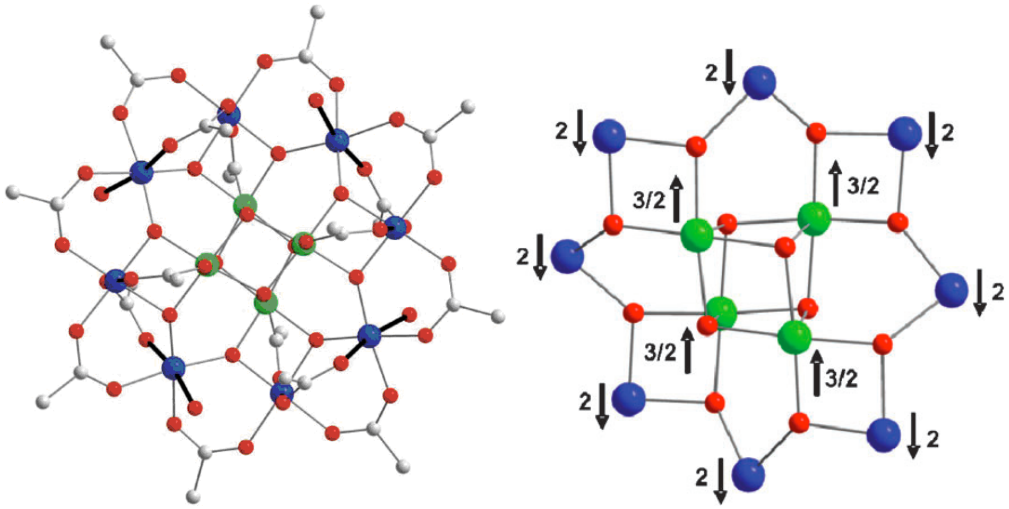

Figure 3. Crystal structure of the first "Mn_{12}" cluster and the arrangement of the spins in the ground state cluster.

Having a high spin alone does not ensure SMM behaviour. Another requirement is a large negative magnetic anisotropy (D), which, when coupled with a high overall spin (*S*), enables a slow relaxation of magnetisation upon application of a magnetic field (Equation 5). Finally, intermolecular interactions must be negligible, so that the magnetic response is of the individual molecule and not of the bulk material.

Equation 5: $U = S^2|D|$

This barrier to relaxation of magnetisation (U) gives rise to a hysteresis loop in a graph of the magnetisation versus the magnetic field (Figure 4), showing that an SMM can retain memory of the external magnetic field. One diagnostic characteristic of the hysteresis loop of an SMM is that the curve is not smooth, but rather descends in "steps" as a result of quantum tunnelling, which occurs when electrons jump to different states, passing barriers they should not have enough energy to overcome.[13]

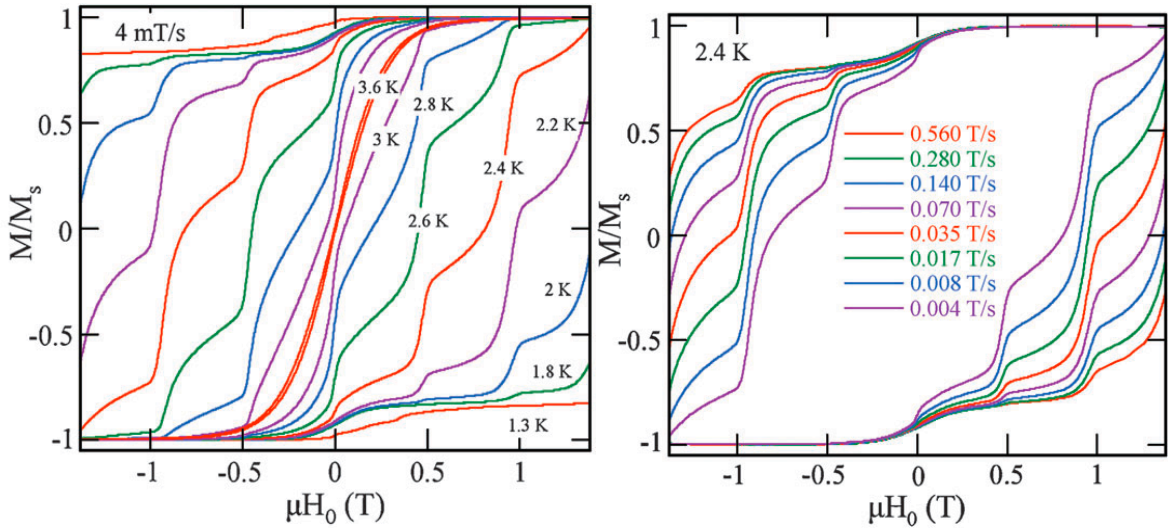

Figure 4. Hysteresis loops of a Mn_{12} cluster a) varying temperature at a fixed sweep rate and b) varying sweep rate strength at a fixed temperature.[13]

Studies are ongoing to determine whether modifications can be made to Mn_{12} SMMs in order to give the maximum possible barrier to magnetisation relaxation.[14] Most reported SMMs contain Mn, however several others have been reported using other transition metal centes, including Fe(II)[15], Fe(III)[16], Co(II)[17], V(III)[18] and Mo(III)[19]. Another avenue that is enjoying some success is mixed d-f metal clusters[20], and recently f-block metal clusters

have also been shown to be good SMMs, with a $Dy(III)_4$ cluster showing the highest known barrier to relaxation of magnetisation.[21]

1.3 QUANTUM COMPUTING

The concept of quantum computing was suggested as early as 1981 by Richard Feynman, with the idea being that quantum effects would be used as opposed to electronic effects in computing.[22] However, it was not until Shor[23] and Grover[24] published algorithms which showed how the theory could be put into practice, that many different approaches have been considered. Despite these efforts, a system that is functional on a practical scale remains elusive.

1.3.1 Qubits

A quantum bit (qubit) is a unit of quantum information. It is analogous to a bit in a regular data storage system, and thus requires a two-state system (comparable to 1 and 0 of a regular bit). The only difference is that where a regular bit can be $|1\rangle$ or $|0\rangle$, a qubit can be 1, 0 or a superposition of the two. Consequently, any two-state system may be considered as a qubit, and various single-spin candidates have been outlined, such as electron spin and nuclear spin. These are attractive as they are natural two-state systems (spin up and spin down) and because their decoherence times are unusually large for what is expected of their spin degree of freedom.[25] Another possibility is a multiple state system, in which two states are sufficiently isolable so as to be considered independently of any other excited states.

In 2003, a theoretical publication by Loss *et al*. outlined the possibility of using multi-nuclear metallic clusters as qubits.[3,4] The candidates for this were not only 1D, in the forms of odd-numbered spin chains, but also 2D in the shape of bipartite lattices, geometrically frustrated systems such as anti-ferromagnetically coupled triangles and larger molecular clusters such as the heterometallic wheels synthesised by Winpenny *et al.* Provided that these compounds have a well isolated, single spin ground-state of $S = ½$, the advantages of using molecules instead of single spins are great as the control over them needs only to be on the molecular scale instead of the atomic scale.

1.3.2 Quantum Gates

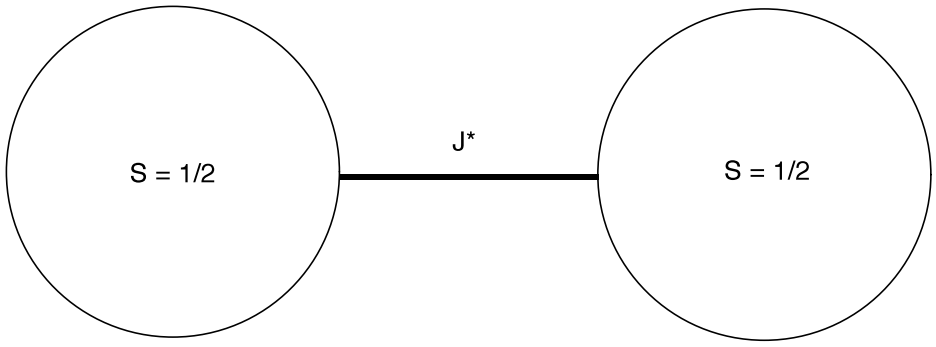

Figure 5. A schematic of a universal set of quantum gates.

In order for qubits to be applied to working computational systems, it is necessary to form a two-qubit quantum gate. This principle was first suggested by Deutsch in 1985[26], who compared a quantum logic gate to a conventional logic gate. To realise such a gate, two qubits with $S = ½$ must be linked together by a molecule that allows a degree of electronic coupling between the qubits, giving an inter-cluster magnetic exchange interaction, J^*, that can be modulated by some kind of physical change within the linking unit (Figure 5).

This intramolecular exchange allows entanglement of the qubits, which means that the qubits may no longer be considered as individuals but as one system. By entanglement of an n-qubit system, 2^n states are obtainable. QIP algorithms would take advantage of this entanglement to perform certain tasks exponentially quicker than current computer systems.

The linked ring assemblies we aim to synthesise during this project are designed to possess the properties characteristic of such a quantum gate and therefore may prove to be promising prototype systems.

1.4 CYCLIC METALLIC CLUSTERS IN THE LITERATURE

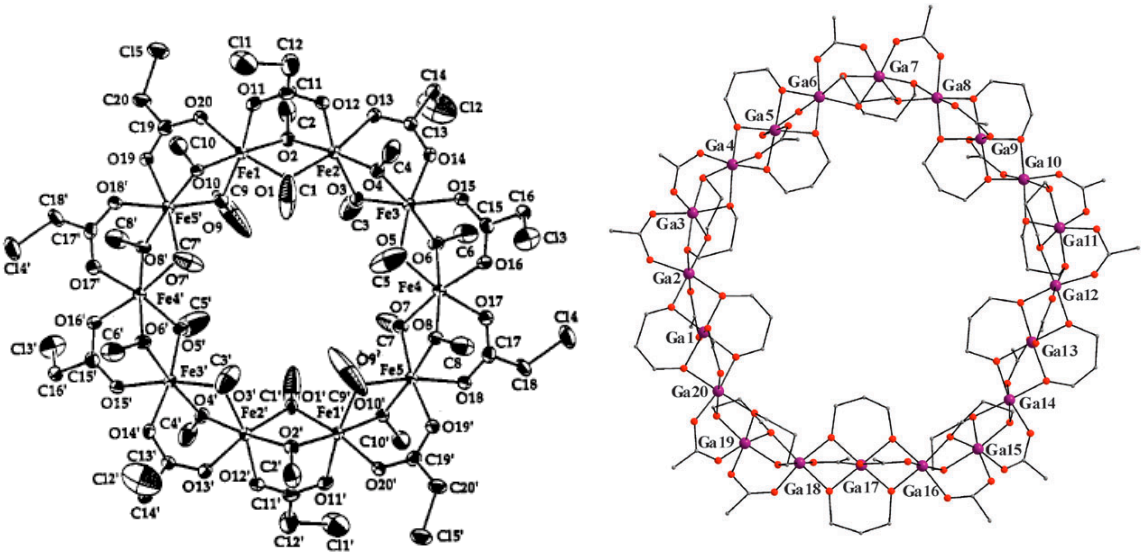

Figure 6. A selection of monolayered wheels; Lippard's "Ferric Wheel"[27] and Christou's "Gallic Wheel".[28]

The first homometallic wheel published outside of the USSR was Lippard's "Ferric Wheel" in 1994[27], a decametallic cyclic cluster formed by self assembly from a mixture of $[Fe_3O(O_2CCH_2Cl)_6(H_2O)_3](NO_3)\bullet 4H_2O$, $Fe(NO_3)_3\bullet\cdot 9H_2O$ and methanol (Figure 6). Each of the ten Fe^{III} ions are bridged by one monochloroacetate and two methoxide ligands, forming an almost planar arrangement of metal centres. Since then, the catalogue of metallic wheels in the literature has been ever expanding, with some of the more impressive cyclic structures including a single-layered Ga_{20} "Gallic Wheel"[28] (Figure 6) and a number of multilayered homo-metallic wheels with 84[29], 154[30] and 176[31] (the largest to date) metal centres in their backbones (Figure 7).

Wheel-shaped complexes have also been synthesised using Fe(II)[32], Cr(III)[33], V(III)[34], V(IV)[35], Hg(II)[36], Dy(III)[37], Ni(II)[38], Cu(II)[39], Co(II)[40] and Ti(IV)[41] in a variety of even numbered sizes, with 4-20 metal centre containing mono-layered wheels being readily accesible. Very few homometallic odd-numbered metallic wheels have been synthesised, only 5 and 9-membered wheels.[42,43] In addition to the wheels discussed in Section 1.5, a small number of heterometallic even-numbered examples have been published recently.[44,45]

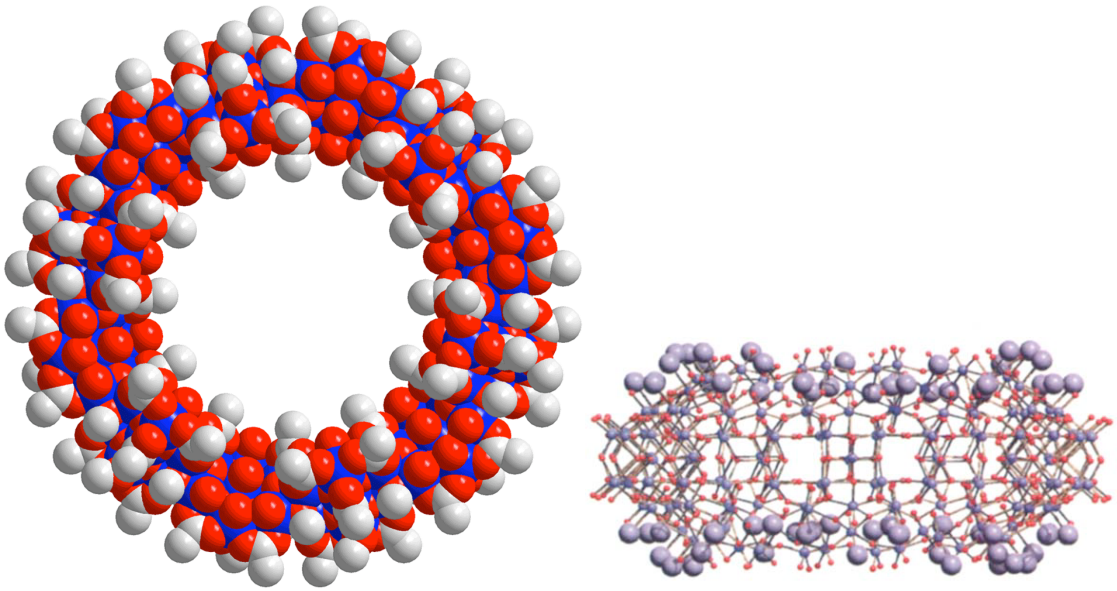

Figure 7. A selection of multi-layered wheels; Christou's Mn_{84} wheel[29] and Müller's Mo_{154} wheel.[30]

The metal centres in these wheels are found in a variety of geometries, and it is possible to impose a great deal of control over wheel size by careful consideration of the reaction conditions, solvent and bridging ligands. Most metal centres in these wheel-shaped structures are coupled together anti-ferromagnetically, but ferromagnetic interactions are observed in a few cases, leading to high ground-state spins and in some cases SMM properties.[46,47]

1.5 – REVIEW OF THE HETEROMETALLIC WHEEL FAMILY

1.5.1 – $[Cr_8F_8(O_2CCMe_3)_{16}]$

The family of heterometallic wheels was derived from the homometallic cluster, $[Cr_8F_8(O_2CCMe_3)_{16}]$, which was first synthesised in 1985.[48] Refluxing $CrF_3 \bullet 4H_2O$ and pivalic acid in DMF for 24 h allowed the self-assembly of this homometallic ring, the structure of which was confirmed by X-ray crystallography and can be seen in Figure 8. Each Cr^{III} ion exhibits a slightly distorted octahedral geometry and is bridged to each adjacent Cr^{III} ion *via* one fluoride and two pivalate anions. The fluorides point into the centre of the wheel and the pivalate ligands take one of two arrangements; either an

equatorial position in the plane of the ring or an axial position alternating in front and behind the ring.

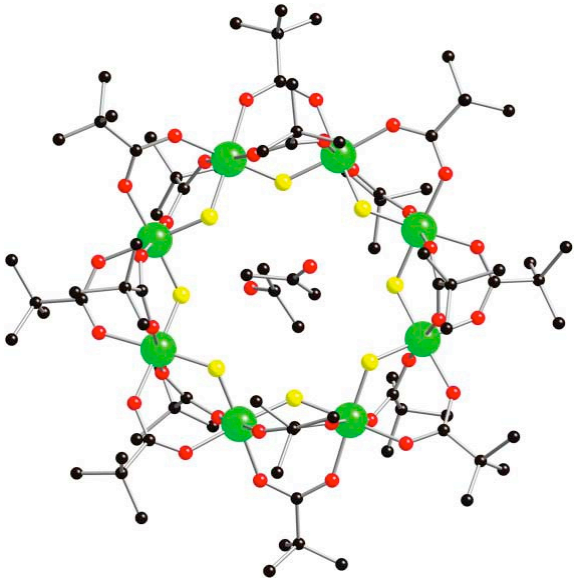

Figure 8. X-Ray Crystal Structure of $[Cr_8F_8(O_2CCMe_3)_{16}]$.[48]

Situated in the cavity of the wheel in Figure 8 can be seen two acetone molecules, demonstrating the ability of such wheels to act as hosts for small organic molecules.[49] Magnetic studies of this wheel showed that the Cr^{III} ions are coupled anti-ferromagnetically to each other, giving an overall ground state spin of 0.[50] The properties of this homometallic wheel have been studied in detail and thus it was chosen as a basis for the formation of heterometallic analogues.

1.5.2 –Heterometallic Wheels

1.5.2.1 – Synthesis

It was found that addition of a divalent metal to the reaction mixture allowed a heterometallic wheel to be formed.[5] By using $2NiCO_3{\bullet}3Ni(OH)_2{\bullet}4H_2O$ it was possible to synthesise an octametallic wheel containing seven Cr^{III} ions and one Ni^{II} ion in the backbone. Exchanging a trivalent metal with a divalent metal caused the wheel to become anionic instead of neutral and thus a molecule of protonated dimethylamine, which was formed by acid hydrolysis of the DMF, sits in the cavity of the ring. The homometallic Cr_8 wheel was formed as a by-product that could easily be separated from the anion-cation pair of the heterometallic wheel by column chromatography.

However, the yield of this reaction was only 45% and it was found that a higher yield could be achieved by carrying out the reaction with the carboxylic acid as both solvent and reagent and by use of a primary or secondary amine which, upon protonation, provides a template for the wheel formation. This approach produced a wheel templated about the protonated amine in a relatively high yield of approximately 70% after crystallisation.

1.5.2.2 – Constitution of the Wheels

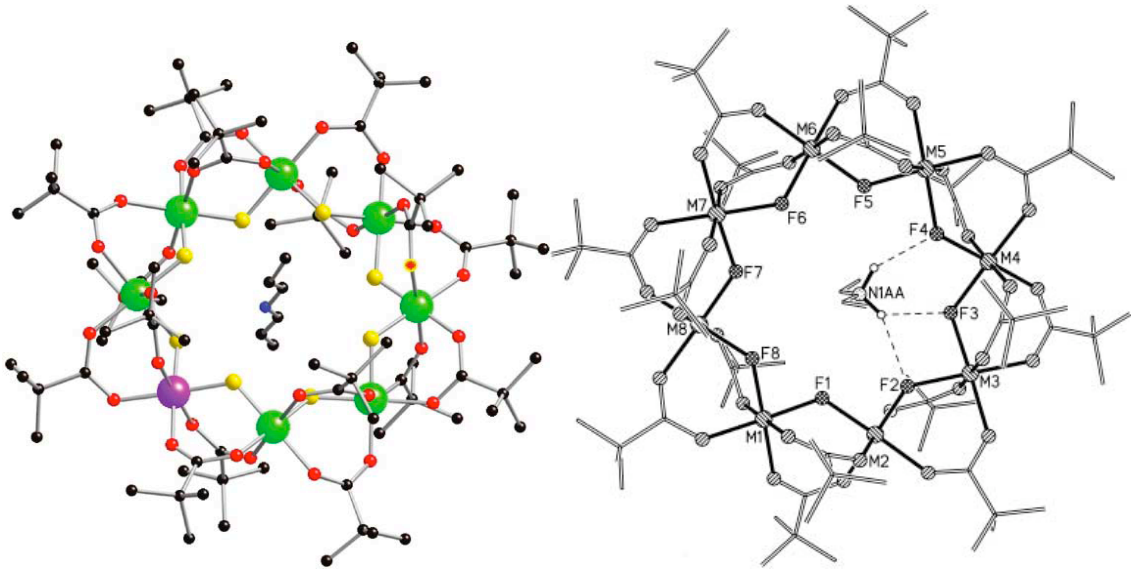

Figure 9. Crystal structure of $[Pr_2NH_2][Cr_7NiF_8(O_2CCMe_3)]_{16}$ and hydrogen bonding in a heterometallic wheel.[5]

In a fashion similar to the Cr_8 wheel previously described, there are eight metal centres coupled anti-ferromagnetically, seven of which are Cr^{III}, d^3 with a spin of $^3/_2$ and one of which is Ni^{II}, d^8 with a spin of 1. Each metal centre is bridged by two carboxylates and one fluoride, giving a total of sixteen carboxylates and eight fluorides within the backbone. This gives the wheel an overall ground state spin of ½ and a charge of –1. The wheel is templated about a protonated amine, the amine being held in the cavity of the wheel by hydrogen bonds to three of the fluorides, which point into the centre of the wheel. A molecular structure (Figure 9) helps to visualise this concept.

1.5.2.3 – Physical Properties

This Cr_7Ni compound has been well studied in order to verify its potential for use as a qubit in quantum computing.[6] Magnetic studies show that the heterometallic wheel behaves in a similar fashion to the homometallic wheel and the metal centres couple anti-ferromagnetically to each other, as evidenced by the magnetism, $\chi_M T$, of the system decreasing as the temperature is decreased (Figure 10).

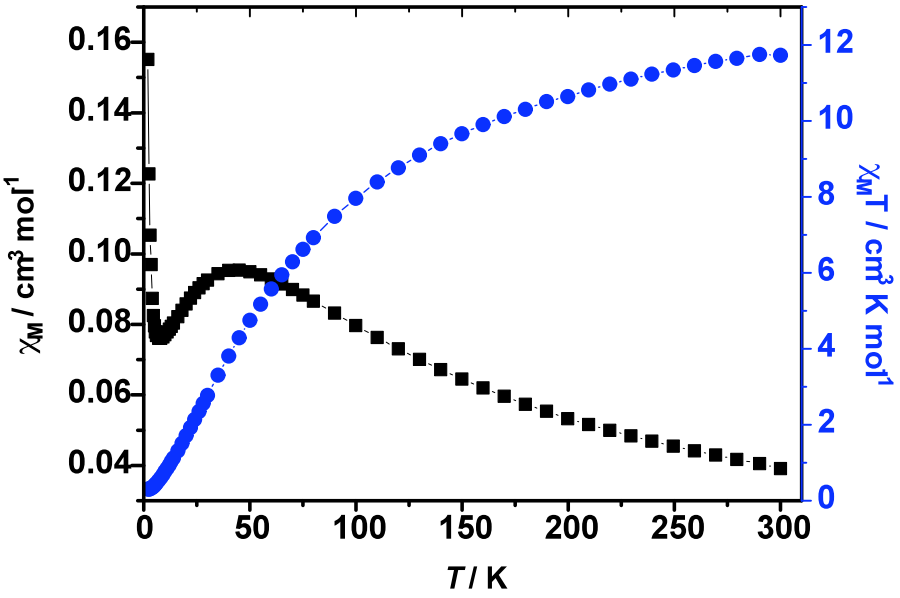

Figure 10. SQUID magnetism studies on a Cr_7Ni wheel.[6]

The Q-band EPR spectra of these Cr_7Ni wheels confirm that at low temperatures they have a spin of ½, with axial symmetry ($g_{xy} = 1.781$, $g_z = 1.740$) giving rise to a single absorption feature (Figure 11).

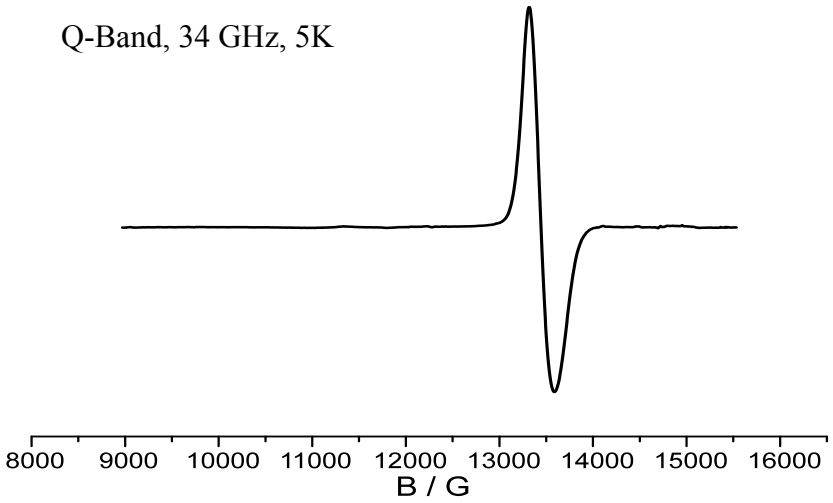

Figure 11. The Q-Band EPR Spectrum of a Cr_7Ni wheel.[6]

1.5.2.4 – Application of the DiVincenzo Criteria to the Wheels

In order for the wheels to be potentially useful in quantum computing, they must follow the four criteria for qubits outlined by DiVincenzo[51]:

i. It must exist in two stable states. For magnetic wheels, this requires that the ground state is a "pure" $S = ½$ and does not contain a mixture of higher spin states. For Cr_7Ni-containing wheels, 99% of the molecules are in a stable $S = ½$ configuration which means that they can be considered as a two state (binary) system in which $M_S = \pm ½$ corresponds with the 0 (off) and 1 (on) states.

ii. The energy gap to the first excited state must be large, in order to prevent the population of higher spin states. For Cr_7Ni wheels, the energy difference between the $S = ½$ ground state and the first excited state with $S = {}^3/_2$ is 13 K, meaning that at low temperatures $M_S = \pm ½$ are the only states to be significantly populated.

iii. The $M_S = \pm ½$ states must separate significantly in energy (due to Zeeman splitting) when an external magnetic field is applied, so that one of them can be selectively populated without significant leakage to higher S states. This creation of a "bit" of information as 0 or 1 is known as initialisation. For Cr_7Ni wheels, the Zeeman splitting is 2.4 K (at a field of 2 T) and the energy gap to the lowest level arising from the $S = {}^3/_2$

quartet excited state is 9.4 K. Therefore, there should be no leakage and the molecule will still behave as a two state system.

iv. There should be no significant loss of information (decoherence) within the system. For Cr_7Ni rings there are two possible sources of decoherence. The first source is a dipolar exchange between molecules, which can be minimised by placing them in a matrix of diamagnetic Cr_8 wheels. The second source is hyperfine interactions between unpaired electrons in the metal atoms and nuclear spins in the fluoride ions. These interactions are not strong enough to be resolved in EPR spectroscopy but may still cause decoherence.

1.5.3 – Variations on the Wheels

The majority of this project focuses on the use of Cr_7Ni containing wheels, but there is an ever-increasing family of closely related wheels formed by varying one or more features. Changing any or all of the trivalent wheel, the divalent metal, the fluoride, the carboxylate and the ammonium template has led to a family that could number over 1400 rings.

1.5.3.1 – The Trivalent Metal

Chromium is the trivalent metal of choice for this project, but heterometallic wheels with a $M^{III}{}_7Ni$ backbone have also been synthesised with M = vanadium or iron, as the fluorides of these metals are readily accessible.[52] In air, hydrolysis of iron and oxidation of vanadium can occur, so the synthesis of these wheels must be performed under inert conditions.

More recently, the group 13 metals aluminium, gallium and indium, have also been used in place of chromium.[53] These were used in order to allow study of the paramagnetic M^{II} ion in a wheel arrangement with other diamagnetic ions, and also to test how far this family of rings can be expanded. In all cases, the wheels formed are isostructural with their Cr analogues, but the reaction yields can vary depending on the size of the metal. The best yields of between 70 and 90 % occur with Ga^{III} which is of a similar size to Cr^{III}, while the worst (less than 10 %) are for Al^{III}, perhaps because its small size is less well-suited for forming an octametallic wheel.

1.5.3.2 The Divalent Metal

Nickel is the divalent metal of choice for this project as when incorporated into a Cr_7Ni wheel it gives the most stable molecules and its overall spin of ½ affords the most interesting wheels. However, related wheels have also been formed for Cr_7M^{II} where M^{II} = Co, Fe, Mn, Cd, Zn or Mg.[52] All of these ions have an octahedral coordination geometry and therefore form structures analogous to the Cr_7Ni rings, but with differing ground state spins. Consequently, their potential uses may be expanded, not only to QIP data storage devices but also to magnetic refrigeration.[54]

Usually, the paramagnetism that occurs in heterometallic wheels precludes the use of NMR spectroscopy as a characterisation tool. However, Cr_7Co wheels are amenable to paramagnetic NMR studies, due to the fast relaxation times of the Co which counteracts the slow relaxation times of the Cr, affording only slightly broadened peaks. Such studies may aid in the characterisation of linked-wheel systems before crystallisation,[55] and the knowledge gained may be applied by inference to analogous Cr_7Ni systems.

1.5.3.3 The Carboxylate

The only restriction on the carboxylate used in the synthesis of these rings with a variety of templates is that it must be a liquid at *ca.* 160 °C, as a requirement of the preferred synthetic procedures. This requirement has lead to the formation of a family of wheels containing over 14 different carboxylates.[52] If the carboxylate is not liquid at 160 °C then DMF can be used as a solvent, but the templating species will be $[Me_2NH_2]^+$. The principal carboxylate considered in this project is pivalate, as it gives the best balance between the solubility and stability of the Cr_7Ni wheels.

1.5.3.4 The Amine

Various amines have been used as templates for the heterometallic wheels. Altering the amine can affect the size and shape of the wheels, as the ammonium cation is always found in the centre. Cr_7Ni wheels have been formed around protonated primary or linear secondary amines such as di(*n*-propyl)amine. It is also possible to use more complex primary or secondary amines as templates, for example using an amine such as 4-(ethylaminomethyl) pyridine can allow the synthesis of a wheel that is able to coordinate to

metal centres through its template. By moving from simple linear alkyl chains in the secondary amine to branched chains, it is possible to increase the size of the ring from octametallic to nonametallic,[56] an example of which can be seen in Figure 12. Use of a tertiary amine has been found to lead to the formation of a decametallic wheel, of type Cr_9M, which can also be seen in Figure 12.[57]

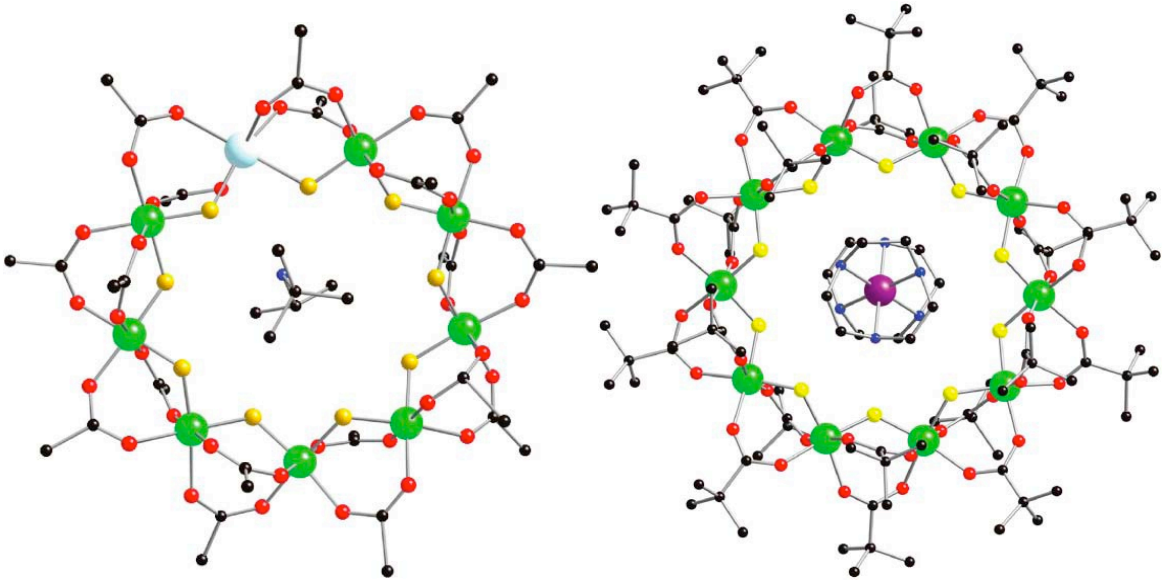

Figure 12. Examples of a nona- and deca-metallic wheel.[56,57]

Cyclic metal complexes have also been utilised as templates for decametallic wheels.[58] The use of a simple aza crown species, such as 1,4,7-triazacyclononane (tacn) in a reaction otherwise identical to those carried out with other amines, allows the formation of a decametallic wheel with the complex $[Ni(tacn)_2]^{2+}$ as the template. Consequently, the metallic composition of these ten-membered wheels is Cr_8M_2 because the template is a dication, as confirmed by elemental analyses.

In theory, it should be possible to use these different amine templates to synthesise a full range of wheels for each combination of available trivalent and divalent metal ions.

1.5.3.5 The Fluoride

The reaction of chromium(III) nitrate with sodium pivalate in water at 40 ˚C allowed the formation of $[Cr_8(OH)_8(O_2CCMe_3)_{16}]$ homometallic wheels.[59] The change of ligand, from fluoride to hydroxide, did not affect the structure of the wheel, with the hydroxides pointing into the centre. However, the d-d transitions of the wheel were altered

significantly and thus the hydroxide analogue is a deep purple colour instead of green. Attempts to apply this modification directly to heterometallic systems have proved unsuccessful. This is possibly due to the H-atoms of the hydroxy groups pointing into the ring centre upon formation, preventing encapsulation of the protonated amine template by H-bonding. It appears that it is this encapsulation that drives the formation of the fluoride-containing heterometallic wheels.

1.5.3.6 "Purple Wheels"

The presence of eight fluoride ions has until very recently appeared to be essential for the synthesis of these rings. It was believed that it would not be possible to form heterometallic rings of any form without fluorides bridging each metal centre. However, following the precedent with hydroxide (see above), the use of an aminopolyol as a template has led to the synthesis of a new "sugared" wheel,[60] which can be seen in Figure 13. The polyol, either *N*-ethyl-*D*-glucamine or *N*-methyl-*D*-glucamine, becomes fully deprotonated and the resulting poly-alkoxide replaces five of the fluoride bridging ligands, producing $[Cr_7NiF_3(O_5C_8H_{14}N)(O_2C^tBu)_{15}(H_2O)]$ in a yield of approximately 40%. The presence of five oxygens in place of five fluorides alters the d-d transitions of the Cr^{III} ions and thus, in a similar fashion to the $[Cr_8(OH)_8(O_2CCMe_3)_{16}]$ wheel, the Cr_7Ni wheels appear purple coloured.

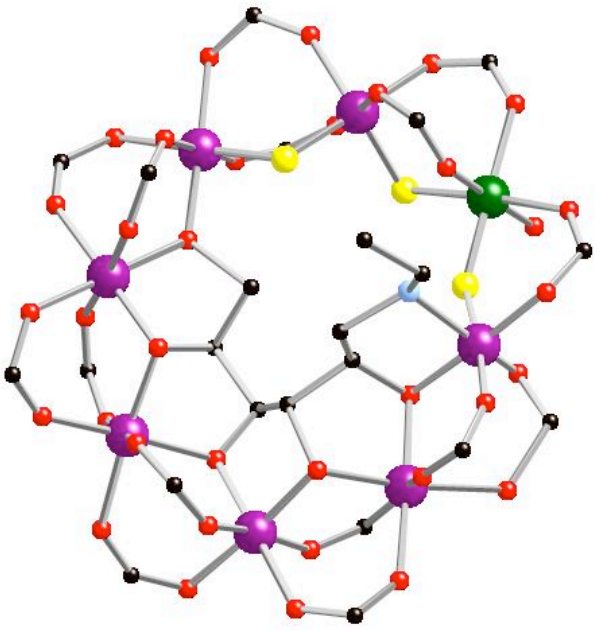

Figure 13. A "Sugared Wheel", $[Cr_7NiF_3(O_5C_8H_{14}N)(O_2C^tBu)_{15}(H_2O)]$.[60]

The nitrogen of the "template" also coordinates to a Cr^{III} ion adjacent to the divalent metal, taking up a site that should contain a bridging pivalate. Consequently a free site becomes available at the divalent metal and a solvent molecule coordinates to it. Interestingly, as the aminopolyol does not act as a template, but instead coordinates into the wheel, this wheel is neutral. This wheel has been synthesised using chromium, iron or gallium as the M^{III} ion and nickel, cobalt, zinc or manganese as the M^{II} ion.

The purple wheels are more anisotropic than green wheels due to their lack of symmetry. This can be observed in their Q-band EPR sprectra (Figure 14). It is also possible that having a smaller number of fluorides within the structure may lead to decreased decoherence in linked wheel systems.

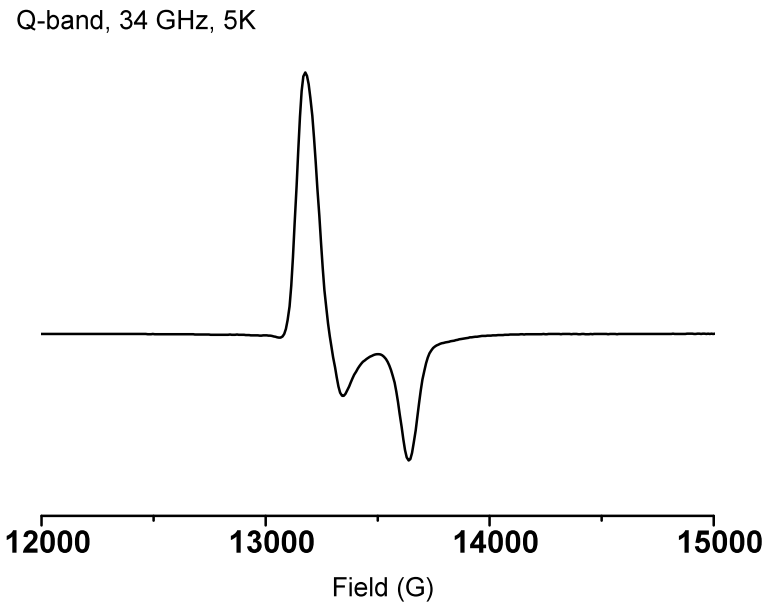

Figure 14. Q-Band EPR Spectrum of a purple Cr_7Ni wheel.

1.5.3.7 Summary of Tuning Capabilities

When designing the wheels, it is therefore possible to use different approaches to tune not only the chemical structures of the wheels and their derivatives, but also their physical properties, as follows:

a) The ground state spin (*S*) by varying the metal ions, for examples see Table 1.

Table 1. Overall ground state spins on $M^{III}_7M^{II}$ wheels by varying metal centres.

		M^{II}				
		Ni^{II}	Co^{II}	Zn^{II}	Fe^{II}	Mn^{II}
M^{III}	Cr^{III}	$^1/_2$	1	$^3/_2$	$^1/_2$	1
	V^{III}	0	$^1/_2$	1	1	$^3/_2$
	Fe^{III}	$^3/_2$	2	$^5/_2$	$^1/_2$	0
	Ga^{III}	1	$^3/_2$	0	2	$^5/_2$

b) The zero field splitting (D) by use of particular metal ions for example both Cr_7Mn and V_7Zn have a ground state spin of 1, but D is larger for the latter as the wheel is derived from more anisotropic ions.

c) The solubility and stability of the wheels by varying the carboxylate used as the reaction solvent. For example, using pivalic acid produces a wheel that is insoluble in acetonitrile, while using *tert*-butyl acetic acid produces a wheel that dissolves in acetonitrile.

1.5.4 Other Shapes in the Heterometallic Wheel Family

1.5.41 "Hourglasses"

The synthesis of heterometallic "hourglass" clusters is achieved by including a dicationic metal in the reaction, which does not adopt an octahedral coordination geometry. An example is the use of copper(II) carbonate in the presence of $CrF_3•4H_2O$, pivalic acid and a secondary amine, giving the salt compound $[R_2NH_2]_2[Cr_{10}Cu_2F_{14}(O_2CCMe_3)_{22}]$ which contains a distorted dodecametallic wheel (Figure 15).[61]

The copper centres are five-coordinate and connected to one Cr^{III} ion through one bridging fluoride and two pivalates and to another Cr^{III} ion through one fluoride and only one pivalate. The Cr^{III} ion that is only doubly bridged to the Cu^{II} ion also has a terminal fluoride ligand. The presence of two divalent metal ions in this distorted ring gives an overall charge of –2 and two protonated secondary amine cations are found in the centre of the structure, sitting in the cavities as a result of H-bonding to the centrally oriented fluoride ions.

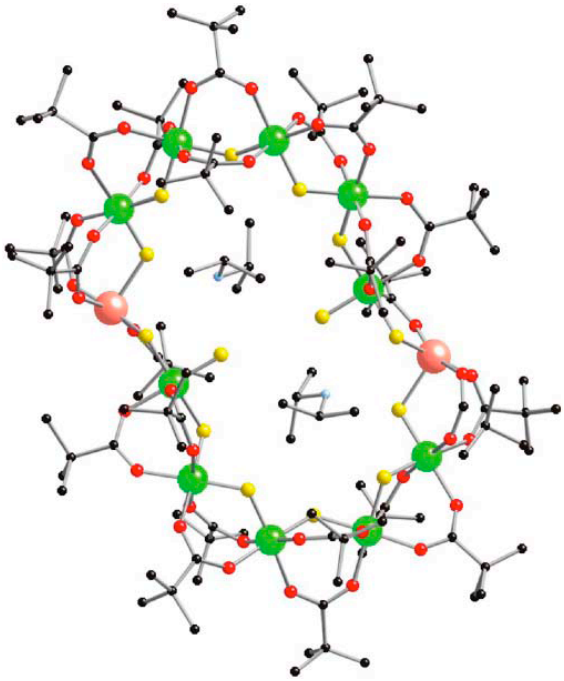

Figure 15. Molecular hourglasses.[61]

1.5.4.2 "Horseshoes"

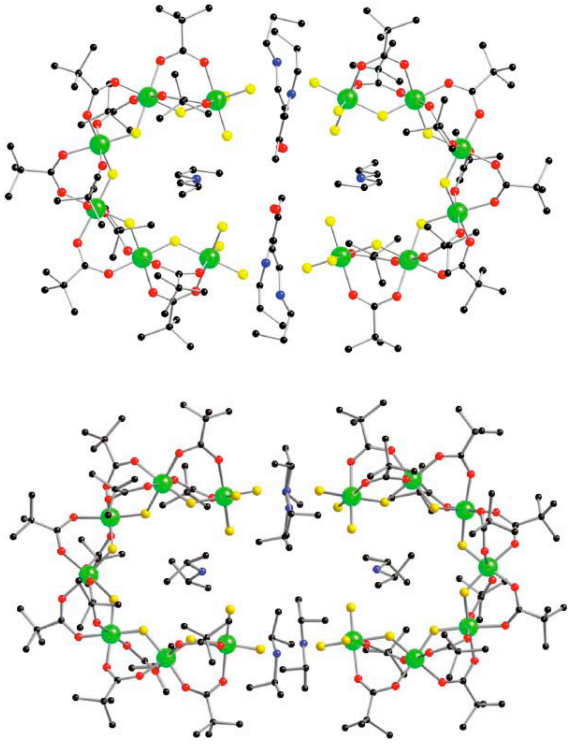

Figure 16. Molecular horseshoes.[61]

Homometallic "horseshoes" (Figure 16) can be formed by excluding the divalent metal from the reaction. For example by reacting $CrF_3 \bullet 4H_2O$ with a secondary amine in pivalic

acid, a pair of horseshoe-shaped clusters is formed, with an overall formula of $[R_2NH_2]_6[Cr_6F_{11}(O_2CCMe_3)_{10}\}(sol)]_2$ (R = Et, ^nPr, $^nC_5H_{11}$, sol = solvent).[61] When using a bulkier secondary amine, such as iso-propyl diamine, as the horseshoe template the horseshoe clusters formed contain seven Cr^{III} ions instead of six.

It is not yet fully understood why one template causes the formation of a hexametallic and another a heptametallic horseshoe. One possibility is that in all reactions both derivatives are formed and it is during crystallisation that the most stable arrangement for a particular template is isolated. Another possibility is that the bulk of the template has a role in the size of the horseshoe synthesised. The three linear diamines used as templates produced hexametallic horseshoes, whereas the bulkier branched diamine produced heptametallic versions, potentially due to the larger cavity size in the seven-membered horseshoe. A similar principle operates in the heterometallic wheel systems.

The crystal structures of the horseshoes showed that the arrangement of the internal Cr^{III} ions is identical to those found in wheel structures. Each Cr^{III} pair is bridged by two pivalate ions and one fluoride ion. The terminal Cr^{III} sites of the horseshoe bind to the adjacent Cr^{III} ion through two pivalate ions and one fluoride ion, but they also have three terminal fluoride ligands which are H-bonded to the protonated secondary amine cations situated between the two clusters. There are six protonated amines associated with each horseshoe pair. One amine sits in the cavity of each horseshoe and two can be found at each terminus of the horseshoe. They are held in place by H-bonding to fluorides.

1.5.4.3 "Seahorses"

A heterometallic "seahorse" cluster was formed by using a large macrocyclic templating amine, 1,4,7,10-tetraazacyclododecane (cyclen), as the template and can be seen in Figure 17.[58]

Reacting cyclen with $CrF_3 \bullet 4H_2O$ and nickel(II) carbonate afforded an open-chain complex with a $[Ni(cyclen)]^{2+}$ unit at each end and one central Ni^{II} ion connecting two Cr_6 "horseshoes" to give $[\{Ni(cyclen)\}_2Cr_{12}NiF_{20}(O_2CCMe_3)_{22}]$**.** The crystal structure showed that the twelve Cr^{III} ions are joined together in two hexametallic chains. The coordination geometries of the internal ions of these chains are the same as in the hexametallic Cr_6 horseshoes. The two internal ends of the chains are linked *via* two fluorides and one

pivalate bridge each to a central Ni^{II} ion, thus creating an "S" shape. The terminal ends of the chains are each attached to a Ni(cyclen) complex *via* one fluoride and one pivalate bridge. The metal core of this molecule is virtually planar and the Ni(cyclen) complexes are held in place with a single N–H---F bond to the fluorides attached to the central Ni^{II} ion.

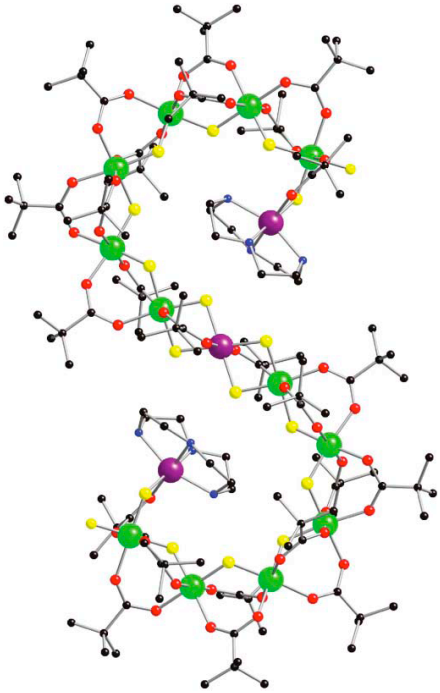

Figure 17. A "Seahorse" Cluster Structure, $[\{Ni(cyclen)\}_2Cr_{12}NiF_{20}(O_2CCMe_3)_{22}]$.[58]

1.6 LINKED WHEEL SYSTEMS

In order to fulfil the requirements needed for applications in QIP, two wheels must be linked together to form a two-qubit quantum gate. The extent of interaction between the wheels must be controllable, so studies have been undertaken to assess what factors affect this.

1.6.1 Linking Wheels Indirectly through the Template

1.6.1.1 Syntheses

Initial studies to link together the wheels were focussed on linking through the template. Two different methods were attempted to achieve this goal. The first method was to template the formation of two wheels around a single linker molecule, using for example a

simple linear diamine. The synthesis of this genre of linked wheel system was carried out in an identical fashion to that of a single wheel system, although the quantity of templating molecules added to the reaction was halved. Purification was achieved by recrystallisation, as the products could not be placed on a column for reasons of stability. This approach has been employed with 1,8-diaminooctane and longer chain molecules;[62] a representative crystal structure of one of the products can be seen in Figure 18.

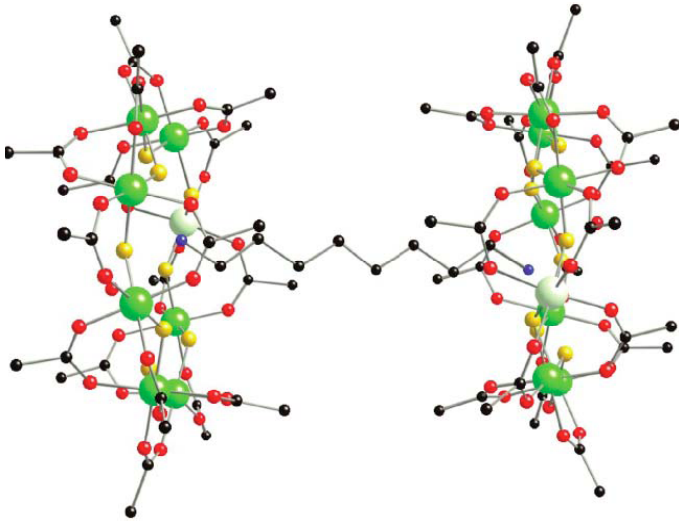

Figure 18. X-ray Crystal Structure of $[\{H_3NC_8H_{16}NH_3\}\{Cr_7NiF_8(O_2CCMe_3)_{16}\}_2]$.[62]

Another method for linking heterometallic rings involved the synthesis of a wheel around a pyridyl-functionalised amine, for example 4-(ethylaminomethyl)pyridine, followed by coordination of the pendant pyridyl units with a metal complex.[62] Following the synthesis of a pyridyl-functionalised wheel, two wheels were linked together *via* first row transition metal centres. Preliminary studies involved the linking of wheels through copper, nickel, cobalt and ruthenium dimers[63] by reaction at room temperature in toluene and in some cases diethyl ether. Gentle evaporation of the reaction solvent gave crystalline products, which in some cases could be characterised using X-ray crystallography. The crystal structure of one such assembly, $[\{Cu_2(O_2CCMe_3)_4\}\{[EtNH_2CH_2C_5H_4N][Cr_7NiF_8(O_2CCMe_3)_{16}]\}_2]$, can be seen in Figure 19.

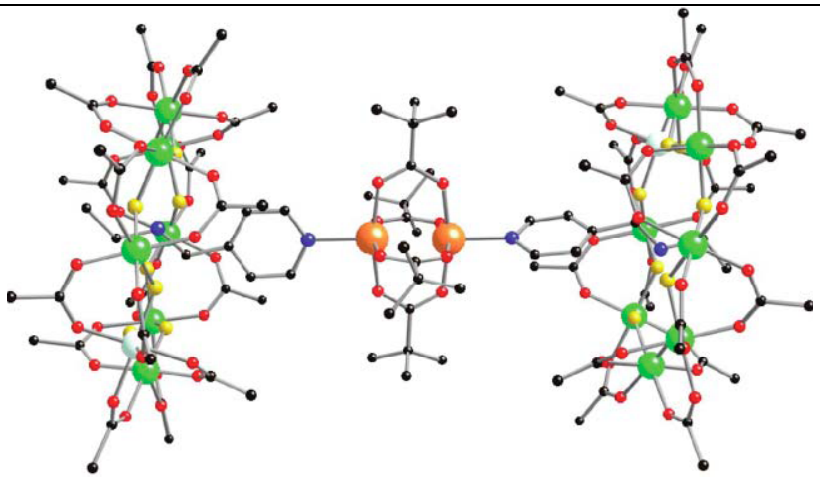

Figure 19. X-ray crystal structure of $[\{Cu_2(O_2CCMe_3)_4\}\{[EtNH_2CH_2C_5H_4N][Cr_7NiF_8(O_2CCMe_3)_{16}]\}_2]$.[63]

It was also possible to link wheels together through single metal centres, such as copper and nickel.[64] An example of such a molecule containing copper can be seen in Figure 20.

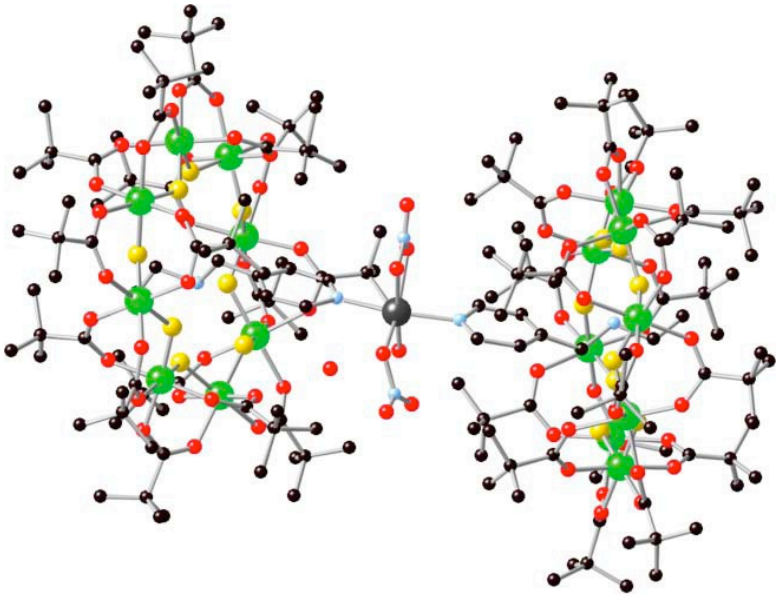

Figure 20. Wheels linked indirectly through a single copper centre.[64]

1.6.1.2 Magnetic Studies

A working two-qubit quantum gate must display a significant and controllable electronic coupling between the magnetic components. Magnetic susceptibility and specific heat studies of all indirectly linked wheel systems have revealed negligible interaction between the two rings. Such systems therefore correspond to an "off state", showing that the wheels can be in close proximity without affecting each other (not an unexpectedly as

there is no direct linkage between the wheels). The requirement for an "on state" has led to investigations into the formation of a direct link between two wheels.

1.6.2 Linking the Wheels Directly through the Backbone

1.6.2.1 Syntheses

Heterometallic wheels have recently been linked together directly using a novel method.[65] For the traditional "green" wheels, a two-step process was required in order to form the links. The first step was to functionalise the wheel, by external modification of the backbone, with a linking moiety. The second step was to introduce a metal centre through which two wheels may be joined together using coordination chemistry.

The general synthetic procedure for such a substitution involves heating the wheel with an approximately four-fold excess of the incoming carboxylate in propan-1-ol under reflux.[65] The carboxylic acids are not very soluble in propan-1-ol, so the reaction takes place over approximately 24 h. The first substitution reaction was attempted with nicotinic acid as it has a relatively good solubility. However, isonicotinic acid (ISNA) substitutes into the wheel more efficiently, so this project focuses on ISNA-functionalised wheels.

This substitution process was selective, as the Ni^{II} ion is much more labile than the relatively inert Cr^{III} ions, so both the primary and secondary substitutions occur at the nickel and one of the adjacent chromium ions. Column chromatography on silica gel was used to isolate the product, eluting initially with toluene to bring off the unsubstituted wheel, then increasing the gradient using a 40:3 mixture of 40/60 °C petroleum ether and ethyl acetate to bring off products with higher degrees of substitution. With ISNA, both the mono and disubstituted products have been isolated, characterised and used for further synthetic studies. Crystal structures of these substituted wheels can be seen in Figure 21.

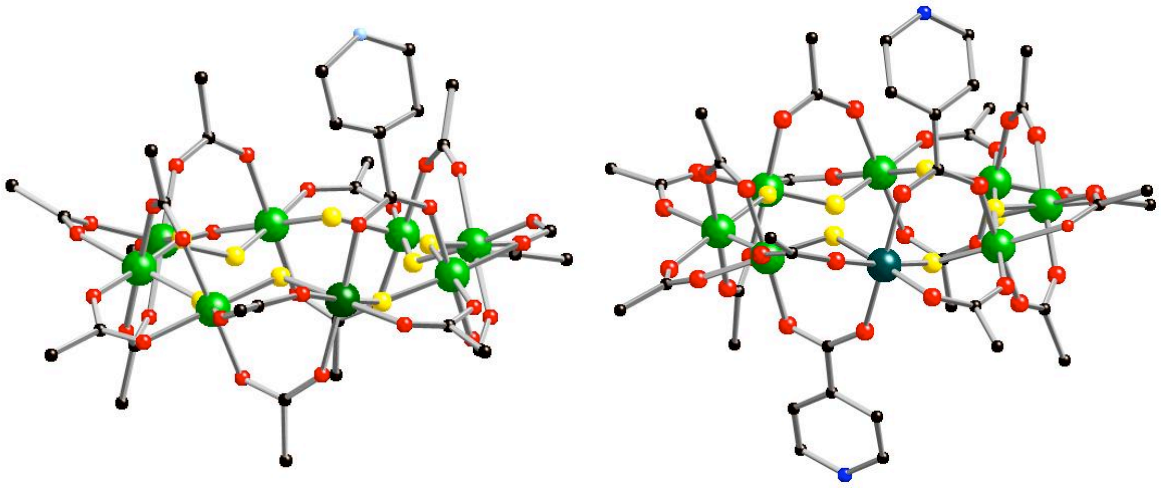

Figure 21. A mono- and di-substituted wheel containing ISNA.[65]

Microwave and solvothermal techniques have also been used to achieve substitution of carboxylates into the wheels, but these approaches caused more decomposition than standard methods.[66] Different solvents can be used for reactions of wheels with other carboxylate groups; for example, using *tert*-butyl acetate in place of pivalate groups allows the substitution reactions to be carried out in acetonitrile.

By altering the pendant group on the incoming carboxylate, it is possible to alter the chemistry that can be achieved with the substituted product. Using a pyridyl unit allows the wheel to act as a potential bulky ligand, while using an alkyne substituent allows the wheel to undergo 'Click chemistry' to join together two wheels. Thiol substituents may allow the wheels to attach directly to gold surfaces in self-assembled monolayer formations.

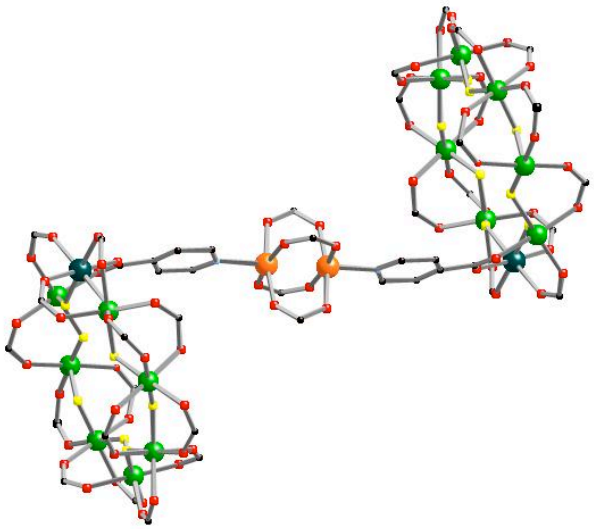

Figure 22. Wheels linked directly through copper dimers.[65]

The ISNA-substituted wheels can act as bulky ligands with first row transition metal centres.[65] Reaction of such a wheel with $[Cu_2(O_2CCMe_3)_4(HO_2CCMe_3)_2]$ at room temperature in toluene afforded a linked wheel system (Figure 22). Heating the ISNA-substituted wheels with $Cu(NO_3)_2 \bullet 2.5H_2O$ in acetone allowed the formation of another type of linked wheel system (Figure 23).

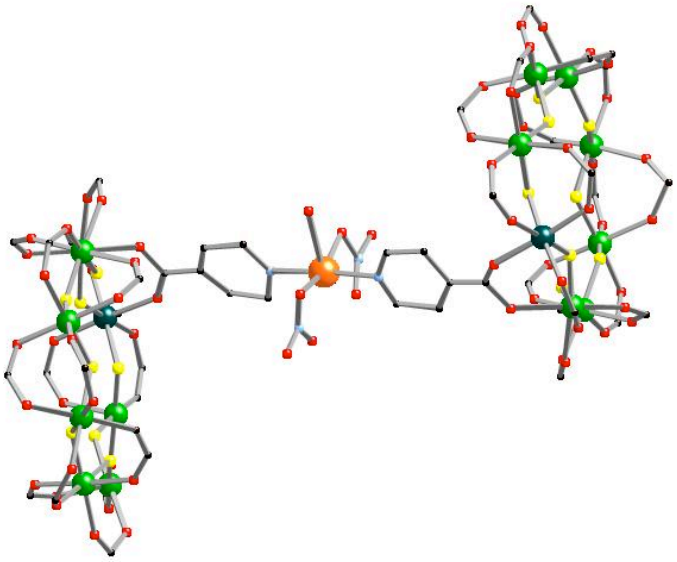

Figure 23. Wheels linked directly through a single copper centre.[65]

Reaction of a disubstituted wheel with a metal complex, such as $[Cu_2(O_2CCMe_3)_4(HO_2CCMe_3)_2]$, allows the formation of a polymeric structure where two metal complexes are linked together through a wheel.[66] An example of such a structure can be seen in Figure 24.

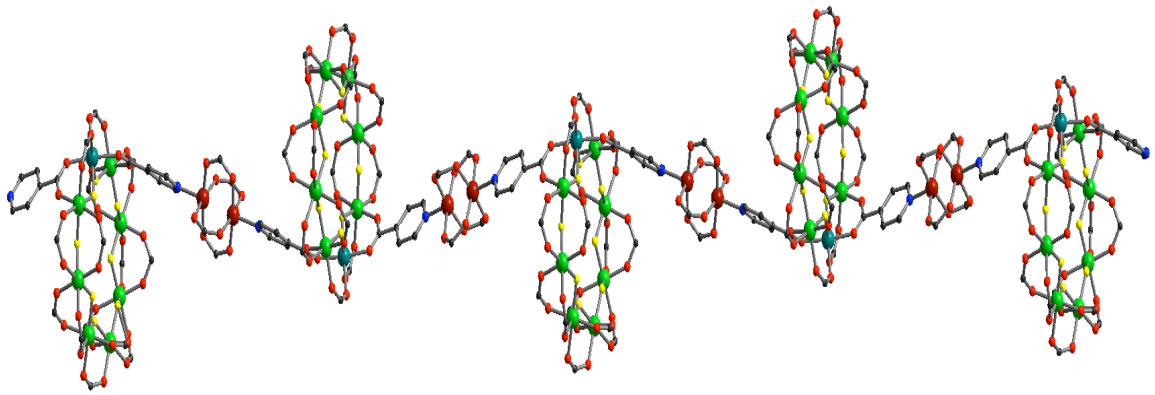

Figure 24. Polymer formed by disubstituted wheels linked through copper dimers.[66]

1.6.2.2 Magnetic Studies

EPR studies on a system with two ISNA-substituted wheels joined through a copper dimer showed no interaction between the wheels, because the spectrum is identical to that of the uncomplexed wheel (Figure 25).[65] This result is predictable as the two paramagnetic copper centres in the dimer are very strongly anti-ferromagnetically coupled, forming a diamagnetic, partially conjugated moiety that prevents any communication between the two wheels.

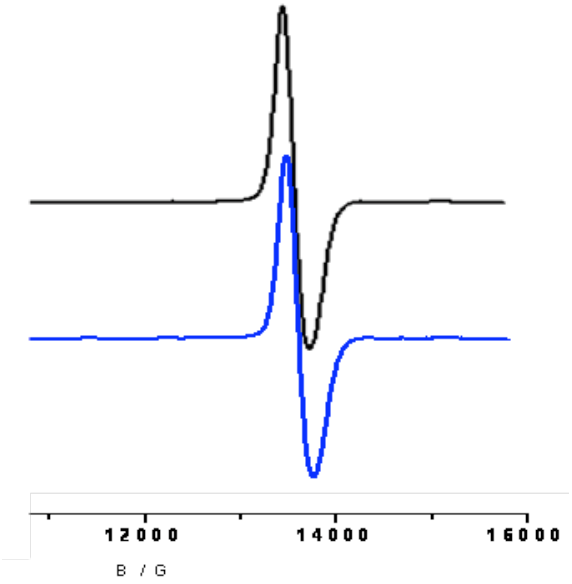

Figure 25. Q-Band EPR Spectra of Individual Cr_7Ni Ring (black) and 2 Cr_7Ni wheels linked through a Cu dimer (blue).[65]

When the Cr_7Ni wheels are linked through a single copper centre, however, a very different EPR spectrum was observed.[65] The spectrum of the linked wheel system, shown in red in Figure 26, was much more complex than the simple singlet observed for a single Cr_7Ni wheel. This observation is due to the paramagnetic nature of the Cu centre and the conjugated links between the two Cr_7Ni wheels allowing interactions between them.

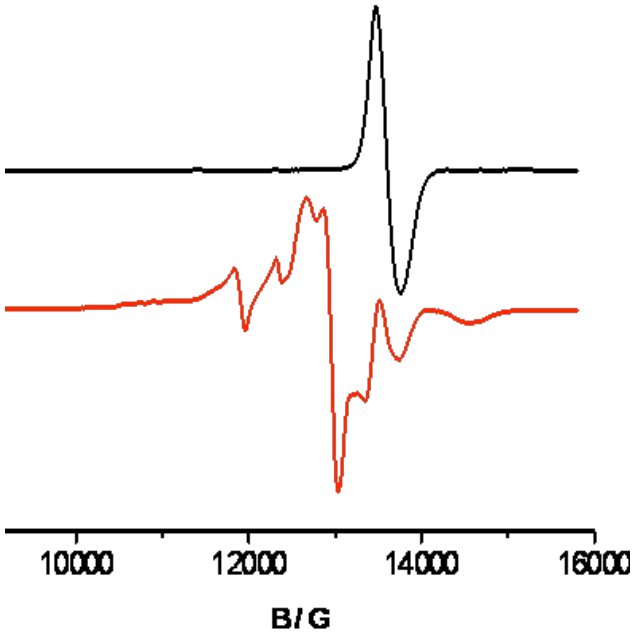

Figure 26. Q-Band EPR Spectra of Individual Cr_7Ni Ring (black) and two Cr_7Ni wheels linked together through a single Cu centre (red).[65]

It has therefore been demonstrated that by linking the wheels together directly it is possible to observe both the "on" and "off" states required for uses in QIP. However, for such an application, the "on" and "off" states must be generated within the same molecule.

1.6.3 Linking Purple Wheels together

While it is plausible that purple wheels could be linked together directly in a manner identical to that used for green wheels, a novel route was considered taking advantage of the spare coordination site available on the divalent metal centre.[60] Molecules containing two or more pendant pyridyl groups have been used to link wheels together, with the pyridyl coordinating to the divalent metal.

1.6.3.1 Syntheses

Reactions of a purple cluster with 4-picoline (4-pic) in acetone allowed substitution of the coordinated water molecule to produce $[Cr_7NiF_3(O_5C_8H_{14}N)(O_2C^tBu)_{15}(4\text{-pic})]$ which has also been structurally characterised,[60] confirming the coordination of 4-pic to the Ni^{II} centre. This concept was then extended to molecules containing two pendent pyridyl groups, such as 4,4′-bipyridine (bpy) and *trans*-1,2-bis(4-pyridyl)ethylene (bpe), in order

to form linked wheel systems. The synthetic procedures used are straightforward and involve a short period of heating in a low boiling point solvent such as acetone or dichloromethane. Once the linked wheel systems were formed they were isolated by crystallisation, and characterised by X-ray crystallography and elemental analyses.

1.6.3.2 Magnetic Studies

Systems containing wheels linked through organic moieties did not show any difference in their SQUID measurements. This is to be expected as the interactions between the two wheels are relatively weak, and more significant interactions are required to affect SQUID measurements. EPR spectroscopy can detect much weaker interactions and consequently a difference in spectra may be observed between two wheels linked through bpy and an individual wheel (Figure 27). The spectrum of the linked wheel system, corresponds to an S = 1 ground state below 10 K, meaning the wheels are coupled ferromagnetically to each other.

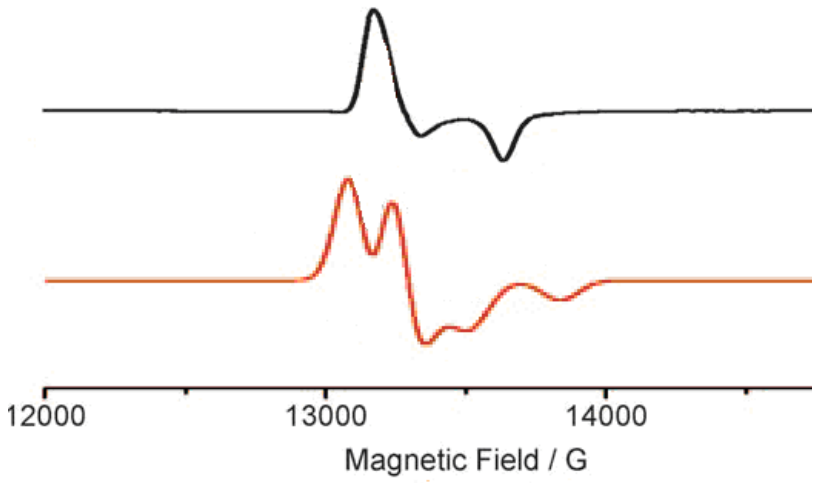

Figure 27. EPR spectrum of unlinked purple Cr_7Ni wheels (black) and linked through bpy (red).[60]

1.7 ATTACHING WHEELS TO SURFACES

In order to apply these systems, it will be necessary to attach them to surfaces. Consequently, studies have been carried out to ascertain the suitability of different methods for this purpose. Further to investigations with Mn_{12} clusters,[67] the viability of attaching Cr_7Ni wheels to gold surfaces has been studied. [68,69] Wheels were deposited on Au(111)

surfaces in a one-step procedure, by immersing a 5 mM solution in either tetrahydrofuran or dichloromethane over 10 minutes. The treated surfaces were then studied using scanning tunnelling microscopy (STM) and X-ray photoemission spectroscopy (XPS).

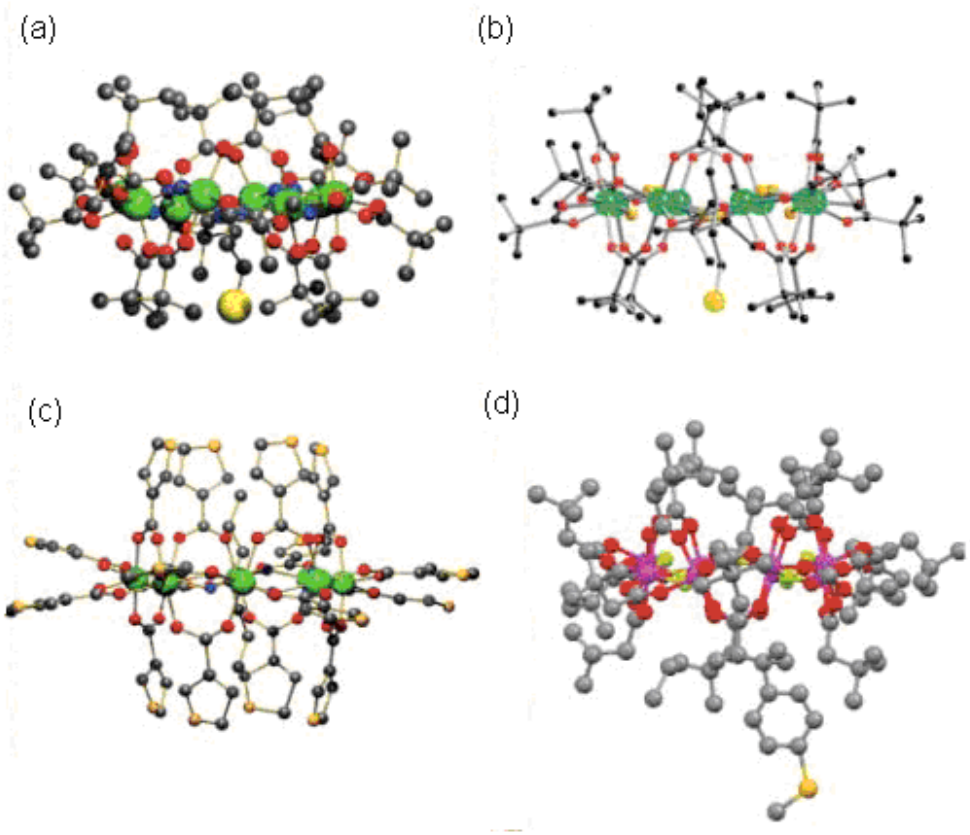

Figure 28. Thio-functionalised wheels for attachment to gold surfaces; (a) and (b) thiols in template, (c) and (d) thiols in backbone.[68,69]

Four thio-functionalised wheels (Figure 28) and three other functionalised wheels (Figure 29) have been used for these experiments; three of these (a, b and e) contained the surface-binding functionality in the template of the wheel and four were functionalised in their backbones (c, d, f and g). The former showed inefficient grafting, with only 2–10% coverage of the surface area by wheels; this was primarily caused by the wheels detaching from their templates, leaving a self-assembled monolayer (SAM) of the templates alone. However, the backbone-functionalised wheels adsorbed much more successfully, giving up to 35% surface coverage.

In keeping with the known high affinity of sulfur for gold, the thio-functionalised wheels adsorbed most strongly, but reasonable surface coverages were nevertheless observed for the other wheels. Physical studies showed that the electronic properties of the surface-

attached wheels remained largely unchanged when compared with their behaviour in solution.[70] However, surface binding did cause a reduction in the coupling constants between Cr and Ni, which in turn lowered the energy gap between the $S = ½$ ground state and other excited states.

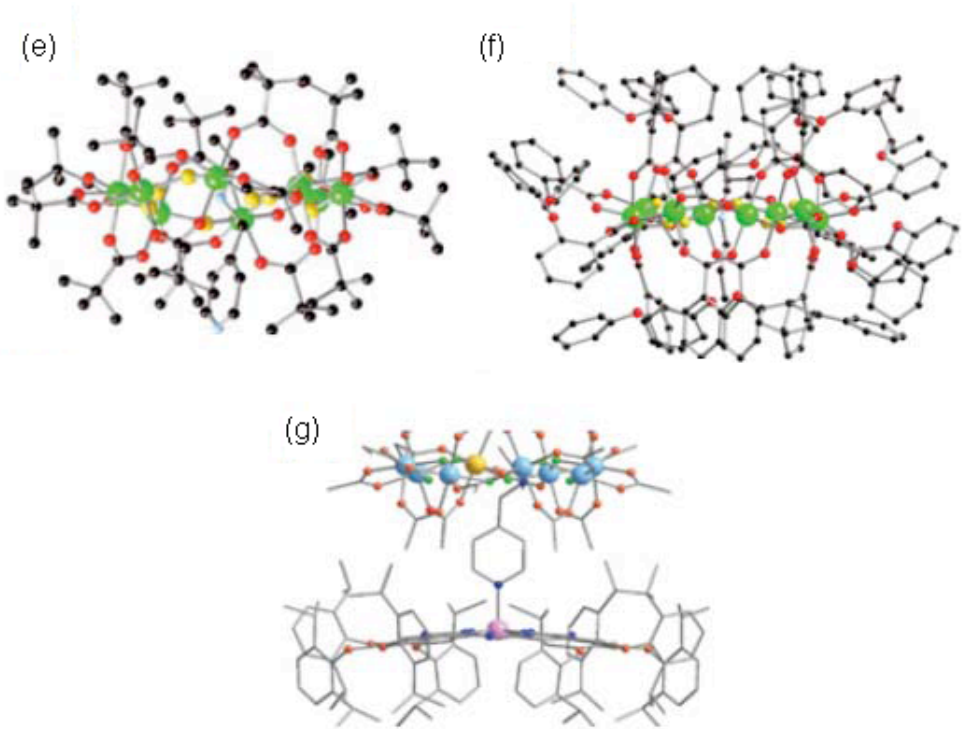

Figure 29. Non-thio functionalised wheels for gold surface studies.[71]

Wheels have also been adsorbed onto highly-oriented pyrolytic graphite (HOPG).[71] The wheels synthesised for this purpose contained large alkyl or benzyl groups (Figure 30), which can bind to HOPG by van der Waal's (VdW) or π-π interactions. Two techniques were used in this study, the first being a one-step method whereby the substrate is dipped into a toluene solution of the wheel. The wheels adsorbed readily onto the HOPG surface on bulk, but using 10^{-4} M concentrations gave only sub-monolayers. The second technique involved two-steps. First, a SAM of the salt $CH_3(CH_2)_{15}SO_3Na$ was applied to the surface, then a cationic wheel was bound by interaction with the anionic $–SO_3^-$ groups. The electrostatic bonds formed were strong and the wheels remained on the surface, even after a strong rinse with dichloromethane.

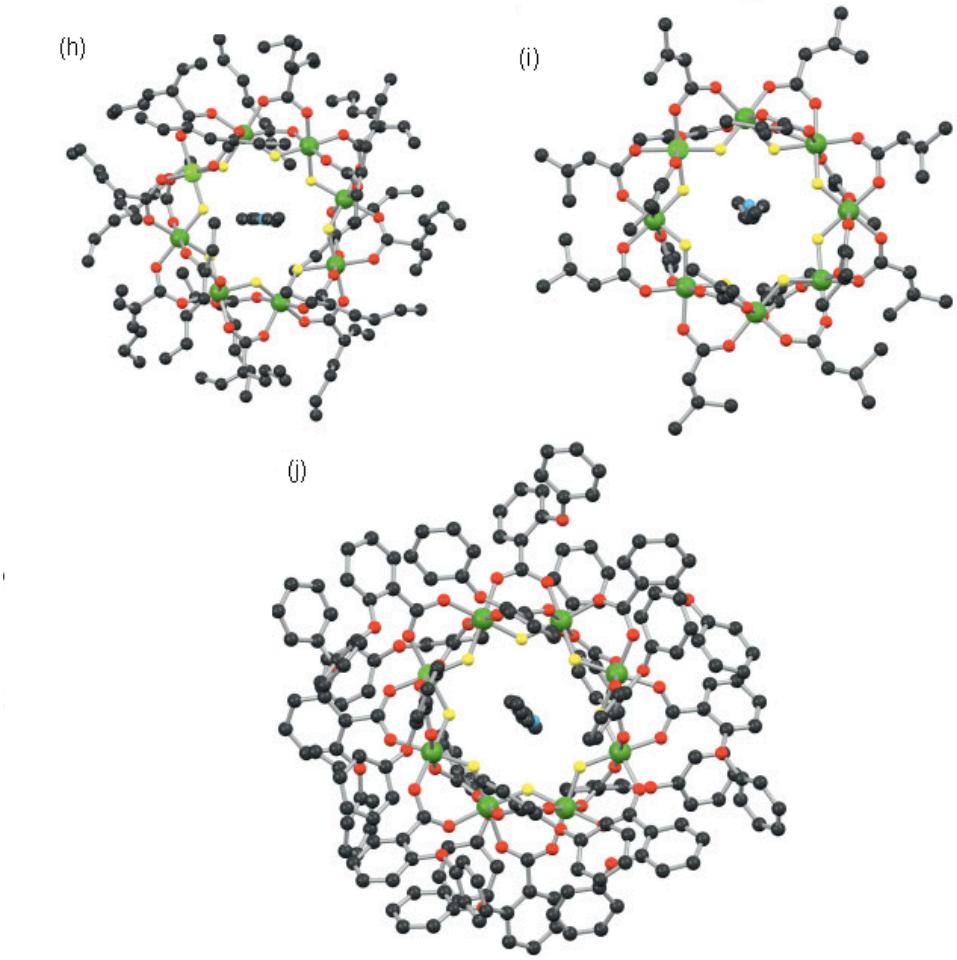

Figure 30. Wheels for attachment to HOPG surfaces.[71]

1.8 FORMING NOVEL LINKED WHEEL SYSTEMS

1.8.1 Non-Switchable Systems

While it is desirable to link wheels together through molecules that are able to act as a switch for quantum gate applications, it is also important to be able to understand how wheels interact when linked through various moieties. Therefore, some target linker molecules were identified, primarily for studying the interactions they mediate as opposed to creating switchable systems.

In order for qubits to become entangled, there must be a direct path for magnetic interactions, so one line of investigation considered is fully conjugated organic molecules. As purple wheels have already been linked together and shown to interact through 4,4′-bpy and bpe, extended versions of these molecules are viable options for probing how the length of the linkage affects the communication between the wheels (Figure 31).

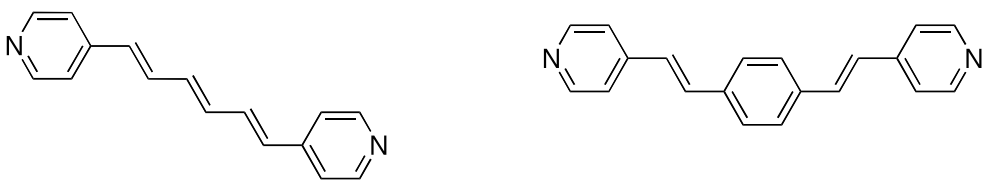

Figure 31. Target organic linker moieties.

In the case of green wheels linked directly by using an ISNA-functionalised carboxylate in the backbone, it has been possible to observe interaction by linking through a paramagnetic metal centre. Insertion of a diamagnetic centre between the two wheels acts as a break in the circuit and prevents any interaction. There are two variables by which we can further study these wheels. The first is to attempt substitution reactions with other functionalised carboxylates (Figure 32) that may be able to act as ligands to metal centres. By comparing EPR spectra of analogous ISNA compounds, it may be possible to probe the effects of varying the carboxylate on the entanglement of the wheels. The second variable is the transition metal centre. So far, wheels have been linked together directly using copper and copper dimers. It would be interesting to observe what effect other metal centres will have on the interaction occurring between the wheels. Some of the metal centres considered for linking wheels are; $M^{II}(CF_3COCHCOCF_3)_2$ where M^{II} = Cu, Ni and Mn, *fac*-$ReCl(CO)_3$ and the triangular system, $Fe_2NiO(O_2CCMe_3)_6$.

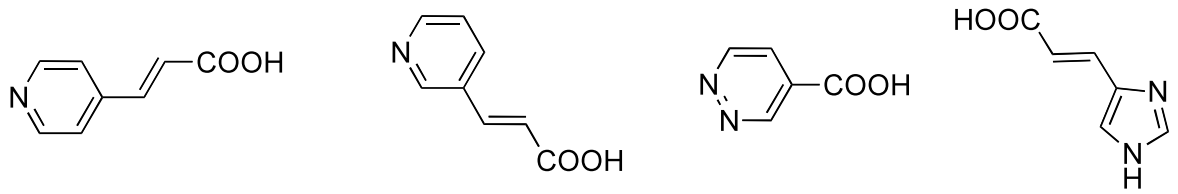

Figure 32. Target carboxylic acids to undergo substitution into wheels.

The final area of consideration for non-switchable systems is that of mixed-wheel systems. It has been shown that green wheels with pyridyl functionalised carboxylates may act as ligands to transition metal centres.[65] The purple wheel has a free coordination site on the divalent metal centre, so it may be possible to attach a green wheel to a purple wheel simply by adding them together.

1.8.2 Switchable Systems

Many recent studies have focused on the concept of "molecular switches", molecules that can exist in two or more stable states. Conversion between these states can be achieved by various means; either by exploiting photoexcitation[72,73] or redox activity,[74] or by alteration of other external conditions, such as pH[75] or temperature.[76] An example of a photoswitchable compound can be seen in Figure 33. The orange bead-like molecule can sit around either the green or the purple functional group dependent on its environment.[77]

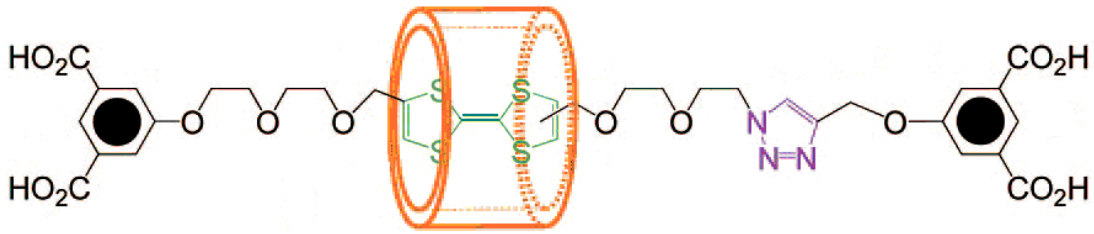

Figure 33. An example of a photoswitchable rotaxane synthesised by Stoddart *et al*.[77]

A relevant example of a molecular switch was published in 2000 by Irie and Matsuda, who showed that it is possible to control the interaction between two radicals by linking them through a diarylethene molecule.[78] Exposure of the sample to UV light, caused a ring closing reaction to occur, allowing full conjugation in the linking molecule (Figure 34). Differences were observed in the magnetic SQUID measurements and electrochemistry of the two compounds as a result of intramolecular anti-ferromagnetic interactions.

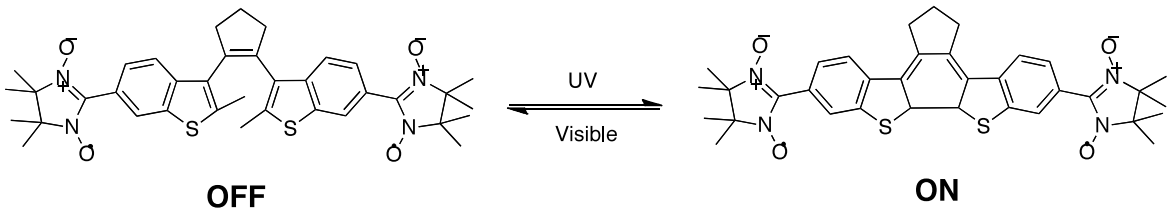

Figure 34. Irie's molecular switch involving an intramolecular magnetic interaction.[78]

This project is particularly focused on the use of photo-excitable or redox-active compounds as switches that may be able to modulate interaction between the wheels. Systems to be considered include viologens, $[M(bpy)_3]^{2+}$ (M = Fe or Ru) and *fac*-$ReCl(CO)_3(bpy)$-based MLCT chromophores.

1.8.2.1 Viologens

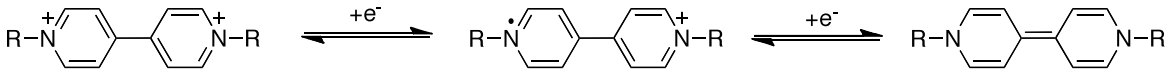

Figure 35. The redox chemistry of the viologens.

The viologens are a series of bis-quaternised derivatives of 4,4′-bpy, which can undergo two reversible one electron reductions (Figure 35). The first reduction produces a mono-radical cation, which is an intense blue colour,[79] and further reduction produces a quinoid. Synthesis is generally achieved by refluxing a halogenated alkane (RX) with 4,4′-bpy in a polar solvent to allow the bis-quaternisation to occur. Use of a less polar solvent allows the formation of the mono-quarternised product. Viologens have proved to be useful in many areas, such as solar energy conversion, herbicides, electrochromic devices and molecular electronics,[80] and have been tested recently as molecular switches for quantum computing purposes, by controlling electron transport between gold nano-particles and an electrode surface.[81] This type of molecule (Figure 36) will only be considered for linking wheels indirectly due to the synthetic limitations inherent in attaching cationic species to the backbone of wheels.

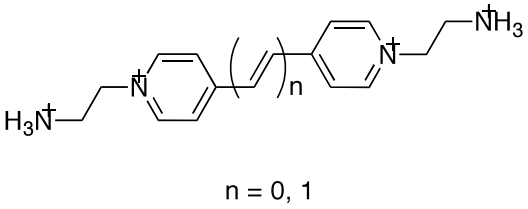

n = 0, 1

Figure 36. Target viologen for linking wheels together indirectly.

1.8.2.2 Photo- and Redox-Active Metal Complexes

Another type of switchable system considered for use as a linking molecule between the wheels is a MLCT-active complex. In such complexes, charge-transfer can occur upon excitation in the UV or short wavelength visible light regions allowing an electron to be promoted from a d-orbital on the metal centre to a low-lying π* anti-bonding orbital on the ligand. These transitions are both Laporte and spin allowed, so their molar extinction co-efficients are in the region of 10^4, and the majority of MLCT chromophores are very strongly coloured.

There are many types of MLCT chromophore. However, this project will focus on ruthenium polypyridyl and rhenium α-diimine systems (Figures 37 and 38) as these are very well studied, and known to have long excited-state lifetimes that may be sufficient for our purposes. In both cases the diamagnetic ground-state, low spin d^6 metal centres (Ru^{II} or Re^{I}) lose an electron temporarily upon MLCT excitation and become paramagnetic with a low spin d^5, S = ½, configuration. This change from dia- to paramagnetism should greatly affect any interactions between the wheels.

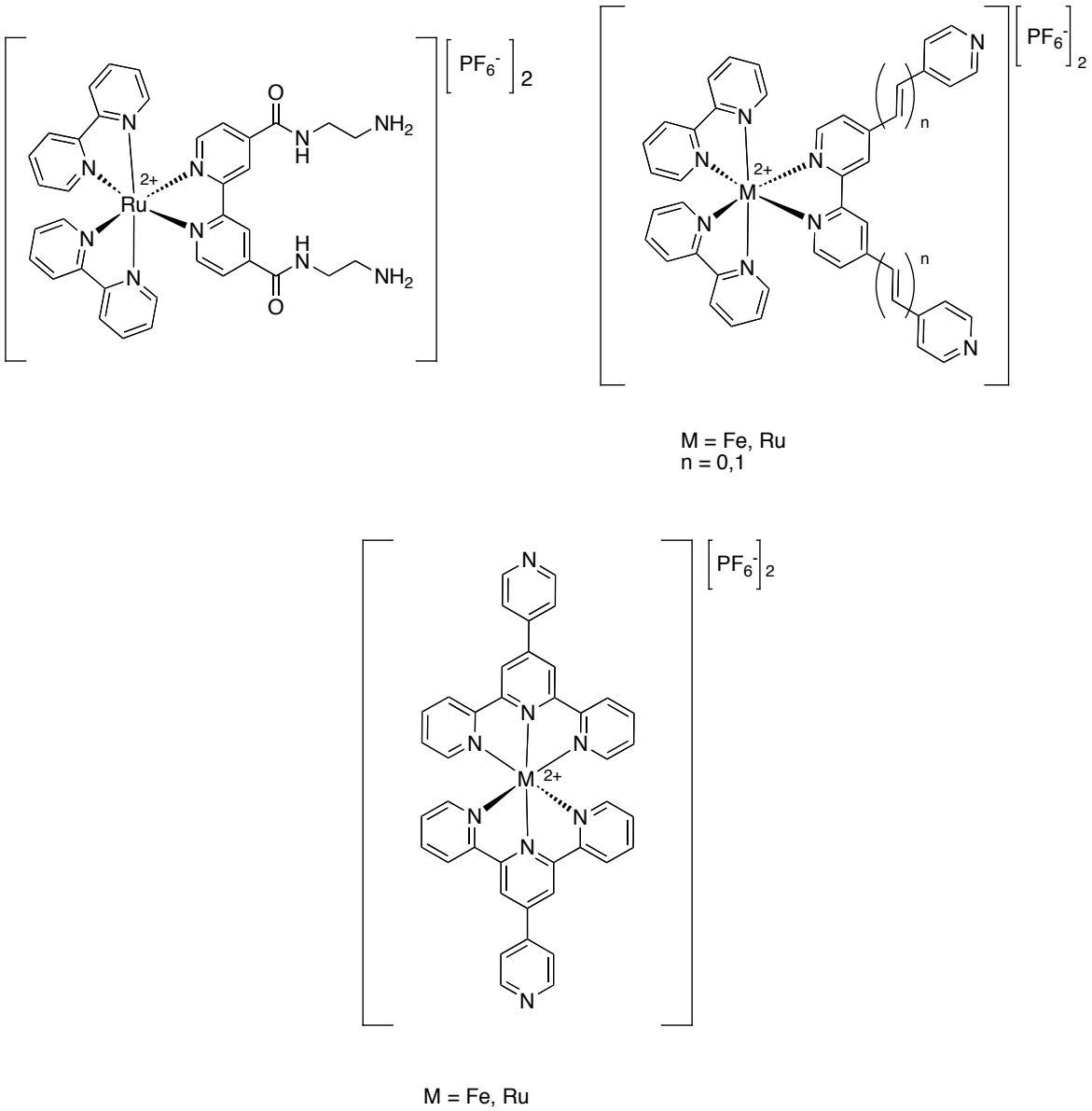

Figure 37. Target Ru and Fe MLCT/redox-active complexes.

The photochemical properties of $[Ru(bpy)_3]^{2+}$ have been very well studied.[82] The UV-vis spectrum of this complex has two absorptions due to ligand-based excitations at 185 and

285 nm, and two MLCT transitions at 240 and 450 nm. If excited at these wavelengths, long-lived luminescence (on the 100–3000 ns scale) is observed.[83] Another much used MLCT chromophore is *fac*-$ReCl(CO)_3(bpy)$, which shows an MLCT absorption band at 370 nm.[84] The lifetime of this excited state (on the 10–500 ns scale) is shorter than that of $[Ru(bpy)_3]^{2+}$ because of intramolecular quenching, caused by the chloride ligand. The advantage of both of these types of complexes is that the α-diimine ligands can be altered readily, allowing control over the absorption and emission properties.

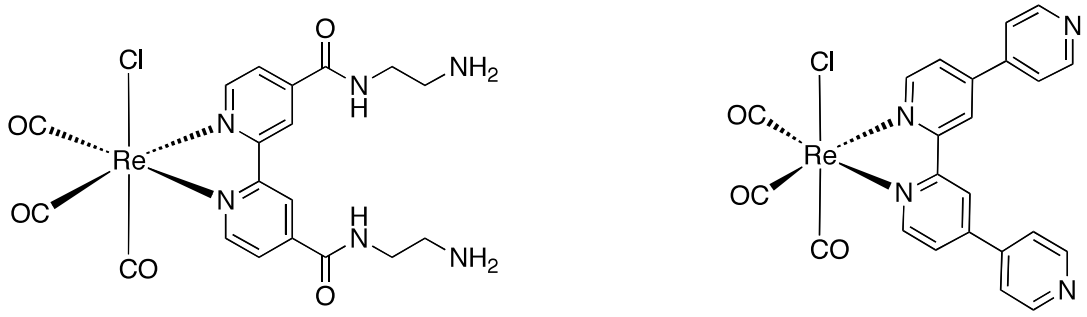

Figure 38. Target Re-based linker molecules.

The ruthenium complexes synthesised should also show a reversible $Ru^{II/III}$ oxidation which can be observed by electrochemical techniques. Replacement of the ruthenium centre with iron will also give reversible redox properties, although Fe^{II} has lower $E_{1/2}$ values and is thus more readily oxidised than Ru^{II}. Chemical or electrochemical redox is clearly related to MLCT and may provide an alternative method of switching the interaction between the wheels.

1.9 ANALYTICAL TECHNIQUES

1.9.1 Paramagnetic ^{1}H NMR Spectroscopy

In general, NMR spectroscopy is an inappropriate analytical technique for systems containing Cr_7M wheels as the overly fast relaxation of the paramagnetic Cr^{III} ions broadens the spectrum severely. However, it is possible to use NMR spectroscopy with the Cr_7Co analogues of the wheels, as the slow relaxation of the Co^{II} ion counteracts the effects of the Cr^{III} ions and thus a spectrum may be observed. Previous studies have been carried out on simple symmetrical Cr_7Co wheels, demonstrating that a degree of information can be obtained.[55]

The spectra obtained are a lot broader than expected for a regular diamagnetic sample, and consequently splitting of the peaks cannot be observed. The chemical shifts of the peaks, instead of being restricted between 0 and 10 ppm, are changed greatly and can be found between –80 and 15 ppm. Also, the integration of the peaks is not always very accurate. Although this technique is not ideal, it can prove useful to probe how a paramagnetic molecule is arranged in solution, while X-ray crystallography is applicable to the solid state only.

1.9.2 EPR Spectroscopy

EPR spectroscopy is a technique used for studying paramagnetic species. It is very similar to NMR spectroscopy, but probes electron- as opposed to nuclear-spin transitions. EPR can be studied by varying either the magnetic field or the frequency of radiation, but in general the frequency is kept the same while the magnetic field varies. At The University of Manchester, a number of machines of different frequency are used to run EPR spectra; X-band (8–10 GHz), K-band (24 GHz), Q-band (35 GHz) and W-band (95 GHz).

Samples can be run in a variety of states; gases, single crystals, solutions, powders and frozen solutions. The spectrum is usually shown as a first derivative of the absorption spectrum, to reduce noise seen on the absorption spectrum.

The g-factor, which is a unitless measurement of the magnetic moment of a particular electron (the moment of a free electron is 2.0023), and analogous to the chemical shift in NMR spectrum can be calculated using Equation 6, where h is Planck's constant (6.626×10^{-34} J s^{-1}), ν is the frequency of radiation (s^{-1}), β is the Bohr magnetron (9.274×10^{-24} J T^{-1}) and B is the strength of the magnetic field (T).

Equation 6:

$$g = \frac{h\nu}{\beta B}$$

Hyperfine splitting is possible in EPR spectra, either through coupling of the electron to its own nucleus' spin or through coupling to that of a nearby nucleus. As in NMR spectra, the coupling ratio follows Pascal's triangle of intensities. The hyperfine constant, a, which is the distance between two of the peaks can be converted into a value, A, in Hz by using Equation 7.

Equation 7: $hA = g\beta a$

Another factor that can affect the EPR spectrum of a molecule is anisotropy, i.e. orientation-dependence. The g-factor is split into three components; g_x, g_y and g_z. If $g_x = g_y = g_z$, the spectrum is considered to be isotropic. When $g_x = g_y \neq g_z$, the spectrum is said to be axial. If g_z is larger than g_x and g_y, then a small peak is seen at low field and a large peak is seen at high field. If g_z is smaller than g_x and g_y, a large peak is observed at low field and a small peak at high field. When $g_x \neq g_y \neq g_z$, the spectrum is said to be rhombic and 3 large peaks are observed, corresponding to the different values of g. The wheels under study here are axially symmetrical and g_z is smaller than g_{xy}.

1.10 INITIAL AIMS OF THE PROJECT

The aims of this project are to extend the series of linked wheel systems in order to better understand how the link affects interaction between the wheels. This is to be investigated by three different synthetic strategies.

1. Functionalisation of the wheel followed by coordination to a metal centre.

Functionalisation of green wheels may be achieved by selective substitution of a pivalate group for a carboxylate containing a pendant coordinating group. The product may then be used as a bulky ligand in the synthesis of transition metal complexes, forming linked wheel systems. A number of carboxylates will be used to assess their suitability as substituents and their behaviour as bulky ligands in previously used metal complexes. The series of metal complexes used with these wheels will also be expanded to include some potential switchable MLCT active Ru^{II} and Re^{I} complexes.

2. Coordination of pyridyl to a vacant site on the divalent metal in purple wheels.

As previously discussed in Section 1.6.3, linking of purple wheels is carried out by coordinating a pyridyl ligand to the spare site on the divalent metal. Attempts will be made to link wheels using more lengthy organic molecules with the aim of studying how the interaction between the wheels is affected by the length of the link. Another avenue of

investigation to be considered is the linking of purple wheels through some MLCT active transition metal complexes based upon quaterpyridyl ligands.

3. Linking the wheels through hydrogen-bonds to a template molecule.

Wheels can be linked indirectly either through direct formation of wheels about a pre-made template containing two amine groups or by using a wheel templated about a pyridyl containing amine as a ligand in a coordination complex. A variety of switchable templating molecules will be synthesised in order to attempt direct synthesis of linked wheel systems.

Chapter 2 – Linked Green Wheel Systems

2.1 INTRODUCTION

The attempted formation of two qubit quantum gates using Cr_7Ni heterometallic wheels first began by linking the wheels together through their templates.[62] While some success was achieved in the synthesis of these systems, the properties desired for use in quantum computing were not observed.[64] Consequently an alternative method was devised, whereby the wheels were linked together directly by replacing one of the pivalates with a carboxylate with a pendent coordinating group such as a pyridyl ring. To date, the isonicotinate-substituted wheel $[Pr_2NH_2][Cr_7NiF_8(O_2CCMe_3)_{15}(O_2CPy)]$, **203**, has been the most used as it can be produced in a reasonable yield and has been proven to act as a bulky ligand in simple coordination chemistry under mild conditions.[65]

Magnetic studies on two different copper complexes demonstrated that by linking the wheels together directly it is possible to obtain the two states (ON/OFF) required in a two-qubit quantum gate.[65] The first complex, a copper dimer $Cu_2(O_2CCMe_3)_4$(**203**)$_2$, shows no interaction of spins of the wheels. However, the second copper complex, $Cu(NO_3)_2(H_2O)_2$(**203**)$_2$, shows a coupling of the wheels, observable in the EPR spectrum (Figure 39).

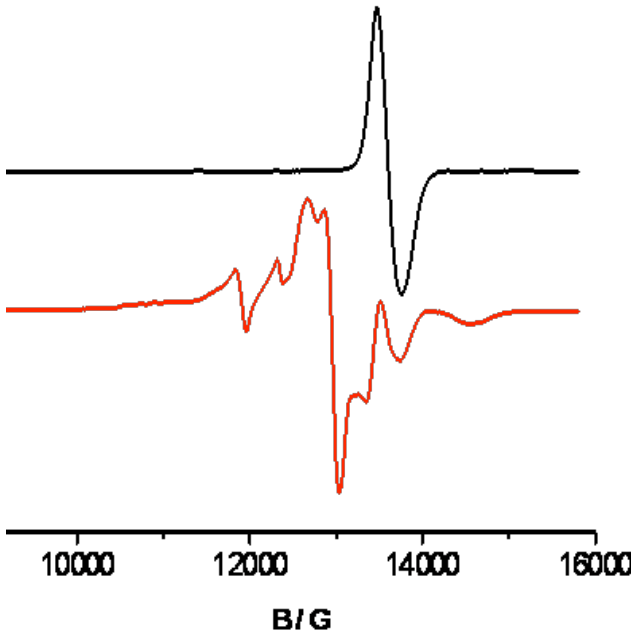

Figure 39. EPR spectrum of individual wheel (black) versus Cu linked-wheel system (red).[65]

The work in this chapter includes the further development of the series of mono- and disubstituted wheels, and the resultant metal complexes that can be obtained by using them as bulky ligands. Studies have been undertaken into the abilities of **203** as a ligand under more harsh conditions, for use with second and third row transition metal centres. Of particular interest in this respect are Ru^{II} and Re^{I} complexes, which are well known to demonstrate MLCT excited states with relatively long lifetimes, that may enable an ON/OFF state switching to occur.

2.2 EXPERIMENTAL PROCEDURES

2.2.1 Materials and Procedures

The compounds $[Co(O_2CCMe_3)_2]_n$[85], $[Pr_2NH_2][Cr_7NiF_8(O_2CCMe_3)_{16}]$[5], $[Pr_2NH_2][Cr_7CoF_8(O_2CCMe_3)_{16}]$[5], $[Pr_2NH_2][Cr_7NiF_8(O_2CCMe)_{15}(O_2CPy)]$ **203**[65], $[Pr_2NH_2][Cr_7NiF_8(O_2CCMe_3)_{14}(O_2CPy)_2]$ **208**[66], $Cu_2(O_2CCMe_3)_4([Pr_2NH_2][Cr_7NiF_8(O_2CCMe_3)_{15}(O_2CPy)])_2$ **214**[65], *fac*-$ReCl(CO)_3(bpy)$[84], *cis*-$Ru(bpy)_2Cl_2•2H_2O$[86], $Cu_2(O_2CCMe_3)_4(HO_2CCMe_3)_2$[87], $Ni(hfac)_2(H_2O)_2$ (hfac = $F_3CCOCHCOCF_3$)[88] and $Fe_2NiO(O_2CCMe_3)_6(HO_2CCMe_3)_3$[89] were synthesised by literature methods. All other materials were purchased commercially and used as supplied.

2.2.2 Physical Measurements

All studies were carried out at the University of Manchester unless stated otherwise. Paramagnetic ^1H NMR spectra were run by Dr Louise Natrajan and Mr Thomas Faust on a Bruker Advance 400 MHz spectrometer. IR data were recorded using a Varian Bio-Rad Excalibur series IR instrument and UV data were recorded on a Shimadzu UV-2401 PC UV-VIS spectrophotometer. Elemental analyses were performed by the Microanalytical Laboratory, and mass spectra were obtained using electrospray analysis on a Micromass Platform spectrometer. Linked wheel systems were sent to Dr Lindsay Harding at the University of Huddersfield for analysis using a Bruker MicroTOF-Q mass spectrometer with an electrospray ionisation source. EPR studies were performed by Dr Floriana Tuna and Mr John Machin; Q-Band EPR was run on an Elexsys E500 spectrometer equipped with a Bruker 2 tesla magnet, and variable temperature studies used an Oxford VT liquid helium cryostat between 5 and 30 K.

2.2.3 Syntheses

$[Pr_2NH_2][Cr_7NiF_8(O_2CCMe_3)_{15}(O_2CCHCH\text{-}4\text{-}Py)]$ 204

$[Pr_2NH_2][Cr_7NiF_8(O_2CCMe_3)_{16}]$ (5.035 g, 2.19 mmol) and *trans*-3-(pyrid-4-yl)acrylic acid (4-pyac) (1.291 g, 8.77 mmol) were refluxed in propan-1-ol (100 ml) for 19.5 h before the solvent was removed under vacuum. The impure product was extracted into diethyl ether,

the solution filtered and the solvent removed under vacuum. The solid was then washed with acetonitrile and dried thoroughly before further purification by column chromatography on silica column, initially eluting with toluene to remove the starting material. The eluent was then changed to a 20:1 mixture of 40–60 °C petroleum ether/ethyl acetate to separate the mono-substituted wheel from more highly substituted products. Once a band had become fully distinguishable, a gradient up to 8:1 40–60 °C petroleum ether/ethyl acetate was used to remove the desired product as a green solid. Yield: 0.628 g (12%). +ve electrospray: *m/z*: 2342 $[MH]^+$, 2364 $[MNa]^+$. –ve electrospray: *m/z*: 2340 $[M - H]^-$, 2239 $[M - Pr_2NH_2]^-$. Elemental analysis calcd. (%) for $C_{89}H_{157}Cr_7F_8N_2NiO_{32}$: C 45.65, H 6.76, N 1.20, Cr 15.54. Found: C 45.40, H 6.88, N 1.07, Cr 15.49.

$[Pr_2NH_2][Cr_7NiF_8(O_2CCMe_3)_{15}(O_2CCHCH\text{-}3\text{-}Py)]$ 205

This compound was prepared and purified in manner similar to **204** by using $[Pr_2NH_2][Cr_7NiF_8(O_2CCMe_3)_{16}]$ (5.093 g, 2.22 mmol) and *trans*-3-(pyrid-3-yl)acrylic acid (1.288 g, 8.75 mmol) with a reflux time of 20 h, giving a green solid. Yield: 0.335 g (6%). +ve electrospray: *m/z*: 2342 $[MH]^+$, 2364 $[MNa]^+$. –ve electrospray: *m/z*: 2340 $[M - Pr_2NH_2]^-$, 2340 $[M - H]^-$. Elemental analysis calcd. (%) for $C_{89}H_{157}Cr_7F_8N_2NiO_{32}$: C 45.65, H 6.76, N 1.20, Cr 15.54. Found: C 45.80, H 6.92, N 1.09, Cr 15.18.

$[Pr_2NH_2][Cr_7NiF_8(O_2CCMe_3)_{15}(O_2CPyd)]$:Pyd = 4-pyridazine 206

This compound was prepared and purified in manner similar to **205** by using $[Pr_2NH_2][Cr_7NiF_8(O_2CCMe_3)_{16}]$ (5.10 g, 2.22 mmol) and 4-pyridazine carboxylic acid (4-pyd) (1.063 g, 8.57 mmol), giving a green solid. Yield: 2.27 g (44%). +ve electrospray: *m/z*: 2316 $[MH]^+$, 2339 $[MNa]^+$. –ve electrospray: *m/z*: 2214 $[M - Pr_2NH_2]^-$. Elemental analysis calcd. (%) for $C_{86}H_{154}Cr_7F_8N_3NiO_{32}$: C 44.58, H 6.70, N 1.81, Cr 15.71. Found: C 44.70, H 7.05, N 1.76, Cr 15.52.

$[Pr_2NH_2][Cr_7CoF_8(O_2CCMe_3)_{15}(O_2CPy)]$ 207

This compound was prepared and purified in manner similar to **205** by using $[Pr_2NH_2][Cr_7CoF_8(O_2CCMe_3)_{16}]$ (5.118 g, 2.23 mmol) and ISNA (0.836 g, 6.79 mmol) with a reflux time of 17 h, giving a green solid. Yield: 1.24 g (24%). +ve electrospray:

2316 $[MH]^+$, 2339 $[MNa]^+$. Elemental analysis calcd. (%) for $C_{87}H_{155}CoCr_7F_8N_2O_{32}$: C 45.12, H 6.75, N 1.21, Cr 15.72. Found: C 44.65, H 6.73, N 1.17, Cr 16.11.

$[Pr_2NH_2][Cr_7NiF_8(O_2CCMe_3)_{14}(O_2CPyd)_2]$ 209

This compound was prepared and purified in manner similar to **206**, but the desired product was eluted from the column after the mono-substituted product by using 20:3 40–60 ºC petroleum ether/ethyl acetate, giving a green solid. Yield: 310 mg (6%). +ve electrospray: *m/z*: 2361 $[MNa]^+$. –ve electrospray: *m/z*: 2335 $[M - Pr_2NH_2]^-$, 2338 $[M - H]^-$. Elemental analysis calcd. (%) for $C_{86}H_{148}Cr_7F_8N_5NiO_{32}•C_4H_8O$: C 45.43, H 6.60, N 2.82, Cr 14.66. Found: C 45.88, H 6.90, N 2.61, Cr 14.23.

$[Pr_2NH_2][Cr_7CoF_8(O_2CCMe_3)_{14}(O_2CPy)_2]$ 210

This compound was prepared and purified in a manner similar to **207**, but the desired product was eluted from the column after the mono-substituted product by using 20:3 40–60 ºC petroleum ether/ethyl acetate, giving a green solid. Yield: 143 mg (3%). +ve electrospray: *m/z*: 2359.6 $[MNa]^+$. Elemental analysis calcd. (%) for $C_{88}H_{150}CoCr_7F_8N_3O_{32}$: C 45.23, H 6.47, N 1.80, Cr 15.57. Found: C 45.36, H 6.69, N 1.65, Cr 15.24.

$Cu_2(O_2CCMe_3)_4([Pr_2NH_2][Cr_7NiF_8(O_2CCMe_3)_{15}(O_2CCHCH\text{-}4\text{-}Py)])_2$ 211

$Cu_2(O_2CCMe_3)_4(HO_2CCMe_3)_2$ (38.0 mg, 0.052 mmol) was added to a solution of **204** (253 mg, 0.108 mmol) in toluene (10 ml) and the mixture was stirred at room temperature for 15 min. The mixture was refluxed for 5 min, cooled to room temperature and stirred for 95 min then covered and left to stand overnight. Slow evaporation of the solvent at room temperature afforded the green crystalline product. Yield: 38.8 mg (14%). Elemental analysis calcd. (%) for $C_{198}H_{350}Cr_{14}Cu_2F_{16}N_4Ni_2O_{72}$: C 45.60, H 6.76, N 1.07, Cr 13.96, Cu 2.44. Found: C 45.70, H 6.85, N 1.02, Cr 13.59, Cu 2.48.

$Cu_2(O_2CCMe_3)_4([Pr_2NH_2][Cr_7NiF_8(O_2CCMe_3)_{15}(O_2CCHCH\text{-}3\text{-}Py)])_2$ 212

This compound was prepared and purified in manner similar to **211** by using $Cu_2(O_2CCMe_3)_4(HO_2CCMe_3)_2$ (38.6 mg, 0.052 mmol) and **205** (252 mg, 0.108 mmol),

giving a green crystalline product. Yield: 78 mg (64%). Elemental analysis calcd. (%) for $C_{198}H_{350}Cr_{14}Cu_2F_{16}N_4Ni_2O_{72}$: C 45.60, H 6.76, N 1.07, Cr 13.96, Cu 2.44. Found: C 43.76, H 6.81, N 0.92, Cr 13.93, Cu 2.37.

$Cu_2(O_2CCMe_3)_4([Pr_2NH_2][Cr_7NiF_8(O_2CCMe_3)_{15}(O_2CPyd)])_2$ 213

This compound was prepared and purified in manner similar to **211** by using $Cu_2(O_2CCMe_3)_4(HO_2CCMe_3)_2$ (38.8 mg, 0.053 mmol) and **206** (250 mg, 0.108 mmol), giving a green crystalline product. Yield: 125 mg (44%). Elemental analysis calcd. (%) for $C_{192}H_{344}Cr_{14}Cu_2F_{16}N_6Ni_2O_{72}$: C 44.65, H 6.71, N 1.63, Cr 14.09, Cu 2.46. Found: C 44.78, H 6.84, N 1.51, Cr 13.27, Cu 2.47.

$Cu(NO_3)_2(H_2O)([Pr_2NH_2][Cr_7NiF_8(O_2CCMe_3)_{15}(O_2CCHCH\text{-}4\text{-}Py)])_2$ 215

$Cu(NO_3)_2$•$2.5H_2O$ (11.6 mg, 0.050 mmol) was added to a warm solution of **204** (302 mg, 0.129 mmol) in acetone (40 ml). The reaction was stirred for 5 min then filtered. The flask and sinter were washed with further acetone (5 ml) and the solution left covered at room temperature for 48 h, affording green crystals. Yield: 126 mg (52%). Elemental analysis calcd. (%) for $C_{178}H_{316}Cr_{14}CuF_{16}N_6Ni_2O_{71}$: C 43.73, H 6.51, N 1.72, Cr 14.89, Cu 1.30, Ni 2.40. Found: C 43.51, H 6.55, N 1.71, Cr 14.94, Cu 1.32, Ni 2.35.

$Cu(hfac)_2([Pr_2NH_2][Cr_7NiF_8(O_2CCMe_3)_{15}(O_2CPy)])_2$ 216

To a solution of **203** (101 mg, 0.043 mmol) in refluxing acetone (20 ml) was added $Cu(hfac)_2(H_2O)_2$ (10.8 mg, 0.021 mmol). The solution was heated with stirring for 5 mins during which time the product formed as a green precipitate, which was collected by filtration, washed with acetone and dried in air. Yield: 46 mg (43%). Elemental analysis calcd. (%) for $C_{184}H_{312}Cr_{14}CuF_{28}N_4Ni_2O_{68}$: C 43.25, H 6.15, N 1.10, Cr 14.25, Cu 1.24, Ni 2.30. Found: C 43.15, H 6.18, N 1.11, Cr 13.88, Cu 1.23, Ni 2.29.

$Ni(hfac)_2([Pr_2NH_2][Cr_7NiF_8(O_2CCMe_3)_{15}(O_2CPyd)])_2$ 217

To a solution of **206** (103 mg, 0.044 mmol) in warm acetone (15 ml) was added a solution of $Ni(hfac)_2(H_2O)_2$ (10.8 mg, 0.021 mmol) in acetone (5 ml). The reaction was heated for 5 min then cooled to room temperature, covered and left for 24 h. The resulting green

crystals were collected by filtration, washed with a small amount of acetone and dried under vacuum. Yield: 42 mg (39%). Elemental analysis calcd. (%) for $C_{182}H_{310}Cr_{14}F_{28}N_6Ni_3O_{68}$: C 42.81, H 6.12, N 1.65, Cr 14.26, Ni 3.45. Found: C 42.47, H 6.00, N 1.59, Cr 13.85, Ni 3.46.

$Mn(hfac)_2([Pr_2NH_2][Cr_7NiF_8(O_2CCMe_3)_{15}(O_2CPyd)])_2$ 218

This compound was prepared and purified in manner similar to **218** by using **206** (106 mg, 0.046 mmol) and $Mn(hfac)_2(H_2O)_2$ (14.4 mg, 0.031 mmol) in place of $Ni(hfac)_2(H_2O)_2$. The crystalline product was collected after 48 h at room temperature. Yield: 56 mg (47%). Elemental analysis calcd. (%) for $C_{182}H_{310}Cr_{14}F_{28}MnN_6Ni_2O_{68}$•$2Me_2CO$: C 43.27, H 6.22, N 1.61, Cr 13.95, Mn 1.05. Found: C 43.15, H 6.19, N 1.66, Cr 13.64, Mn 0.80.

$Fe_2NiO(O_2CCMe)_6([Pr_2NH_2][Cr_7NiF_8(O_2CCMe_3)_{15}(O_2CCHCHPy)])_3$ 219

$Fe_2NiO(O_2CCMe_3)_6(HO_2CCMe_3)_3$ (26.4 mg, 0.024 mmol) and **204** (101 mg, 0.043 mmol) were dissolved in *n*-hexane (10 ml) and stirred at room temperature for 20 h before the solvent was allowed to evaporate to dryness. Crystals suitable for X-ray crystallography were obtained by evaporation of a diethyl ether/acetone solution at room temperature. Yield: 71 mg (63 %). Elemental analysis calcd. (%) for $C_{297}H_{525}Cr_{21}F_{24}Fe_2N_6Ni_4O_{109}$: C 45.62, H 6.77, N 1.07, Cr 13.97, Ni 3.00. Found: C 43.76, H 6.65, N 0.93, Cr 12.26, Ni 3.02.

$ReCl(CO)_3([Pr_2NH_2][Cr_7NiF_8(O_2CCMe_3)_{15}(O_2CPy)])_2$ 220

$ReCl(CO)_5$ (30.9 mg, 0.085 mmol) and **203** (499 mg, 0.22 mmol) were refluxed in toluene (10 ml) for 24 h, then the reaction solvent was removed under vacuum. Column chromatography on alumina was used to isolate the pure product, which was the first green band to be brought off using toluene as an eluent. The solvent was removed under vacuum and the product recrystallised by evaporation of a solution in 3:2 acetone/*n*-pentane at room temperature. Yield: 263 mg (62%). +ve electrospray: *m/z*: 4939 $[MH]^+$. υ_{max} (cm^{-1}): 2029 (C≡O), 1931 (C≡O), 1890 (C≡O). Elemental analysis calcd. (%) for $C_{177}H_{310}ClCr_{14}F_{16}N_4Ni_2O_{67}Re$: C 43.06, H 6.33, N 1.13, Cr 14.74, Re 3.77. Found: C 42.73 H 6.32, N 1.07, Cr 14.36, Re 3.85.

$ReCl(CO)_3([Pr_2NH_2][Cr_7CoF_8(O_2CCMe_3)_{15}(O_2CPy)])_2$ 221

This compound was prepared and purified in manner similar to **222** by using $ReCl(CO)_5$ (20.0 mg, 0.055 mmol) and **207** (303 mg, 0.131 mmol), giving a green solid. Recrystallisation was achieved as for **222** using a 3:2 acetone/*n*-pentane mixture at room temperature. Yield: 87.7 mg (35%). υ_{max} (cm^{-1}): 2021 (C≡O), 1930 (C≡O), 1887 (C≡O). Elemental analysis calcd. (%) for $C_{177}H_{310}ClCo_2Cr_{14}F_{16}N_4O_{67}Re$: C 43.05, H 6.33, N 1.13, Cr 14.74, Re 3.77. Found: C 43.00, H 6.62, N 1.04, Cr 14.54, Re 3.79.

$[Re\{[Pr_2NH_2][Cr_7NiF_8(O_2CCMe_3)_{15}(O_2CPy)]\}(CO)_3(bpy)][PF_6]$ 222

To a solution of *fac*-$ReCl(CO)_3(bpy)$ (0.106 g, 0.230 mmol) and **203** (2.53 g, 1.09 mmol) in refluxing toluene (55 ml) was added a solution of $AgBF_4$ (54 mg, 0.276 mmol) in toluene (5 ml). The reaction mixture was refluxed for 3 h then filtered warm to remove AgCl before the filtrate was refluxed for a further 23 h. The warm solution was filtered once more and the solvent was removed from the filtrate under vacuum. The product was extracted into acetonitrile (200 ml), which was then removed under vacuum. The solid was dissolved in a minimal amount of THF and metathesis to the PF_6^- salt was effected by addition of aqueous NH_4PF_6. The green product was collected by filtration, washed with a large amount of water and dried under vacuum. Yield: 186 mg (28%). +ve electrospray: *m/z*: 2915 $[MNa]^+$, 2742 $[M - PF_6]^+$, 2337 $[\{Pr_2NH_2\}\{Cr_7NiF_8(O_2CCMe_3)_{15}(O_2CPy)\}Na]^+$, 2315 $[\{Pr_2NH_2\}\{Cr_7Ni\ F_8(O_2CCMe_3)_{15}(O_2CPy)\}]^+$. υ_{max} (cm^{-1}): 2037 (C≡O) (s), 1926 (C≡O) (br). Elemental analysis calcd. (%) for $C_{100}H_{165}Cr_{14}F_{14}N_4NiO_{67}PRe$: C 41.57, H 5.76, N 1.94, Cr 12.60. Found: C 41.48, H 5.78, N 1.73, Cr 12.39.

$[Ru(bpy)_2([Pr_2NH_2][Cr_7NiF_8(O_2CCMe_3)_{15}(O_2CPy)])_2][PF_6]_2$ 223

cis-$Ru(bpy)_2Cl_2 \cdot 2H_2O$ (52 mg, 0.108 mmol) and $AgCF_3SO_3$ (87 mg, 0.339 mmol) were refluxed in ethanol (25 ml) for 3 h, giving a deep red solution. The solution was filtered warm to remove AgCl before **203** (1.174 g, 0.507 mmol) was added and further refluxing for 16.5 h produced an orange-green solution. The solution was cooled and filtered and the solvent was removed under vacuum. The product was extracted into acetonitrile, removing the starting wheel, and to the solution was added aqueous NH_4PF_6 to form an orange-brown precipitate, which was collected by filtration, washed with water and dried under

vacuum. Yield: 174 mg (32%). +ve electrospray: *m/z*: 2522 $[M - 2PF_6]^{2+}$, 5193 $[M - PF_6]^{+}$. λ_{max} (ε/mol^{-1} dm^3 cm^{-1}): 433 (12300), 367 (15600), 291 (67200). Elemental analysis calcd. (%) for $C_{194}H_{326}Cr_{14}F_{28}N_8Ni_2O_{64}P_2Ru \bullet 1.5NH_4PF_6$: C 41.76, H 6.00, N 2.38, Cr 13.05. Found: C 41.57, H 5.90, N 2.34, Cr 12.98.

$[Cu(NO_3)_2(H_2O)([Pr_2NH_2][Cr_7NiF_8(O_2CCMe_3)_{14}(O_2CPy)_2])]_n$ 224

To a warm solution of **208** (107 mg, 0.046 mmol) in acetone was added $Cu(NO_3)_2 \bullet 2.5H_2O$ (13.2 mg, 0.057 mmol) in acetone (10 ml) and the solution was refluxed for 10 min. During this time a green precipitate began to form. The reaction was allowed to cool to room temperature and left covered for 24 h, affording a precipitate. This solid was collected by filtration, washed with acetone and dried under vacuum. X-ray quality crystals were grown by evaporation of a tetrahydrofuran/toluene solution. Yield: 114 mg.

2.3 RESULTS AND DISCUSSION

2.3.1 Synthetic Studies

2.3.1.1 Substitution into Wheels

The primary starting materials, $[Pr_2NH_2][Cr_7MF_8(O_2CCMe_3)_{16}]$ where M = Ni (**201**) and Co (**202**) were synthesised following published procedures.[5] The cobalt analogue, however, required additional purification by washing the product through a silica column with toluene to remove impurities prior to recrystallisation.

Functionalisation of the wheels was achieved following a procedure used with the previously published ISNA wheel **203**[65] (Scheme 1). Refluxing a roughly four-fold excess of a second carboxylic acid with **201** or **202** in propan-1-ol allowed this acid to be incorporated into the wheel. In order to aid the removal of the anionic pivalate ligands a polar solvent is required, but the solubility of the wheels must also be considered. Consequently, propan-1-ol was considered to be the most appropriate solvent for this reaction.

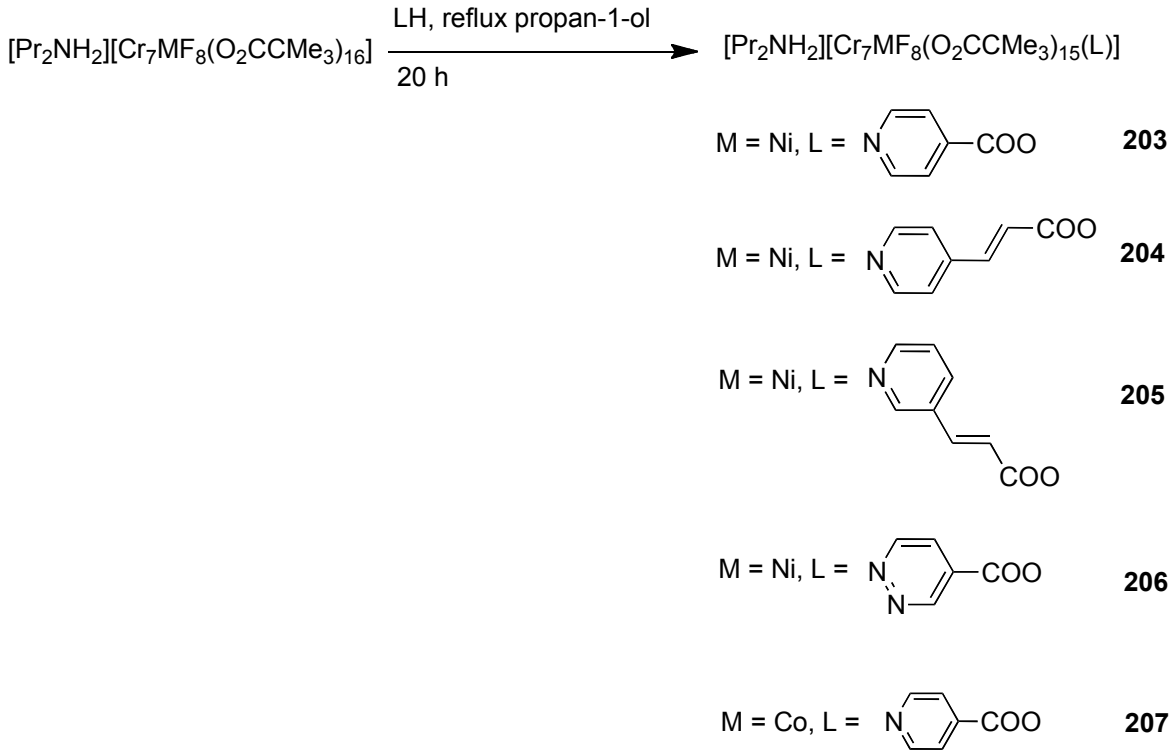

Scheme 1. Synthesis of substituted wheels.

Isolation of the product was achieved by column chromatography on silica gel, eluting initially with toluene to remove the starting material, before increasing the gradient of the eluent using a 40–60 ºC petroleum ether/ethyl acetate mixture (2 L:100 ml). Once the band of the mono-substituted product, $[Pr_2NH_2][Cr_7NiF_8(O_2CCMe_3)_{15}(L)]$, had separated from bands of more highly substituted products, the amount of ethyl acetate was increased to elute the desired product faster.

For certain substitution reactions, it is also possible to obtain disubstituted products (Scheme 2), although the yields of these are significantly lower than those of the comparable mono-substituted wheels. These minor products were brought off the same silica columns used to isolate the mono-substituted wheels simply by increasing the relative ethyl acetate content of the eluent.

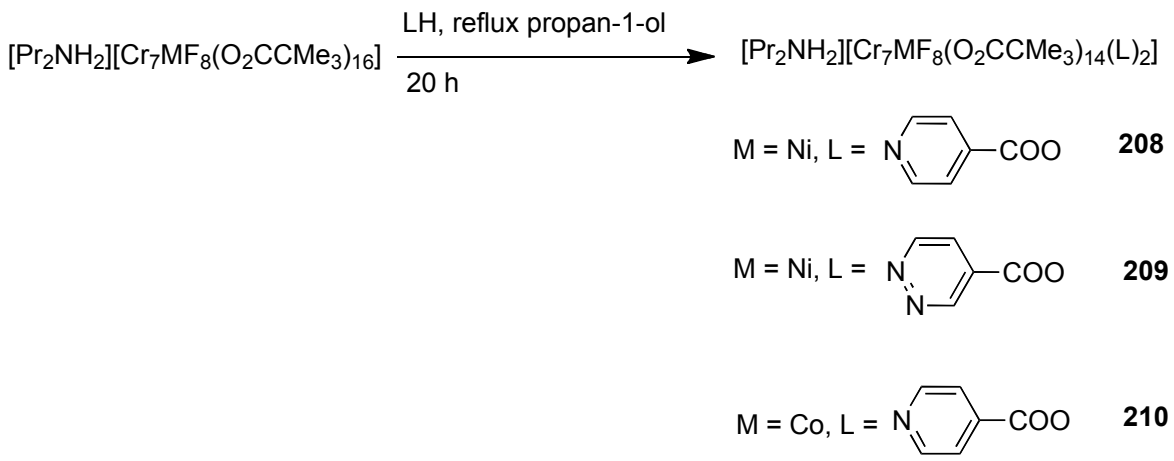

Scheme 2. Synthesis of disubstituted wheels.

Substitution of the carboxylate occurs across the divalent metal and one of the Cr^{III} ions, because the former is much more kinetically labile. The substitution takes place in the axial position due to the trans effect of the opposite π-accepting carboxylate ligands. The equatorial pivalate groups are trans to π-donating fluoride ligands which strengthens their bonds to the metal centre. The second substitution also occurs on the divalent metal ion and an adjacent Cr^{III} ion. As it is preferential for the substitution to occur in the axial position, it occurs on the Cr^{III} ion that has not already been involved in the first substitution.

Table 2. Yields of substitution reactions.

Product	Yield (%)
203	32
204	12
205	6
206	44
207	24
208	3
209	6
210	3

The efficiency of the substitution reactions appears to vary widely (see Table 2), which has been attributed to a number of factors. Firstly, and most obviously, the solubility of the substituting carboxylic acid in propan-1-ol plays a major role as none of the carboxylic acids used are fully soluble, even at reflux. Another potentially important factor is the pK_a of the incoming acid. The lower this pK_a, the higher the anticipated yield, due to the increased ability of the acid to dissociate into the anionic species required to substitute into the wheel.

2.3.1.2 Reactions of Substituted Wheels with First Row Transition Metals

Initial coordination chemistry of these novel functionalised wheels was attempted with first row transition metal centres. Due to the relative weakness of the bonds formed, coordination to first row d-block metals can generally occur readily, without the requirements of harsh conditions or much purification. It is not anticipated that selective control of magnetic interactions will be possible with these linked-wheel systems. However, preliminary work with the previously synthesised substituted wheel, **203**, had already produced some interesting results, so this approach provides a good basis to compare the effectiveness of the various substituents in terms of metal ion coordination.

Systems of the type $Cu_2(O_2CCMe_3)_4([Pr_2NH_2][Cr_7NiF_8(O_2CCMe_3)_{15}(L)_2])_2$ were formed by reaction of the mono-substituted wheels with $Cu_2(O_2CCMe_3)_4(HO_2CCMe_3)_2$ in toluene. Stirring the reaction at room temperature and then at reflux produced the desired linked-wheel compounds and slow evaporation of the solvent afforded crystals. The wheels **204**, **205** and **206** formed **211**, **212** and **213**, respectively (Scheme 3).

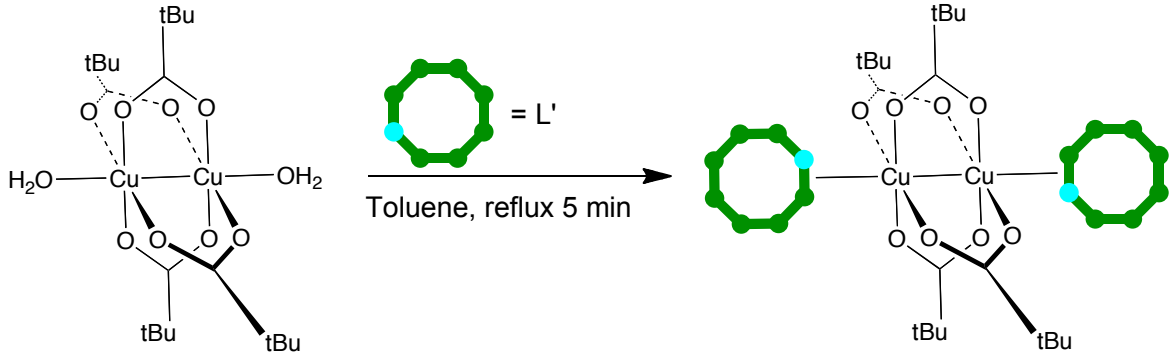

Scheme 3. Synthesis of Cu dimer linked-wheel systems.

Crystals suitable for X-ray diffraction were obtained for the products **211** and **213**, but those of **212** did not diffract strongly enough. Hence, **212** has been characterised by elemental analysis only. **211** and **213** have been characterised by elemental analysis and X-ray crystallography

Following the experimental procedures used in the synthesis of the ISNA analogue **214**, **204** was linked through a single copper centre to form **215** (Scheme 4).[65] An acetone solution of $Cu(NO_3)_2 \cdot 2.5H_2O$ and **204** was heated for 5 min and then left to stand covered for 2 days forming crystals, which have been characterised by X-ray crystallography and elemental analyses. When a similar reaction was attempted with **206** however, crystals were not obtained. Therefore, the solution was allowed to stand only partially covered, producing some crystalline material. However, elemental analyses showed only trace quantities of copper, indicating that this material was unreacted **206**.

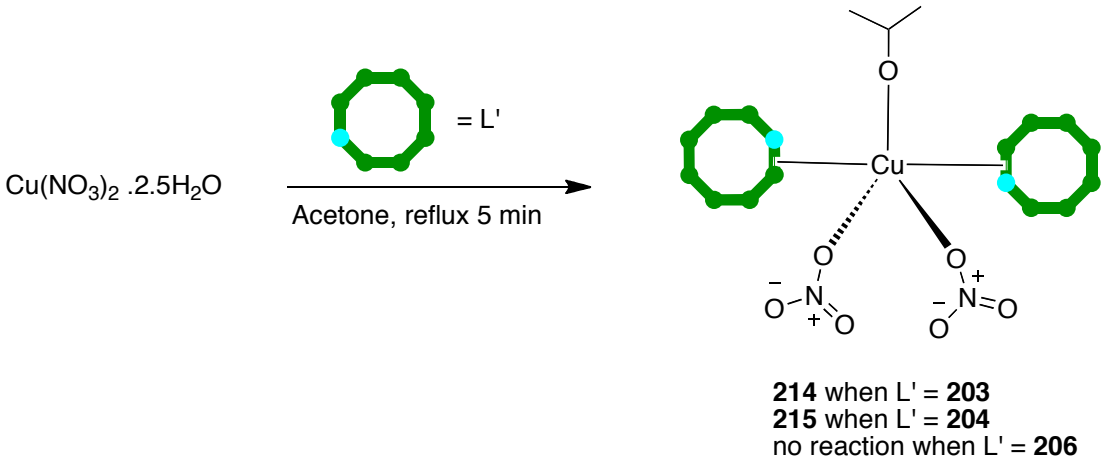

Scheme 4. Synthesis of copper nitrate linked wheel systems.

Having encountered difficulties in attempting to synthesise a linked-wheel system previously using **206** as a ligand, it was decided to investigate its general suitability as a ligand, using some alternative metal centres of type *trans*-M(hfac)$_2$(H$_2$O)$_2$ where M = Cu, Ni or Mn (Scheme 5). In a similar fashion to other reactions with first row neutral metal complexes, a 2:1 ratio of wheel to metal complex was mixed and allowed to crystallise, using the insolubility of the linked-wheel system to drive its formation. The first complex to be considered was the copper one, as it was with another copper complex where the problems had been discovered initially. In a similar fashion to the reaction described previously, no crystalline material was produced, so the solution was allowed to partially evaporate. However, elemental analyses on the material produced showed no copper to be present, so no link had been made. In stark contrast, use of **203** as a ligand afforded a crystalline material, **216**, within five minutes.

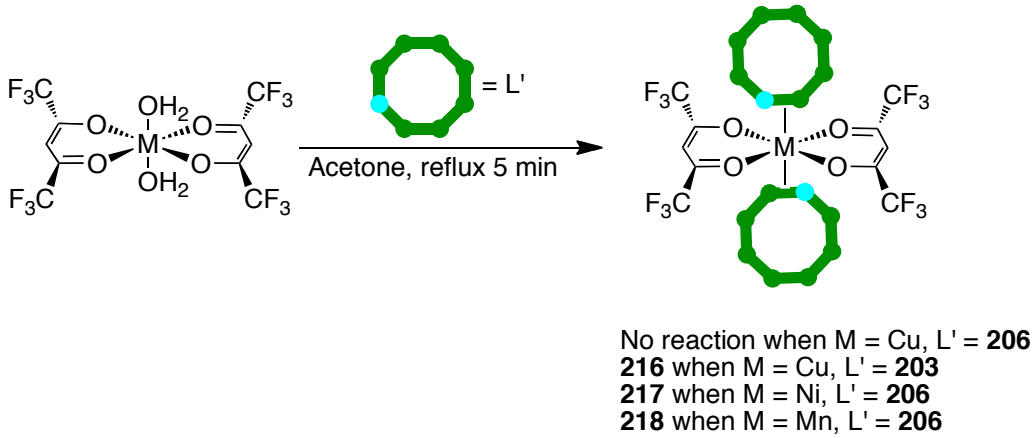

No reaction when M = Cu, L' = **206**
216 when M = Cu, L' = **203**
217 when M = Ni, L' = **206**
218 when M = Mn, L' = **206**

Scheme 5. Synthesis of *trans*-M(hfac)$_2$(L)$_2$ (M = Cu, Ni or Mn) complexes.

Reacting **206** with *trans*-Ni(hfac)$_2$(H$_2$O)$_2$ in warm acetone for 5 mins afforded **217** in a 62% isolated yield. **217** was characterised by X-ray crystallography and elemental analyses, showing that **206** can be used as a monodentate ligand with nickel centres. Reaction of **206** with *trans*-Mn(hfac)$_2$(H$_2$O)$_2$ also appeared to be successful. However, the complexation occurred much more slowly when compared with the analogous Ni system. taking 5 days. As yet, crystals of **218** suitable for x-ray diffraction have not been produced.

It is unknown why **206** does not appear capable of coordinating in a monodentate fashion to a single copper centre, when it does form linked-wheel systems through other metal

centres, especially as there is previously published evidence of 4-pyridazine being used as a monodentate ligand with copper.[90] However 4-pyridazine is an electron deficient ligand with the ortho-nitrogen removing electron density from the coordinating nitrogen, which may have an impact on its coordinating abilities.

A tri-wheel system was synthesised by reacting 3 equivalents **204** with $Fe_2NiO(O_2CCMe_3)_6$ $(HO_2CCMe_3)_3$ in *n*-hexane at room temperature (Scheme 6). Crystallisation of the linked-wheel system formed (**219**) was attempted by many methods, but slow evaporation of a diethyl ether/acetone solution gave the best quality crystals, confirming the coordination of three wheels. However, satisfactory elemental analyses are still required before pursuing magnetic and EPR studies on this product. A similar reaction has also been attempted with **203**, but there has been no evidence to date of successful synthesis of a linked-wheel system.

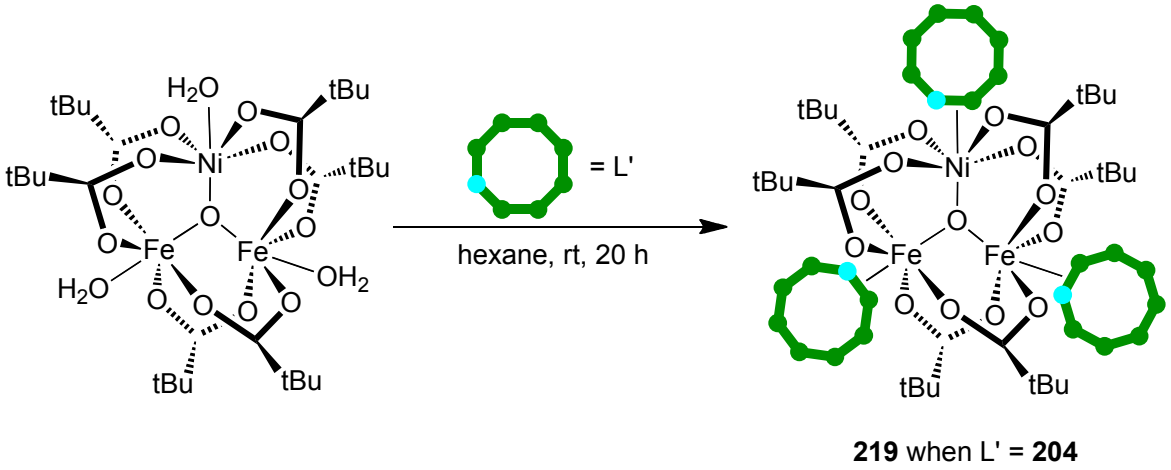

Scheme 6. Synthesis of **219**.

2.3.1.3 Reactions with Second and Third Row Transition Metals

Reactions with first row transition metals occur very readily, allowing mild conditions and (often) facile crystallisation directly from the reaction solution. However, the coordination of second and third row transition metal centres is expected to provide more interesting systems from the perspective of redox/photo-activity, and also more stable products. The only substituted wheels considered in this section are the ISNA derivatives **203** and **207**.

By reacting **203** with $ReCl(CO)_5$ in refluxing toluene for 24 h, it is possible to form the linked-wheel system **220** (Scheme 7). Purification was achieved on an alumina column

using toluene as the eluent. An analogous reaction using **207** in place of **203** produced **221**, but in a yield only half of that obtained for **222**. Both of these products have been characterised using IR spectroscopy and elemental analyses, and the structure of **220** has been proven using X-ray crystallography.

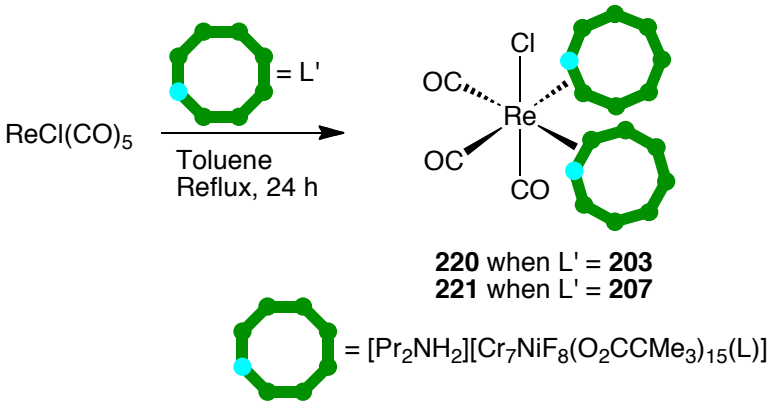

Scheme 7. Synthesis of Re-linked wheel systems.

Although it is possible to form linked-wheel systems from reactions with $ReCl(CO)_5$, such species are not expected to demonstrate any potentially useful photo/redox-activity. One method of introducing photoactivity into the system is to include a relatively low energy MLCT chromophore, using a co-ligand such as 2,2′-bipyridine.[91] Consequently, it was decided to react **203** with the known complex *fac*-$ReCl(CO)_3$(bpy) to form **222**. It was expected that only one wheel would coordinate to the Re centre due to selective substitution of the chloride ligand. However, it might be possible to use a complex such as *fac*,*fac*-$\{ReCl(CO)_3\}_2$(bpym) (bpym = 2,2′-bipyrimidine) to link two wheels.

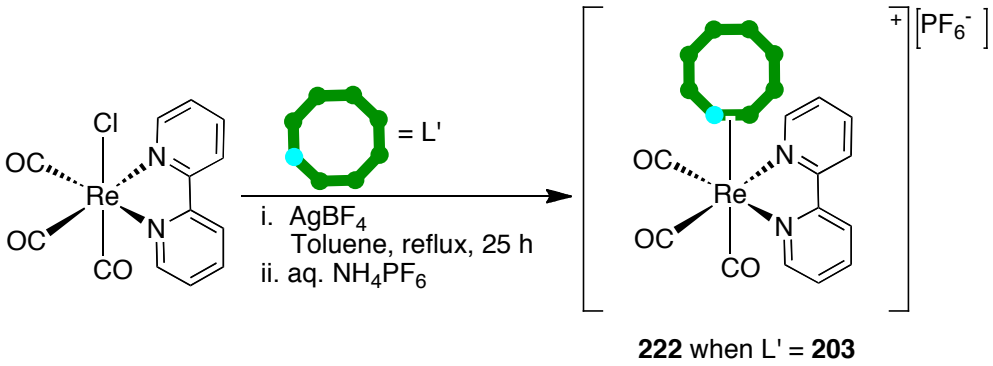

Scheme 8. Synthesis of **222**.

222 was synthesised using a previously unpublished one-step method, recommended by Dr Mike Coogan of the University of Cardiff (Scheme 8). 1 equivalent of *fac*-

$ReCl(CO)_3(bpy)$ was refluxed with 1.2 equivalents of $AgBF_4$ and 5 equivalents of **203** in toluene. After 3 h, the reaction mixture was filtered to remove AgCl, and the filtrate was refluxed for a further 22 h. Purification was achieved by metathesis to the PF_6^- salt, followed by chromatography on an alumina column. Attempts to grow diffraction-quality crystals via slow evaporation of an acetone/methanol solution proved unsuccessful, but **222** has been characterised by elemental analyses, mass spectrometry and IR spectroscopy.

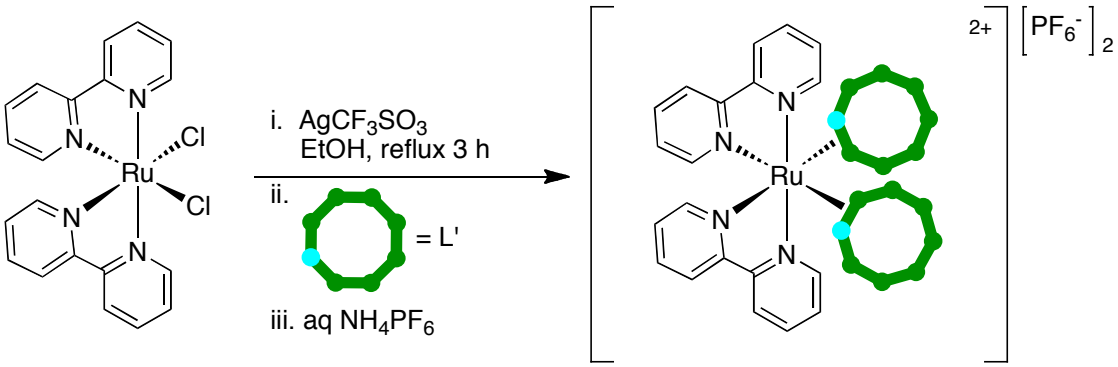

223 when L' = **203**

Scheme 9. Synthesis of **223**.

The reaction of **203** with *cis*-$Ru(bpy)_2Cl_2•2H_2O$ produced **223** in ca. 30% yield, via a two-step method based on a literature procedure,[92] that involves $AgCF_3SO_3$ in ethanol to generate the solvento intermediate *cis*-$[Ru(bpy)_2(EtOH)_2][CF_3SO_3]_2$ (Scheme 9). Again, no crystals have been grown, but characterisation of **223** has been achieved using mass spectrometry, UV/vis spectroscopy, cyclic voltammetry and elemental analyses.

2.3.1.4 Formation of polymers

A polymer of structure $\{Cu(NO_3)_2(H_2O)([Pr_2NH_2][Cr_7NiF_8(O_2CCMe_3)_{14}(O_2CCPy)_2])_2\}_n$, **224**, was formed by reacting the disubstituted wheel **208** with $Cu(NO_3)_2•2.5H_2O$ (Scheme 10). Diffraction-quality crystals were obtained by slow evaporation of a THF/toluene solution.

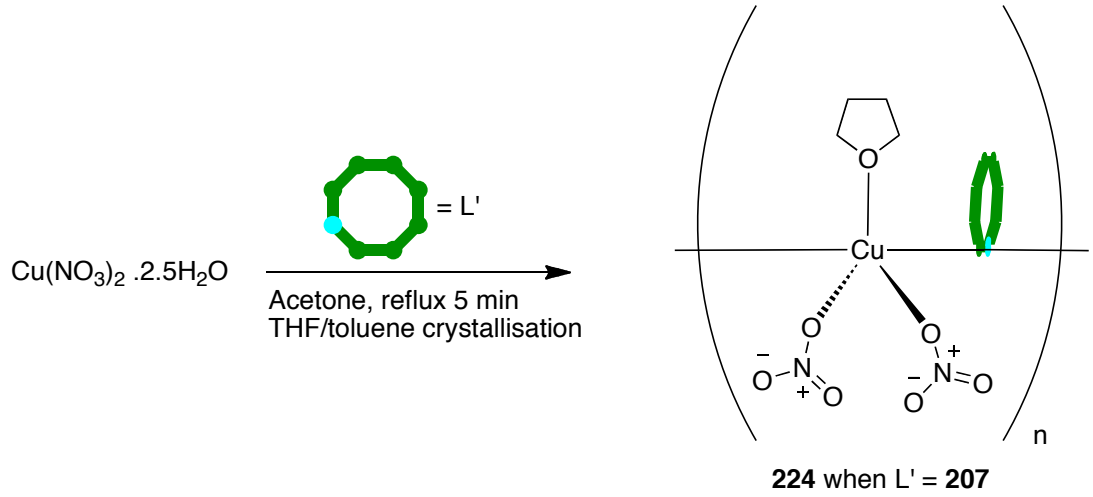

224 when L' = **207**

Scheme 10. Synthesis of **224**.

2.3.2 Mass Spectrometry Studies

Mass spectrometry (MS) is a technique that has proved quite useful in the identification of "wheel" systems, as NMR spectroscopy cannot be used in general due to the fast relaxation of the Cr^{III} nuclei contained in the backbones of the wheels. Previous investigations on single wheels had deduced that the best technique to observe the presence of the wheels is electrospray MS in THF, due to solubility factors. The ISNA-substituted wheel, **203**, shows peaks for the $[MH]^+$ and $[MNa]^+$ ions in the positive electrospray spectrum. In the negative electrospray spectrum a peak is observed for the $[M - Pr_2NH_2]^-$ (wheel without template) ion. Each of the novel monosubstituted and disubstituted wheels, **204**–**210**, has been characterised by MS, all showing the anticipated peaks.

The unusually high molecular weights are an issue when analysing linked-wheel systems. Each wheel has a molecular weight of approximately 2300 Da and the electrospray MS machine used at The University of Manchester can only measure $^m/_z$ to a maximum value of 3000, so the $[M]^+$ peaks cannot be observed for linked-wheel systems. However, analysis of **223** showed that MS is still a viable technique because a peak can seen quite clearly at $^m/_z = 2523$, which is associated with the $[M - 2PF_6]^{2+}$ dication. Simulation of this peak pattern (Figure 40) shows agreement with the observed spectrum.

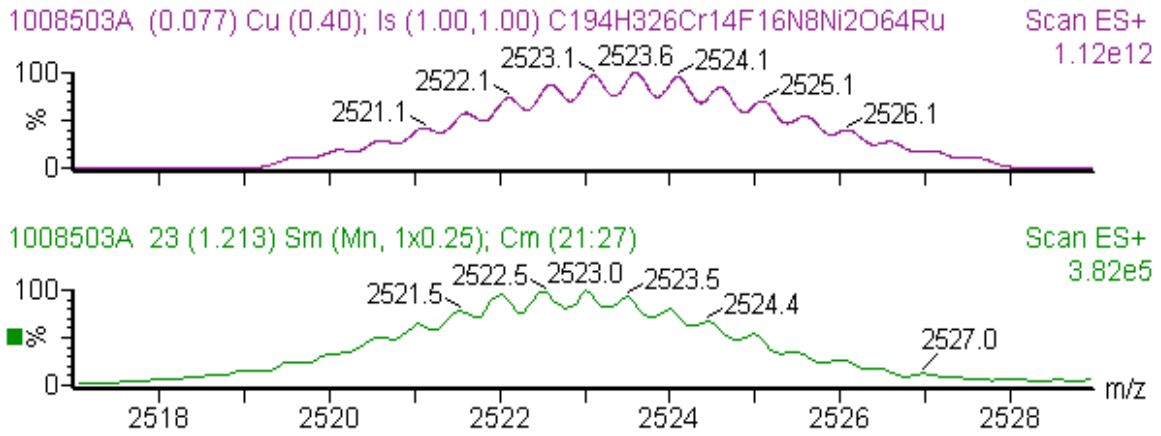

Figure 40. Electrospray MS of the $^{2+}$ ion of **223** (top = predicted, bottom = observed).

Later on in the project a collaboration was commenced with Dr Lindsay Harding of the University of Huddersfield who offered to study some of the linked-wheel systems using an ESI-TOF machine, which has a wider mass range. Two linked green wheel systems were analysed successfully, **220** and **223**. The spectrum of **220** shows a peak for $[MH]^+$ at $^m/_z$ = 4939, and a peak is seen at $^m/_z$ = 5193 in the spectrum of **223** corresponding to $[M - PF_6]^+$. The mass peak of the three-wheel system, **219**, however is not observed as its molecular weight of 7818 Da appears to be too high for even this technique.

2.3.3 Infrared Spectroscopy

Infrared spectra have been recorded for the three Re-based compounds, **220**, **221** and **222**. The spectra of **220** and **221** are virtually identical, which is as expected as the only difference between these two compounds is the divalent metal contained in the wheels. Three ν(CO) bands can be seen between 2030 and 1885 cm^{-1}, as expected for *fac*-$Re(CO)_3$ complex fragments.[93] As can be seen in Table 3, these bands occur at energies similar to those reported for the model complex *fac*-$ReCl(CO)_3(py)_2$, indicating that the presence of the wheels does not have a significant electronic effect on the Re centre. In a similar fashion, the bands associated with the wheel ligands are not shifted upon coordination to the Re centre, as shown by direct comparison of the spectra for **203** and **220** (Figure 41).

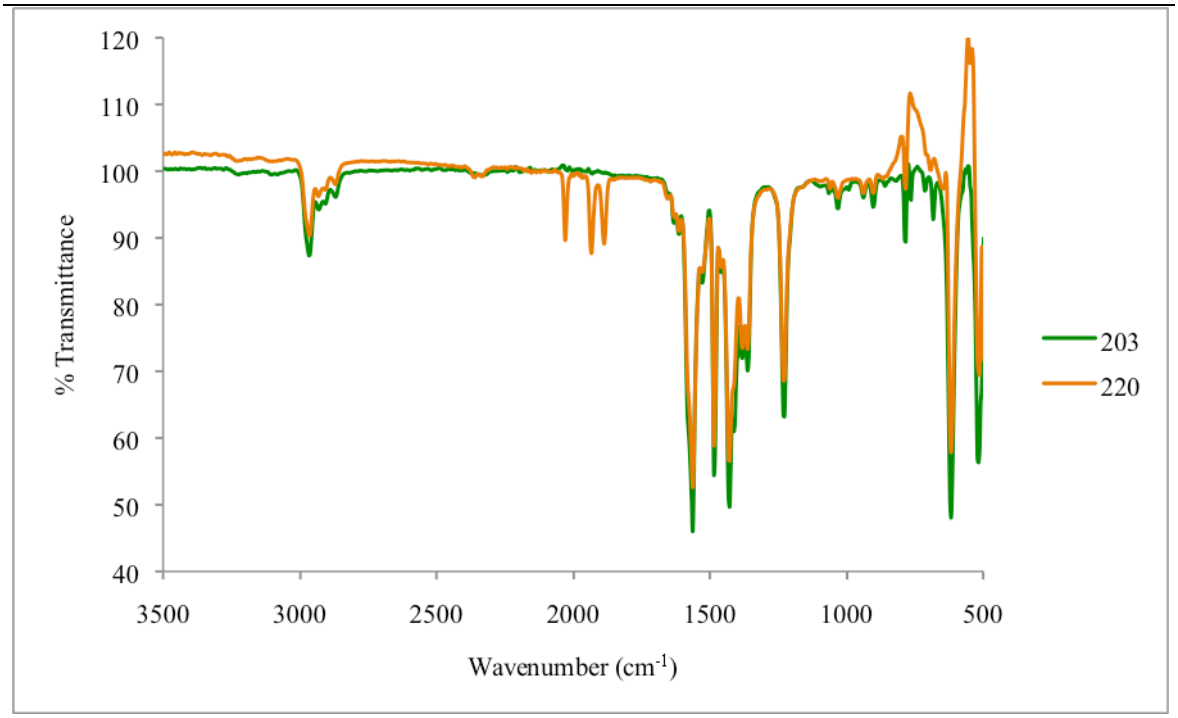

Figure 41. IR Spectra of of **203** and **220**.

Table 3. IR data for novel and reference Re complexes in the CO stretching region.

Compound	**Bands, cm^{-1}**		
fac-ReCl(CO)$_3$(py)$_2$[93]	2025	1920	1885
220	2029	1931	1890
221	2021	1930	1887
222	2037	1926 (br)	
fac- [Re(py)(CO)$_3$(bpy)]$^{+}$[94]	2026	1906 (br)	

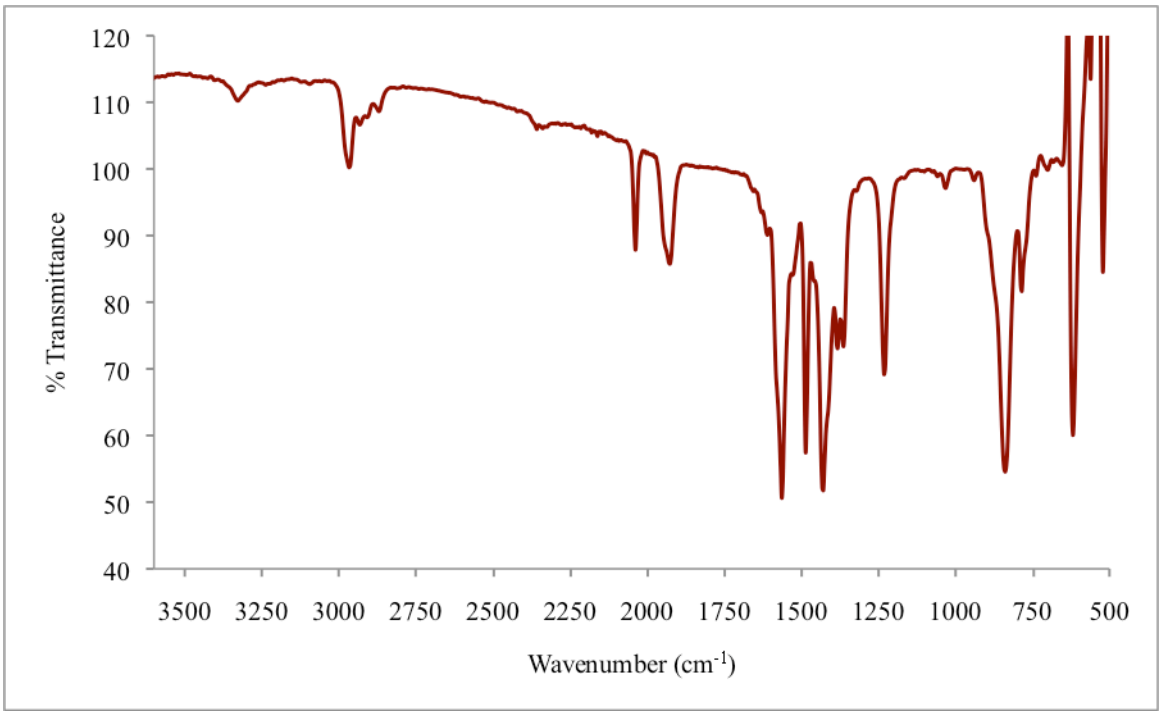

Figure 42. IR Spectrum of **222**.

The IR spectrum of **222** (Figure 42) shows only two ν(CO) bands. The two lower energy bands, instead of being well defined, are merged into one broad band which is a common observation for complexes containing $[ReL(CO)_3(bpy)]^+$ fragments.[95]

2.3.5 UV/Visible Spectroscopy

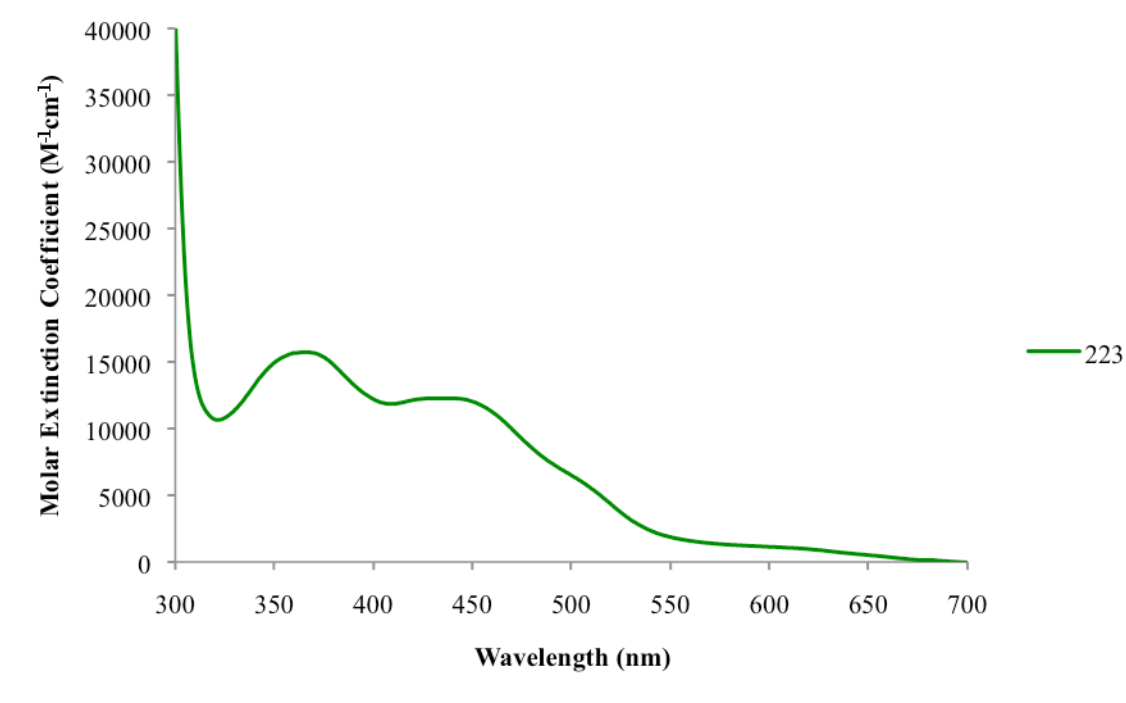

Figure 43. UV/vis spectrum of **223** in acetonitrile.

The UV/vis spectrum of **223** can be seen in Figure 43. As expected, two d→π* MLCT bands are observed, which are not dissimilar from the literature data obtained for *cis*-$[Ru(bpy)_2(py)_2][PF_6]_2$, helping to confirm that the expected product has been formed.[96] A shoulder is observed at approximately 500 nm, which could be attributable to d→π* interactions between the Ru centre and the wheel ligand.

2.3.6 Electrochemistry

A cyclic voltammogram of **223** was run in a 0.1 M $[NBu^n_4][PF_6]$ solution in acetonitrile, and a representative trace is shown in Figure 44. The trace is very weak due to the high molecular mass of the product as well as its poor solubility in acetonitrile. What appears to be a reversible $Ru^{III/II}$ oxidation can be seen at 1.43 V vs. Ag-AgCl (ΔE_p = 55 mV), a potential 0.13 V higher than that observed for *cis*-$[Ru(bpy)_2(py)_2][PF_6]_2$,[97] implying a

greater stability of the Ru^{II} oxidation state. Three irreversible waves can also be seen at -1.27 V, –1.35 V and –1.60 V vs. Ag-AgCl related to ligand reductions.

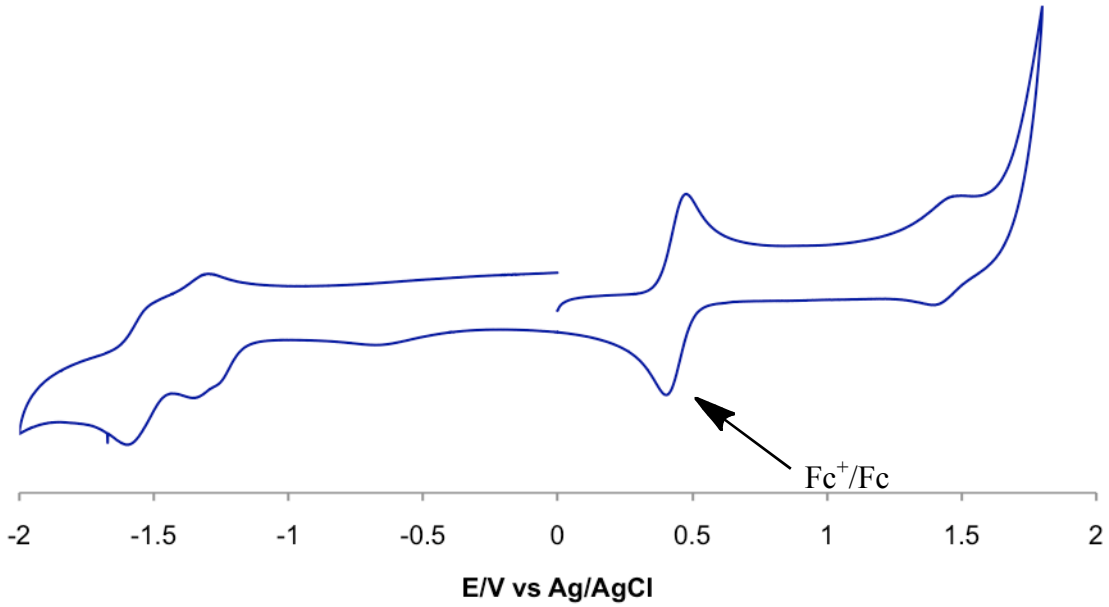

Figure 44. Cyclic voltammogram of **223** in acetonitrile at a scan rate of 200 mV s^{-1}.

2.3.7 EPR Studies

The EPR spectra of the copper dimer linked-wheel systems **211** and **213** have been recorded. In a fashion similar to the previously published ISNA system,[65] these spectra show no changes when compared with that of the unlinked wheel (Figure 45), with a simple $S = ½$ signal. It appears that the strongly antiferromagnetically coupled copper dimer moiety prevents coupling between the wheels. The Re linked-wheel system **221** shows an essentially identical spectrum.

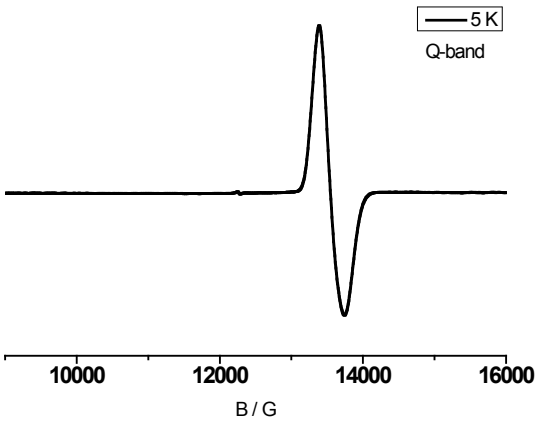

Figure 45. Q-band EPR spectrum of an individual wheel at 5 K.

However, the EPR spectrum of **215** differs significantly from that of the individual wheel. The spectrum of **215** together with that of the previously published compound **214** can be seen in Figure 46. While the parameters have not yet been established for **215** it is anticipated that the interaction between the wheels will be weaker than for **214**.

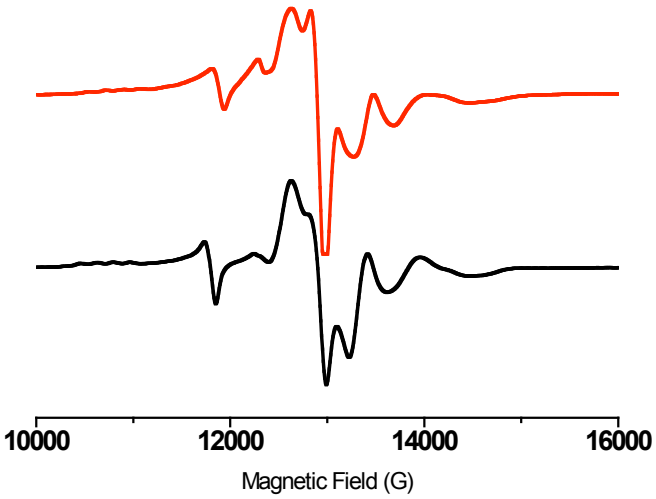

Figure 46. Q-band EPR spectra of **214** (red) and **215** (black).

The EPR spectrum of the copper linked polymeric chain of wheels was also run, giving a broad spectrum. The spectrum is too broad to be modelled, but differs from the unlinked wheels hence interaction of some sort is occurring.

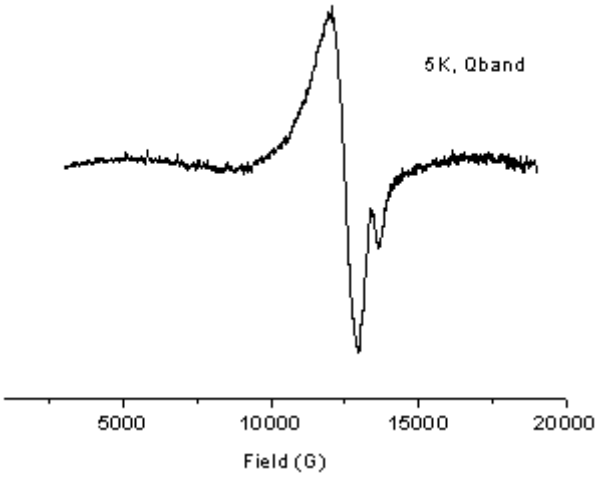

Figure 47. Q-band EPR spectrum of **224**.

2.3.9 X-Ray Crystallography

Due to the magnetic nature and large size of these linked-wheel systems, it is very difficult to confirm their structures without using X-ray crystallography. Many of these systems have therefore been characterised by this method.

Crystal structures of **206**, **207** and **210** have been determined. However, these structures have not been fully solved due to pronounced disorder of the divalent metal and hence the substituted carboxylate. Also, the mass spectra for these compounds confirm the formation of the desired structures, showing an instantaneously recognisable pattern, so having only low-quality X-ray structures is sufficient for our purposes.

For all of the compounds discussed in this chapter, the structures of the wheels are consistent, and agree with previously published structures. The Cr–F bond lengths average between 1.90 and 1.92 Å and the Cr–O bond lengths are between 1.94 and 1.99 Å. The Ni–F bond lengths are slightly longer, between 2.00 and 2.02 Å with the Ni–O bond lengths averaging at 1.99–2.01 Å. In all cases the $[Pr_2NH_2]^+$ template can be seen in the central cavity of all the wheels, held in place by N–H---F bonds. The only differences observed are the carboxylates that are substituted into the wheels.

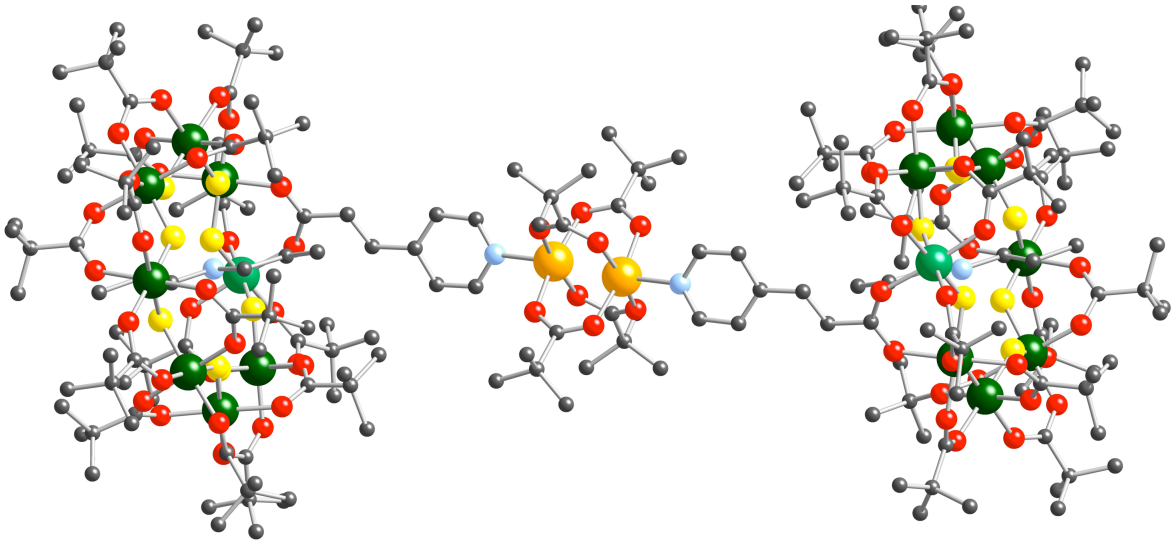

Figure 48. A representation of the molecular structure of **211**.

Structures have been obtained for **211** (Figure 48) and **213** (Figure 49), from crystals formed directly from their reaction mixtures in toluene. Both form monoclinic systems, with **211** adopting a space group C_12/C_1 and **213** P_12_1/C_1. Both structures show identical

central regions with a Cu paddlewheel dimer linking the wheels together. The only significant difference between the two central portions is the Cu–N bond distances, with that in **211** being ca. 0.03–0.04 Å shorter than that in **213**. This observation might explain the poor yield obtained for **213**, with a weaker bond being formed between the pyridazine ring and Cu centre. The disordered nature of the six-membered rings precludes any meaningful comparisons of their geometric parameters. The Cu–N bond in **213** (2.183(5) Å) is also significantly longer than that in a monodentate pyridazine Cu complex found in the literature[90] (1.984(2) Å), suggesting that the attached wheel may weaken the effectiveness of **209** as a ligand.

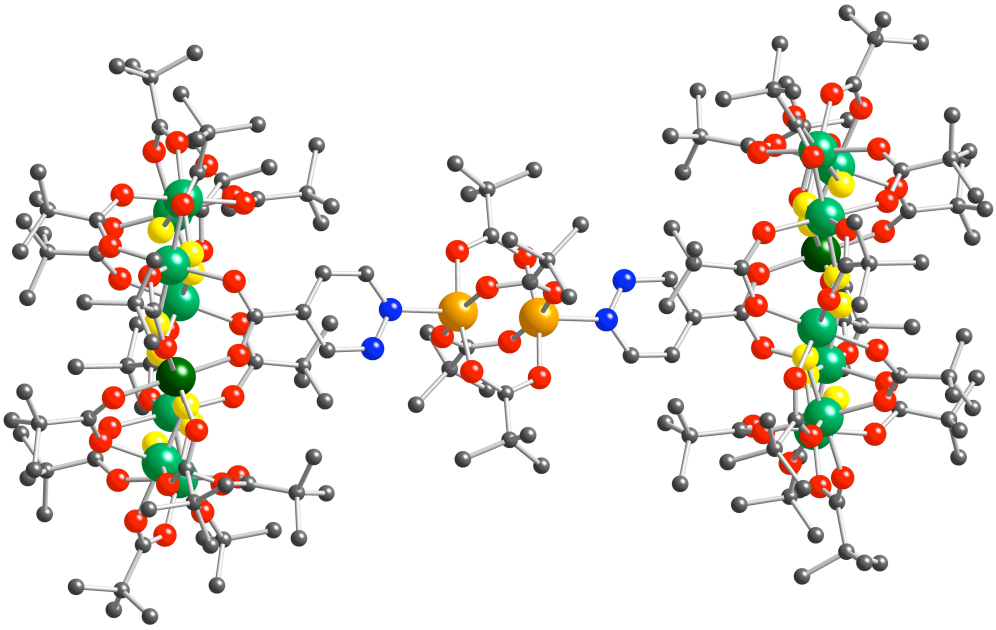

Figure 49. A representation of the molecular structure of **213**.

Measurable crystals of **215** were grown upon formation of the product in an acetone solution. The crystals were twinned, and thus a poor final R_1-factor of 0.1789 was obtained. A picture of the structure can be seen in Figure 50. The crystals are triclinic in the $P\bar{1}$ space group. The wheels are linked in a virtually trans arrangement, with an N–Cu–N angle of 172.0(3)º, through a five-coordinate Cu centre. Also coordinated are two monodentate nitrate ligands and an acetone solvent molecule, which demonstrates Jahn-Teller distortion with a Cu–O bond distance of 2.431(6) Å as opposed to the shorter nitrate Cu–O bonds which have an average length of 1.975 Å. The two nitrate groups are apparently coordinated in a monodentate fashion, due to a significant difference in the Cu–O distances (0.65 Å and 0.77 Å). However, 0.77 Å is still shorter than the combined values of the Van der Waals radii of the Cu and O atoms, so it is plausible that at least one

of the nitrate ligands could be bidentate. The arrangements of the other Cu-ligand bonds, which are all close to 90º, support the idea of an octahedral structure.

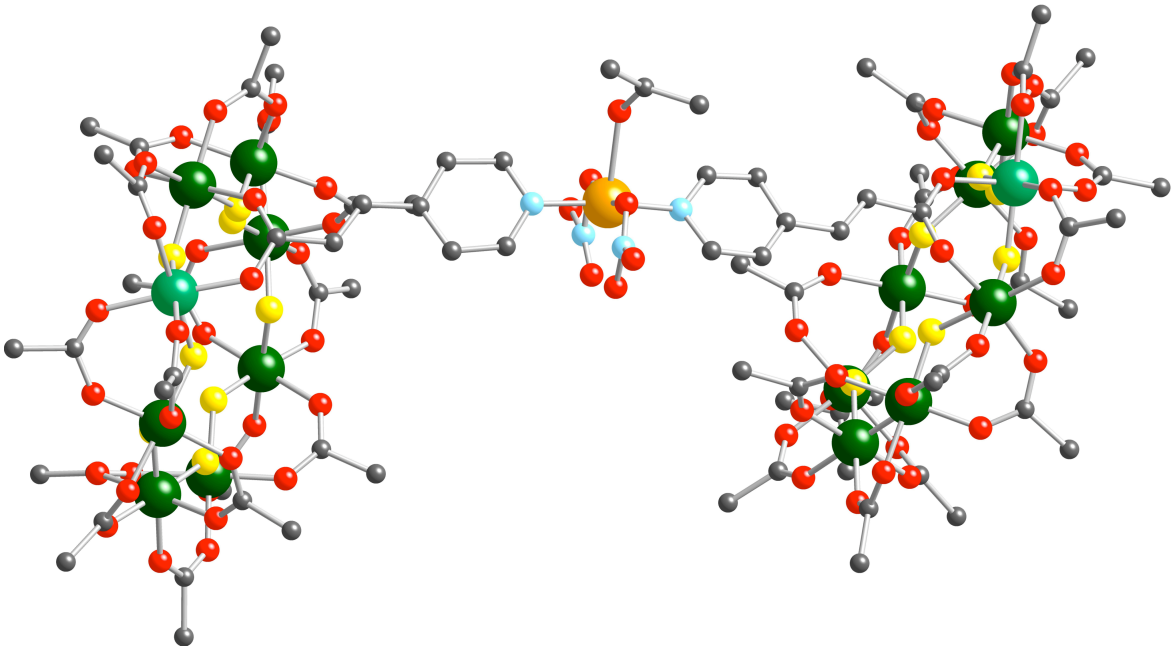

Figure 50. A representation of the molecular structure of **215**.

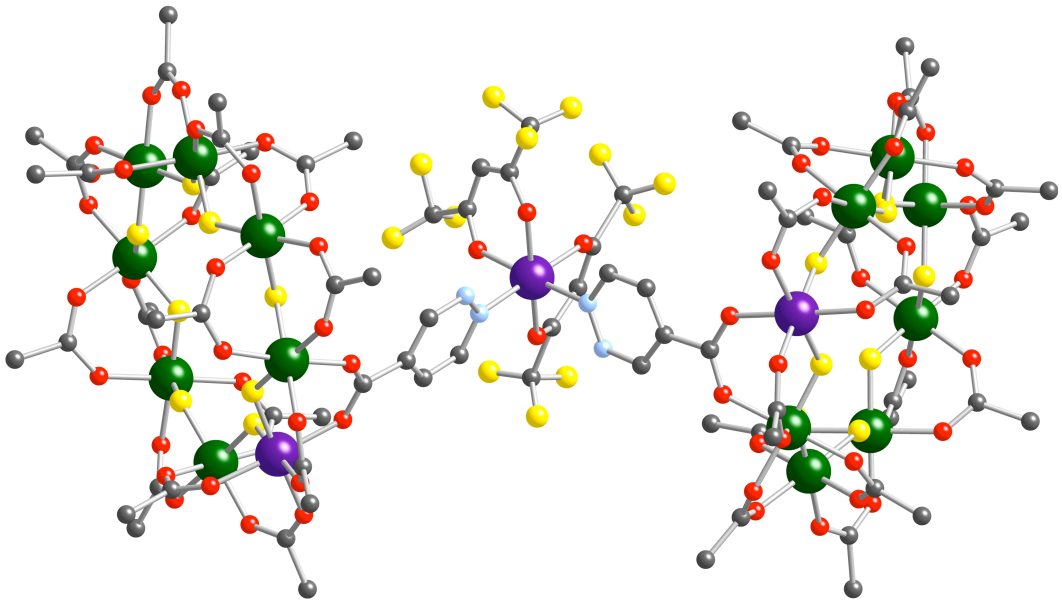

Figure 51. A representation of the molecular structure of **217**.

In a similar fashion to the crystal structures mentioned thus far, crystals of **217** were obtained directly from the reaction to produce this compound in acetone. This structure is orthorhombic in the *Pccn* space group, and has the wheels coordinated in a *cis* geometry (Figure 51), with an N–Cu–N angle of 89.9(4)º. In contrast, the ISNA analogue shows a

trans disposition of the wheels.[98] As in the structure of **213**, the ortho nitrogens in **217** are disordered over two sites.

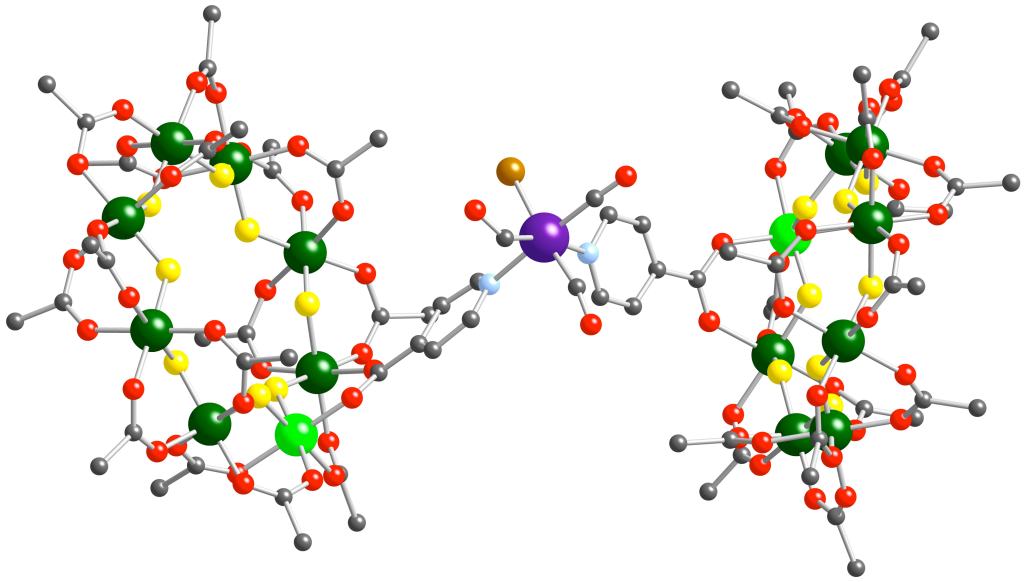

Figure 52. A representation of the molecular structure of **220**.

Crystals of **220** were grown by evaporation of an *n*-pentane/acetone solution. The crystals are monoclinic in a $P2_1/c$ space group and the molecular structure can be seen in Figure 52. Unfortunately, due to disorder about the Re centre the R_1 factor is very high at 14%. However, it is clear that the desired compound has been formed. The Re atom is disordered over two sites, with N–Re–N angles of 86–88º.

The crystal structure of **219** adopts the triclinic $P\bar{1}$ space group. This complex (Figure 53) contains three wheels coordinated through 4pyac to the central triangular metal cluster. The central oxygen is positioned almost symmetrically, with the Ni–O bond being only slightly longer (~0.02 Å) than the Fe–O bonds. The three metal centres in the triangle have very slightly distorted octahedral geometries, with bond angles in the range 82–97º.

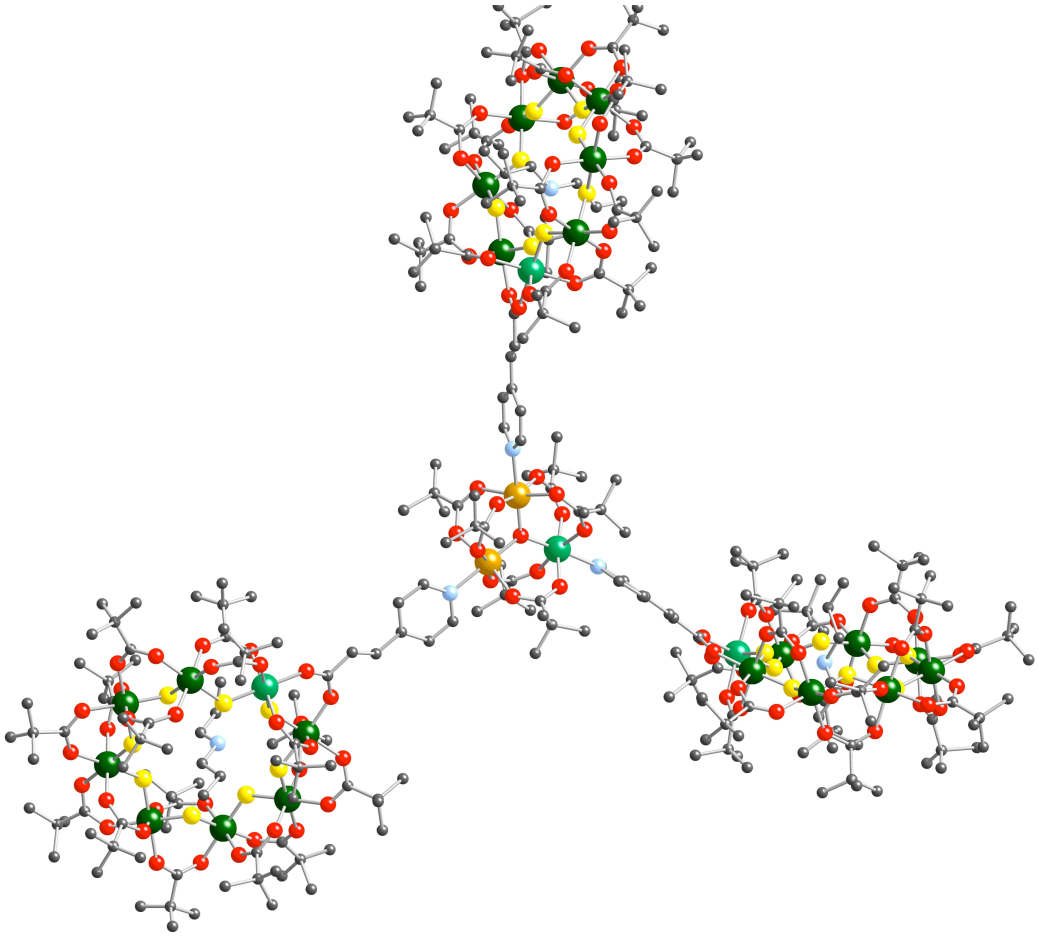

Figure 53. A representation of the molecular structure of **219**.

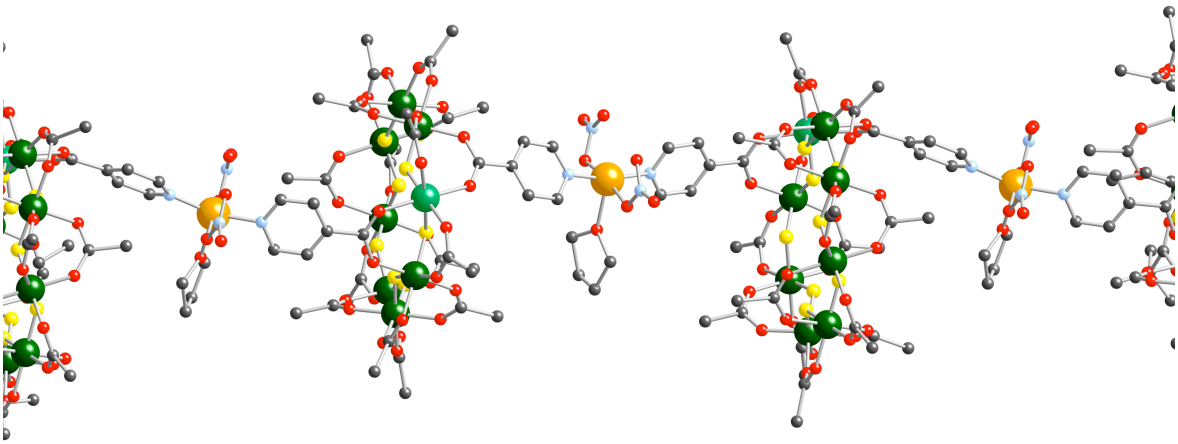

Figure 54. A representation of the molecular structure of **224**.

The final structure to be considered is that of **224**, crystals of which were grown by evaporation of a THF/toluene solution at room temperature. **224** adopts the monoclinic space group $P2_1/n$, and the polymeric complex (Figure 54) contains coordinated THF derived from the substitution of water during crystallisation. As with the monomeric

structure, **215**, the Cu–O bond to this solvent molecule (2.249 (12) Å) is between 0.23 and 0.41 Å longer than the other Cu–O bonds. The structure of the disubstituted wheel is clearly resolved and as observed previously,[98] with both ISNA groups coordinated to the divalent metal centre and an adjacent Cr^{III} ion.

2.4 CONCLUSIONS

The series of mono- and disubstituted wheels has been extended with varying degrees of success. These novel wheels have been reacted with a variety of 1st row transition metal complexes, in order to assess their suitability as ligands. **204** appears to behave well in complexation reactions, but **206** has not been coordinated to single Cu metal centres. However, crystal structures have been obtained for the **206**-containing complexes **213** and **217**, proving that it can act as a ligand in certain situations. EPR studies have been carried out on the **204**-containing system **215**, and comparison with the **203**-containing **214** demonstrates that the interaction between the wheels weakens as the link extends on moving from ISNA to 4-pyridylacrylate.

Some further work has been undertaken with **203** as a ligand for 2nd and 3rd row Re and Ru complexes expected to form MLCT/redox-active complexes. An X-ray crystal structure has been obtained for **220**, confirming the coordination to the Re centre. While no crystal structure has of yet been obtained for **223**, the data available indicate that the desired product has been formed and that it shows MLCT absorption bands and a fully reversible $Ru^{2+/3+}$ oxidation, suggesting that switchability may be possible with this system.

Reaction of a bis-ISNA-substituted wheel with $Cu(NO_3)_2 \bullet 2.5H_2O$ produces a polymeric structure, which has been fully characterised. The EPR spectrum shows some evidence of interaction occurring between the wheels, but the spectrum is too broad to be able to model any parameters.

2.6 FURTHER WORK

While a crystal structure has been solved for **220**, a better structure will be required for publication purposes. The use of different solvent systems could be attempted in order to grow crystals of higher quality, or the existing crystals could be sent to a synchrotron in order to get better data. Obtaining a crystal structure of **223**, which is a good candidate for switching studies, is an important objective in order to fully characterise this product. This complex is extremely soluble as its PF_6^- salt, and consequently anion metathesis may be the best option to allow effective crystallisation. Metathesis to a bulkier anion such as

BPh_4^- may improve the potential for packing in a lattice, as the complex itself is relatively large. Once a hypothetically switchable system containing two wheels has been fully characterised, then physical studies to assess the possibilities for potential qubit behaviour will be pursued.

Further substitution reactions into the wheels could be attempted using polypyridyl carboxylic acids, such as those shown in Figure 55. These could produce excellent ligands for coordination to metal centres such as Ru^{II} or Re^{I}, leading to the possibility of having low energy MLCT excitations directed at the wheels themselves.

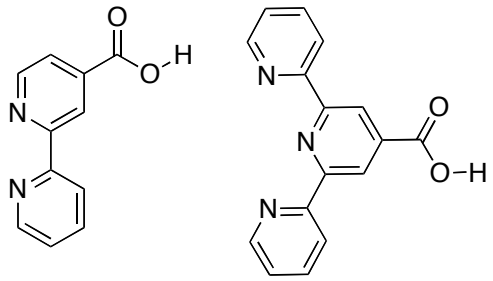

Figure 55. Examples of polypyridyl carboxylic acids, potentially suitable for substitution into the wheels.

While initial studies have involved attaching **203** to Re cores, using as precursors $ReCl(CO)_5$ and *fac*-$[ReCl(CO)_3(bipy)]PF_6$, other Re complexes may be considered in order to access systems that show low energy MLCT bands and also contain multiple wheels. One such complex precursor is $\{$*fac*-$ReCl(CO)_3\}_2$(bpym), which should be amenable to chloride substitutions. If this approach were to prove successful, then the same chemistry should be extendable to include larger polynuclear Re systems, such as triangles and squares.[99]

Chapter 3 – Linked Purple Wheel Systems

3.1 INTRODUCTION

Purple wheels were first synthesised when experimenting with altering the templating amine molecule to observe what effect it would have on the size and shape of the resultant complex. Purple wheels differ from their green counterparts, in that the "template" used to form the wheel, in this case a sugared amine, *N*-ethyl-D-glucamine, coordinates directly into the wheel, replacing five of the eight fluorides. The purple derivatives also contain one less carboxylate ligand, allowing the template to coordinate twice to the chromium adjacent to the divalent metal, leaving a spare site at the divalent metal. In the uncoordinated purple wheel a solvent molecule can be found at this site, but this can be replaced easily by a good coordinating group such as a pyridine.

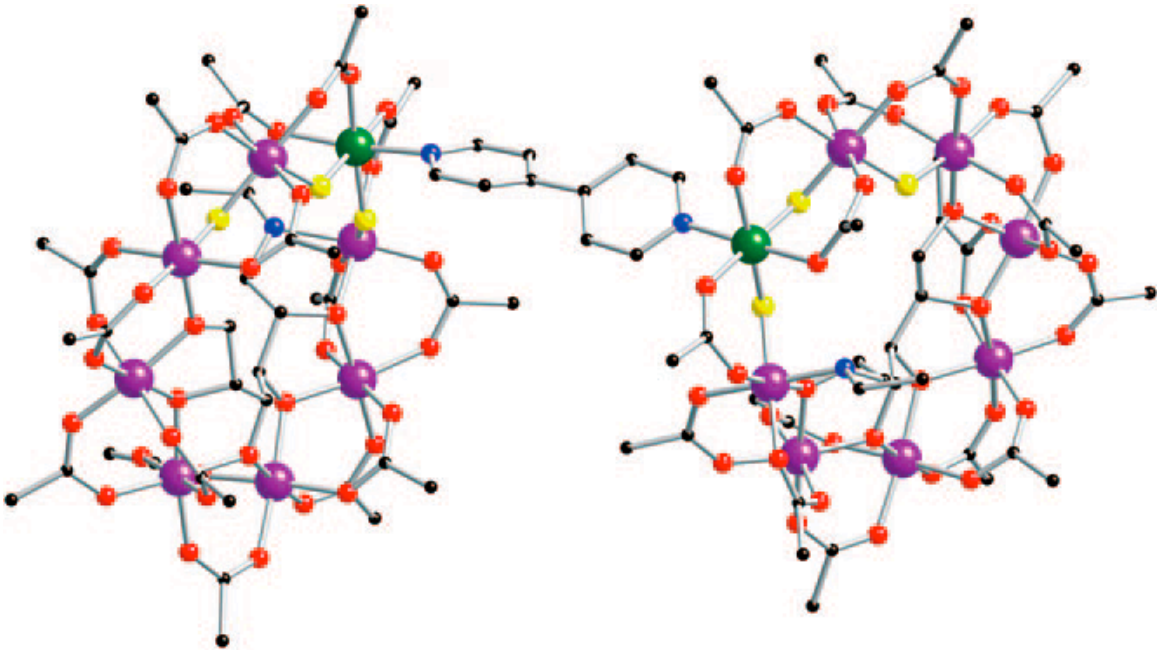

Figure 56. Purple wheels linked through 4,4´-bpy.[60]

A reaction was attempted using 4,4´-bpy as the coordinating ligand, forming a linked-wheel system (Figure 56).[60] Other reactions using the slightly longer linker bpe and molecules with more than two pendant pyridyl groups also proved successful. Applying this principle opens the door to systems linked by not only other organic molecules but also transition metal complexes that contain ligands with terminal pyridyl groups such as quaterpyridine (qpy) and its derivatives. By using such complexes it may be possible to

construct switchable systems. Rhenium(I) and ruthenium(II) complexes often display long-lived MLCT excited states and ruthenium(II) and iron(II) complexes undergo reversible oxidations.

Various organics and metal complexes (Figure 57) have been identified as suitable potential target linker molecules; some of these are already known in the literature, while others are novel. The work covered in this chapter includes the further development of novel linked-wheel systems with organic bridges, as well as studies towards the creation of a series of transition metal polypyridyl linked-wheel complexes.

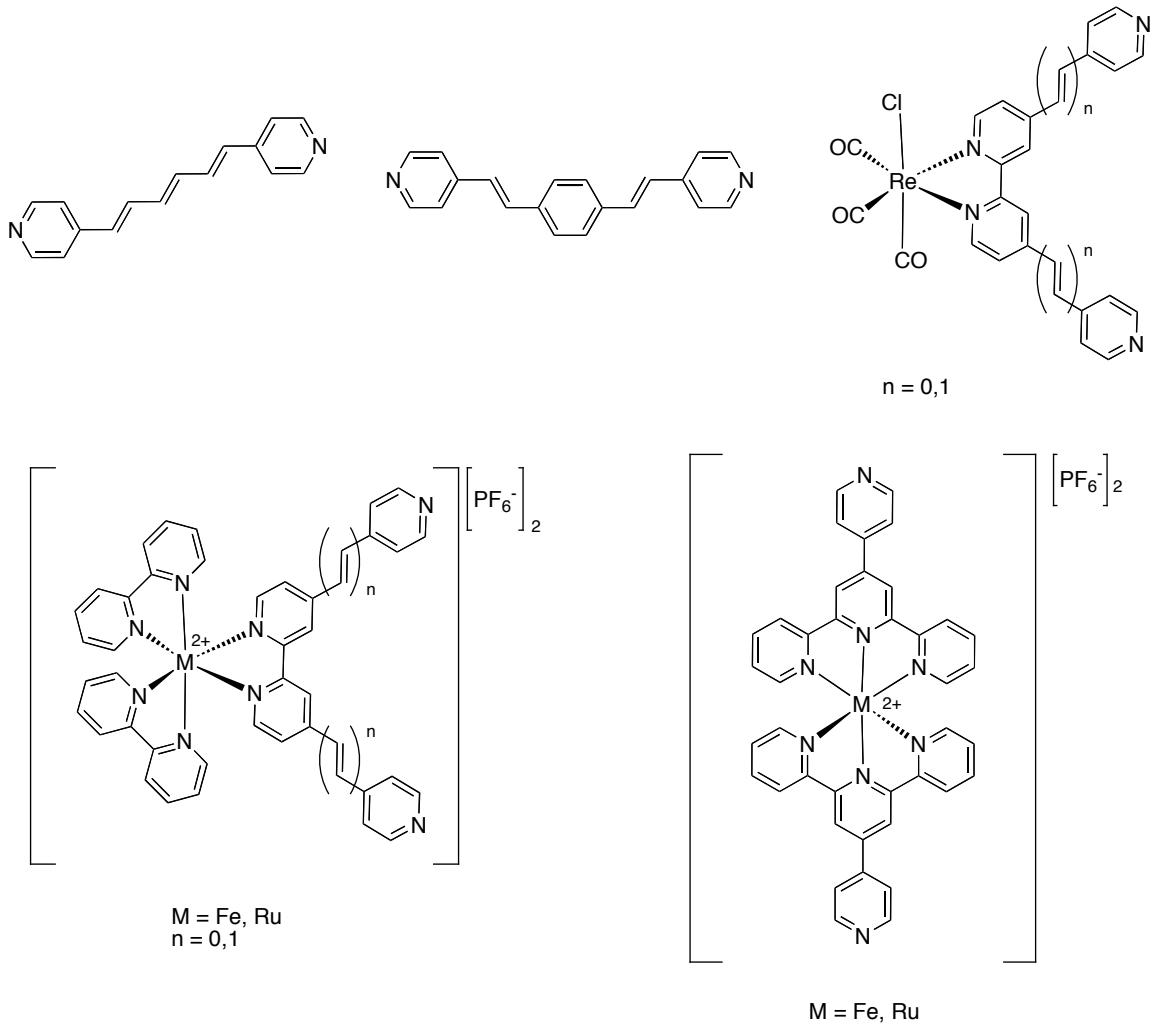

Figure 57. Target compounds for linking purple wheels together.

3.2 EXPERIMENTAL PROCEDURES

3.2.1 Materials and Procedures

The compounds (*E*,*E*,*E*)-1,6-bis(4-pyridyl)-1,3,5-hexatriene (bph),[100] 1,4-bis[*E*-2-(4-pyridyl)ethenyl]benzene (bpvb),[101] 2,2′:4,4′′:4′,4′′′-quaterpyridyl (qpy),[102,103] 4,4′-bis-[(*E*)-2-(4-pyridyl)vinyl]-2,2′-bipyridyl (bbpe),[104] 4′-(4′′′-pyridyl)-2,2′:6′2′′-terpyridine (pytpy),[105] $[Fe(pytpy)_2][BF_4]_2$,[105] $[Ru(pytpy)_2][PF_6]_2$,[106] *cis*-$[Ru(bipy)_2(qpy)][PF_6]_2$,[107] *fac*-$ReCl(CO)_3(qpy)$[108] and $[Cr_7NiF_3(O_2CCMe_3)_{15}(EtGlu)(H_2O)]$[60] were synthesised by literature methods. All other starting materials were purchased commercially and used as supplied.

3.2.2 Physical Measurements

All ^1H NMR spectra were recorded on Bruker Ultrashield 500 MHz or 300 MHz spectrometers. IR data were recorded using a Varian Bio-Rad Excalibur series IR instrument and UV data were recorded on a Shimadzu UV-2401 PC UV-VIS spectrophotometer. Elemental analyses were performed by the Microanalytical Laboratory, University of Manchester. Mass spectra were obtained using electrospray analysis on a Micromass Platform spectrometer at The University of Manchester. Linked-wheel systems were sent to Dr Lindsay Harding at the University of Huddersfield for analysis, and spectra were run using a Bruker MicroTOF-Q mass spectrometer with an electrospray ionisation source. EPR studies were performed by Dr Floriana Tuna and John Machin at The University of Manchester. Q-Band EPR was run on an Elexsys E500 spectrometer equipped with a Bruker 2 tesla magnet. Variable temperature studies were achieved using an Oxford VT liquid helium cryostat between 5 K and 30 K.

3.2.3 Syntheses

[(bph){[$Cr_7NiF_3(O_2CCMe_3)_{15}$(EtGlu)]}$_2$] 301

A solution of bph (27.3 mg, 0.117 mmol) in dichloromethane (10 ml) was added to a solution of [$Cr_7NiF_3(O_2CCMe_3)_{15}$(EtGlu)($H_2O$)] (513 mg, 0.231 mmol) in dichloromethane (10 ml) and the reaction stirred at room temperature for 15 h. The solvent was removed under vacuum and the dry product was washed with acetone to remove any excess starting material, producing a purple solid. The product was then recrystallised by evaporation at room temperature of a dichloromethane/acetone solution. Yield: 318 mg (58%). Elemental analysis calcd. (%) for $C_{182}H_{312}Cr_{14}F_6N_4Ni_2O_{70}$•$CH_2Cl_2$: C 46.56, H 6.70, N 1.19, Cr 15.42, Ni 2.49. Found: C 46.70, H 6.84, N 1.06, Cr 15.11, Ni 2.09.

[(bpvb){[$Cr_7NiF_3(O_2CCMe_3)_{15}$(EtGlu)]}$_2$] 302

This compound was prepared and purified in a manner similar to **301** by using bpvb in place of bph (34.4 mg, 0.121 mmol) and [$Cr_7NiF_3(O_2CCMe_3)_{15}$(EtGlu)($H_2O$)] (509 mg, 0.230 mmol) in dichloromethane (20 ml), forming a purple solid. Diffraction-quality crystals were obtained by evaporation of a tetrahydrofuran/acetonitrile solution. Yield: 208 mg (38%). +ve electrospray: 4687 $[MH]^+$, 2485 [{M –[$Cr_7NiF_3(O_2C$-$CMe_3)_{15}$(EtGlu)]}H]$^+$. Elemental analysis calcd. (%) for $C_{186}H_{314}Cr_{14}F_6N_4Ni_2O_{70}$ •CH_2Cl_2: C 47.08, H 6.68, N 1.17, Cr 15.26, Ni 2.46. Found: C 47.15, H 6.71, N 1.15, Cr 15.26, Ni 2.56.

[{[$Cr_7NiF_3(O_2CCMe_3)_{15}$(EtGlu)]}(qpy){[$Cr_7NiF_3(O_2CCMe_3)_{15}$(EtGlu)]}$_2$ 303

To a solution of [$Cr_7NiF_3(O_2CCMe_3)_{15}$(EtGlu)($H_2O$)] (610 mg, 0.274 mmol) in dichloromethane (15 ml) was added a solution of qpy (42.0 mg, 0.134 mmol) in dichloromethane (5 ml) and the reaction was stirred at room temperature for 30 mins. The solution was then heated to reflux for a further 10 mins. The solution was concentrated under vacuum until only approximately 5 ml remained, then acetone (25 ml)

was added and the resultant solution was refluxed for 1 h. A purple precipitate was formed during this time and upon cooling of the solution it was collected by filtration, washed with acetone and dried in the air. Yield: 336 mg (53%). Elemental analysis calcd. (%) for $C_{269}H_{459}Cr_{21}F_9N_7Ni_3O_{105}$: C 46.75, H 6.69, N 1.42, Cr 15.80, Ni 2.55. Found: C 47.09, H 6.55, N 1.67, Cr 15.46, Ni 2.55.

[{[$Cr_7NiF_4(O_2CCMe_3)_{14}$(EtGlu)]}(bbpe){[$Cr_7NiF_3(O_2CCMe_3)_{15}$(EtGlu)]}$_2$ 304

To a solution of [$Cr_7NiF_3(O_2CCMe_3)_{15}$(EtGlu)($H_2O$)] (503 mg, 0.226 mmol) in dichloromethane (10 ml) was added bbpe (29.0 mg, 0.080 mmol) in dichloromethane, and the reaction stirred at room temperature for 15 h. The solvent was removed under vacuum and an acetone/acetonitrile recrystallisation gave a purple solid. Yield: 58 mg (10%). Elemental analysis calcd. (%) for $C_{273}H_{463}Cr_{21}F_9N_7Ni_3O_{105}$: C 47.09, H 6.70, N 1.41, Cr 15.68, Ni 2.53. Found: C 46.94, H 6.80, N 1.40, Cr 15.37, Ni 2.51.

***fac*-ReCl(CO)$_3$(bbpe) (attempted) 306**

A solution of $ReCl(CO)_5$ (100 mg, 0.276 mmol) and bbpe (105 mg, 0.290 mmol) in a 3:1 mixture of THF and toluene (20 ml) was refluxed for 8 h. The solution was allowed to cool, then filtered and the insoluble orange solid washed with toluene. Yield: 152 mg (69%). ν(cm^{-1}): 2015 s (C=O), 1841 br (C=O). Elemental analysis calcd. (%) for $C_{27}H_{18}ClN_4O_3Re\cdot{}^1/_3ReCl(CO)_5$: C 43.66, H 2.30, N 7.10, Re 31.48. Found: C 43.93, H 2.43, N 6.93, Re 28.56.

***cis*-[Ru(2,2′-bpy)$_2$(bbpe)][PF_6]$_2$ 308**

A solution of *cis*-$RuCl_2$(2,2′-bpy)$_2$•$2H_2O$ (101 mg, 0.194 mmol) and bbpe (70.5 mg, 0.195 mmol) in ethylene glycol (20 ml) was heated at reflux under argon for 1 h. The bright orange-red solution was cooled to room temperature and filtered. Aqueous NH_4PF_6 was added to the filtrate yielding a red precipitate, which was collected by filtration and washed with water. The crude product was purified on a silica gel column eluting with 0.3 M NH_4PF_6 in 1:1 acetone/acetonitrile, affording the product as the 3rd fraction off the column. Purification of this fraction was achieved by evaporating to

dryness then redissolving in a minimal amount of acetonitrile and adding aqueous NH_4PF_6. The precipitate was filtered off, washed with water and dried. A final reprecipitation from acetone/diethyl ether, collection by filtration, washing with diethyl ether and air drying gave a dark red solid. Yield: 94 mg (35%). ^{1}H NMR (CD_3CN) δ_H/ppm: 7.45 (4 H, t, *J* = 5.6 Hz, bpy), 7.60 (4 H, d, *J* = 7.3 Hz, bpy), 7.76 (2 H, d, *J* = 5.5 Hz, bpy) 7.78–7.84 (8 H, bpy, CH=CH), 7.99 (4 H, d, *J* = 6.6 Hz, bpy), 8.11 (4 H, t, *J* = 7.8 Hz, bpy), 8.55 (4 H, d, *J* = 8.3 Hz, bpy), 8.70 (4 H, d, *J* = 6.6 Hz, bpy), 8.84 (2 H, s, bpy). +ve electrospray: *m/z* = 920 $[(M - PF_6)]^+$, 388 $[(M - 2PF_6)]^{2+}$. λ_{max}/nm (ε/M^{-1} cm^{-1}): 472 (24,500), 376 (18,800), 289 (105,300), 257 (45,600). Elemental analysis calcd. (%) for $C_{44}H_{34}F_{12}N_8P_2Ru \bullet 2HPF_6$: C 38.92, H 2.67, N 8.25, P 9.13. Found: C 39.95, H 2.61, N 8.34, P 8.02.

***cis*-[Fe(2,2′-bpy)$_2$(bbpe)][PF$_6$]$_2$ 311**

A portion of bbpe (69.0 mg, 0.190 mmol) was heated in acetone (50 ml) until fully dissolved. To this solution was added 2,2′-bpy (60.0 mg, 0.384 mmol) in acetone (5 ml) and the solution heated to reflux. A solution of $[Fe(H_2O)_6][BF_4]_2$ (66.0 mg, 0.196 mmol) in acetone (5 ml) was added dropwise to the solution causing an instantaneous colour change to blood red. The solution was stirred and heated for a further 5 min then filtered and the solvent was removed under vacuum. Metathesis of the impure product to the PF_6^- salt was achieved by addition of aqueous NH_4PF_6 to a concentrated acetonitrile solution. Purification was achieved on a silica gel column, eluting initially with 0.1 M NH_4PF_6 in 1:1 acetone/acetonitrile to remove $[Fe(2,2'\text{-bpy})_3][PF_6]_2$, then 0.1 M NH_4PF_6 in 4:1 acetone/acetonitrile to isolate the desired product. Yield: 74 mg. ^{1}H NMR ($(CD_3)_2CO$) δ_H/ppm: 7.62 (4 H, t, *J* = 6.2 Hz, bpy), 7.76–7.82 (6 H, bpy), 7.90 (2 H, d, *J* = 5.3 Hz, bpy), 7.94 (4 H, s, HC=CH), 8.00 (4 H, d, *J* = 4.0 Hz, bpy), 8.31 (4 H, t, *J* = 6.9 Hz, bpy), 8.88 (8 H, d, *J* = 6.9 Hz, bpy), 9.13 (2 H, s, bpy). λ_{max}/nm: 536, 410, 336, 300 nm. Elemental analysis calcd. (%) for $C_{44}H_{34}FeF_{12}N_8P_2$: C 51.76, H 3.36, N 10.98, P 6.07. Found: C 35.70, H 2.36, N 7.34, P 5.97.

cis-[Fe(2,2′-bpy)$_2$(qpy)][PF$_6$]$_2$ (attempted) 310

This compound was prepared in a fashion identical to **311** but using 2,2′-bpy (61.2 mg, 0.392 mmol) in acetone (5 ml), qpy (59.8 mg, 0.193 mmol) in acetone (45 ml) and [Fe(H$_2$O)$_6$][BF$_4$]$_2$ (65.0 mg, 0.193 mmol) in acetone (5 ml) forming a blood red solid. Currently this has not been isolated in a pure form.

fac-[ReCl(CO)$_3$(qpy){[Cr$_7$NiF$_3$(O$_2$CCMe$_3$)$_{15}$(EtGlu)]$_2$}] 312

fac-ReCl(CO)$_3$(qpy) (48.2 mg, 0.133 mmol) and [Cr$_7$NiF$_3$(O$_2$CCMe$_3$)$_{15}$(EtGlu)(H$_2$O)] (547 mg, 0.246 mmol) were dissolved in dichloromethane (25 ml) and the reaction stirred at room temperature in the dark for 25 h. The solvent was then removed under vacuum. The residue was dissolved in 2:1 acetone/acetonitrile (30 ml), stirred briefly and allowed to sit partially covered overnight to give a precipitate. Recrystallisation was effected by gentle evaporation of a dichloromethane/acetonitrile solution. Yield: 206 mg (32%). +ve electrospray: 2201 [{Cr$_7$NiF$_3$Piv$_{15}$EtGlu}H]$^+$, 2224 [{Cr$_7$NiF$_3$Piv$_{15}$EtGlu}Na]$^+$, 5020 [MH]$^+$; –ve electrospray: 616 [ReCl(CO)$_3$(qpy)]$^-$, 2199 [{Cr$_7$NiF$_3$Piv$_{15}$EtGlu} – H]$^-$. ν(cm^{-1}): 2026 (C=O), 1933 (C=O), 1910 (C=O). λ_{max}/nm (ε/M^{-1} cm^{-1}): 556 (1,600), 419 (6,600), 308 (25,500). Elemental analysis calcd. (%) for C$_{189}$H$_{312}$ClCr$_{14}$F$_6$N$_6$Ni$_2$O$_{73}$Re •2CH$_2$Cl$_2$: C 44.22, H 6.14, N 1.62, Cr 14.03, Re 3.59. Found: C 43.86, H 6.09, N 1.57, Cr 14.21, Re 3.68.

cis-[Ru(2,2′-bpy)$_2$(qpy){[Cr$_7$NiF$_3$(O$_2$CCMe$_3$)$_{15}$(EtGlu)]}$_2$)][PF$_6$]$_2$ 313

A solution of *cis*-[Ru(2,2′-bpy)$_2$(qpy)][PF$_6$]$_2$ (45.6 mg, 0.045 mmol) and [Cr$_7$NiF$_3$(O$_2$CCMe$_3$)$_{15}$(EtGlu)] (203 mg, 0.091 mmol) in acetone (20 ml) was stirred at room temperature for 18 h. The solution was filtered and the solvent removed under vacuum. The product was extracted into acetonitrile, the solution filtered and evaporated to dryness under vacuum. Extraction into toluene in a similar manner produced a purple-red powder. Yield: 145 mg (60%). λ_{max}/nm (ε/M^{-1} cm^{-1}): 463 (16,700), 360 (13,100), 288 (71,200), 250 (72,000). Elemental analysis calcd. (%) for C$_{206}$H$_{340}$Cr$_{14}$F$_{18}$N$_{10}$

$Ni_2O_{70}P_2Ru•C_7H_8$: C 46.35, H 6.36, N 2.54, Cr 13.19, Ni 2.13, P 1.12. Found: C 46.29, H 6.40, N 2.30, Cr 12.90, Ni 1.94, P 1.32.

cis-[Ru(2,2′-bpy)$_2$(bbpe){[Cr$_7$NiF$_3$(O$_2$CCMe$_3$)$_{15}$(EtGlu)]}$_2$)][PF$_6$]$_2$ 314

This compound was prepared and purified in a manner similar to **313** by using *cis*-[Ru(2,2′-bpy)$_2$(bbpe)][PF$_6$]$_2$ (25.0 mg, 0.018 mmol) and [Cr$_7$NiF$_3$(O$_2$CCMe$_3$)$_{15}$(EtGlu)] (115 mg, 0.052 mmol) in acetone (15 ml), forming a purple-red solid. Yield: 56 mg. λ_{max}/nm (ε/M^{-1} cm^{-1}): 478 (12,900), 386 (10,100), 289 (55,300). Elemental analysis calcd. (%) for $C_{210}H_{344}Cr_{14}F_{18}N_{10}Ni_2O_{70}P_2Ru$: C 46.03, H 6.33, N 2.56, Cr 13.29, Ni 2.14, P 1.13. Found: C 45.47, H 6.40, N 1.91, Cr 13.01, Ni 2.06, P 1.43.

[Fe(pytpy)$_2$){[Cr$_7$NiF$_3$(O$_2$CCMe$_3$)$_{15}$(EtGlu)]})$_2$][BF$_4$]$_2$ 315

This compound was prepared and purified in a manner similar to **313** by using [Fe(pytpy)$_2$][BF$_4$]$_2$ (68.7 mg, 0.081 mmol) and [Cr$_7$NiF$_3$(O$_2$CCMe$_3$)$_{15}$(EtGlu)] (503 mg, 0.227 mmol) in acetone (25 ml), forming a bright purple solid. Yield: 77 mg (18%). Elemental analysis calcd. (%) for $C_{206}H_{338}B_2Cr_{14}F_{14}FeN_{10}Ni_2O_{70}$: C 47.01, H 6.47, N 2.66, Cr 13.83, Ni 2.23. Found: C 47.25, H 6.33, N 2.43, Cr 13.29, Ni 2.15.

3.3 RESULTS AND DISCUSSION

3.3.1 Synthesis of Organic Linker Molecules and Ligands

All organic molecules and ligands used in this chapter (Figure 58) were synthesised via published experimental procedures; Dr Simon Foxon provided all of these compounds, with the exception of pytpy.

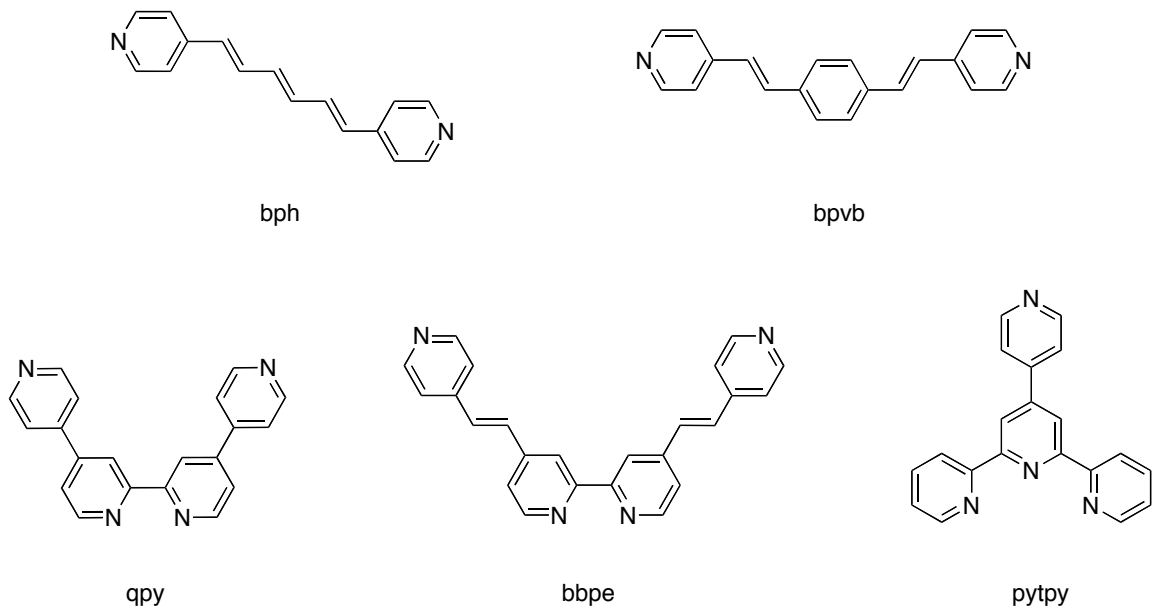

Figure 58. Organic linker molecules.

A slightly adapted method was used to synthesise pytpy (Scheme 11), due to problems encountered when trying to isolate the product of the first step, 1,5-bis(2-pyridyl)-3-(4′-pyridyl)pentane-1,5-dione. The literature method[105] indicated that upon completing the first step of the reaction, the intermediate product may be formed as an orange gum and the addition of methanol would allow the isolation of a white solid. It was discovered that this approach did not work as the initially formed white solid almost instantaneously reverted to orange gum and the addition of further methanol redissolved the product. Many different solvent combinations, primarily methanol and water mixtures, were attempted to allow isolation of the white solid, but without success. Consequently, it was decided to attempt the second step of the reaction using the orange gum, isolated by decanting off the reaction solvent. This strategy worked, albeit in a less effective manner

than published, and the pytpy was isolated in an 8.6% yield as off-white crystals, which were characterised by ^{1}H NMR, mass spectrometry and elemental analysis.

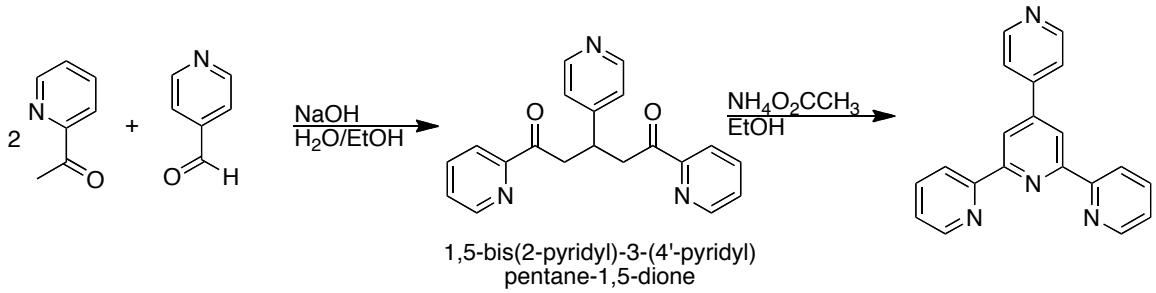

Scheme 11. Synthesis of pytpy.

3.3.2 Synthesis of Organic Linked-wheel systems

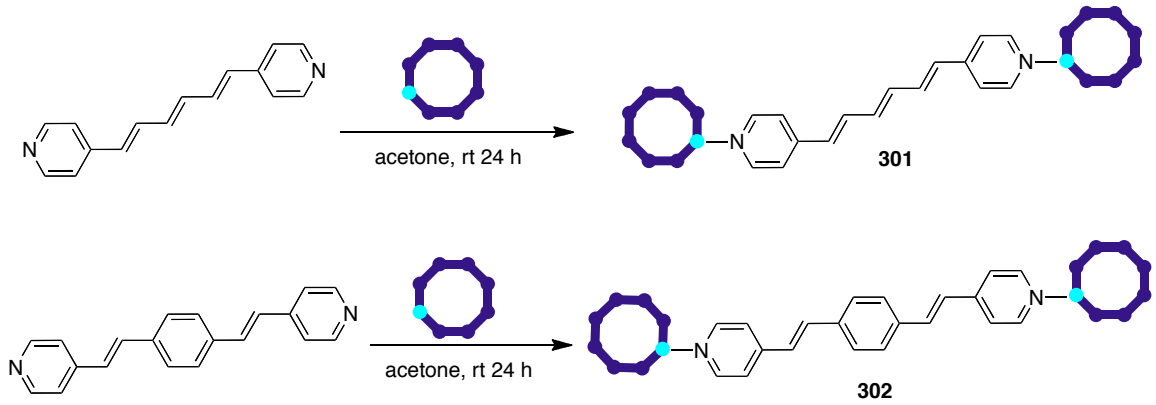

Scheme 12. Synthesis of two-wheel systems with organic linkers.

In a fashion similar to the method used for the previously synthesised 4,4´-bipy and bpe linked-wheel systems[60], the syntheses of **301** and **302** were achieved simply by reacting the two starting materials together at room temperature (Scheme 12). Isolation of the products was achieved by exploiting their differences in solubility when compared to both starting materials. Various attempts were made at crystallising **301** and **302**. The crystallisation approach considered, as for most wheel systems, was evaporation of a mixed solvent system at room temperature. A THF/acetonitrile solution proved successful in producing diffraction-quality crystals of **302**, but no measurable crystals have been obtained for **301** to date.

The compound qpy is an ideal ligand to link wheels through metal centres due to its free terminal pyridyl groups available upon chelation to metal centres.[108] Prior to reacting the wheels with qpy complexes, the wheels were reacted with qpy alone. Using a 2.5:1 ratio of wheel to qpy, followed by gentle evaporation of a diethyl ether/acetone solution, produced an interesting crystal structure.

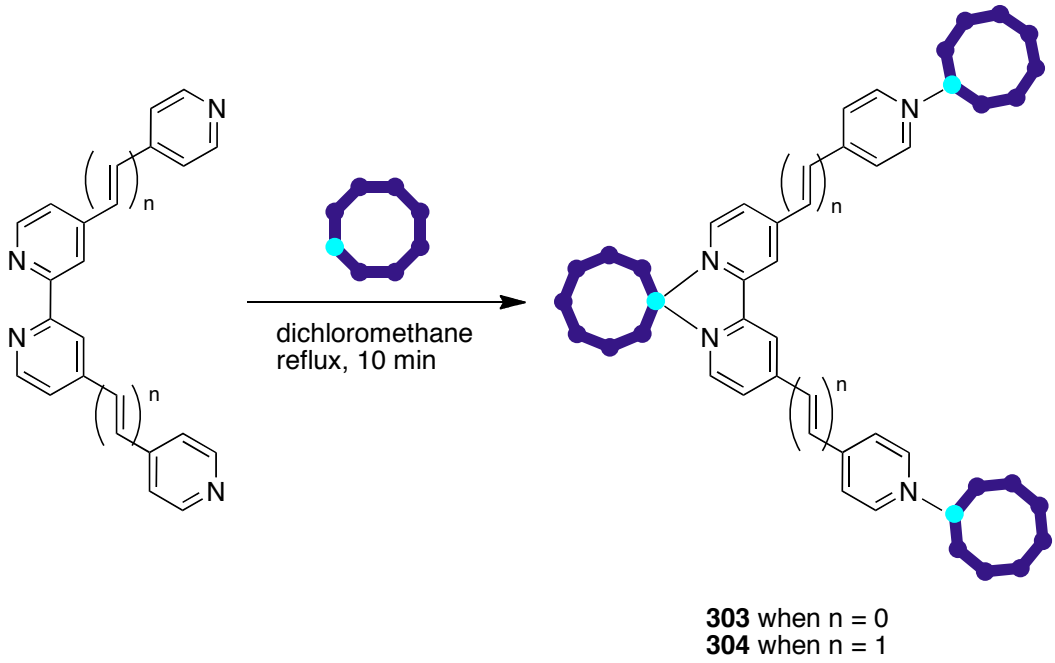

Scheme 13. Synthesis of three-wheel systems.

Instead of the anticipated two-wheel system, a three-wheel system had formed (Scheme 13). This was not wholly unexpected as qpy has 4 free nitrogen atoms available for coordination to the metal wheels. What is unexpected is that the two adjacent nitrogens allow bidentate coordination of the third wheel. This is made possible by the release of one pivalate oxygen atom from the nickel centre, freeing up an extra site for coordination. While previous studies had involved only replacement of the aquo ligand in the wheels, chelation clearly provides a driving force for this pivalate substitution.

A similar reaction was attempted using a slightly extended version of qpy, bbpe, to form **304**. The reaction was carried out in an identical fashion to that used to form **303**, but the addition of acetone to the reaction mixture caused no precipitation. A product has been isolated from this reaction by recrystallisation, involving gentle evaporation of an acetone/acetonitrile solution at room temperature. The elemental analyses obtained on

this sample suggested the formation of the desired product was achieved, but a crystal structure is required in order to confirm its structure.

3.3.3 Synthesis of Metal Complex Linker Molecules

Various rhenium, ruthenium or iron polypyridyl complexes have been synthesised for use as linker molecules. These were chosen for their expected MLCT photoexcitation and/or redox properties. Some have been prepared following previously published literature procedures, whereas others are new.

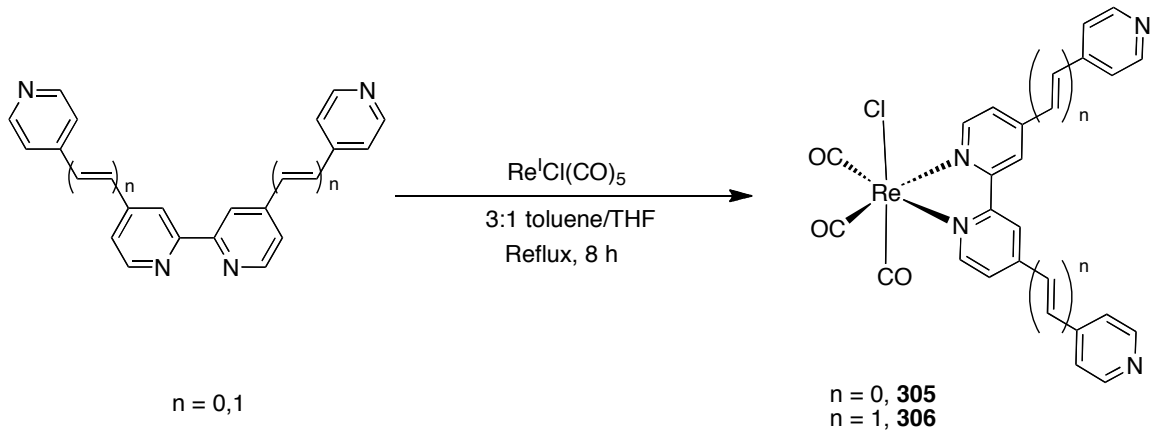

Scheme 14. Synthetic procedure for Re-based linkers.

The synthesis of **305** was achieved following a literature procedure by Thomas et al.[108] The synthesis of the bbpe analogue, *fac*-ReCl(CO)$_3$(bbpe), **306**, was attempted in an identical fashion (Scheme 14). Characterisation of the product proved very difficult due to poor solubility. Elemental analyses suggest some contamination by the ReCl(CO)$_5$ starting material, and the solid-state IR spectrum shows two ν(CO) bands (one sharp, the other broader) between 2015 and 1840 cm^{-1} as expected for compounds of this type. Repeating this reaction using an excess of bbpe might provide a pure sample of **306**, but as this material could not be further reacted with wheels because of its incredibly poor solubility, this possibility was not further investigated.

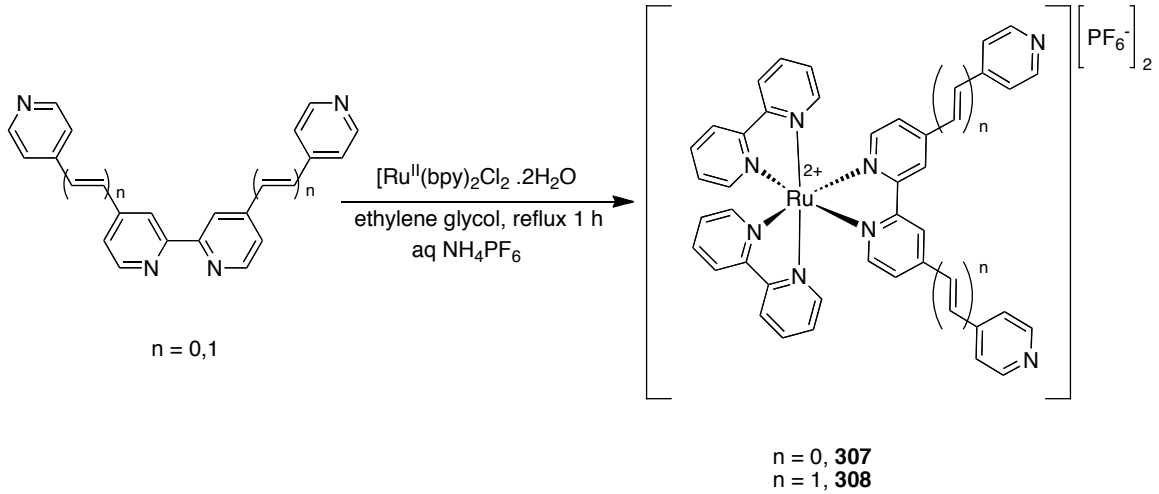

Scheme 15. Synthetic procedure for Ru-based linkers .

The synthesis of **307** was achieved using a literature method by Ward et al[107] and the product fully characterised (Scheme 15). The same method was applied to form the novel compound **308** using bbpe as the incoming ligand in place of qpy. Purification of **308** was achieved by column chromatography on silica gel and the product was characterised by ^{1}H NMR and UV-vis spectroscopies and elemental analyses.

Complex salt **309** was synthesised according to a literature method (Scheme 16).[105]

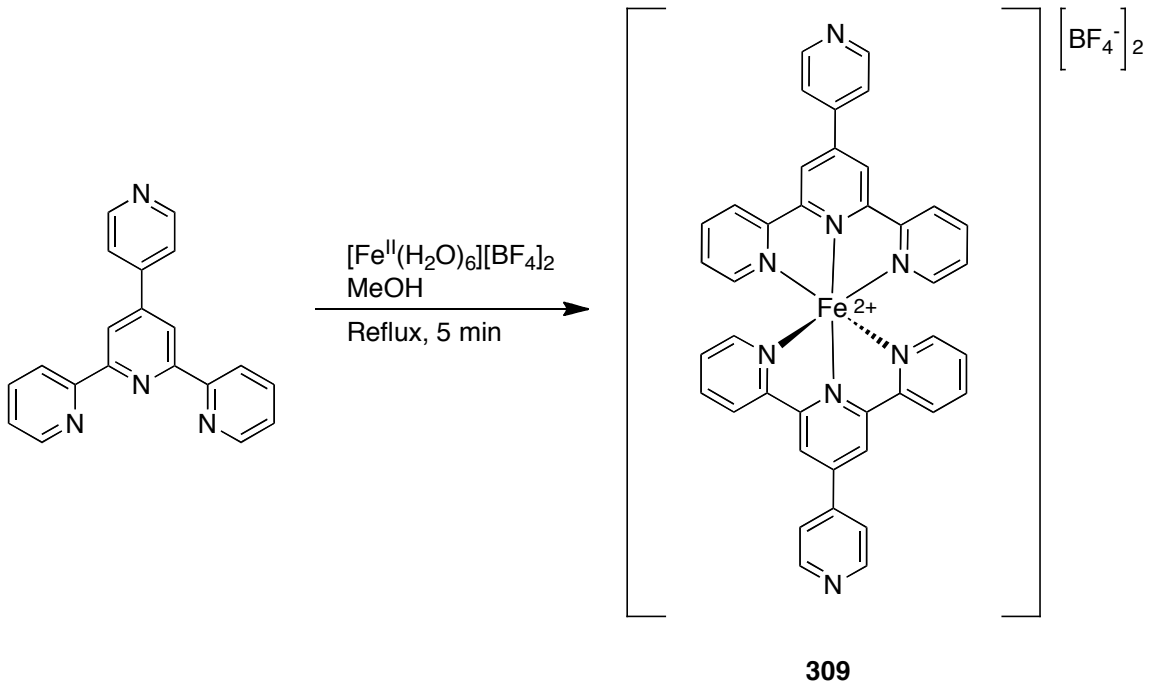

Scheme 16. Synthesis of **309**.

The formation of unsymmetrical Fe^{II} tris-chelate complexes of type $[Fe(L)_2(L')]^{2+}$ has not been widely reported in the literature. However, two different methods have been used to form such compounds. The first approach[109] involves simply reacting a 2:1 ratio of the respective ligands 2,2′-bpy (L) and a variety of extended 2,2′-bpy viologen derivatives (L′) with $Fe^{II}SO_4 \bullet 7H_2O$ in water for 1 h at room temperature to form the desired products by precipitation. The products were obtained in quantitative yields and seemed pure by elemental analysis. However, as the only step of purification was recrystallisation and as there was no evidence of characterisation by ^{1}H NMR this does not seem like a reliable reference. The second published method[110] involves a two-step synthesis at –30 °C to form an intermediate of type $[Fe^{II}(2,2'\text{-bpy})_2(S)_2]^{2+}$ (where S = H_2O or MeCN) in situ before addition of the second ligand, an extended 2,2′-bpy derivative, to form the desired product in a yield of approximately 70%.

A simple approach was used to synthesise **311**, based on the first method reported (Scheme 17). One equivalent of $[Fe^{II}(H_2O)_6][BF_4]_2$ was added to a refluxing acetone solution of the two ligands, 2,2′-bpy and bbpe, forming products instantaneously. Purification was achieved in a similar fashion to that used for the Ru^{II} analogues on silica gel. The separation of similarly coloured bands on the column showed that a mixture of products formed, and the lower than anticipated yield of **311** suggests strongly that the previously published work did not in fact produce the expected compounds in pure form simply by recrystallisation. Despite obtaining a good ^{1}H NMR spectrum of this compound (Section 3.3.5), the elemental analyses obtained are unsatisfactory. Therefore, this product has not been further reacted with wheels.

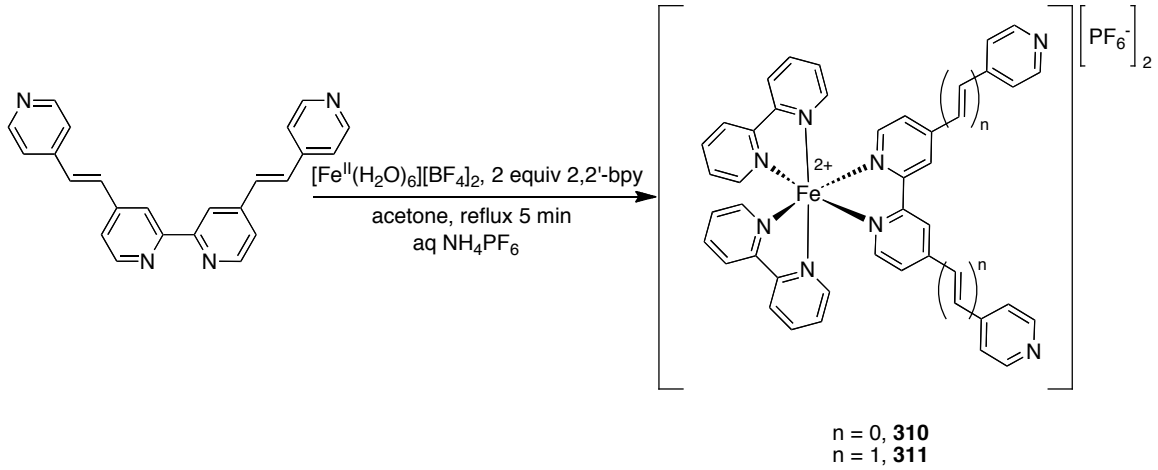

Scheme 17. Synthesis of novel asymmetric Fe^{II} tris-chelate complex salt.

In a similar fashion, a reaction was attempted to form the qpy analogue, **310**. Although a pure product has not yet been isolated, the electrospray mass spectrum of the impure product shows peaks at 822 and 339 corresponding to $[M - PF_6]^+$ and $[M - 2PF_6]^{2+}$, respectively.

3.3.4 Synthesis of Systems with Wheels Linked Through Metal Centres

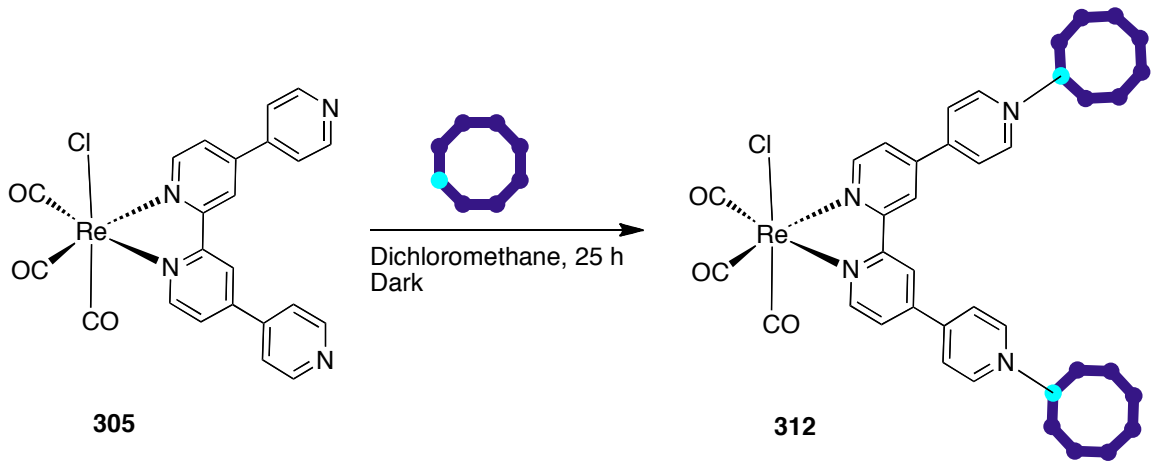

Scheme 18. Synthesis of **312**.

A simple procedure was used to link wheels through **305** (Scheme 18). Purification was achieved by gentle evaporation of an acetone/acetonitrile solution and then a dichloromethane/acetonitrile solution, producing a crystalline material. **312** was characterised using mass spectrometry, elemental analyses, IR and UV/Vis

spectroscopies and cyclic voltammetry. Unfortunately, no crystal structure has been obtained to date, but the large amount of data obtained on this compound leaves little doubt concerning its structure.

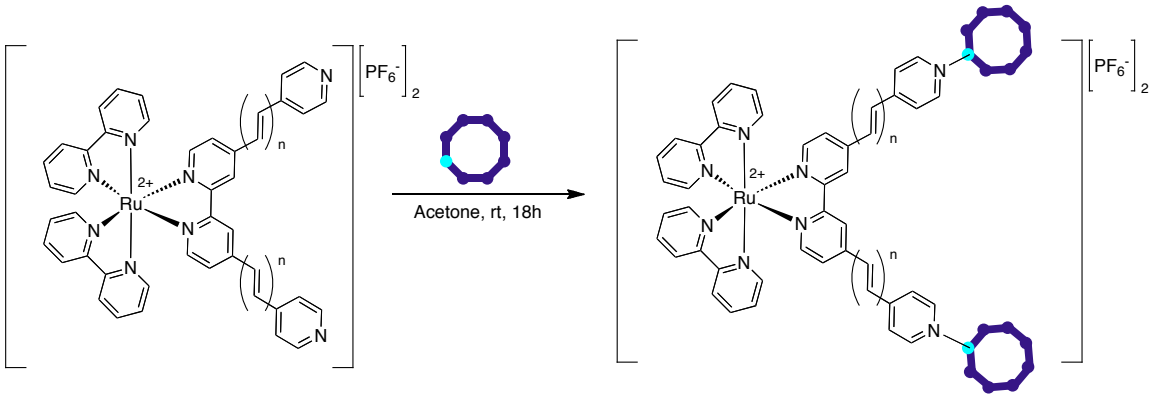

Scheme 19. Synthesis of Ru-containing linked-wheel systems.

The synthesis of **313** and **314** was achieved simply by reacting a 2:1 ratio of wheel and metal complex at room temperature (Scheme 19). The increased solubilities of the products enabled separation from the starting materials, by first extracting into acetonitrile then into toluene. **313** and **314** were characterised by elemental analyses, mass spectrometry, UV-vis spectroscopy and cyclic voltammetry.

The synthesis of **315** was achieved in a fashion identical to **313** and **314** (Scheme 20), and the product was characterised by elemental analyses, mass spectrometry, cyclic voltammetry and UV-vis spectroscopy.

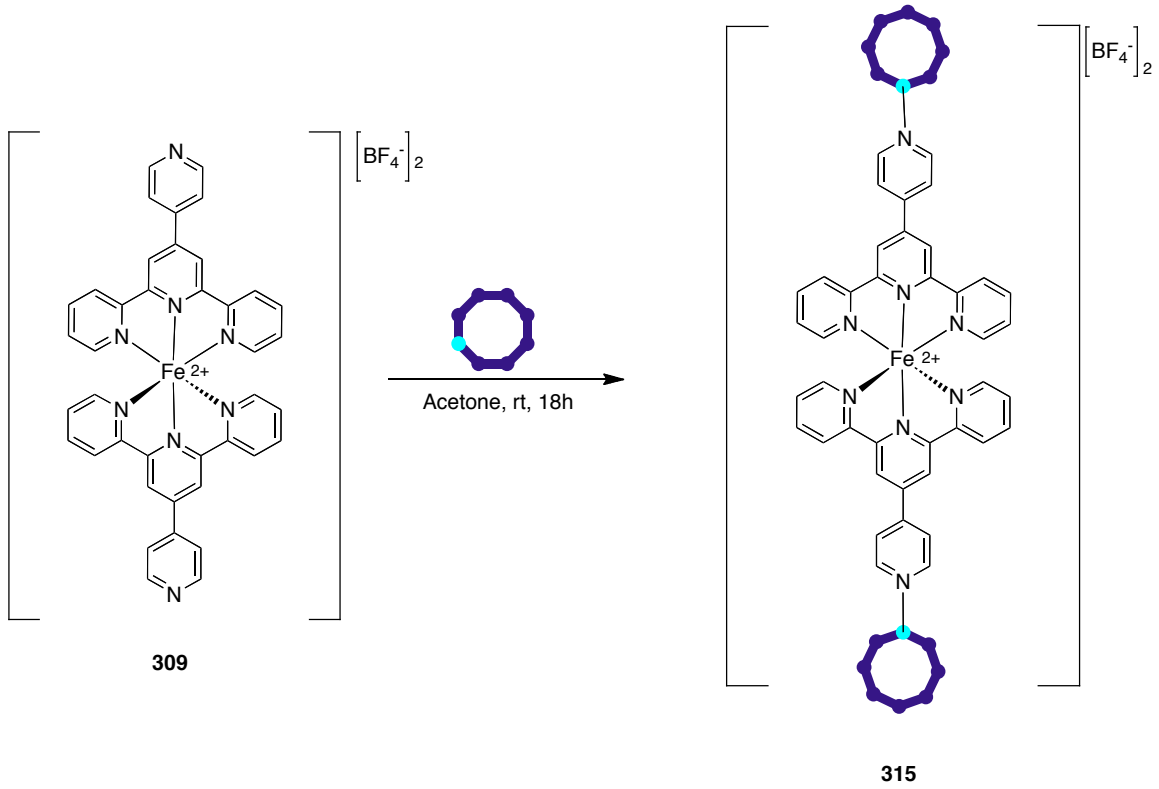

Scheme 20. Synthesis of **315**.

3.3.5 ^{1}H NMR Studies

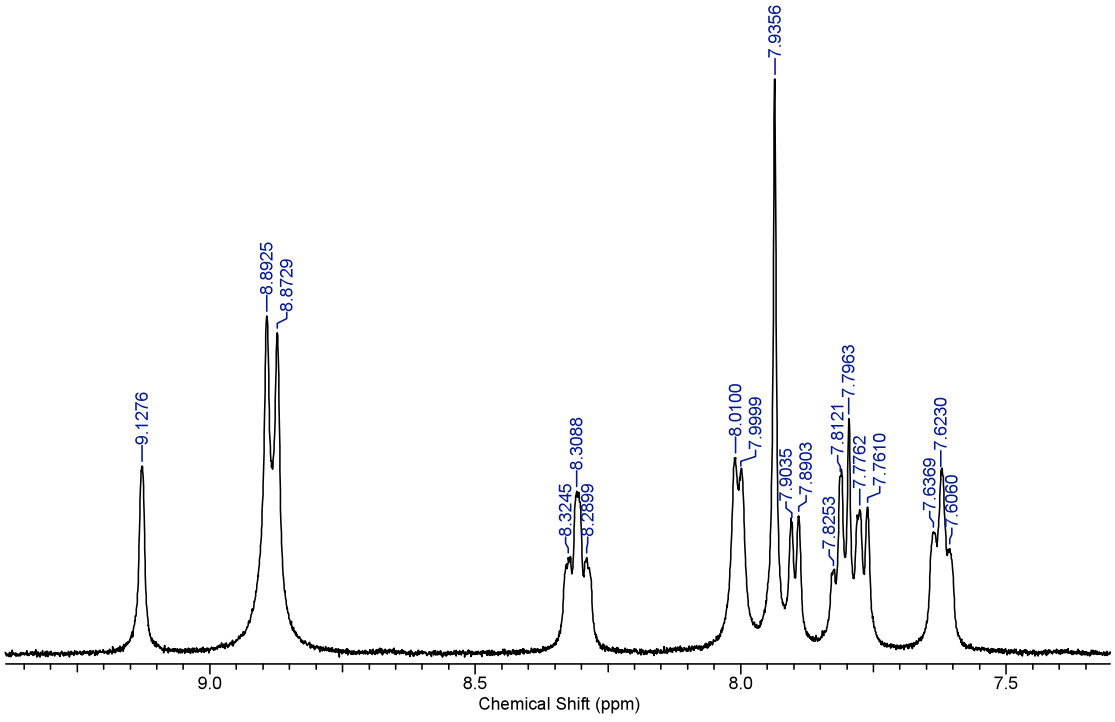

Figure 59. ^{1}H NMR spectrum of **311** in acetone-d_6 at 293 K.

^{1}H NMR spectra were recorded for the two novel metal complex salts **308** and **311**. The spectrum of **311**, shown in Figure 59, displays a series of peaks in the aromatic region, which correlate to the 15 different proton environments of this compound, with a number of signals overlapping.

3.3.6. Mass Spectrometry

Mass spectrometry has been used to identify the linked-wheel compounds. Spectra recorded at The University of Manchester show peaks corresponding to the linking molecule and the purple wheel without a water molecule attached. In collaboration with Dr Lindsay Harding of the University of Huddersfield, the spectra of **302**, **303**, **312**, **313** and **314** have been obtained. As for **219**, the molecular ion peak is not observed for **303** as the mass of this product is too high. However, the spectra of the other compounds do show peaks correlating with their molecular masses.

3.3.7. IR Spectroscopy

The IR spectrum of the novel linked-wheel system **312** and can be seen in Figure 60. The major differences in the spectra of that and that of **305** occur above 1600 cm^{-1}, where **312** has extra bands due to the pivalate groups on the wheel. The distinctive ν(C=O) peaks are positioned very similarly in these two compounds, suggesting that the wheels do not exert significant electronic effects on the Re centre.

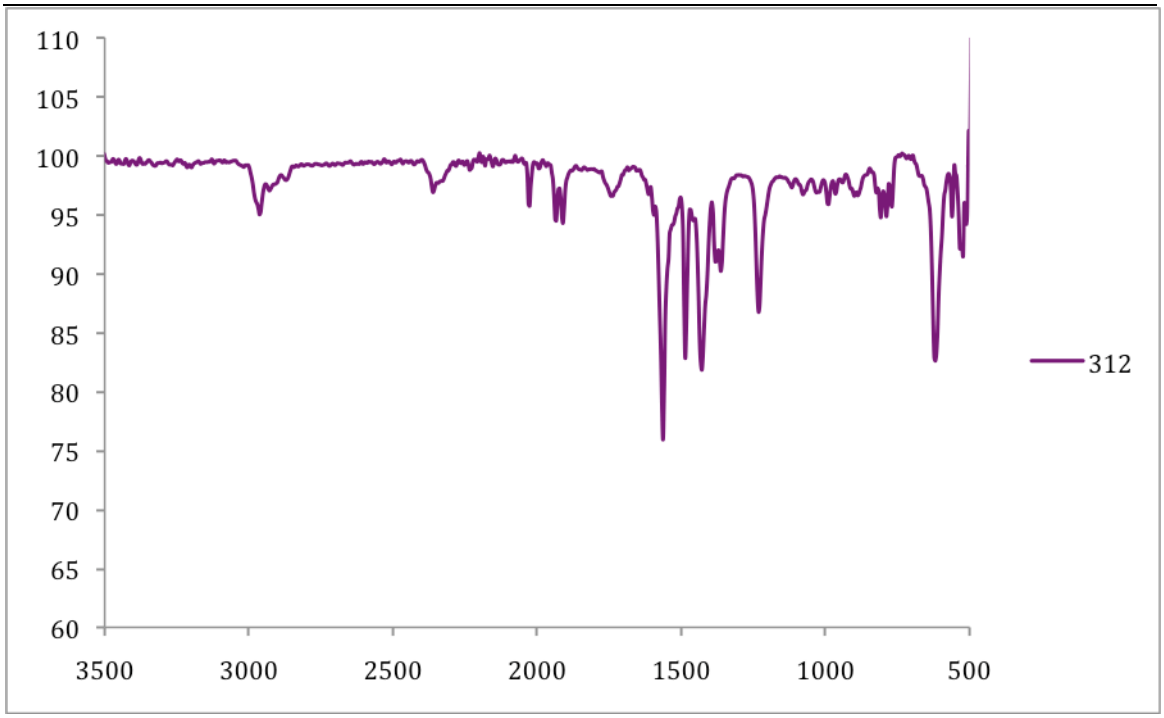

Figure 60. IR absorption spectra of **312**.

3.3.8. UV-Visible Spectroscopy

The UV-vis absorption spectra of the various complexes have been recorded in order to observe any d→π* MLCT transitions. These studies have been carried out at 293 K in acetonitrile, except for **305** and **312**, which have been studied in dichloromethane due to solubility considerations. The resulting data can be seen in Table 4.

Table 4. UV-vis data for compounds **305**, **307**–**308** and **311**–**314**.

Compound	λ_{max}/nm (ε/M^{-1} cm^{-1})	Assignment
305 [a]	413 (3 900)	d→π*
	307 (16 600)	π→π*
307 [b]	462 (16 500)	d→π*
	356 (13 000)	d→π*
	288 (70 300)	π→π*
	254 (51 100)	π→π*
308 [b]	472 (24 500)	d→π*
	376 (18 800)	d→π*
	289 (105 300)	π→π*

	257 (45 600)	$\pi \rightarrow \pi^*$
311 [b]	536 [c]	d→π^*
	410 [c]	d→π^*
	336 [c]	$\pi \rightarrow \pi^*$
	300 [c]	$\pi \rightarrow \pi^*$
312 [a]	556 (1 600)	d→d
	419 (6 600)	d→π^*
	308 (25 500)	$\pi \rightarrow \pi^*$
313 [b]	563 (2 600)	d→d
	463 (16 700)	d→π^*
	360 (13 100)	d→π^*
	288 (71 200)	$\pi \rightarrow \pi^*$
	250 (72 000)	$\pi \rightarrow \pi^*$
314 [b]	555 (2 300)	d→d
	478 (55 300)	d→π^*
	386 (10 100)	d→π^*
	289 (12 900)	$\pi \rightarrow \pi^*$

[a] Solutions in dichloromethane. [b] Solutions in acetonitrile. [c] Values of ε have not been calculated due to unsatisfactory elemental analyses.

The data for **305** agree with those in the literature,[108] with the peak at 307 nm being assigned to a $\pi \rightarrow \pi^*$ transition and that at 413 nm being assigned to a d→π^* transition. As can be seen in Figure 61, the position of the MLCT band changes little, but the apparent intensity does increase upon coordination of the wheels. However, the increased ε value may be attributable to overlap with wheel-based absorption(s). This is an observation that is remarked upon in more detail in Chapter 4. The broad band in the spectrum of **312** at $\lambda_{max} \approx 560$ nm arises from d-d transitions within the Cr_7Ni wheels. The Cr_7Ni wheel precursor shows a band at a very similar wavelength.

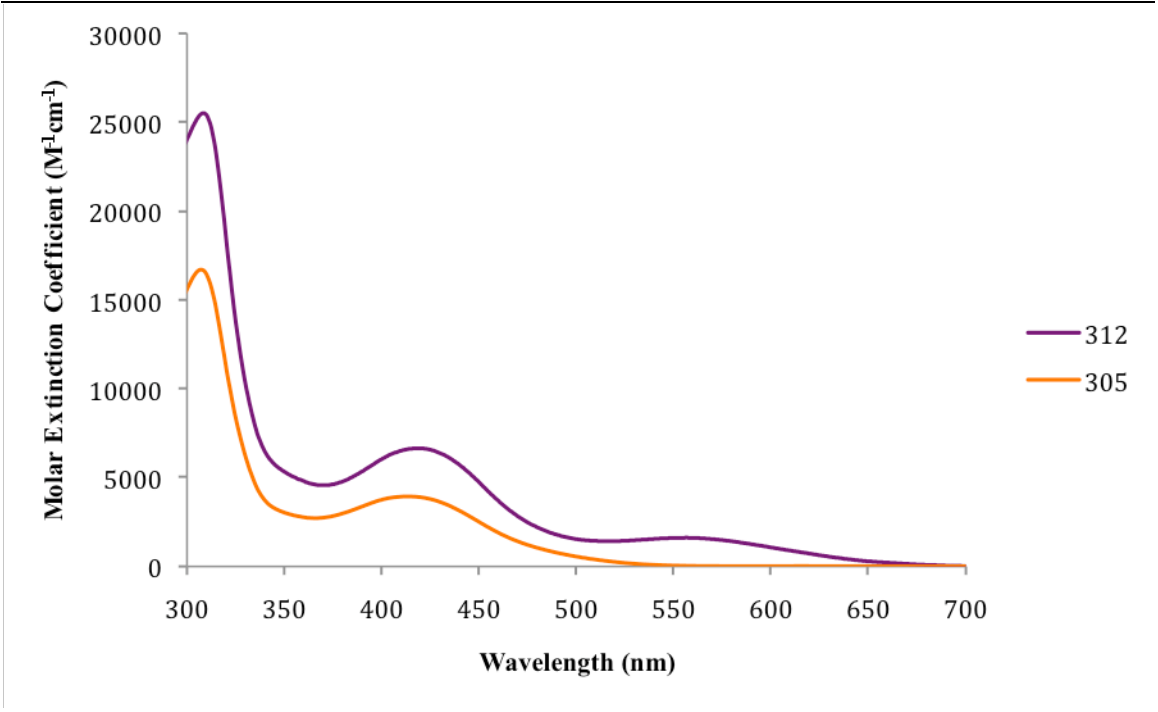

Figure 61. UV-vis absorption spectra of **305** and **312** in dichloromethane at 293 K.

The UV-vis spectra of **307**, **308**, **313** and **314** can be seen in Figure 62. In a similar fashion to the previously discussed spectra, addition of wheels to a complex (moving from **307** to **313**) does not significantly alter the position of the MLCT bands, and in this case neither does it appreciably affect the band intensities. A weak band at $\lambda_{max} \approx 560$ nm in the spectrum of **313** is once again assigned to d-d transitions within the wheels. The spectrum of **308** shows bathochromic shifts in comparison to that of **307**, with changing the ligand from qpy to bbpe also giving a hyperchromic effect. Both of these observations are attributable to the extended π-conjugation and increased orbital overlap within the ligand.

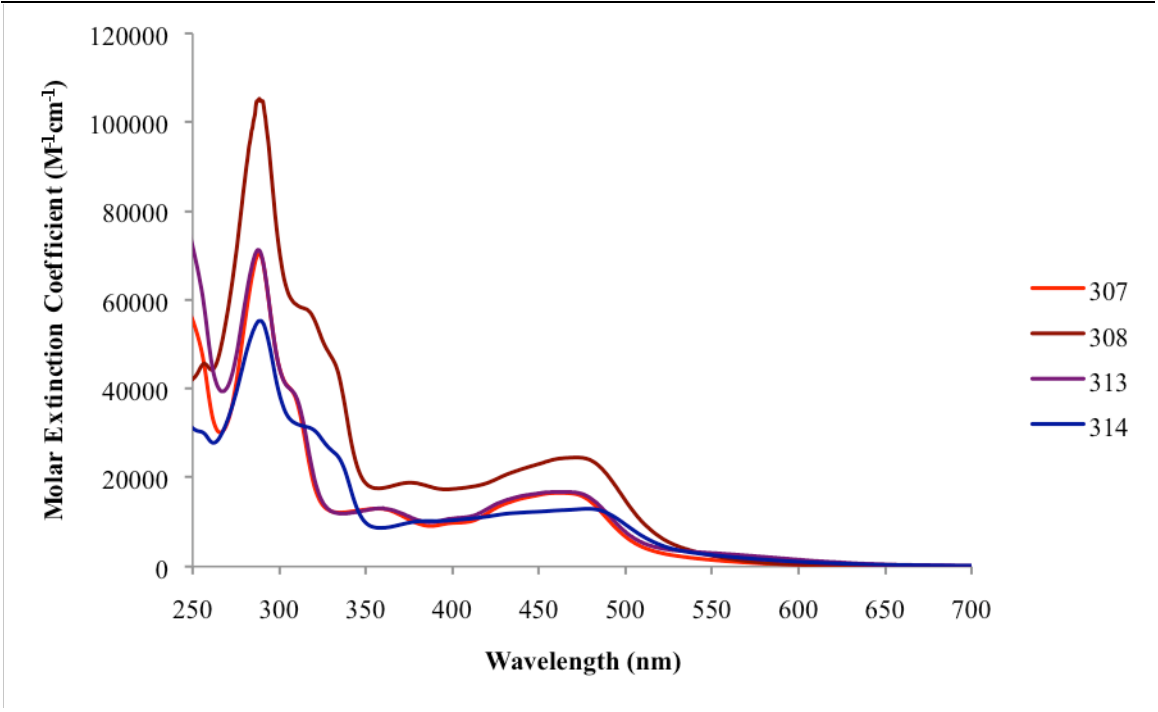

Figure 62. UV-vis absorption spectra of **307**, **308**, **313** and **314** in acetonitrile at 293 K.

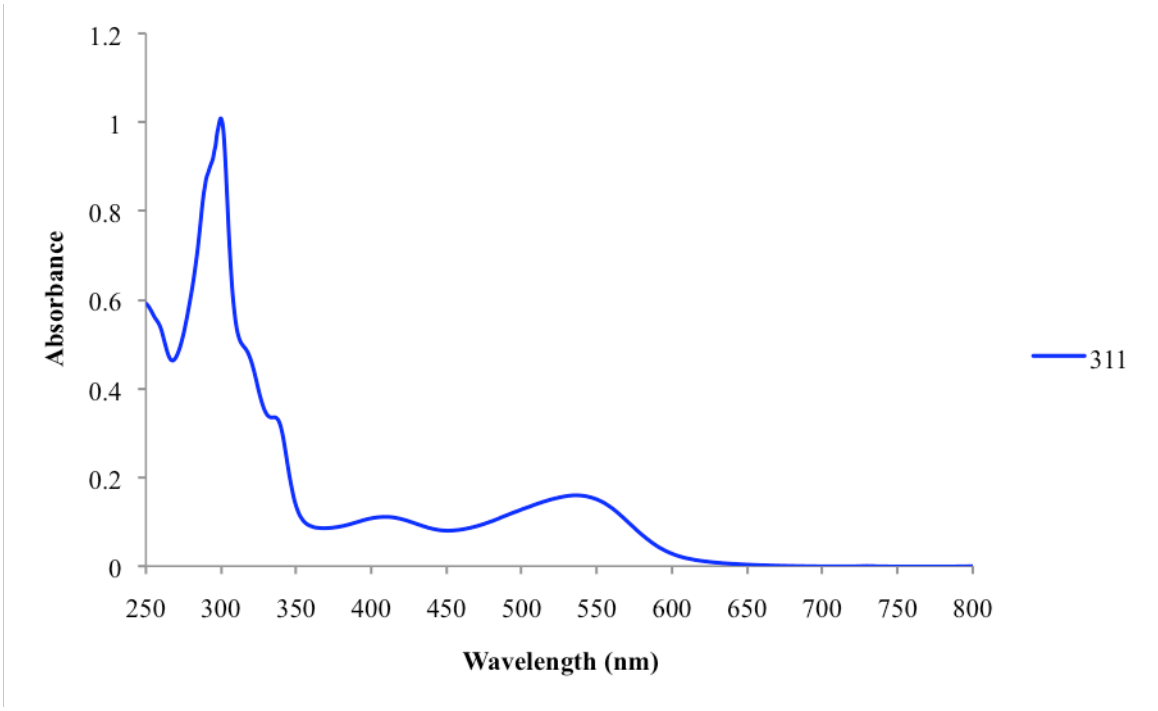

Figure 63. UV-vis absorption spectrum of **311** in acetonitrile at 293 K.

While valid molar extinction coefficients cannot be derived for **311** due to unsatisfactory elemental analyses, its spectrum (Figure 63) clearly displays two low energy absorptions

assigned to MLCT transitions. These bands occur at wavelengths that are consistent with data found in the literature for similar $[Fe^{II}(2,2'\text{-bpy})_2(L)]^{2+}$ complexes (where L is a α-diimine ligand).[110]

3.3.9. Electrochemistry

Cyclic voltammetric studies have been carried out with the novel linked-wheel systems and their precursors **305**, **307**–**309** and **311**–**315**, and the results are shown in Table 5. The presence of terminal pyridyl groups did create difficulties due to coating of the working electrode, but good data were obtained nonetheless.

Table 5. Electrochemical data for purple wheel complexes.

Compound	$E_{1/2}$/V or E_{pc}/V vs. $M^{III/II}$	Ag/AgCl (ΔE_p/mV) [c] Ligand Waves[d]
305 [a]		–1.10 –0.78 (E_{pa})
307 [b]	1.39 (100)	–1.11 (60)
308 [b]	1.34 (70)	–1.13 (60) –0.57
309 [a]	1.24 (40)	–1.04 (54) –1.21 (76)
311 [b]	1.12 (100)	–0.67 –1.11 (85) –1.39
312 [a]		–1.06 (80)
313 [b]	1.41 (40)	–1.09

314 [b]	1.35 (70)	–1.13 –0.87
315 [a]	1.30 (90)	–0.80 –0.95 (80) –1.17 (70)

[a] In dichloromethane. [b] In acetonitrile. [c] Solutions ca. 10^{-4} M in analyte and 0.1 M in $[NBu^n_4][PF_6]$ at a Pt disc working electrode with a scan rate of 200 mV s^{-1}. Ferrocene reference $E_{1/2}$ = 0.44 V, ΔE_p = 65 mV. [d] E_{pc} value unless stated otherwise.

The cyclic voltammograms of **305** and its corresponding linked-wheel system **312** can be seen in Figure 64. As anticipated for Re^I-diimine systems, no redox activity is observed for the Re centre within the window measured, since such complexes normally show an irreversible $Re^{II/I}$ oxidation above 1.5 V vs. Ag/AgCl. In **305**, irreversible processes are observed between –0.5 and –1.2 V, corresponding to ligand-centred reductions, in accord with literature studies.[108] In contrast, **312** shows a single, quasireversible reduction wave with $E_{1/2}$ = –1.06 V vs. Ag/AgCl. Therefore, it appears that coordination of the pyridyl N atoms to the purple wheels improves the reversibility of the reductive chemistry of **305**.

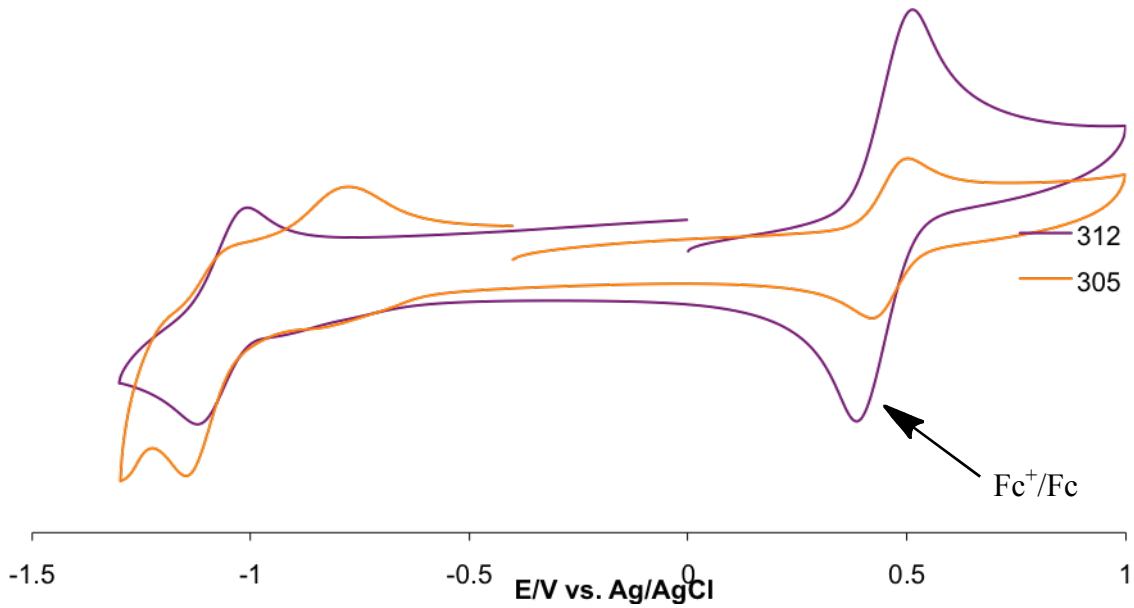

Figure 64. CVs of **305** and **312** in acetonitrile 0.1 M in $[NBu^n_4][PF_6]$ at 200 mV s^{-1}.

The cyclic voltammograms of **307** and **313** can be seen in Figure 65. The data obtained for **307** agree with those in the literature.[111] The trace obtained for **313** is of poorer quality when compared with that of **307**, probably due to the high molecular mass and lower solubility of **313**. However, comparison of the two voltammograms reveals that the $Ru^{III/II}$ $E_{1/2}$ value is not affected significantly by coordination of the wheels, although the ligand-based reduction at $E_{1/2}$ = –1.11 V vs. Ag/AgCl for **307** becomes irreversible in **313**. This provides an interesting contrast with the behaviour of the Re^{I}-containing pair **305** and **312**.

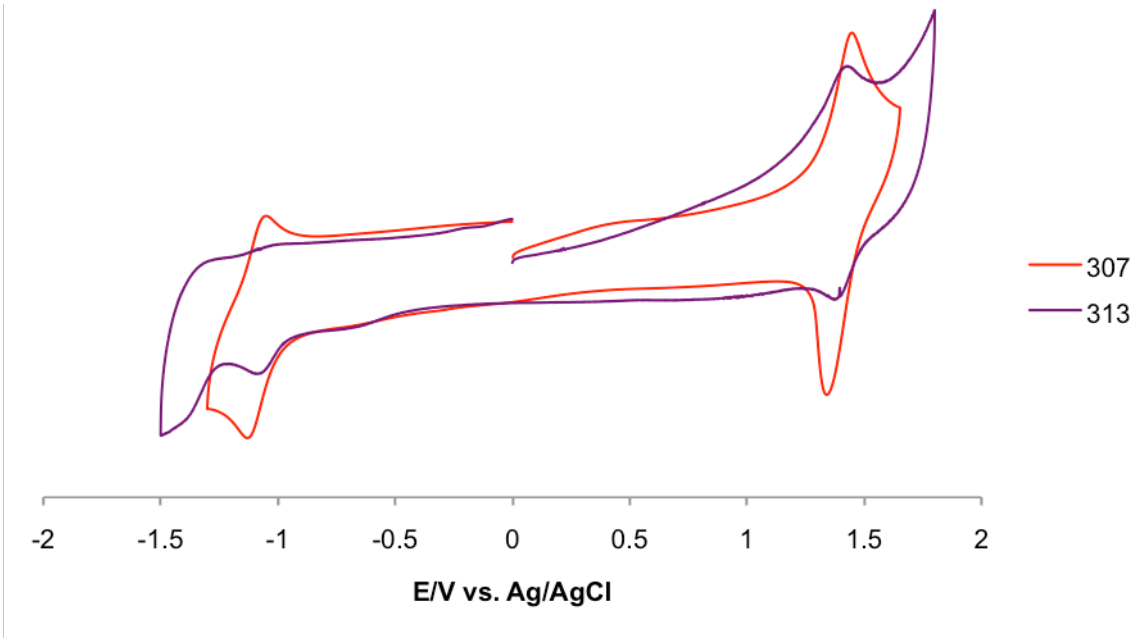

Figure 65. CVs of **307** and **313** in acetonitrile 0.1 M in $[NBu^{n}_{4}][PF_6]$ at 200 mV s^{-1}.

The cyclic voltammograms of **308** and **314** show a pattern similar to those obtained for **307** and **313**, with a much weaker signal for **314** when compared with **308**. Once more the $Ru^{III/II}$ $E_{1/2}$ value is not altered and the ligand based reduction at $E_{1/2}$ = –1.13 V vs. Ag/AgCl becomes irreversible upon addition of the wheels. The irreversible reduction wave at –0.57 V vs. Ag/AgCl in **308** is attributable to the presence of the ethenylene groups.

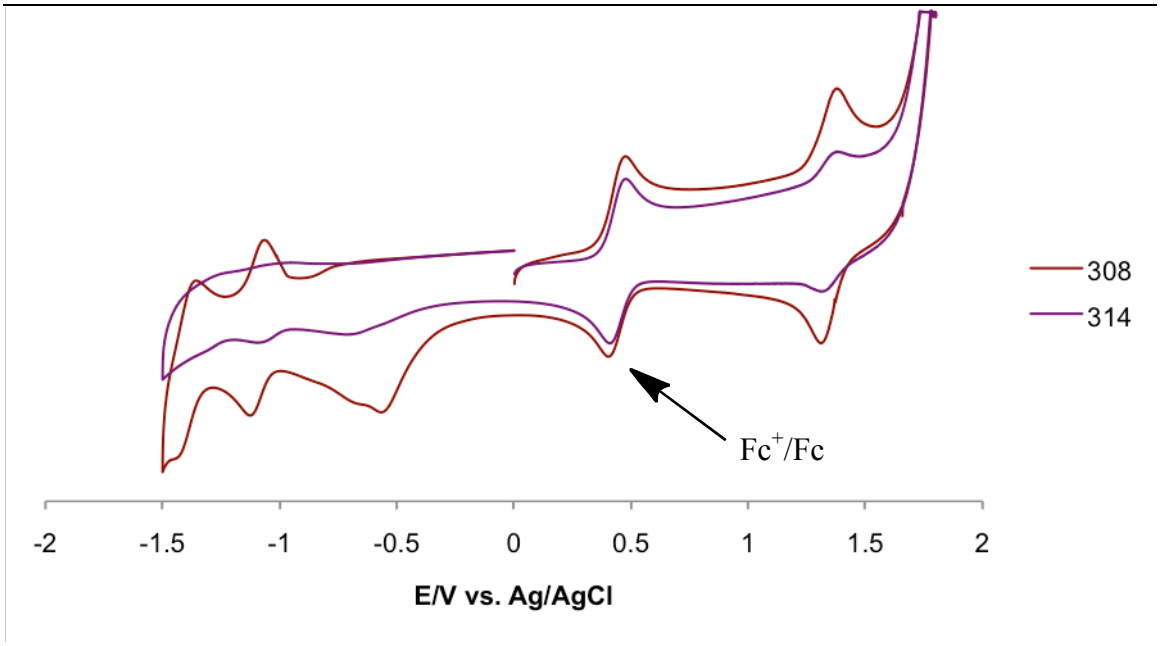

Figure 66. CVs of **308** and **314** in acetonitrile 0.1 M in $[NBu^n_4][PF_6]$ at 200 mV s^{-1}.

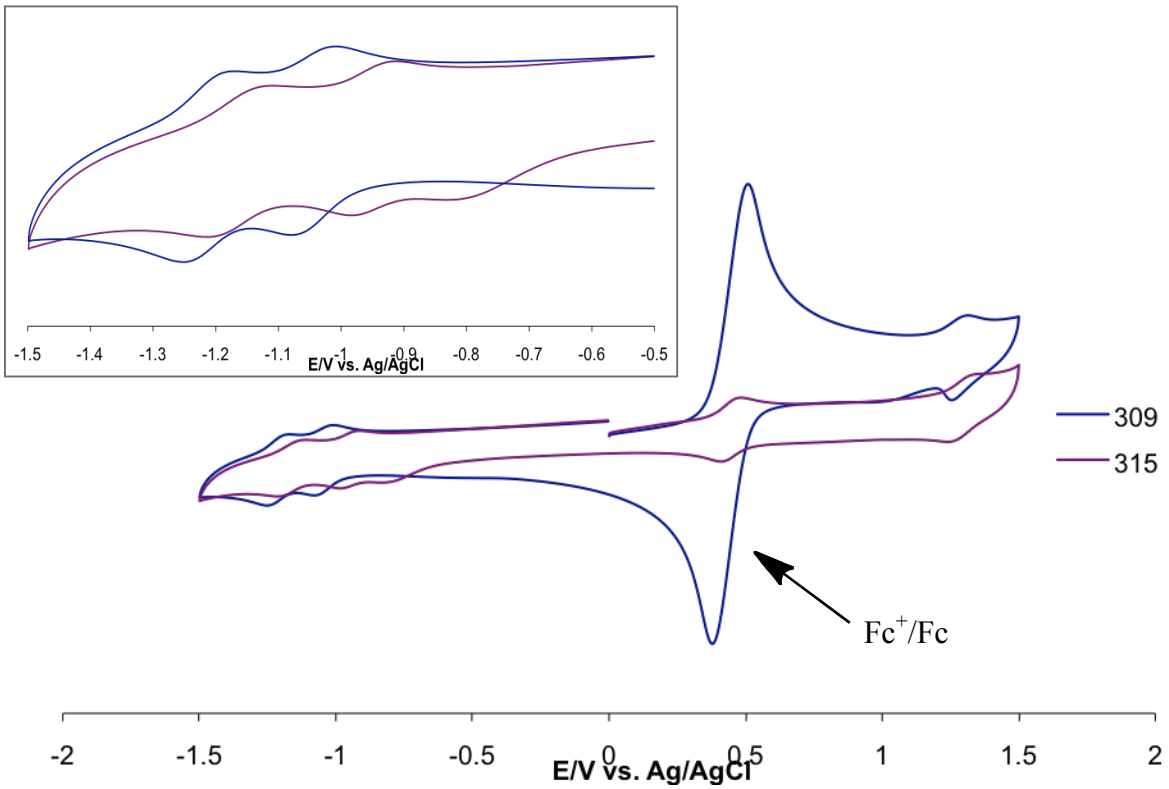

Figure 67. CVs of **309** and **315** in dichloromethane 0.1 M in $[NBu^n_4][PF_6]$ at 200 mV s^{-1}. Inset: Close up of ligand based reductions.

The redox behaviour of **309** and **315** varies once again only in the ligand reduction region (Figure 67). As anticipated from literature results,[108] **309** shows two reversible ligand

based reduction waves. **315** seems to show two reversible ligand based reductions, at –0.95 V and –1.17 V vs. Ag/AgCl with an irreversible band appearing at -0.80 V.

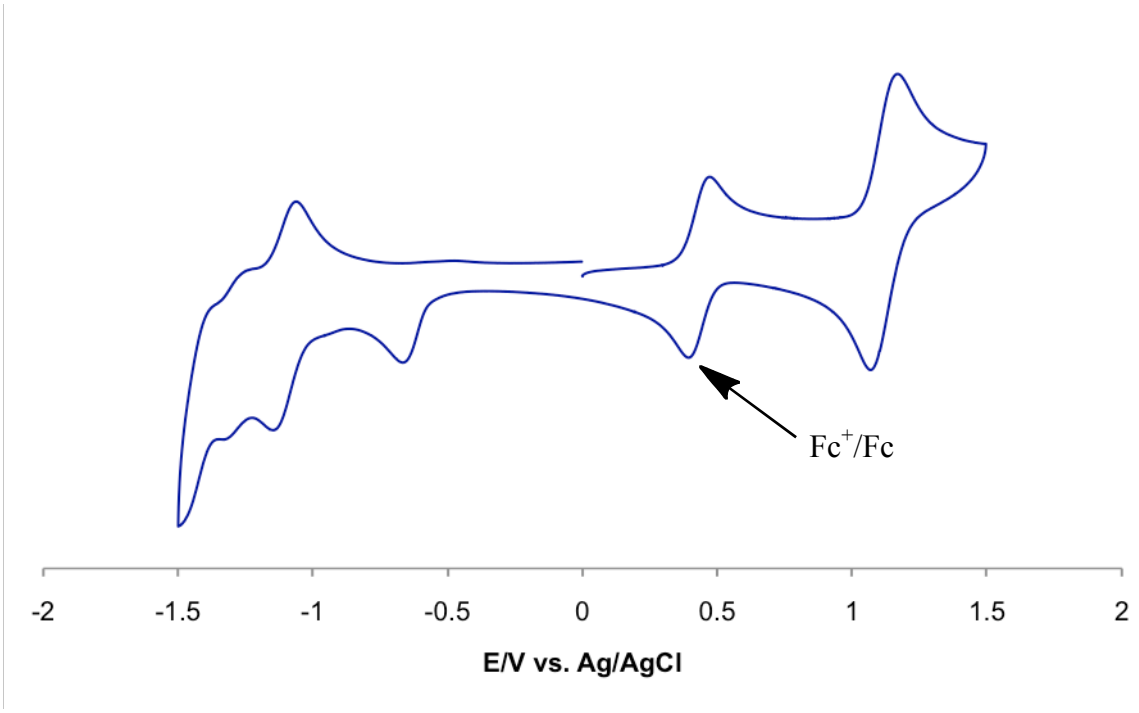

Figure 68. Cyclic voltammogram of **311** in acetonitrile at a scan rate of 200 mV s^{-1}.

The cyclic voltammogram of **311** (Figure 68) shows a quasi-reversible $Fe^{III/II}$ oxidation wave with $E_{1/2}$ = 1.12 V vs. Ag/AgCl. Several ligand-centred reduction processes are also observed, one of which appears to be reversible. As for **308**, the irreversible reduction wave at –0.67 V vs. Ag/AgCl in **311** arises from the presence of the ethenylene units.

3.3.10. Luminescence Studies

Some initial luminescence studies have been run on the Re^{I} complexes **305** and **312**. **305** shows a broad emission band at 650 nm upon excitation at 400 nm, which agrees with literature data and is assigned to emission from a MLCT excited state. In contrast, **312** displays no luminescence upon 400 nm excitation, showing that it is quenched due to the presence of the wheels. Presumably, this observation reflects a shortening of the MLCT excited state lifetime due to nonradiative decay via other electronic excited states, possibly of ligand-field nature. Further, more detailed luminescence studies (also

involving the Ru^{II} complexes) will be required in order to clarify the behaviour of the new linked-wheel systems.

3.3.11. X-Ray Crystallography

Crystal structures have been solved for **302** and **303**. Both adopt orthorhombic space groups; $C222_1$ for **302** and $P22_12_1$ for **303**.

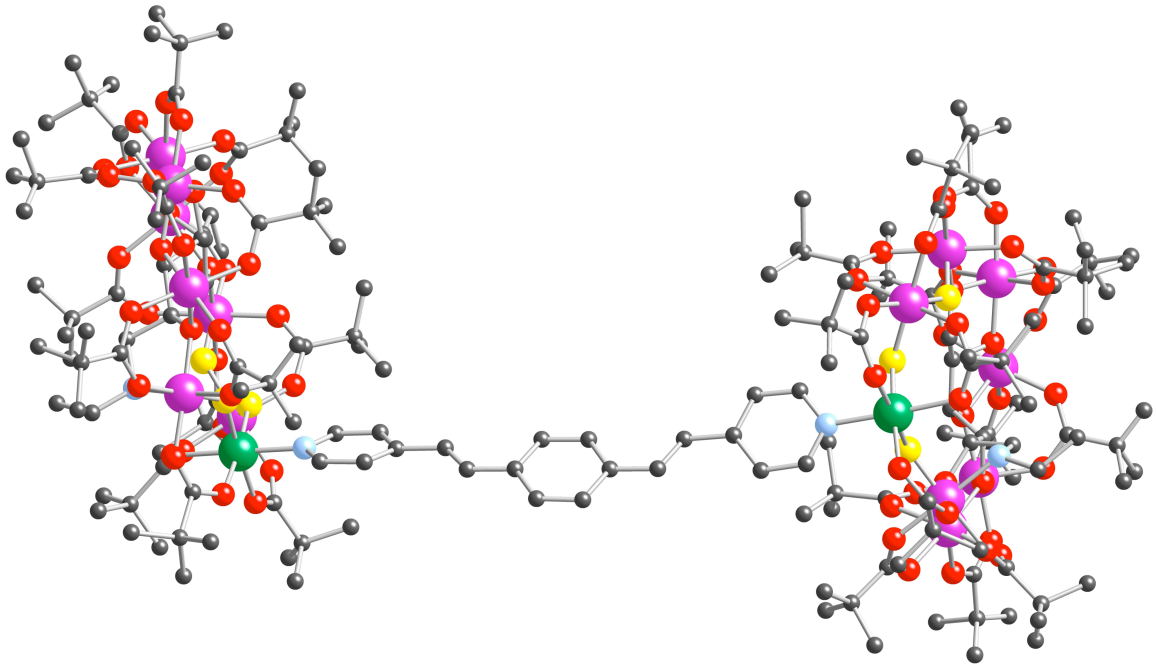

Figure 69. Crystal Structure of **302**.

The crystal structure of **302** can be seen in Figure 69. The two N–Ni bond distances of 2.057(4) Å are similar to those observed in the previously published 4,4′-bpy linked-wheel system. The bpvb linker molecule is not planar and twists about the ethenylene bridges with torsion angles of almost 20º.

The structure of **303** (Figure 70) shows an interesting arrangement of wheels not seen previously. The qpy ligand is coordinated to three wheels, with chelation to the central one. All four N–Ni distances are approximately 2.1 Å, showing no significant shortening upon chelation. An equatorial O (*), originally coordinated to the Ni^{II} centre, has been

released, leaving a monodentate pivalate group attached to the adjacent Cr^{III} ion. All other bonds in the structure of the chelated wheel remain as expected.

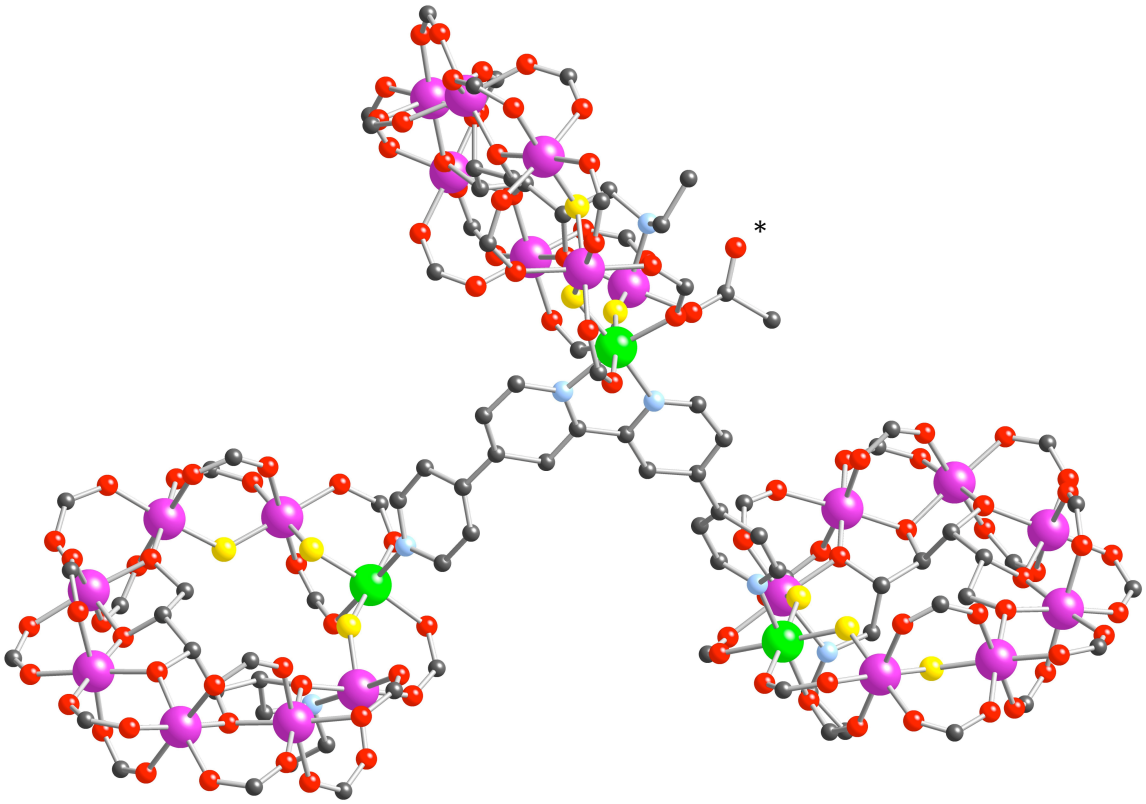

Figure 70. Crystal structure of **303**.

3.4. CONCLUSIONS

Three systems linked through purely organic moieties have been synthesised, with **302** and **303** characterised by X-ray crystallography. Two novel transition metal-containing linker molecules (**308** and **311**) have been prepared using the ligand bbpe, and both have been characterised using ^{1}H NMR spectroscopy. **308** and three other Re, Ru or Fe complexes have been reacted with wheels to form linked-wheel systems. Unfortunately, to date no diffraction-quality crystals have been grown of any of the systems containing metal-based linkers, but enough evidence has been gathered to indicate that the desired products have been formed. UV-vis studies show no significant changes in the MLCT absorption spectra due to wheel coordination. However, the emission spectrum of **312** shows quenching of the luminescence observed for the precursor compound **305**. Cyclic voltammetry on the linked-wheel systems shows that while the metal-based oxidation processes remain essentially unchanged, in every case the ligand-centred reductions are altered significantly due to the presence of the wheels.

3.5. FURTHER WORK

Ideally, crystal structures are required for the compounds not yet characterised by X-ray diffraction. For the Re-containing linked-wheel system **312**, it should be possible to form suitable crystals by subtle alterations to the crystal growing solvents, as the formation of crystalline material has been observed using a dichloromethane/acetonitrile solution. For the Ru/Fe-containing linked-wheel systems, crystal growing may prove to be more challenging due to the relatively high solubilities of these products. Metathesis to a salt, such as a chloride, that would be less soluble in solvents like acetonitrile may give more promising results. Alternatively, using a bulkier anion such as BPh_4^- may facilitate the production of crystals by improving the efficiency of crystal packing.

Studies to assess the switchable properties of the new photo and/or redox-active linked-wheel systems will be a high priority. One way of doing this may be to use an EPR machine in combination with a pulsed laser, in order to cause MLCT excitation at the appropriate wavelength. Time resolved EPR spectroscopy has been used to study short-

lived excited states in the past[112,113], with some studies involving the MLCT excitations of Re^{I} and Ru^{II} polypyridyl complexes.[114]

It will be desirable to complete the synthesis of the series of Fe and Ru polypyridyl systems in order to be able to determine which is the most promising for our purposes. Three compounds in this series have either not yet been synthesised or reacted with wheels (Figure 71). **310** must be isolated to a satisfactorily pure degree, and a method to purify **311** remains to be established. The complex salt $[Ru(pytpy)_2][PF_6]_2$ is known in the literature.

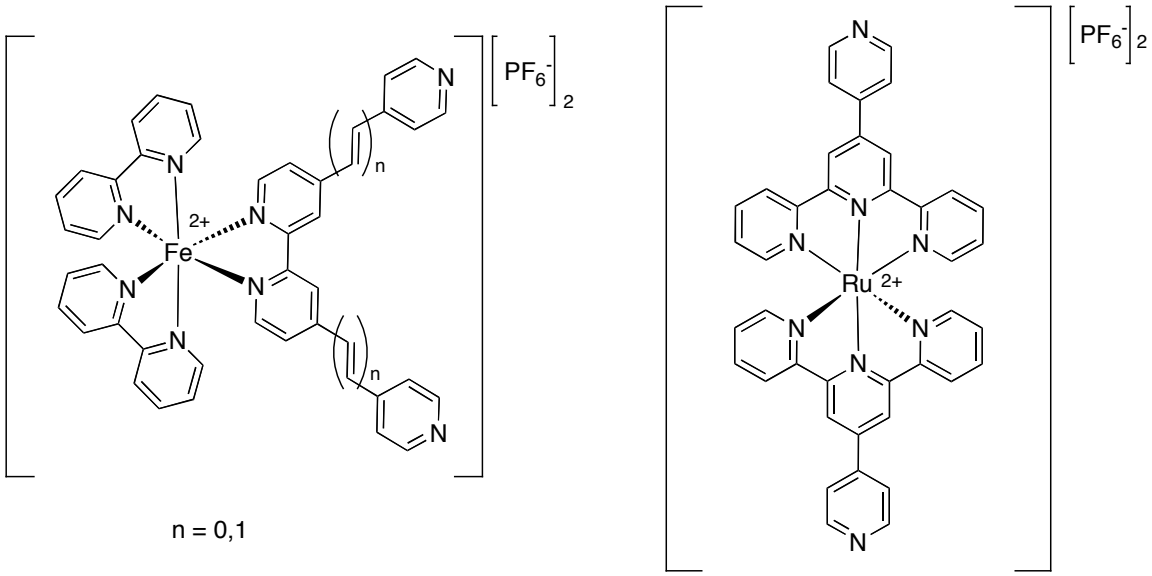

Figure 71. Remaining Fe/Ru species to be coordinated to purple wheels.

Chapter 4 – Mixed Wheel Systems

4.1 INTRODUCTION

As described in Chapters 2 and 3, developments have been made in the synthesis of linked wheel systems using both mono-substituted green wheels and sugar-templated purple wheels. Until now, however, the two genres of wheels have only been considered separately. Having demonstrated the various capabilities of linking each genre of wheel, it became apparent that purple and green wheels have the potential to be linked together, by coordinating the terminal pyridyl group of the green wheel to the vacant site on the divalent metal in the purple wheel. With the latter being a first row transition metal, it is anticipated that the reaction conditions should not need to be extreme and coordination should occur readily.

This is an interesting series to study, as the length of the link between the two wheels is not the only variable that can be considered. Changing the divalent metal in the Cr_7M wheels may affect the interaction occurring between the wheels, and the coordination of the divalent metal may also play an important role – in the green wheels the link involves both the divalent metal and the adjacent chromium centre, whereas with the purple wheels the link is formed through only the divalent metal.

A series of mixed wheel systems has been synthesised by reacting four different mono-substituted green wheels (**203**, **204**, **206** and **207**) with four purple wheels (Cr_7M, where M = Ni, Co, Mn and Zn). A total of fourteen novel systems has been formed, with two of the attempted reactions failing to occur. These linked wheel systems have been characterised by elemental analysis, X-ray crystallography and, in some cases, UV-vis spectroscopy and mass spectrometry. EPR studies on Cr_7Ni-Cr_7Ni linked systems have shown that the strongest interaction occurs when using isonicotinate as a link, with 4-pyridazine carboxylate giving the weakest coupling. Studies have also been undertaken on Cr_7Ni-Cr_7Mn and Cr_7Ni-Cr_7Zn systems, with the former showing interactions and the latter showing none.

4.2 EXPERIMENTAL PROCEDURES

4.2.1 Materials and Procedures

$[Cr_7NiF_3(O_2CCMe_3)_{15}(EtGlu)(H_2O)]$[60] and $[Pr_2NH_2][Cr_7NiF_8(O_2CCMe_3)_{15}(O_2CPy)]$[5] were synthesised by literature methods. The syntheses of the other green wheels are discussed in Chapter 2 and the Cr_7Mn, Cr_7Zn and Cr_7Co analogues of the purple wheels were synthesised according to unpublished methods by Dr Grigore Timco.

4.2.2 Physical Measurements

Elemental analyses were performed by the Microanalytical Laboratory, University of Manchester. Mass spectrometry was performed either using electrospray on a Micromass Platform spectrometer at The University of Manchester or using a Bruker MicrTOF-Q mass spectrometer with an electrospray ionisation source by Lindsay Harding at the University of Huddersfield. EPR studies were performed by Dr Floriana Tuna and John Machin at The University of Manchester. Q-Band EPR was run on an Elexsys E500 spectrometer equipped with a Bruker 2 tesla magnet. X-ray crystallographic data was collected in Berkeley, California by Dr Simon J. Teat and the structures were solved by Dr Robin Pritchard at The University of Manchester.

4.2.3 Syntheses

$[Pr_2NH_2][Cr_7NiF_8(O_2CCMe_3)_{15}(O_2CPy)Cr_7NiF_3(O_2CCMe_3)_{15}(EtGlu)]$ 401

To a warm solution of $[Cr_7NiF_3(O_2CCMe_3)_{15}(EtGlu)(H_2O)]$ (1.79 g, 0.807 mmol) in acetone (130 ml) was added a warm solution of $[Pr_2NH_2][Cr_7NiF_8(O_2CCMe_3)_{15}(O_2CPy)]$ (**203**) (1.80 g, 0.777 mmol) in acetone (200 ml) and the reaction was heated under reflux for 5 min. The blue-grey solution was then allowed to sit covered at room temperature until the product formed as a blue-grey crystalline material, which was collected by filtration and washed with a small amount of acetone. Measurable crystals were isolated from the reaction mixture prior to filtration. Yield: 1.92 g (55%). Elemental analysis

calcd (%) for $C_{170}H_{304}Cr_{14}F_{11}N_3Ni_2O_{67}$: C 45.21, H 6.78, N 0.93, Cr 16.12, Ni 2.60. Found: C 45.04, H 6.59, N 0.90, Cr 15.99, Ni 2.64.

All of the other compounds were prepared and isolated as blue-grey solids in a manner similar to **401**; the quantities of reagents used, yields and characterisation data are listed below.

$[Pr_2NH_2][Cr_7NiF_8(O_2CCMe_3)_{15}(O_2CCHCHPy)Cr_7NiF_3(O_2CCMe_3)_{15}(EtGlu)]$ 402

$[Pr_2NH_2][Cr_7NiF_8(O_2CCMe_3)_{15}(O_2CCHCHPy)]$ (**204**) (200 mg, 0.085 mmol) in acetone (20 ml); $[Cr_7NiF_3(O_2CCMe_3)_{15}(EtGlu)(H_2O)]$ (207 mg, 0.093 mmol) in acetone (20 ml). Yield: 292 mg (76%). +ve electrospray: 2199 $[PW - H_2O + H]^+$, 2222 $[PW - H_2O + Na]^+$, 2342 $[GW + H]^+$, 2366 $[GW + Na]^+$. -ve electrospray: 2200 (PW), 2246 (GW – $Pr_2NH_2^+$). Elemental analysis calcd (%) for $C_{172}H_{306}Cr_{14}F_{11}N_3Ni_2O_{67}$: C 45.48, H 6.79; N 0.93, Cr 16.02, Ni 2.58. Found: C 44.88, H 6.76, N 0.82, Cr 16.34, Ni 2.63.

$[Pr_2NH_2][Cr_7NiF_8(O_2CCMe_3)_{15}(O_2CPyd)Cr_7NiF_3(O_2CCMe_3)_{15}(EtGlu)]$ 403

$[Cr_7NiF_3(O_2CCMe_3)_{15}(EtGlu)(H_2O)]$ (151 mg, 0.068 mmol) in acetone (20 ml); $[Pr_2NH_2][Cr_7NiF_8(O_2CCMe_3)_{15}(O_2CPyd)]$ (**206**) (152 mg, 0.066 mmol) in acetone (15 ml). Yield: 154 mg (52%). Elemental analysis calcd (%) for $C_{169}H_{303}Cr_{14}F_{11}N_4Ni_2O_{67}$: C 44.93, H 6.76, N 1.24, Cr 16.11, Ni 2.60. Found: C 44.75, H 6.83, N 1.17, Cr 16.32, Ni 2.71.

$[Pr_2NH_2][Cr_7CoF_8(O_2CCMe_3)_{15}(O_2CPy)Cr_7NiF_3(O_2CCMe_3)_{15}(EtGlu)]$ 404

$[Cr_7NiF_3(O_2CCMe_3)_{15}(EtGlu)(H_2O)]$ (157 mg, 0.071 mmol) in acetone (20 ml); $[Pr_2NH_2][Cr_7CoF_8(O_2CCMe_3)_{15}(O_2CPy)]$ (**207**) (151 mg, 0.065 mmol) in acetone (20 ml). Yield: 135 mg (46%). Elemental analysis calcd (%) for $C_{170}H_{304}CoCr_{14}F_{11}N_3NiO_{67}$: C 45.21, H 6.78, N 0.93, Cr 16.12, Ni 1.30. Found: C 45.13, H 6.92, N 0.92, Cr 15.84, Ni 1.32.

$[Pr_2NH_2][Cr_7NiF_8(O_2CCMe_3)_{15}(O_2CPy)Cr_7CoF_3(O_2CCMe_3)_{15}(EtGlu)]$ 405

$[Cr_7CoF_3(O_2CCMe_3)_{15}(EtGlu)(H_2O)]$ (155 mg, 0.070 mmol) in acetone (20 ml); **203** (156 mg, 0.067 mmol) in acetone (20 ml). Yield: 256 mg (85%). Elemental analysis calcd (%) for $C_{170}H_{304}CoCr_{14}F_{11}N_3NiO_{67}$: C 45.21, H 6.78, N 0.93, Cr 16.12, Ni 1.30. Found: C 43.25, H 6.51, N 0.94, Co 1.28, Cr 15.67, Ni 1.31.

$[Pr_2NH_2][Cr_7NiF_8(O_2CCMe_3)_{15}(O_2CCHCHPy)Cr_7CoF_3(O_2CCMe_3)_{15}(EtGlu)]$ 406

$[Cr_7CoF_3(O_2CCMe_3)_{15}(EtGlu)(H_2O)]$ (150 mg, 0.068 mmol) in acetone (20 ml); **204** (152 mg, 0.065 mmol) in acetone (20 ml). Yield: 197 mg (67%). Elemental analysis calcd (%) for $C_{172}H_{306}CoCr_{14}F_{11}N_3NiO_{67}$: C 45.48, H 6.79, N 0.92, Co 1.30, Cr 16.02, Ni 1.29. Found: C 44.22, H 6.74, N 0.89, Co 1.30, Cr 15.77, Ni 1.22.

$[Pr_2NH_2][Cr_7NiF_8(O_2CCMe_3)_{15}(O_2CPyd)Cr_7CoF_3(O_2CCMe_3)_{15}(EtGlu)]$ 407

$[Cr_7CoF_3(O_2CCMe_3)_{15}(EtGlu)(H_2O)]$ (153 mg, 0.069 mmol) in acetone (20 ml); **206** (153 mg, 0.066 mmol) in acetone (20 ml). Yield: 133 mg (45%). Elemental analysis (%) calcd for $C_{169}H_{303}CoCr_{14}F_{11}N_4NiO_{67}$: C 44.78, H 6.78, N 1.24, Co 1.31, Cr 16.16, Ni 1.30. Found: C 42.27, H 6.65, N 1.24, Co 1.34, Cr 15.08, Ni 1.14.

$[Pr_2NH_2][Cr_7CoF_8(O_2CCMe_3)_{15}(O_2CPy)Cr_7CoF_3(O_2CCMe_3)_{15}(EtGlu)]$ 408

$[Cr_7CoF_3(O_2CCMe_3)_{15}(EtGlu)(H_2O)]$ (155 mg, 0.070 mmol) in acetone (20 ml); **207** (153 mg, 0.066 mmol) in acetone (20 ml). Yield: 159 mg (53%). Elemental analysis calcd (%) for $C_{170}H_{304}Co_2Cr_{14}F_{11}N_3O_{67}$: C 45.20, H 6.78, N 0.93, Co 2.61, Cr 16.12. Found: C 45.24, H 6.91, N 0.99, Co 2.65, Cr 15.96.

$[Pr_2NH_2][Cr_7NiF_8(O_2CCMe_3)_{15}(O_2CPy)Cr_7MnF_3(O_2CCMe_3)_{15}(EtGlu)]$ 409

$[Cr_7MnF_3(O_2CCMe_3)_{15}(EtGlu)(H_2O)]$ (299 mg, 0.135 mmol) in acetone (20 ml); **203** (151 mg, 0.065 mmol) in acetone (20 ml). Yield: 44 mg (15%). Elemental analysis calcd

(%) for $C_{170}H_{304}Cr_{14}F_{11}MnN_3NiO_{67}$: C 45.25, H 6.79, N 0.93, Cr 16.13, Ni 1.30. Found: C 45.18, H 6.80, N 0.92, Cr 16.12, Ni 1.38.

$[Pr_2NH_2][Cr_7NiF_8(O_2CCMe_3)_{15}(O_2CCHCHPy)Cr_7MnF_3(O_2CCMe_3)_{15}(EtGlu)]$ 410

$[Cr_7MnF_3(O_2CCMe_3)_{15}(EtGlu)(H_2O)]$ (313 mg, 0.141 mmol) in acetone (15 ml); **204** (153 mg, 0.065 mmol) in acetone (20 ml). Yield: 169 mg (57%). Elemental analysis calcd (%) for $C_{172}H_{306}Cr_{14}F_{11}MnN_3NiO_{67}$: C 45.52, H 6.80, N 0.93, Cr 16.04, Ni 1.29. Found: C 45.40, H 6.82, N 0.85, Cr 16.31, Ni 1.28.

$[Pr_2NH_2][Cr_7CoF_8(O_2CCMe_3)_{15}(O_2CPy)Cr_7MnF_3(O_2CCMe_3)_{15}(EtGlu)]$ 411

$[Cr_7MnF_3(O_2CCMe_3)_{15}(EtGlu)(H_2O)]$ (308 mg, 0.139 mmol) in acetone (20 ml); **207** (151 mg, 0.065 mmol) in acetone (15 ml). Yield: 106 mg (52%). Elemental analysis calcd (%) for $C_{170}H_{304}CoCr_{14}F_{11}MnN_3O_{67}$: C 45.24, H 6.79, N 0.93, Co 1.31, Cr 16.13, Mn 1.22. Found: C 44.34, H 6.69, N 0.96, Co 1.31, Cr 16.18, Mn 1.14.

$[Pr_2NH_2][Cr_7NiF_8(O_2CCMe_3)_{15}(O_2CPy)Cr_7ZnF_3(O_2CCMe_3)_{15}(EtGlu)]$ 412

$[Cr_7ZnF_3(O_2CCMe_3)_{15}(EtGlu)(H_2O)]$ (306 mg, 0.138 mmol) in acetone (20 ml); **203** (150 mg, 0.065 mmol) in acetone (20 ml). Yield: 112 mg (38%). Elemental analysis calcd (%) for $C_{170}H_{304}Cr_{14}F_{11}N_3NiO_{67}Zn$: C 45.14, H 6.77, N 0.93, Cr 16.09, Zn 1.45. Found: C 45.06, H 6.85, N 0.88, Cr 16.32, Zn 1.44.

$[Pr_2NH_2][Cr_7NiF_8(O_2CCMe_3)_{15}(O_2CCHCHPy)Cr_7ZnF_3(O_2CCMe_3)_{15}(EtGlu)]$ 413

$[Cr_7ZnF_3(O_2CCMe_3)_{15}(EtGlu)(H_2O)]$ (0.1567 g, 0.071 mmol) in acetone (15 ml); **204** (0.1520 g, 0.065 mmol) in acetone (20 ml). Yield: 95 mg (32%). Elemental analysis calcd (%) for $C_{172}H_{306}Cr_{14}F_{11}N_3NiO_{67}Zn$: C 45.41, H 6.78, N 0.92, Cr 16.00, Ni 1.29. Found: C 45.11, H 6.77, N 0.86, Cr 16.05, Ni 1.31.

$[Pr_2NH_2][Cr_7CoF_8(O_2CCMe_3)_{15}(O_2CPy)Cr_7ZnF_3(O_2CCMe_3)_{15}(EtGlu)]$ 414

$[Cr_7ZnF_3(O_2CCMe_3)_{15}(EtGlu)(H_2O)]$ (304 mg, 0.137 mmol) in acetone (20 ml); **207** (155 mg, 0.067 mmol) in acetone (20 ml). Yield: 190 mg (63%). Elemental analysis calcd (%) for $C_{170}H_{304}CoCr_{14}F_{11}N_3O_{67}Zn$: C 45.14, H 6.77, N 0.93, Cr 16.09, Co 1.30. Found: C 44.99, H 6.86, N 0.93, Cr 16.12, Co 1.37.

4.3 RESULTS AND DISCUSSION

4.3.1 Synthetic Studies

By mixing a one-to-one ratio of reactants in refluxing acetone, the straightforward formation of a mixed wheel system occurs (Scheme 21 and Table 6). Simply leaving the reaction mixture covered for between 1 and 10 days affords diffraction-quality crystals of the desired products.

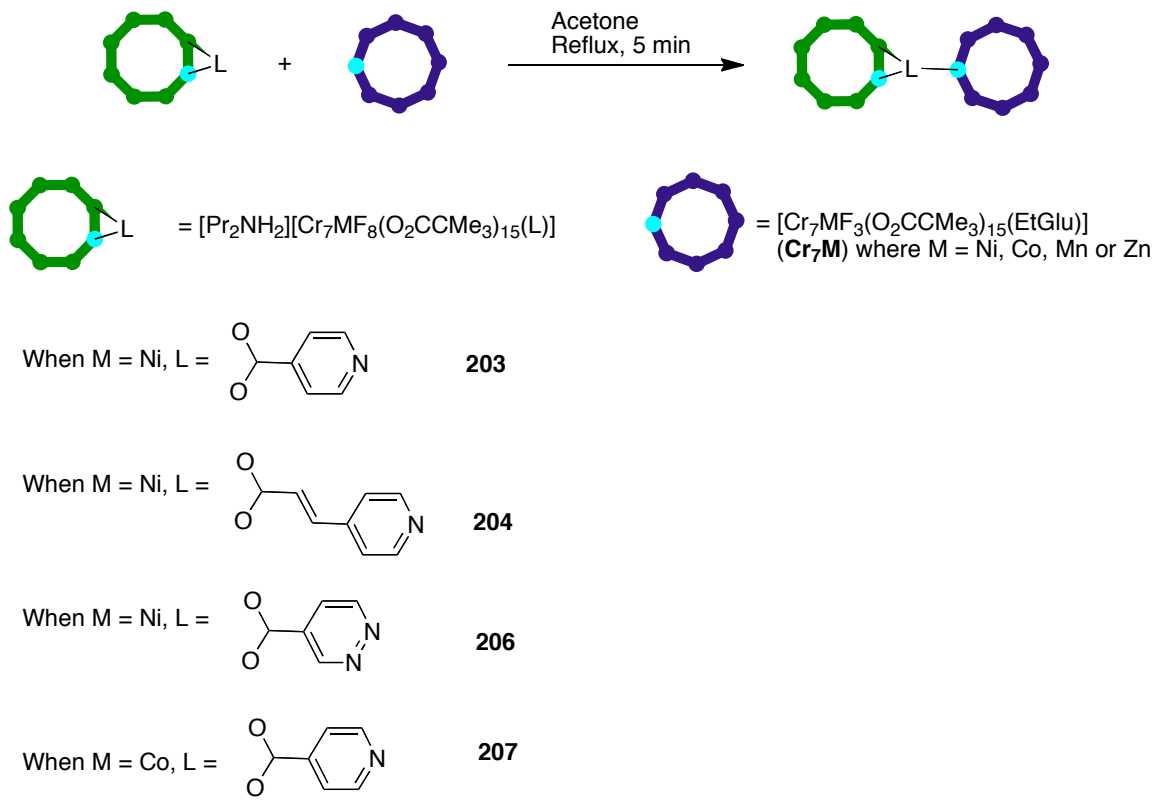

Scheme 21. General procedure for mixed wheel synthesis.

The reaction of **401** was also repeated on a larger scale, where it was found possible to speed up the product formation by stirring the reaction mixture for an hour instead of allowing it to sit covered until crystals formed. The powder formed was proven to be pure by elemental analysis, however crystals suitable for x-ray diffraction were not obtained by this method.

Table 6. Guide to coding of reactions attempted.

↓PW/GW→	203	204	206	207
Cr_7Ni	401	402	403	404
Cr_7Co	405	406	407	408
Cr_7Mn	409	410	---[a]	411
Cr_7Zn	412	413	---[a]	414

[a] Desired product not isolated.

Most of the reactions were successful, but two crystal structures obtained on the products obtained from reactions with the 4-pyd substituted GW **206** showed that the desired mixed-wheel systems did not form. Attempted reactions with the Cr_7Mn and Cr_7Zn PWs lead to only co-crystallisation of the starting materials, with no actual links formed between the two wheels.

4.3.2 Mass Spectrometry Studies

One method of characterisation used with these wheel systems at The University of Manchester is Electrospray mass spectrometry. As mentioned in Chapters 2 and 3, systems containing two wheels are too large to be detected in their entirety, but it is possible to identify peaks characteristic of various fragments. The spectral region between 2200 and 2400 Da contains peaks relating to $[GW]^+$, $[GWNa]^+$, $[PW - H_2O]^+$ and $[PW - H_2O + Na]^+$. The presence of a peak corresponding to the green wheel does not confirm anything about the linked arrangement of the system, but the presence of a peak for a purple wheel without a water (or acetone) molecule implies an originally linked arrangement.

In order to further characterise this type of linked wheel system by mass spectrometry, a representative example (**402**) was also sent to Huddersfield to be studied by Dr Lindsay Harding. The results show that as well as the peaks in the 2200–2400 Da region, a large peak is also visible at 4544 Da, indicative of $[MNa]^+$. This observation confirms that the

wheels remain linked even in solution. It is anticipated that related studies with the other linked-wheel compounds described in this chapter would give similar results.

4.3.3 UV-VIS Spectroscopy

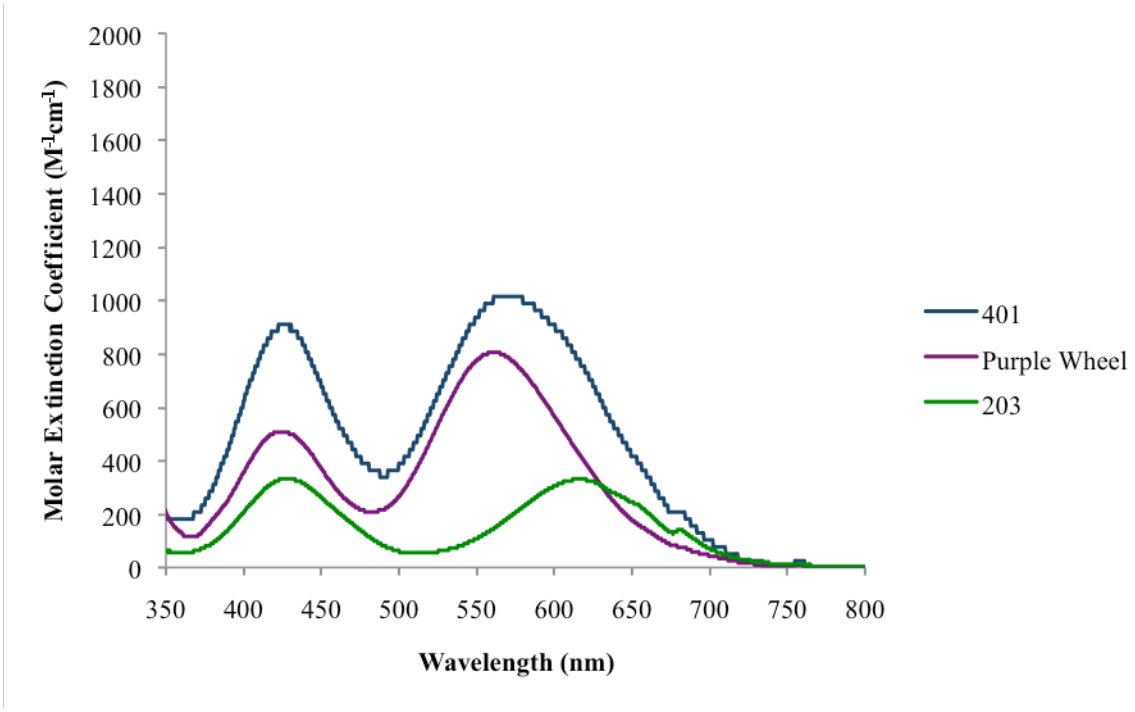

Figure 72. UV-vis spectra of **401** and its components.

The UV-vis spectra of **401** and its component wheels (Figure 72) were run in dichloromethane and directly compared. In all cases, two peaks can be observed between 400 and 700 nm, which are assigned to d-d transitions, and as expected show weak intensities as they are Laporte forbidden. As can be seen in Figure 73, the spectrum for the linked-wheel system corresponds with a pure summation of those of the two starting materials, showing that linking the wheels together has no effect on their electronic transitions.

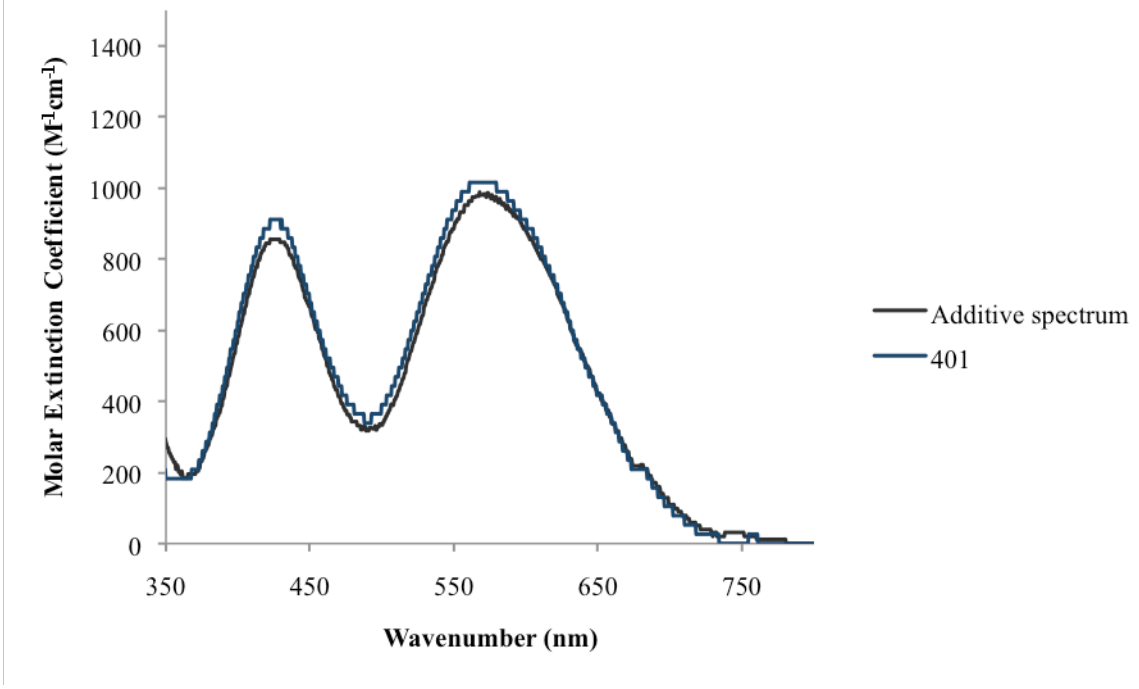

Figure 73. Additive spectrum of the two starting materials against the spectrum of **401**.

The UV-vis spectra of **402** and its starting materials were also studied (Figure 74). Once again an additive effect is observed, so it is anticipated that such behaviour will be seen for all mixed-wheel systems of this type.

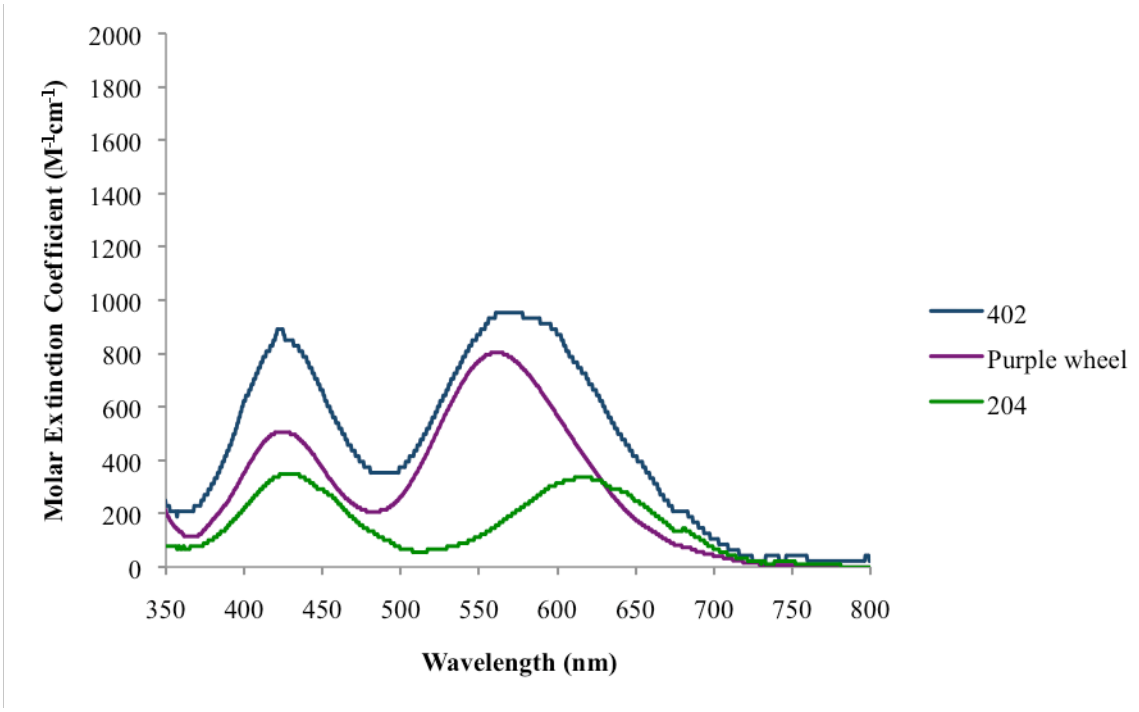

Figure 74. UV-vis spectra of **402** and its components.

4.3.4 EPR Studies

While the interactions between these wheels are not strong enough to be detected using SQUID analysis, EPR spectroscopy is a more sensitive technique that can afford useful information.

The EPR spectra of **401**–**403** can be seen in Figure 75. All three spectra are modelled on the same spin-Hamiltonian parameters (Equation 8), with $S_{eff} = 1$.

Equation 8:

$$\hat{H}_S = \mu_B \mathbf{B}\mathbf{g}\hat{S} + D\left[\hat{S}_Z^2 - \frac{S(S+1)}{3}\right]$$

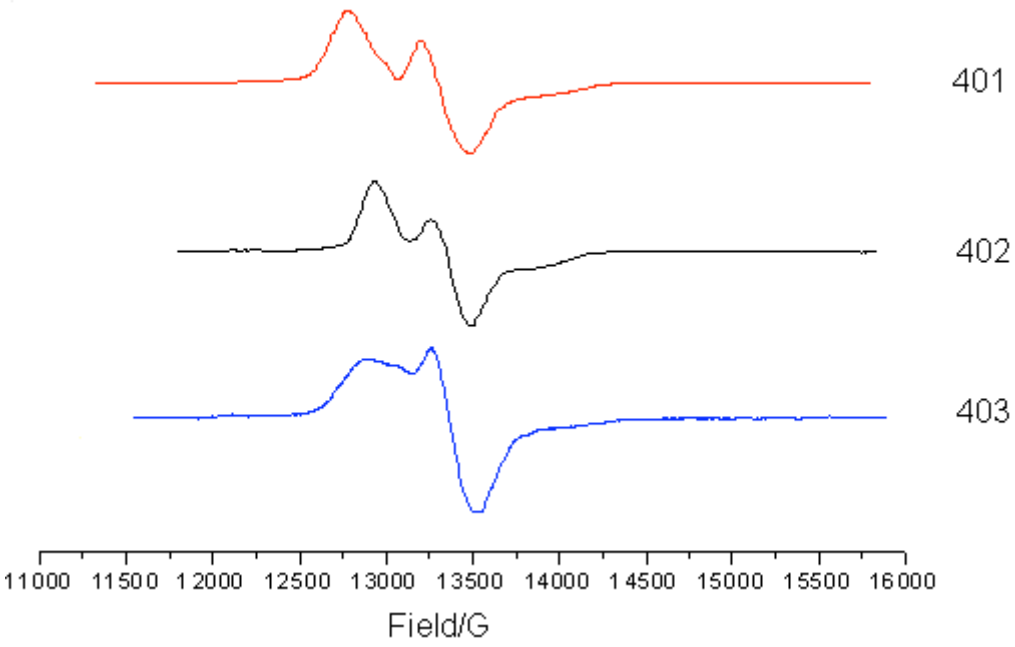

Figure 75. EPR spectra of **401**–**403**.

As can be seen in Figure 76, the simulated spectrum of **403** does not match well with the experimental spectrum. This observation could result from a number of factors, for example it is possible that the compound is rhombic. An alternative suggestion is that the product was perhaps slightly less crystalline than the other linked-wheel systems. It is known that some compounds give different EPR spectra if they are in a powder as

opposed to a crystalline form, which may allow the parameters to better fit the experimental result.

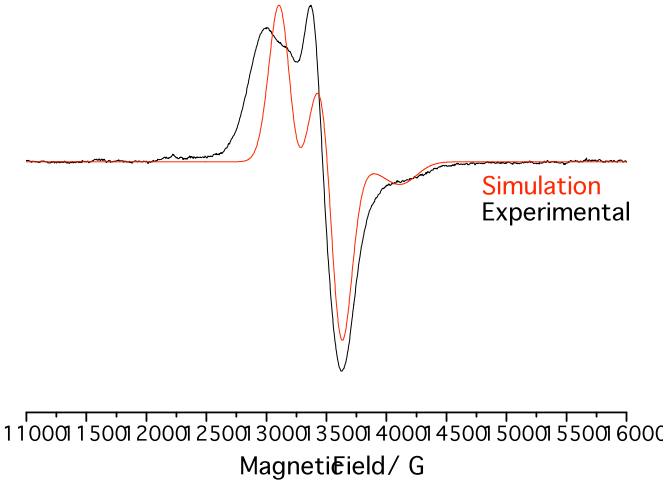

Figure 76. EPR spectrum of **403** and its simulation using the parameters below.

Table 7. EPR parameters for **401**–**403**.

	401	**402**	**403**
g_x	1.82	1.818	1.824
g_y	1.82	1.818	1.824
g_z	1.79	1.8	1.78
Line Widths (G)	120 (isotropic)	x = y =100 ≠ z = 120	x = y = 100 ≠ z = 140
D (cm^{-1})	+0.057	+0.042	+0.036

Table 7 shows the parameters used to obtain the three simulated spectra. As explained above, the parameters used to ascertain the simulation for **403** are not very reliable and more work must be undertaken to improve these results. However, from these results it appears that the strongest interaction between wheels is observed for **401**, as indicated by its relatively large zero field splitting (D value). The smallest D value, and hence the weakest interaction, is observed for **403**; this is interesting as the only structural difference in structure between **401** and **403** is the presence of an N instead of a CH in the ortho position of the pyridyl ring. It may be the case that the greater localisation of electrons within a pyridazine as opposed to a pyridine ring inhibits the interaction

between the wheels. This hypothesis can be supported by previous structural studies on pyridazine,[115] which show unexpected changes in bond length around the ring, not seen in a ring with full aromatic delocalisation.

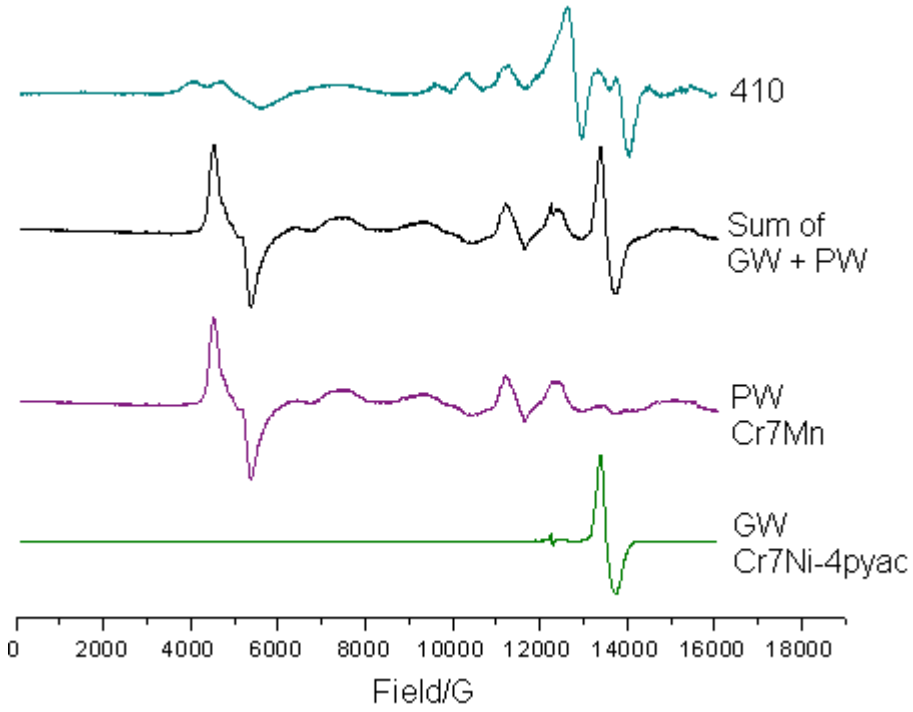

Figure 77. EPR Spectra of **410** and its starting materials.

Figure 77 shows the spectra of **410** and its precursors, together with the summation of the latter spectra. The purple wheel used in this synthesis is Cr_7Mn, with $S_{eff} = 1$ (S of $Mn^{II} = {}^5/_2$). The spectrum of **410** is very different to the sum of those of its starting materials, indicating that some interaction occurs between the wheels. Variable temperature EPR studies will be necessary in order to clarify whether the low-lying $S_{eff} = 2$ excited state of the Cr_7Mn wheel influences the spectra observed.

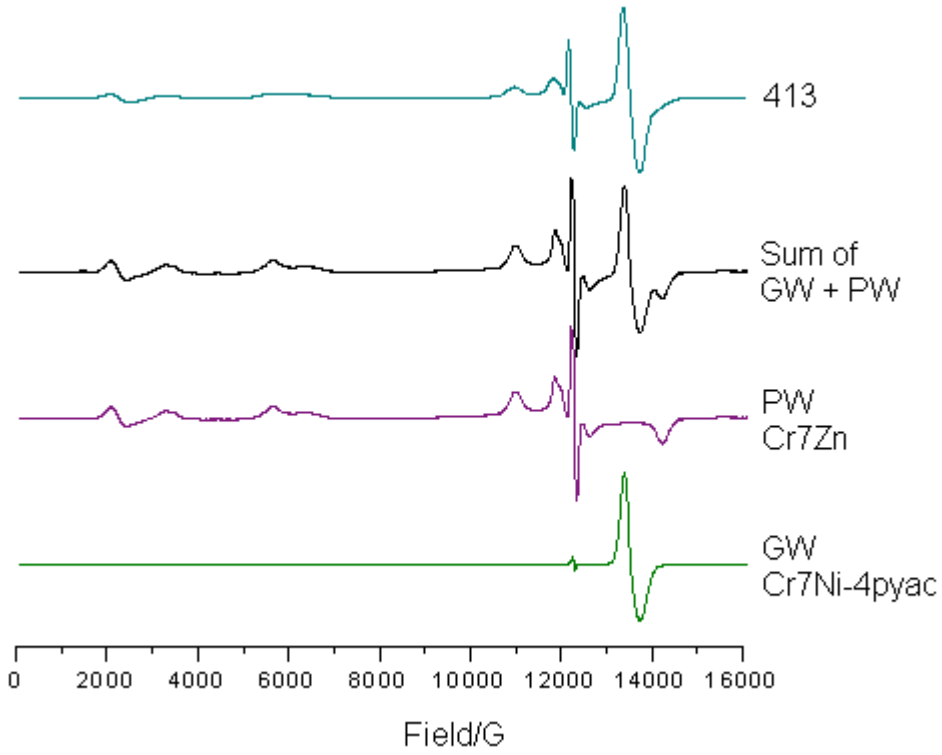

Figure 78. EPR spectra of **413** and its starting materials.

In contrast, the spectrum of compound **413** (Figure 78) is virtually identical to the sum of those of its starting materials, indicating no interaction occurring between the wheels. The only difference between this and **410** is the divalent metal. Zn^{2+} has a full d-subshell, as opposed to Mn^{2+}, thus preventing interaction occurring between the two wheels.

4.3.5 X-Ray Crystallography

Crystal structures were obtained for seven of the new linked-wheel systems (**401**, **402**, **405**, **407**, **409**, **412** and **413**), confirming their expected molecular structures. Two of these structures (**401** and **402**) have been finished and are discussed below, while the others are all very similar so were not deemed worthy of further work. For simplification purposes, the ^{t}Bu groups of the pivalate ligands have not been shown.

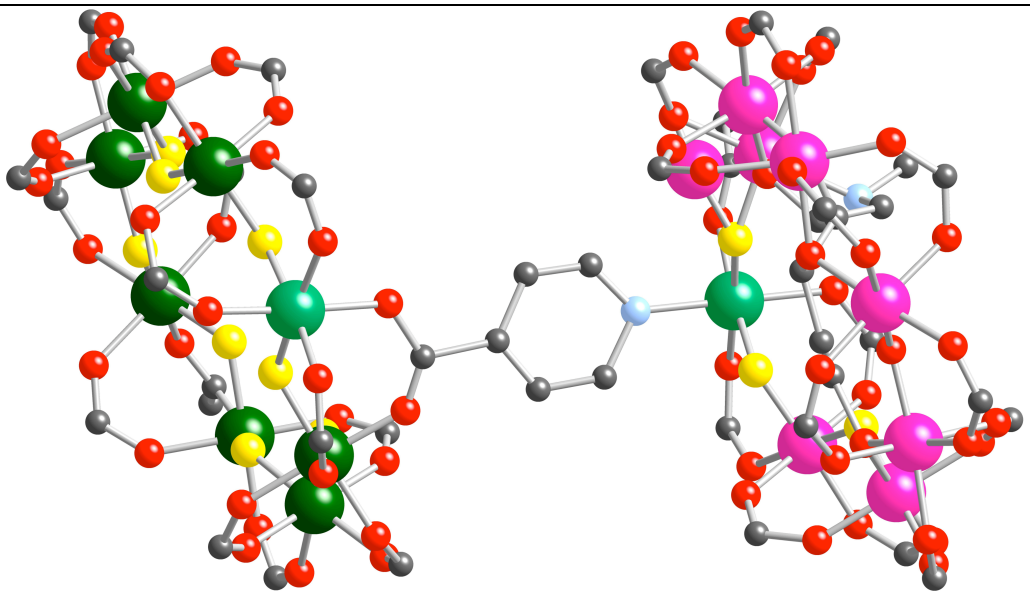

Figure 79. Crystal Structure representation of **401**.

Both crystal structures are monoclinic and adopt the P_12_11 space group. Both have normal Ni–N bond distances in the range 2.03–2.06 Å. The largest difference between the two structures is the relative arrangement of the wheels. In **401** (Figure 79) the wheels are arranged in a transoid orientation, whereas in **402** (Figure 80) they are positioned cis to each other.

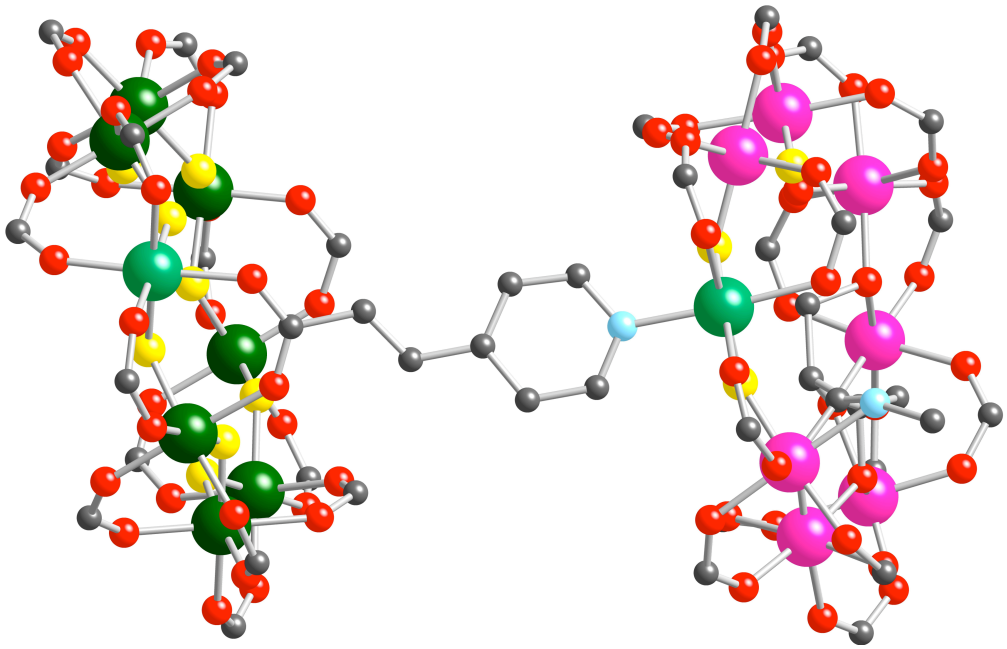

Figure 80. Crystal structure representation of **402**.

4.4 CONCLUSIONS

Purple and green wheels have been successfully linked together in a simple synthetic procedure, and characterised by elemental analysis, mass spectrometry and, in certain cases, X-ray crystallography. Two reactions involving **206** as a starting material were unsuccessful, maybe as a result of the relatively poor monodentate coordinating abilities of the 4-pyridazine carboxylate ligand.

Interaction between the wheels in these systems is weak, and thus has not been detected using SQUID or INS studies. However interaction has been observed using EPR spectroscopy. The strength of interaction decreases in a predictable manner when the link is extended from ISNA to 4-pyac. Using a 4-pyd ring as a link (in **403**) gives the weakest interactions. This observation may be attributable to decreased delocalisation of electrons within the ring, hindering communication between the wheels. Interaction has also been observed via EPR between a Cr_7Ni green wheel and a Cr_7Mn purple wheel, but no interaction is observed when using a Cr_7Zn purple wheel.

4.5 FURTHER WORK

This series of mixed-colour and mixed-metallic wheels merits further studies. To date, studies have involved Cr_7M (M = Ni, Co, Mn and Zn) purple wheels, but only Cr_7Ni and Cr_7Co green wheel systems. By expanding the series of mixed-metal systems to include Cr_7Mn and Cr_7Zn green wheels it would be possible to assess whether interactions occur when Cr_7Zn green wheels are used as opposed to their purple analogues. This may be the case, as in the green wheel systems the linkage is across two metal centres, not only the Zn^{II} ion.

Another possibility would be to synthesise some potentially switchable mixed-wheel systems related to the Ru and Re-containing systems considered in Chapters 2 and 3, some examples of which may be seen in Figure 81. The properties of these species could be compared informatively with those containing two green or two purple wheels.

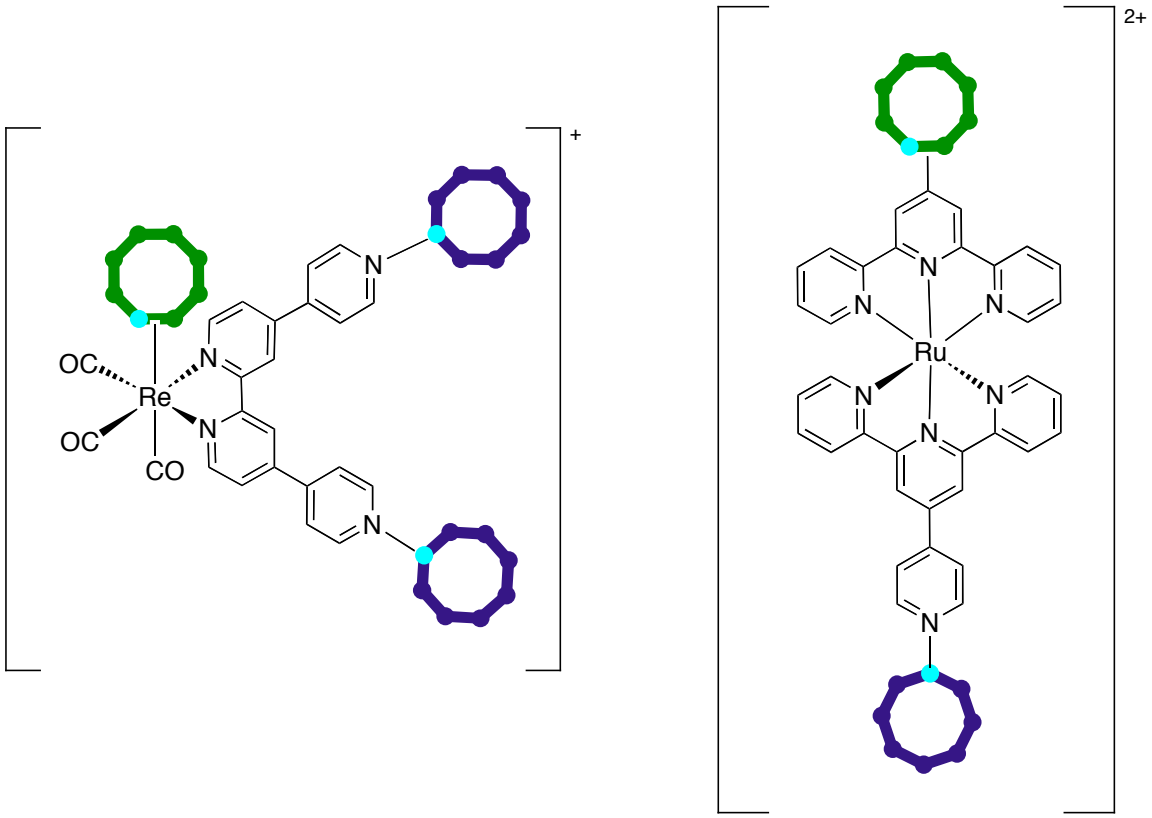

Figure 81. Some target mixed-wheel systems.

Chapter 5 – Linked Wheels through Hydrogen Bonds

5.1 INTRODUCTION

The first examples of linked wheel systems produced by the Winpenny group involved templating two wheels about a simple linear diamine template, such as 1,8-diaminooctane, 1,9-diaminononane and 1,12-diaminododecane.[2] Reactions were carried out in a fashion identical to the synthesis of individual wheels, allowing the formation of two heterometallic wheels around one template. An example of one of these linked wheel systems can be seen in Figure 82.

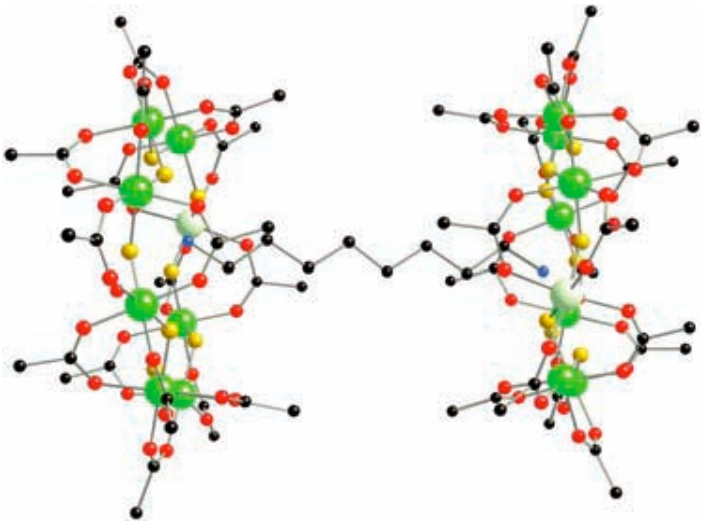

Figure 82. Two Cr_7Ni wheels linked through 1,8-diaminooctane.[2]

Another approach used to link wheels together indirectly was to synthesise a wheel templated about a functionalised secondary amine, such as 4-(ethylaminomethyl)pyridine, and to use the pyridyl group on the template to co-ordinate two wheels to transition metal centres. Primarily, such linked wheel systems were made with first row transition metal dimers,[62] giving products of general formula $M_2(O_2CCMe_3)_4([PyCH_2NH_2Et][Cr_7NiF_8(O_2CCMe_3)_{16}])_2$ (where M = Cu, Ni or Co). Addition of the pre-made wheels to the metal dimer, $M(O_2CCMe_3)_4(L)_2$ (L = H_2O or HO_2CCMe_3) in toluene or diethyl ether, followed by gentle evaporation of the solvents produced X-ray diffraction-quality crystals. An example of such a system can be seen in Figure 83. Further to the synthesis of these compounds, coordination to Ru dimers was also achieved in a similar fashion.[64]

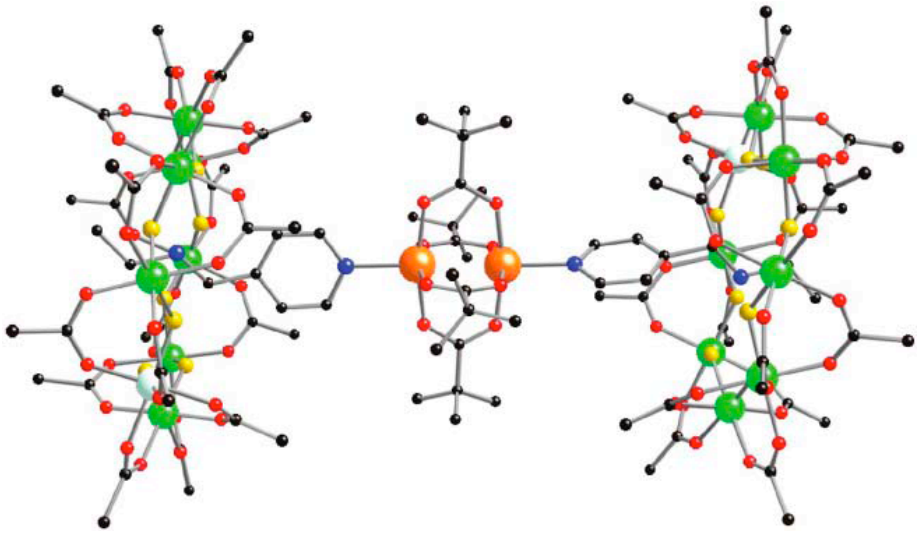

Figure 83. Cr_7Ni wheels linked together indirectly through metal dimers.[64]

Wheels were also linked through a single Cu centre,[64] the crystal structure showing a trans coordination geometry (Figure 84). These wheels are clearly too sterically bulky to be linked in a cis conformation when joined by such a small connecting unit.

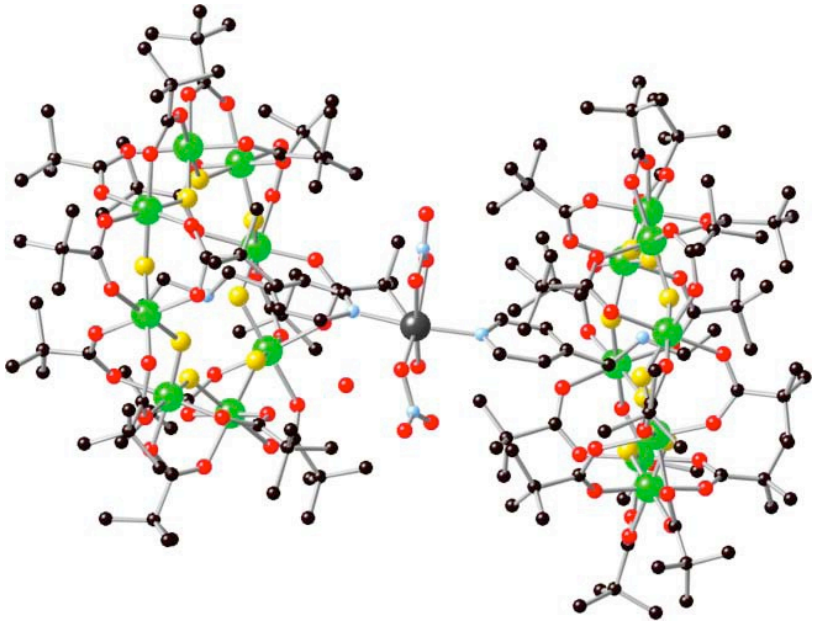

Figure 84. Cr_7Ni wheels linked together indirectly through a single Cu centre.[64]

All of these linked wheel systems were synthesised by using simple procedures and minimal heat, with low boiling solvents. Recrystallisation was the sole means of purification and X-ray diffraction-quality crystals were obtained either directly by gentle

evaporation of the reaction mixture, or as an independent step following removal of the reaction solvent.

A variety of organic compounds and transition metal complexes (Figure 85), which display either redox or photoactivity, were considered as potential linker molecules for the wheels.

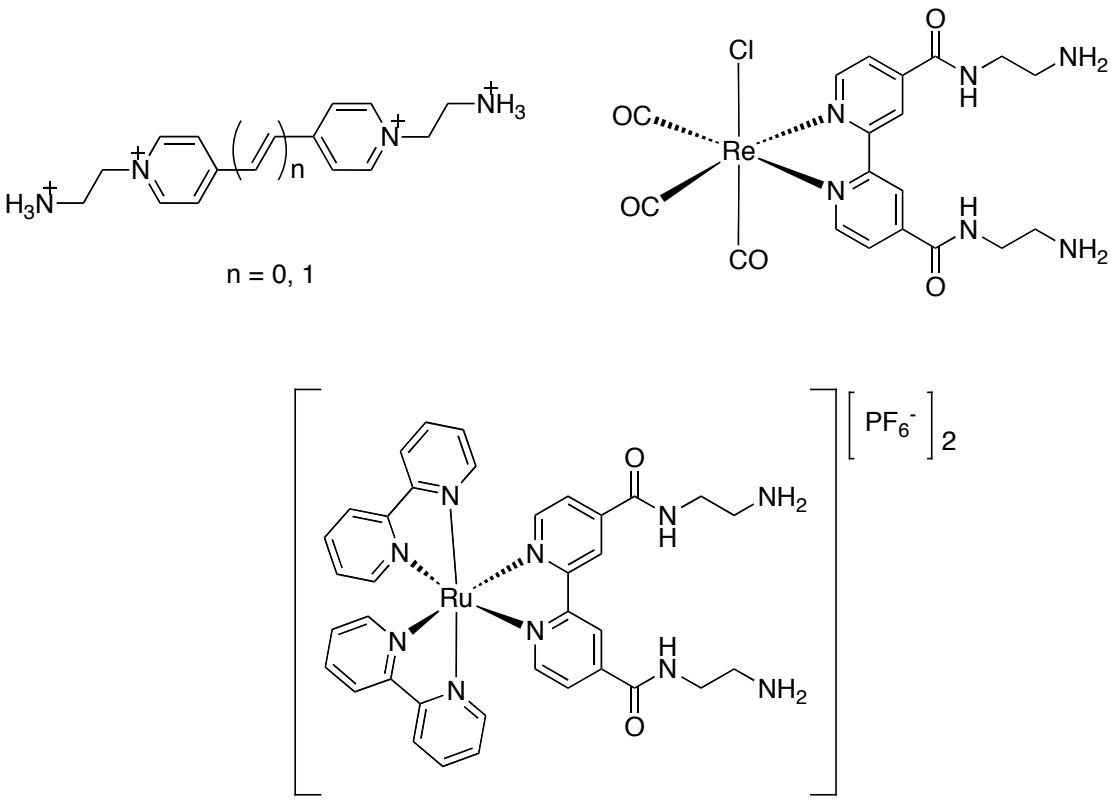

Figure 85. A selection of target linker molecules.

Diquaternary 4,4′-bipyridyl derivatives were considered as potential target linker molecules due to their reversible reductive electrochemistry.[80] Such species are best known as viologens as upon undergoing the first of two possible one-electron reductions they become a mono radical cation, which is an intense blue colour. Upon further reduction, a quinoid is produced which is yellow. The first reduction is of particular interest to this project as the production of an unpaired electron may enable an alteration in the communication occurring between the wheels. The other advantage of using viologens as linkers is that their excited state lifetimes are in the nano-second (ns) scale, making them long-lived enough to affect the interaction. There are numerous papers

reporting the synthesis of bis-quaternised bipyridyl derivatives in the literature, making them an ideal starting point for synthetic studies.[116,117]

Another class of linker template molecules considered are MLCT chromophore-containing Ru^{II} and Re^{I} complexes. It is well established that $[Ru^{II}(bpy)_3]^{2+}$ and *fac*-$Re^{I}Cl(CO)_3(bpy)$ derivatives show long-lived MLCT excited states. $[Ru^{II}(bpy)_3]^{2+}$ derivatives are also known to undergo fully reversible $Ru^{III/II}$ oxidation processes. Coe *et al.* have synthesised the mono-substituted versions of these target linker molecules using 4-carboxy-4′-methyl-2,2′-bipyridine as a starting material.[118] There are also procedures in the literature whereby 4,4′-carboxy-2,2′-bipyridine has been used to synthesise a bis-amide system.[119]

The aims of the project were to identify and synthesise a variety of organic molecules and co-ordination complexes that possess long-lived photo-excited states and/or reversible redox properties. These switchable molecules are intended to act as templates for $[Cr_7NiF_8(O_2CCMe_3)_{16}]^-$ wheels and thus must also contain two terminal amine groups. The molecule may be used as a template to form a linked wheel system directly, or in a substitution reaction to replace the initially used template. A second method to link the wheels together indirectly is to synthesise a wheel templated about an amine with a pendant pyridyl group and to co-ordinate two of these to a metal centre which shows redox and/or photo-activity. Finally, the synthesis and studies of the Cr_7Co analogues of these heterometallic wheels is considered, in order to assess the suitability of ^1H NMR as an analytical tool for these compounds.

5.2 EXPERIMENTAL PROCEDURES

5.2.1 Materials and Procedures

The compounds 4,4′-bis-(carboxy)-2,2′-bipyridine[120], *cis*-bis(2,2′-bipyridine)ruthenium (II) dichloride[86], [4,4′-bis(carboxy)-2,2′-bipyridine]bis(2,2′-bipyridine)ruthenium(II) dichloride[119], $[PyCH_2NH_2Et][Cr_7NiF_8(O_2CCMe_3)_{16}]$[62], $[Pr_2NH_2][Cr_7NiF_8(O_2CCMe_3)_{16}]$[5], $[PyCH_2NH_2Et][Cr_7NiF_8(O_2CCMe_3)_{15}(O_2CPy)]$[62], $[PyCH_2NH_2Et][Cr_7CoF_8(O_2CCMe_3)_{16}]$[62], *fac*-$ReCl(CO)_3(bpy)$[121] and *fac*-$[Re(MeCN)(CO)_3(bpy)]$ $[CF_3SO_3]$[122] were synthesised by previously established methods. They were obtained in yields similar to those of the literature preparations and their identities were confirmed by ^1H NMR spectroscopy, electrospray mass spectrometry and elemental analysis. All other starting materials were purchased commercially and used as supplied.

5.2.2 Physical Measurements

All ^1H NMR spectra were recorded on Bruker Ultrashield 500 MHz or 300 MHz spectrometers. Paramagnetic ^1H NMR spectra were run by Dr Louise Natrajan and Mr Thomas Faust on a Bruker Advance 400 MHz spectrometer at The University of Manchester. Mass spectra were obtained using either electrospray or MALDI analysis on a Micromass Platform spectrometer. Elemental analyses were performed by the Microanalytical Laboratory, University of Manchester. IR data were recorded using a Varian Bio-Rad Excalibur series IR instrument and UV data was recorded on a Shimadzu UV-2401 PC UV-VIS spectrophotometer. Cyclic voltammetry was run in 0.1 M $[NBu^n_4][PF_6]$ in acetonitrile at a Pt disc working electrode with a scan rate of 200 mV s^{-1}.

5.2.3 Syntheses

N,N′-Bis-(2-aminoethyl)-4,4′-bipyridinium tetrabromide 501

4,4′-Bipyridine (255 mg, 1.63 mmol) was added to a refluxing solution of 2-bromoethylamine hydrobromide (926 mg, 4.52 mmol) in acetonitrile (25 ml) and the reaction refluxed for 96 h, affording a yellow precipitate. The solution was allowed to cool to room temperature and then filtered. The precipitate was washed with acetonitrile and diethyl ether and then allowed to dry under vacuum. Purification was achieved by dissolving the impure product in a 2:1 mixture of water and DMF at 80 °C and then adding acetone to give the pure product as a precipitate, which was once again collected by filtration, washed with acetone and dried under vacuum. Yield: 517 mg (56%). ^{1}H NMR (D_2O) δ_H/ppm: 3.68 (4H, t, J = 4.0 Hz, CH_2), 5.00 (4H, t, J = 8.0 Hz, CH_2), 8.55 (4H, d, J = 6.9 Hz, bpy), 9.14 (4H, d, J = 6.4 Hz, bpy). Elemental analysis calcd. (%) for $C_{14}H_{22}Br_4N_4 \bullet H_2O$: C 28.79, H 4.14, N 9.59. Found: C 28.58, H 3.98, N 9.45.

N-(2-aminoethyl)-4,4′-bipyridinium dibromide 502

4,4′-Bipyridine (817 mg, 5.23 mmol) was added to a refluxing solution of 2-bromoethylamine hydrobromide (372 mg, 1.82 mmol) in acetonitrile (25 ml) and the solution was refluxed for 18 h, affording a cream coloured precipitate. The solution was allowed to cool to room temperature and then filtered. The precipitate was washed with acetonitrile and diethyl ether and then allowed to dry under vacuum. Purification was achieved by dissolving the impure product in minimal water and then adding acetone to give a precipitate, which was collected by filtration, washed with acetone and dried under vacuum. Yield: 515 mg (75%); ^{1}H NMR (D_2O) δ_H/ppm: 3.65 (2H, t, J = 7.1 Hz, CH_2), 4.93 (2H, t, J = 6.8 Hz, CH_2), 7.83 (2H, d, J = 6.5 Hz, bpy), 8.40 (2H, d, J = 7.1 Hz, bpy), 8.69 (2H, d, J = 5.8 Hz, bpy), 8.96 (2H, d, J = 7.1 Hz, bpy). +ve electrospray: *m/z*: 200.2 $[M - 2Br]^{2+}$. –ve electrospray: *m/z*: 279.1 $[M - Br]^-$, 360.3 $[M - H]^-$. Elemental analysis calcd. (%) for $C_{12}H_{15}Br_2N_3 \bullet H_2O$: C 38.02, H 4.52, N 11.08. Found: C 37.85, H 4.12, N 11.08.

N-(2-aminoethyl)-trans-1,2-bis(4-pyridyl)ethylene dibromide 503

This compound was prepared and purified in a manner identical to *N*-(2-aminoethyl)-4,4′-bipyridinium dibromide, but using *E*-1,2-bis(4-pyridyl)ethylene (632 mg, 4.20 mmol) instead of 4,4′-bipyridine and 2-bromoethylamine hydrobromide (293 mg, 1.43 mmol) in acetonitrile (35 ml). A cream coloured solid was obtained. Yield: 166 mg (29%); ^{1}H NMR (D_2O) δ_H/ppm: 3.60 (2H, t, J = 6.7 Hz, CH_2), 4.82 (2H, t, J = 7.1 Hz, CH_2), 7.47 (1H, d, J = 16.3 Hz, CH), 7.59 (2H, d, J = 3.6 Hz, bpy), 7.66 (1H, d, J = 16.5 Hz, CH), 8.10 (2H, d, J = 6.2 Hz, bpy), 8.45 (2H, d, J = 5.3 Hz, bpy), 8.73 (2H, d, J = 8.9 Hz, bpy). Elemental analysis calcd. (%) for $C_{14}H_{17}Br_2N_3$•$0.5H_2O$: C 42.45, H 4.58, N 10.61. Found: C 42.42, H 4.21, N 10.60.

2-(tert-Butoxycarbonylamino)ethylammonium)4,4′-bis-(carboxylato)-2,2′-bipyridine 505

Thionyl chloride (2 ml) was added dropwise over 10 min to a suspension of 4,4′-bis-(carboxy)-2,2′-bipyridine (122 mg, 0.500 mmol) in dichloromethane (2 ml). The mixture was stirred at room temperature for 5 h and the solvent was removed under vacuum. The crude acid chloride was dissolved in dry dichloromethane (10 ml) and added over approximately 1 min to a solution of *N*-(*tert*-butoxycarbonyl)-1,2-diaminoethane (243 mg, 1.52 mmol) and triethylamine (327 mg, 3.23 mmol) in dry dichloromethane (10 ml). The reaction was allowed to stir for 4 h, during which time the product formed as a pink precipitate. The precipitate was collected by filtration, washed with dichloromethane and diethyl ether and dried under vacuum. Yield 168 mg (60%); ^{1}H NMR ($(CD_3)_2SO$) δ_H/ppm: 1.36 (18H, s, ^{t}Bu), 2.85 (4H, t, J = 5.5 Hz, CH_2), 3.18 (4H, d, J = 4.8 Hz, CH_2), 7.14 (2H, br s, NH), 7.73 (2H, d, J = 3.8 Hz, bpy), 8.65 (2H, d, J = 7.6 Hz, bpy), 8.76 (2H, s, bpy). +ve electrospray: m/z = 161 (protonated N-(BOC)-1,2-diaminoethane). –ve electrospray: m/z = 243 (mono-deprotonated 4,4′-bis-(carboxy)-2,2′-bipyridine). υ_{max}/cm^{-1}: 3236 (w), 3147 (m), 3068 (m), 2994 (m), 2976 (m), 2881 (m), 2136 (w), 1685 (s, C=O), 1643 (s, C=O), 1582 (s), 1542 (s). Elemental analysis calcd. (%) for $C_{26}H_{40}N_6O_8$: C 55.31, H 7.14, N 14.88. Found: C 55.17, H 7.31, N 14.83.

4,4′-bis-(carbonylamino(2-(tert-butoxycarbonylamino)ethyl))-2,2′-bipyridyl 506

N-(*tert*-butoxycarbonyl)-1,2-diaminoethane (397 mg, 2.48 mmol), 1-hydroxybenzotriazole (HOBT, 452 mg, 3.35 mmol)) and *N*,*N*′-diisopropylcarbodiimide (DIC, 1 ml, 6.62 mmol) were added to a stirred solution of 4,4′-bis(carboxy)-2,2′-bipyridine (256 mg, 1.05 mmol) in dry DMSO (12.5 ml). The reaction was allowed to stir for 24 h, during which time the product formed as a precipitate. The precipitate was collected by filtration, washed with DMSO then acetone, affording the product as a white powder which was dried under vacuum. Yield 354 mg (60%); ^{1}H NMR ($(CD_3)_2NC(D)O$) δ_H/ppm: 1.58 (18H, s, ^{t}Bu), 3.53 (4H, m, CH_2), 3.73 (4H, m, CH_2), 7.15 (2H, m, NH), 8.12 (2H, m, bpy), 9.08 (2H, d, J = 5.5 Hz, bpy), 9.13 (2H, s, bpy), 9.25 (2H, m, NH). MALDI-MS: m/z = 529 $[MH]^+$, 551 $[MNa]^+$, 656, 445, 413, 413, 379, 301, 250. υ_{max} (cm^{-1}):3355 (s), 3303 (s), 3061 (w), 2983 (m), 2936 (m), 1695 (s) (C=O), 1648 (s) (C=O), 1592 (m), 1537 (br, s). Elemental analysis calcd. (%) for $C_{26}H_{36}N_6O_6$•0.4Me_2SO: C 57.50, H 6.91, N 15.01. Found: C 57.45, H 6.89, N 15.34.

(4,4′-Bis(carboxyl(2-(tert-butoxycarbonylamino)ethyl)-2,2′-bipyridine)bis(2,2′-bipyridine)ruthenium(II) bis(hexafluorophosphate) 509

4,4′-Bis-(carbonylamino(2-(*tert*-butoxycarbonylamino)ethyl))-2,2′-bipyridyl•0.4Me_2SO (403 mg, 0.775 mmol) was added to *cis*-$Ru^{II}Cl_2$(bpy)•2H_2O (454 mg, 0.812 mmol) in 9:1 ethanol/water (70 ml). The resulting solution was heated under reflux overnight to give a bright red solution. The solvents were removed under vacuum to give the product as the slightly impure chloride salt. Purification was effected by precipitation from minimal water with an excess of aqueous NH_4PF_6. The solid was then filtered off and washed with water to give the product as an orange red powder. Yield: 757 mg (74%); ^{1}H NMR ($(CD_3)_2CO$) δ_H/ppm: 1.35 (18H, s, ^{t}Bu), 3.32 (4H, d, J = 5.3 Hz, CH_2), 3.53 (4H, d, J = 6.6 Hz, CH_2), 6.24 (2H, m, NH), 7.60 (4H, m, bpy), 7.94 (2H, d, J = 4.5 Hz, bpy), 8.09 (4H, dd, J_1 = 5.9 Hz, J_2 = 4.9 Hz), 8.27 (6H, m, bpy) 8.44 (2H, s, NH), 8.85 (4H, d, J = 8.1 Hz, bpy), 9.18 (2H, s, bpy). +ve electrospray: m/z = 1087 $[(M - PF_6)]^+$, 470 $[(M–2PF_6)]^{2+}$. –ve electrospray: m/z = 145 $[PF_6]^-$. υ_{max} (cm^{-1}): 3435, 2978, 1670 (C=O), 839 (PF_6). λ_{max} (ε/mol^{-1} dm^3 cm^{-1}): 466 (14 100), 351 (9 800), 288 (66 500), 247 (31 400).

Elemental analysis calcd. (%) for $C_{46}H_{52}F_{12}N_{10}O_6P_2Ru•H_2O$: C 44.20, H 4.35, N 11.21. Found: C 43.91, H 4.16, N 11.08.

Tricarbonyl(4,4′-Bis(carboxyl(2-(tert-butoxycarbonylamino)ethyl)-2,2′-bipyridine)chlororhenium(I) 511

4,4′-Bis-(carbonylamino(2-(*tert*-butoxycarbonylamino)ethyl))-2,2′-bipyridyl•0.4Me_2SO (184 mg, 0.329 mmol) was added to $Re^{I}Cl(CO)_5$ (105 mg, 0.290 mmol) in methanol (15 ml) and the solution heated under reflux for 6 h, during which time it became a bright orange colour. The reaction was allowed to cool and the solvent was removed under vacuum. Purification was achieved by reprecipitation from DMF and water, allowing the slightly impure product to be collected as a bright orange solid, washed with water and then dried under vacuum. Yield: 206 mg (85%); ^{1}H NMR ($(CD_3)_2NCDO$) δ_H/ppm: 1.58 (18H, s, ^{t}Bu), 3.54 (4H, d, J = 7.5 Hz, CH_2), 3.75 (4H, d, J = 6.2 Hz, CH_2), 7.18 (2H, s, broad NH), 8.43 (2H, d, J = 6.2 Hz, bpy), 9.40 (2H, s, bpy), 9.49 (2H, s, NH), 9.54 (2H, d, J = 5.0 Hz, bpy). +ve electrospray: m/z = 857 $[MNa]^+$. –ve electrospray: m/z = 833 $[M – H]^-$. υ_{max} (cm^{-1}): 2026 (CO), 1919 (CO), 1880 (CO), 1656 (CO). λ_{max} (ε/mol^{-1} dm^3 cm^{-1}): 398 (4 400), 304 (16 800), 245 (26 400). Elemental analysis calcd. (%) for $C_{29}H_{36}ClN_6O_9Re·3H_2O$: C 39.21, H 4.77, N 9.46, Re 20.96. Found: C 39.19, H 4.55, N 9.34, Re 20.89.

Reaction of $Re^{I}Cl(CO)_5$ and $[PyCH_2NH_2Et][Cr_7NiF_8(Me_3CCO_2)_{16}]$ 516

$Re^{I}Cl(CO)_5$ (37.9 mg, 0.105 mmol) and $[PyCH_2NH_2Et][Cr_7NiF_8(Me_3CCO_2)_{16}]$ (508 mg, 0.218 mmol) were refluxed in toluene (10 ml) for 32 h before the solvent was removed under vacuum. The impure product was placed on an activated neutral alumina column and eluted using toluene. The product was the first green band to be removed, leaving the green starting material on the column. Yield: 126 mg.

$Cu^{II}_2(O_2CCMe_3)_4([PyCH_2NH_2Et][Cr_7CoF_8(Me_3CCO_2)_{16}])_2$ 518

$Cr^{III}F_3 \bullet 4H_2O$ (3.02 g, 16.7 mmol), 4-(ethylaminomethyl)pyridine (0.336 g, 2.47 mmol) and pivalic acid (21.6 g, 213 mmol) were heated at 140 °C for 5 h. $[Co^{II}(Me_3CCO_2)_2]_n$ (0.660 g) was then added and the reaction was further heated for 24 h at 160 °C. The solution was cooled to room temperature and acetonitrile (100 ml) was added. After stirring for 2 h, the green precipitate was collected by filtration and washed with acetonitrile, then dried in a desiccator overnight. The solid was added to hexane (80 ml) and the mixture filtered to remove undissolved material. To this solution was added $Cu^{II}(O_2CC(Me_3)_4(HO_2CC(Me_3)_2$ (0.526 g, 0.71 mmol) dissolved in a minimum amount of hexane. The reaction mixture was stirred overnight at room temperature and then allowed to stand for a further 24 h, affording a green precipitate. The product was collected by filtration, washed with hexane until the filtrate became colourless and then dried under vacuum. Yield: 2.13 g (64% wrt Cu starting material). Elemental analysis calcd. (%) for $C_{196}H_{350}Co_2Cu_2Cr_{14}F_{16}N_4O_{72}$: C 45.34, H 6.79, N 1.08, Cr 14.02. Found: C 45.31, H 7.02, N 1.07, Cr 13.60.

$[PyCH_2NH_2Et][Cr_7CoF_8(Me_3CCO_2)_{16}]$ 517

To $Cu^{II}_2(O_2CCMe_3)_4([PyCH_2NH_2Et][Cr_7CoF_8(Me_3CCO_2)_{16}])_2$ (2.00 g, 0.38 mmol) dissolved in thf (60 ml) was added triethylamine (5 drops) and acetylacetone (4 ml). The mixture was heated at 60 °C for 15 min and then stirred at room temperature for a further 24 h. The solvent was removed under vacuum and the impure reaction mixture was washed with acetonitrile and filtered until the filtrate became colourless. The precipitate was then dried overnight under vacuum and recrystallisation was effected by evaporation of a toluene:thf (2:1) mixture at room temperature. Yield: 1.71 g (97%). +ve electrospray: *m/z*: 2352.6 $[MNa]^+$. –ve electrospray: *m/z*: 2329.7 $[M - H]^-$, 2191.5 $[M - PyCH_2NH_2Et]^-$. Elemental analysis calcd. (%) for $C_{88}H_{157}CoCr_7F_8N_2O_{32}$: C 45.36, H 6.79, N 1.20. Found: C 45.11, H 6.88, N 1.12.

N-(3-carboxyethyl)-4,4′-bipyridine hexafluorophosphate 519

To a refluxing solution of 3-bromopropionic acid (275 mg, 1.60 mmol) in acetonitrile (25 ml) was added 4,4′-bipyridine (769 mg, 4.80 mmol) in acetonitrile (5 ml). The solution was refluxed for 18 h affording a pale yellow precipitate, which was collected by filtration and washed with acetonitrile and diethyl ether before being dried under vacuum. Yield: 374 mg (76%). ^{1}H NMR ($(CD_3)_2CO$) δ_H/ppm: 3.23 (2H, t, J = 6.2 Hz, CH_2), 5.02 (2H, t, J = 6.2 Hz, CH_2), 7.87 (2H, d, J = 6.0 Hz, bpy), 8.55 (2H, d, J = 6.6 Hz, bpy), 8.75 (2H, d, J = 6.0 Hz, bpy), 9.24 (2H, d, J = 6.6 Hz, bpy). Elemental analysis calcd (%) for $C_{13}H_{13}BrN_2O_2 \bullet H_2O$: C 39.81, H 3.19, N 7.14. Found: C 40.16, H 3.28, N 7.43.

5.3 RESULTS AND DISCUSSION

5.3.1 Synthetic Studies

5.3.1.1 Synthesis of Linker Molecules

The first series of linker molecules considered are diquaternised derivatives of 4,4′-bipyridine (4,4′-bpy) or *E*-1,2-bis-(4-pyridyl)ethylene (bpe). Such molecules may show two reversible one-electron reduction processes. Related monoquaternised derivatives could also prove useful for our purposes, because it should be possible for their nonquaternised end to be complexed to redox and/or photoactive metal centres in order to link two wheels. Scheme 22 shows the syntheses of both di- and monoquaternised derivatives.

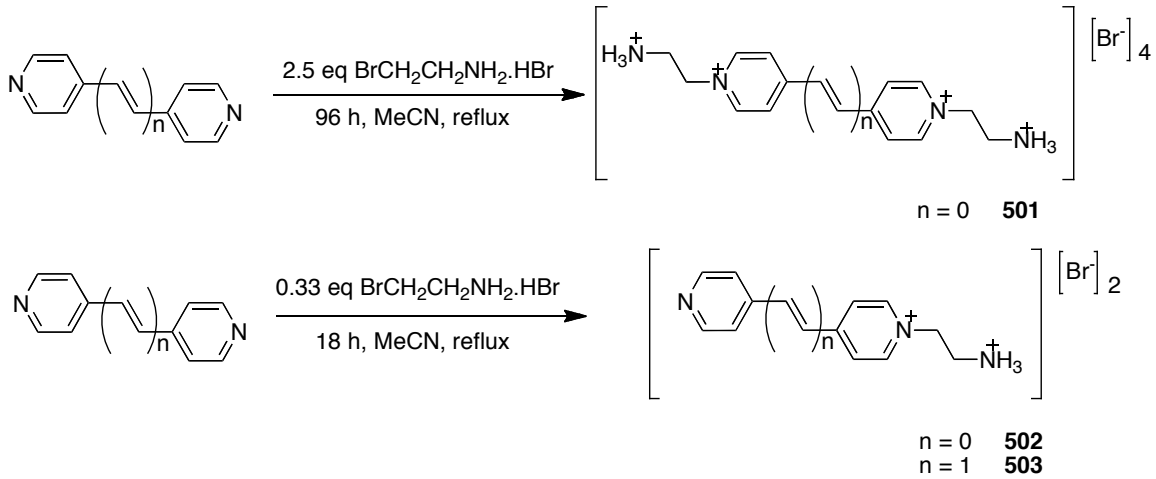

Scheme 22. Reactions used to synthesise quaternised 4,4′-bpy and bpe derivatives.

A previously published paper claimed that *N*,*N*′-bis-(2-aminoethyl)-4,4′-bipyridyl dibromide had been synthesised by reacting 4,4′-bpy with 2-bromoaminoethane hydrobromide in 50:50 DMF/water.[123] This method was attempted, using 2.5 equivalents of 2-bromoaminoethane hydrobromide to 1 equivalent of 4,4′-bpy, but results were unsatisfactory. Upon refluxing the reaction for a period of two days, a colour change was observed. The solution became a dark blue colour, indicating that the desired product may have formed (when such diquaternised bpy derivatives undergo a one-electron

reduction to a mono-cation radical they become a distinctive intense blue). Upon cooling, the solution reverted back to a yellow colour suggesting the reduction was reversible. However, after working up the reaction it appeared that a variety of products was formed as the ^{1}H NMR spectrum showed several sets of peaks. Furthermore, the impure reaction yield was low so the pure product yield would have been unsatisfactory.

As a result, steps were taken to improve on the proposed synthesis adapting from another literature procedure to prepare viologens,[124] this time using acetonitrile as the solvent. The reaction was attempted over a variety of times, from 8 to 96 h, and also using added $AgBF_4$, the formation of highly insoluble AgBr helping to drive the reaction. The use of $AgBF_4$ did appear to increase the speed of the reaction, but it then became very difficult to remove all traces of AgBr. By heating the reaction without $AgBF_4$ for 96 h, the diquaternised product **501** was obtained in a 56% yield. Comparing the results of other reactions attempted over shorter periods of time indicates that the monoquaternised product is formed initially and precipitates out of solution, but its partial solubility in acetonitrile allows the eventual formation of the diquaternised product over longer reaction times. An identical reaction was attempted using bpe in place of 4,4′-bpy, however the diquaternised product was not formed irrespective of reaction timescales. Purification of **501** was achieved by dissolution of the product in a warm mixture of water and DMF and precipitation with acetone, leaving the monoquaternised product in solution.

The synthesis of the monoquaternised compound was achieved by altering the ratio of reactants from that described above to 1 equivalent of 2-bromoaminoethane hydrobromide and 3 equivalents of 4,4′-bpy. Further to the discovery in the previous synthesis that the monoquaternised product **502** is poorly soluble in acetonitrile, the reaction was heated for only 18 h, during which time the product formed as a pale cream coloured precipitate in a 78% yield. A similar reaction using bpe in place of 4,4′-bpy gave the product **503** in a yield of 30%. In both cases purification was achieved by a water/acetone reprecipitation.

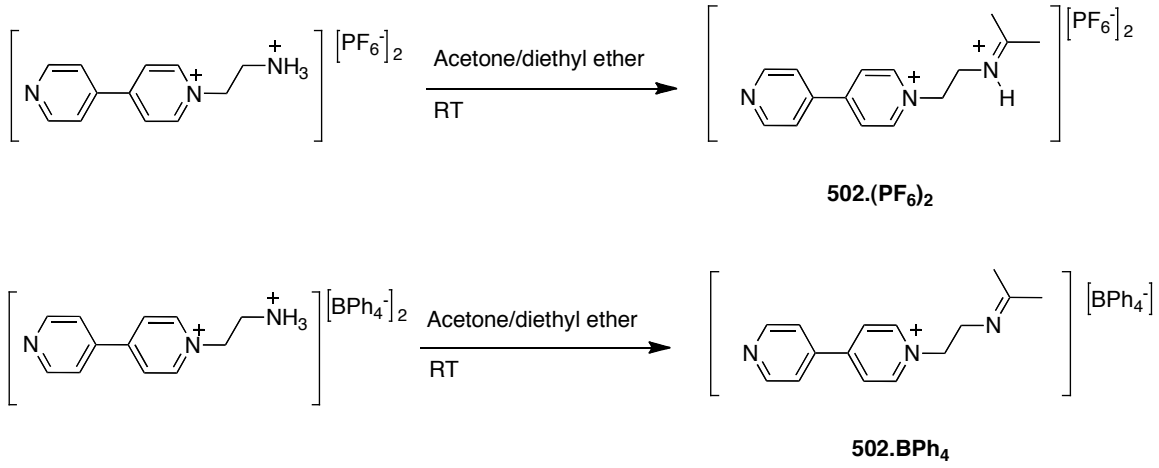

Scheme 23. Synthesis of Schiff base derivatives.

Attempts to crystallise the dication **502** produced some interesting results. Initial attempts to crystallise the bromide salt of this product were not successful so steps were taken to metathesise to the PF_6^- and BPh_4^- salts. In both cases, upon addition of the relevant aqueous salts the expected precipitation did not occur. Consequently, extractions into ethyl acetate were carried out. Diffraction-quality crystals were obtained from both salts, by vapour diffusion of diethyl ether into acetone solutions. However, the structures revealed that the terminal amine groups had reacted with the acetone to form Schiff bases (Scheme 23).

4,4′-Bis-(carbonylaminoethylamine)-2,2′-bipyridyl was viewed as an attractive synthetic target as it has two terminal amine groups and therefore may act as a suitable template molecule for connecting two heteropolymetallic rings. These rings may be attached either to the free pro-ligand or to metal complexes containing this ligand, with facile and reversible redox chemistry of the linkage potentially allowing switching of the magnetic coupling between the rings. Scheme 24 shows the routes attempted to prepare **507**.

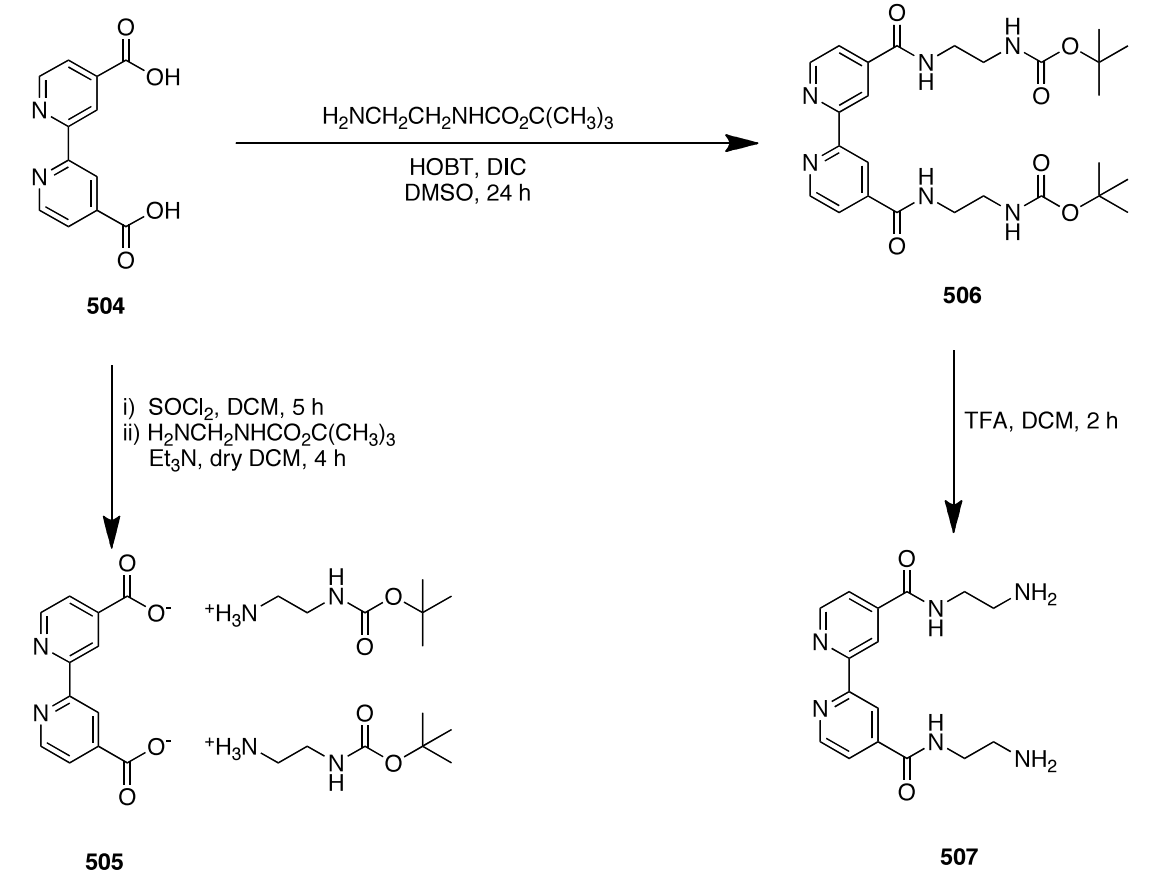

Scheme 24. Route to formation of linker pro-ligand **507**.

4,4′-Bis-(carboxy)-2,2′-bipyridine **504** was synthesised via a literature procedure.[120] Further to a previous report[118], a two-step synthesis to form **506** was attempted. Step one involved reacting **504** with thionyl chloride at room temperature to generate the carbonyl chloride intermediate which was then reacted in step two with N-BOC-ethylenediamine to form the product. However, the product obtained was the salt **505**. This product, while not of direct relevance to the project has been fully characterised and X-ray diffraction-quality crystals were obtained by vapour diffusion of diethyl ether into a DMSO solution.

A potential reason for the formation of **505** as opposed to **506** is that the first step of the reaction had not gone to completion. On reviewing the literature,[125,126] it has been claimed that the diacid **504** requires heating under reflux in thionyl chloride for at least 4 hours to achieve the successful formation of the acid chloride intermediate.

The second method attempted was adapted from a literature procedure[127] and involved the use of the popular amide-coupling reagents diisopropylcarbodiimide (DIC) and 1-hydroxybenzotriazole (HOBT). The C=N bonds of the carbodiimide come under nucleophilic attack from the carboxylic acid group(s), and the reaction is driven by the formation of a highly stable urea by-product. The mechanism of this reaction is depicted in Scheme 25.

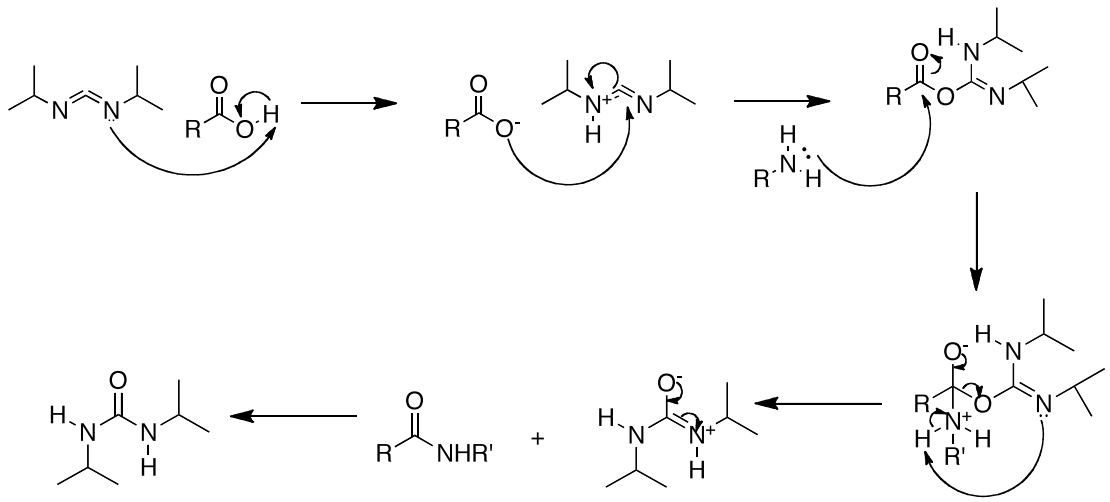

Scheme 25. Mechanism of amide bond formation.

This reaction was carried out in DMF initially, resulting in a precipitate which was shown by ^{1}H NMR analysis to be a mixture of **505** and a monosubstituted BOC product (Figure 86). The reaction solvent was then changed to DMSO and upon stirring overnight at room temperature the desired product **506** formed in a 64% isolated yield. This compound has been fully characterised.

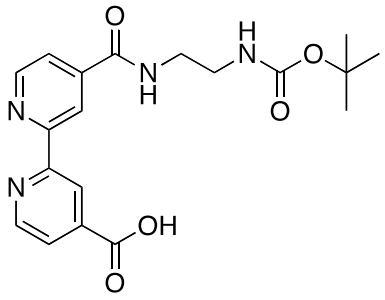

Figure 86. Mono-substituted product formed as a by-product of DMF reaction.

The terminal amine groups of **506** were deprotected by stirring for two hours at room temperature in a mixture of dichloromethane and trifluoroacetic acid. The ^{1}H NMR spectrum of the product clearly shows that the ^{t}Bu groups have been removed, but no new signals are observed for the -NH_2 groups. Problems have also been encountered with the hygroscopic nature of the deprotected compound. One reason for this is the likely formation of the TFA salt of the protonated amine instead of the neutral amine, which may occur due to the large excess of trifluoroacetic acid used in the deprotection step. As a result, no further characterisation has been achieved for this compound (**507**).

Scheme 26 shows the two approaches used to synthesise **509**. The precursors *cis*-$Ru^{II}(bpy)_2Cl_2{\cdot}2H_2O$ and **508** were prepared according to literature methods.[86,119] The first route used to form the complex **509**, which included the direct addition of N-BOC-ethylenediamine to **508**, was explored due to difficulties encountered initially in synthesising the compound **506**.

The BOC protected complex **509** was formed using a method similar to that used to synthesise **506**. This reaction was carried out in DMF and the product was isolated as its PF_6^- salt. Purification was carried out by eluting with an acetonitrile/water/KNO_3 mixture on a silica gel column and the product was obtained in a 45% yield. The ^{1}H NMR and mass spectra are in agreement with the proposed structure. The elemental analysis however indicates that the product is still not fully pure, even when accounting for one equivalent of KPF_6.

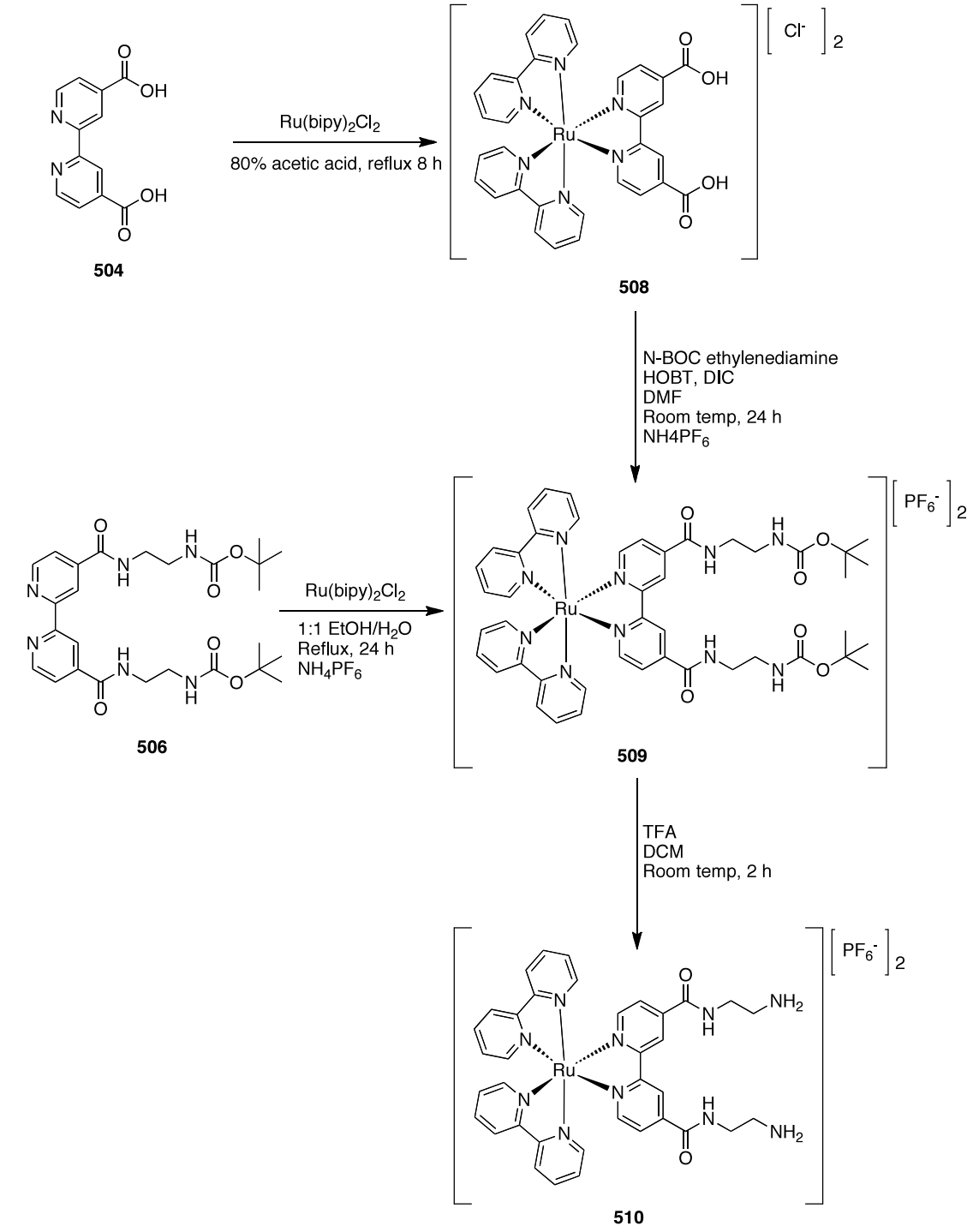

Scheme 26. Synthetic routes to **510**.

Upon completion of the synthesis of the pro-ligand, **506**, it was decided to try reacting this compound directly with *cis*-$Ru(bpy)_2Cl_2 \cdot 2H_2O$ following a method similar to that used by Beer et al.[119] Purification of the product was achieved by anion metathesis, giving a 48% isolated yield. The ^1H NMR spectrum shows this material to be as pure as that obtained from the first attempt using column chromatographic purification. In

addition, elemental analysis shows the product to be pure and this method involving the pre-formed protected pro-ligand appears to be superior to the first approach, as the requirement for column chromatography is eliminated.

Once again, treatment of the BOC-protected complex with TFA in dichloromethane produced an extremely hygroscopic product (**510**). The ^{1}H NMR spectrum of this product shows that it is impure, which could be as a result of a mixture of charged and non-charged species being formed from the TFA treatment.

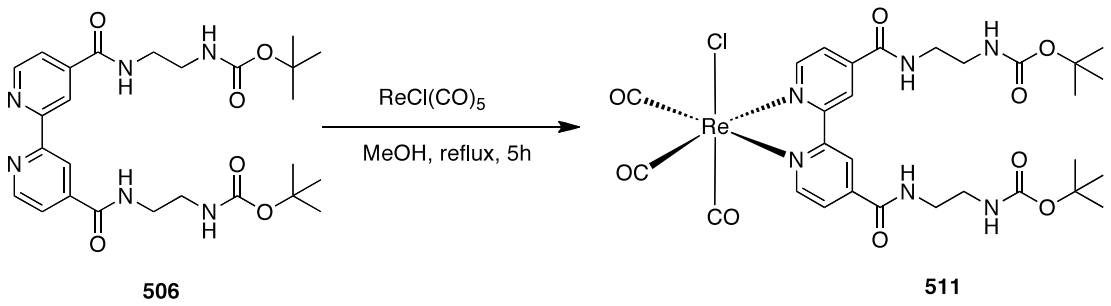

506 **511**

Scheme 27. Route to formation of **511**.

The synthesis of **511** (Scheme 27) was achieved in a fashion similar to a reaction reported previously by Coe *et al.*[118] $Re^{I}Cl(CO)_5$ was reacted with **506** in a 1:1 ratio by heating under reflux in methanol for 5 hours. After reprecipitation from DMF and water, the ^{1}H NMR spectrum implied the formation of a pure product, although the elemental analysis suggested the presence of remaining $Re^{I}Cl(CO)_5$ starting material. Hence, the reaction was repeated using a slight excess of the pro-ligand, affording a pure sample of the desired product **511**.

5.3.1.2 Attempted formation of linked wheel systems

The first approach considered when attempting to link Cr_7Ni wheels together was to substitute the template of a pre-formed ring for one of the target linkers. The only such template-substitution reaction attempted previously had involved using the incoming template as a solvent and thus in a many-fold excess. It was decided to investigate whether it may be possible to tailor this reaction to allow substitution of templates when

using smaller quantities of replacing units, perhaps even less than one equivalent. The approach considered is shown in Scheme 28.

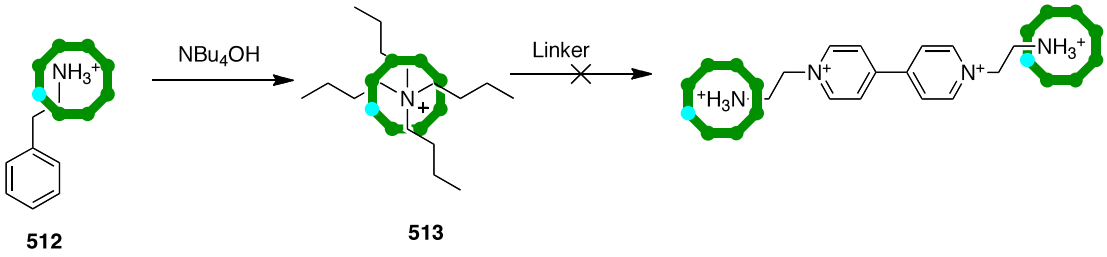

512 **513**

Scheme 28. Attempted substitution of templates to form a linked wheel system.

The starting wheel compound **512** was synthesised in a fashion similar to other wheels by 2-phenethylamine as a template. This starting material was chosen for two reasons. Firstly, its synthesis is straightforward, requiring no column chromatographic purification, and gives a high yield. Second, the use of a primary amine as opposed to a secondary amine as a template should facilitate the swapping for another molecule. The idea for this procedure was to treat **512** with a base, $[Bu_4N]OH$, for an hour to form the intermediate **513** by deprotonating the amine about which the wheel is templated, causing the wheel to "slip off" the template and become associated with Bu_4N^+ instead. The wheel should not be able to sit around the very bulky Bu_4N^+ cation and therefore, upon addition of the new linking molecule, the wheel should associate itself instead with the target template via hydrogen bonding to the protonated amine.

Mass spectrometry studies suggest that the first step of the reaction, the removal of the wheel from the template and subsequent association with Bu_4N^+, was successful. However, following the second step by TLC suggested that only a minimal amount of the desired product was in fact formed. It was decided at this point that the method was too inefficient to warrant further study as potentially more fruitful avenues of investigation were becoming available. It appears that a reasonable rate of substitution requires the linker molecule to be present in a large excess and therefore this method would not be cost effective for more expensive metal complex linkers.

The next approach to the formation of linked wheel systems was to attempt the synthesis of wheels directly about the "linker molecules" in a fashion used for simple linear

diamines previously.[62] The first compound considered in this regard was the monoquaternised product **502**, as shown in Scheme 29.

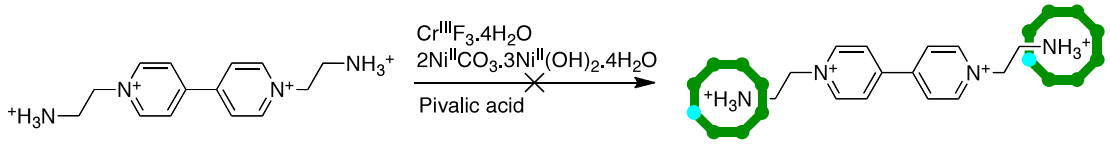

Scheme 29. Direct synthesis of a linked wheel system.

A reaction was attempted by adapting previous syntheses. $Cr^{III}F_3 \bullet 4H_2O$, $2Ni^{II}CO_3 \bullet 3Ni^{II}(OH)_2 \bullet 4H_2O$ and **502** were heated in pivalic acid at 160 °C for 24 h, then cooled before acetonitrile was added to give a precipitate. The resultant mixture was found to contain simply the starting compounds, probably due to a lack of dissolution of **502** in the pivalic acid. With no template, the wheel cannot form. One potential reason for this failure is that all previously used templates are neutral prior to protonation of the amine group, whereas these viologen-type molecules are already doubly charged and thus their solubility properties may be quite different.

The next molecule to be used as a potential template is the pro-ligand **506**. Problems had been experienced when attempting to deprotect the terminal amine groups of this compound in TFA, but this deprotection step is acid-catalysed so it was decided to attempt this in situ as the reaction solvent for wheel formation is an acid (Scheme 30). Once again, this reaction returned only starting materials as the BOC-protected ligand is insoluble in pivalic acid, meaning that pivalic acid is incapable of deprotecting the ligand.

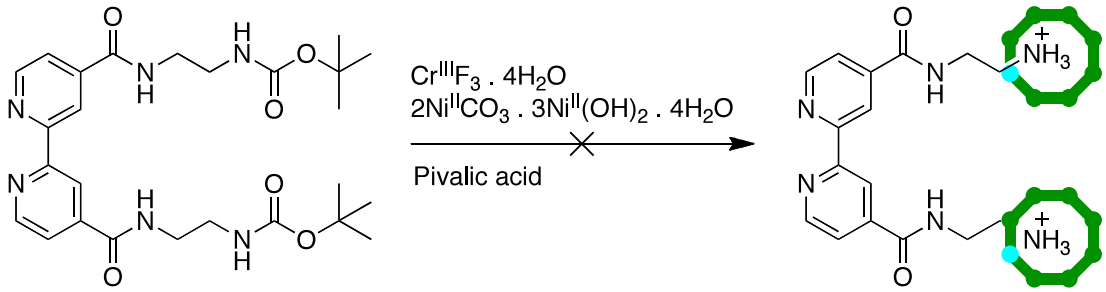

Scheme 30. Attempted synthesis of linked wheel system through **507**.

Attempts were also made to de-protect the pro-ligand in a dichloromethane and pivalic acid mixture and then to remove the dichloromethane to see whether the de-protected ligand would remain dissolved in pivalic acid, but this approach was also unsuccessful. Attempts to form linked wheel systems in an identical fashion using the ruthenium and rhenium complexes **509** and **511** were also unsuccessful. There is a possibility that the use of alternative carboxylic acids as solvents could enable the reaction by dissolving the protected starting material.

5.3.1.3 Coordination chemistry of wheels through their templates

The wheel pro-ligand considered in this section of the chapter **514** was synthesised by a literature preparation.[62] Previous studies using such wheels as bulky pyridyl ligands have only involved coordination chemistry to first row transition metals under very mild conditions. Therefore, we chose to investigate the stability of these wheels under more severe conditions, such as refluxing in high boiling solvents, in order to be able to form complexes of 2nd and 3rd row transition metals.

A 2.5-fold excess of **514** was reacted with $Re^{I}Cl(CO)_5$ in refluxing toluene for 24 h (Scheme 31). The product was isolated by column chromatography, eluting with toluene, and a small amount of diffraction-quality crystals were grown by gentle evaporation of a pentane/acetone solution. The crystal structure obtained shows that the linked wheel system **516** is produced and that the wheels are mutually trans, giving a rarely seen meridional $\{Re^{I}(CO)_3\}^{+}$ core. This is the first reported example of a complex *mer*-$Re^{I}Cl(CO)_3(L)_2$ where L is attached through a pyridyl group, but there are a few related examples in the literature where L is a bulky phosphine.[128,129,130]

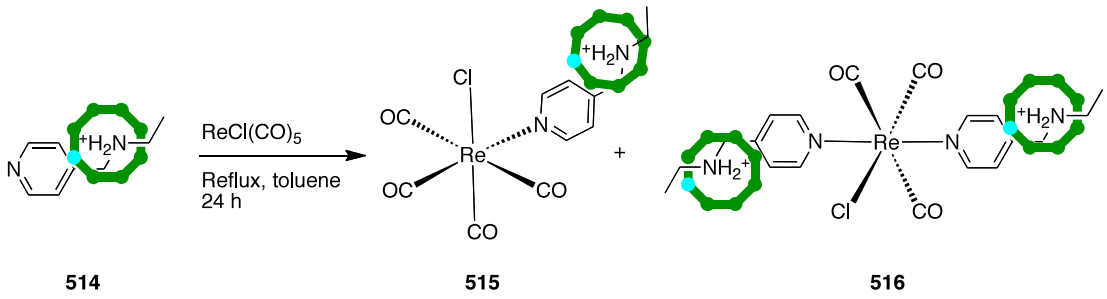

Scheme 31. Reaction of **514** with $Re^{I}Cl(CO)_5$.

Characterisation data, obtained on the product before crystallisation, suggests that the primary product may in fact be the mono-substituted derivative **515**. The IR spectrum and elemental analysis of the powder suggests that it is in fact a rhenium complex containing only one wheel. However, some of the linked wheel system was synthesised. It is believed that approximately 4% of the product formed crystals, and Table 8 shows that the elemental analysis agrees with this allowance.

Table 8. Elemental Analysis of Product from Reaction of **514** with $Re^{I}Cl(CO)_5$.

	Found	**515**	**516**	**515** + 4% **516**
Mol. Wt.	-	2647.54	4965.36	2846.15
C	42.00	41.49	43.30	41.85
H	6.11	5.94	6.37	6.00
N	0.94	1.05	1.13	1.06
Cr	13.76	13.67	14.66	13.81
Re	6.69	6.99	3.75	6.80

Because Ru polypyridyl complexes are the archetypal and most well-studied redox-active MLCT chromophores, a reaction was attempted between *cis*-$Ru(bpy)_2Cl_2$•$2H_2O$ and **514** (Scheme 32).

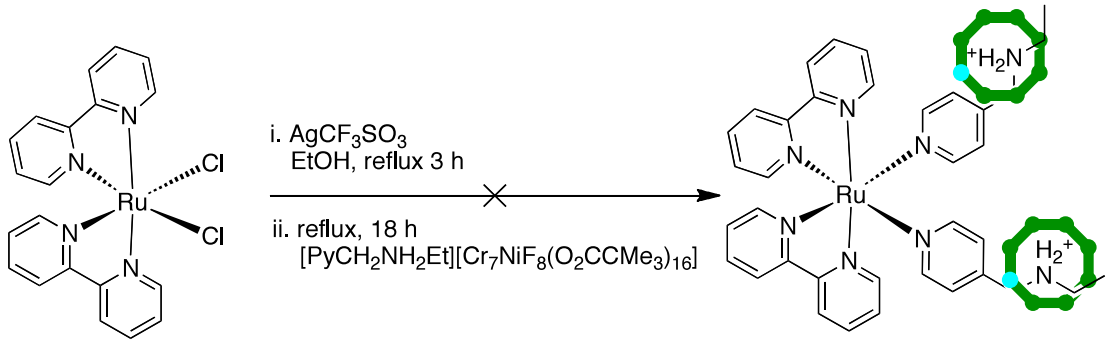

Scheme 32. Attempted synthesis of a ruthenium-based linked wheel system.

Following a well established synthetic approach.[92] *cis*-$Ru(bpy)_2Cl_2$•$2H_2O$ was reacted with silver triflate in ethanol for 3 hours, removing the chloride ligands and forming an intermediate complex with weakly coordinating triflate ligands. This step is driven by

the formation of the highly insoluble AgCl, which was removed from the reaction mixture by filtration before the addition of **514**. The evidence available, suggests that when **514** is used the product contains only one wheel. This seems logical as the wheel-bearing ligands are expected to coordinate cis to each other as *trans*-$\{Ru(bpy)_2\}^{2+}$ complexes are very unstable and undergo isomerism back to their cis forms when exposed to light. Considering the bulk and steric restraints of these wheels and their behaviour in the previously mentioned rhenium example, it seems possible that the system may be too sterically hindered to allow a cis arrangement of the wheels.

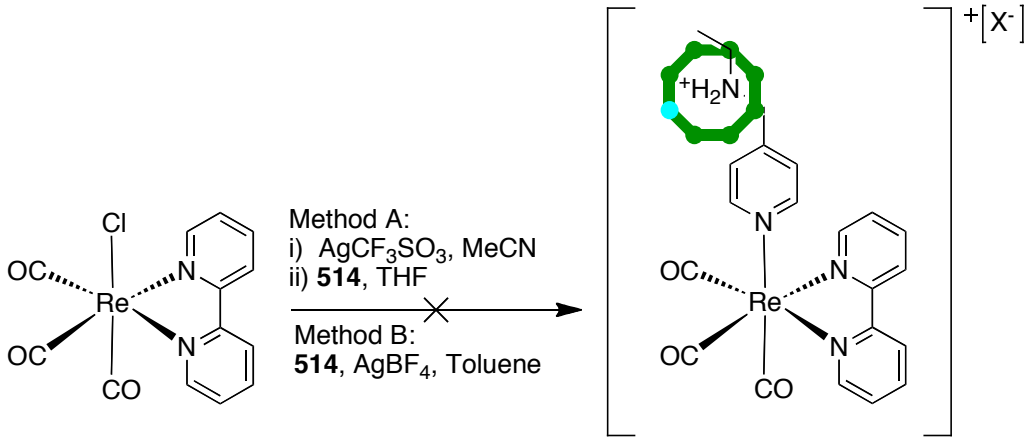

Scheme 33. Attempted synthesis of a rhenium-containing wheel system.

Two reactions have been attempted to synthesise a compound of the general formula *fac*-$[Re([PyCH_2NH_2Et][Cr_7NiF_8(O_2CCMe_3)_{16}])(CO)_3(bpy)]^+$ using **514** (Scheme 33). The first method (A) is an approach commonly found in the literature[131,132] and has two steps, involving firstly the formation of *fac*-$[Re(MeCN)(CO)_3(bpy)][CF_3SO_3]$[133] as an intermediate by reacting *fac*-$ReCl(CO)_3(bpy)$ with silver triflate in acetonitrile. The MeCN complex is isolated and characterised before being added to two equivalents of **514** and refluxed in THF for 4 hours. This reaction proved to be unsuccessful and one of the possible problems is the use of THF as a solvent; previous studies have shown that the wheel in **514** begins to disintegrate upon sitting in THF for a long period of time. Upon refluxing it is likely that degradation will occur more quickly.

As a result and further to discussions with Dr Mike Coogan, a second more direct method (B) was applied, using toluene as a solvent in the knowledge that linked wheel systems have been synthesised previously in refluxing toluene solutions. In this method, silver

tetrafluoroborate was used as a catalyst and **514** was added at the start. However, this approach also proved unsuccessful. In both cases there is evidence to suggest that upon complexation of the template to the rhenium centre loss of the wheel occurs. This is not a wholly unexpected result as the wheels are only attached to the template through hydrogen bonds, which could break under severe conditions.

5.3.1.4 Synthesis of Cr_7Co analogues

One major problem with using heterometallic wheels with a ground state spin is that certain techniques, such as ^1H NMR spectroscopy become unusable as the slow relaxation of the paramagnetic metal centres shifts and broadens the spectra beyond recognition. This means that in general compounds cannot reasonably be identified without obtaining crystal structures. One possible way to deal with this obstacle is to synthesise a series of Cr_7Co analogues of the wheel derivatives that are used as ligands. The fast relaxation time of cobalt(II) counteracts the slow relaxation of chromium(III) and thus proton signals can be identified, even though certain features of the spectrum would be missing, such as proton-proton couplings. This technique has already been used with simple symmetrical Cr_7Co analogues[55] hence it was decided to investigate whether this would be a suitable characterisation tool for non-symmetrical wheels and linked wheel systems.

The Cr_7Co analogue of **514** was synthesised by heating chromium trifluoride and 4-(ethylaminomethyl)pyridine in pivalic acid at 140 °C for 5 hours before adding $\{CoPiv_2\}_n$ and increasing the temperature to 160 °C for a further 24 hours (Scheme 34). The impure product $[C_6H_5CH_2NH_2Et][Cr_7CoF_8(O_2CCMe_3)_{16}]$, **517** was reacted with $[Cu(Piv)_4(HPiv)_2]$ to give pure $Cu_2(O_2CCMe_3)_4([C_6H_5CH_2NH_2Et][Cr_7CoF_8(O_2CCMe_3)_{16}])_2$, **518**. This process removed any "horseshoe" clusters that may have been present. The Cu dimer assembly was then reacted with acetylacetone to release the wheels from the complex and give **517** in its pure form. Both **517** and **518** have been characterised using elemental analysis, paramagnetic NMR spectroscopy, mass spectrometry and X-ray crystallography. Crystals were grown by evaporation of a pentane/acetone solution.

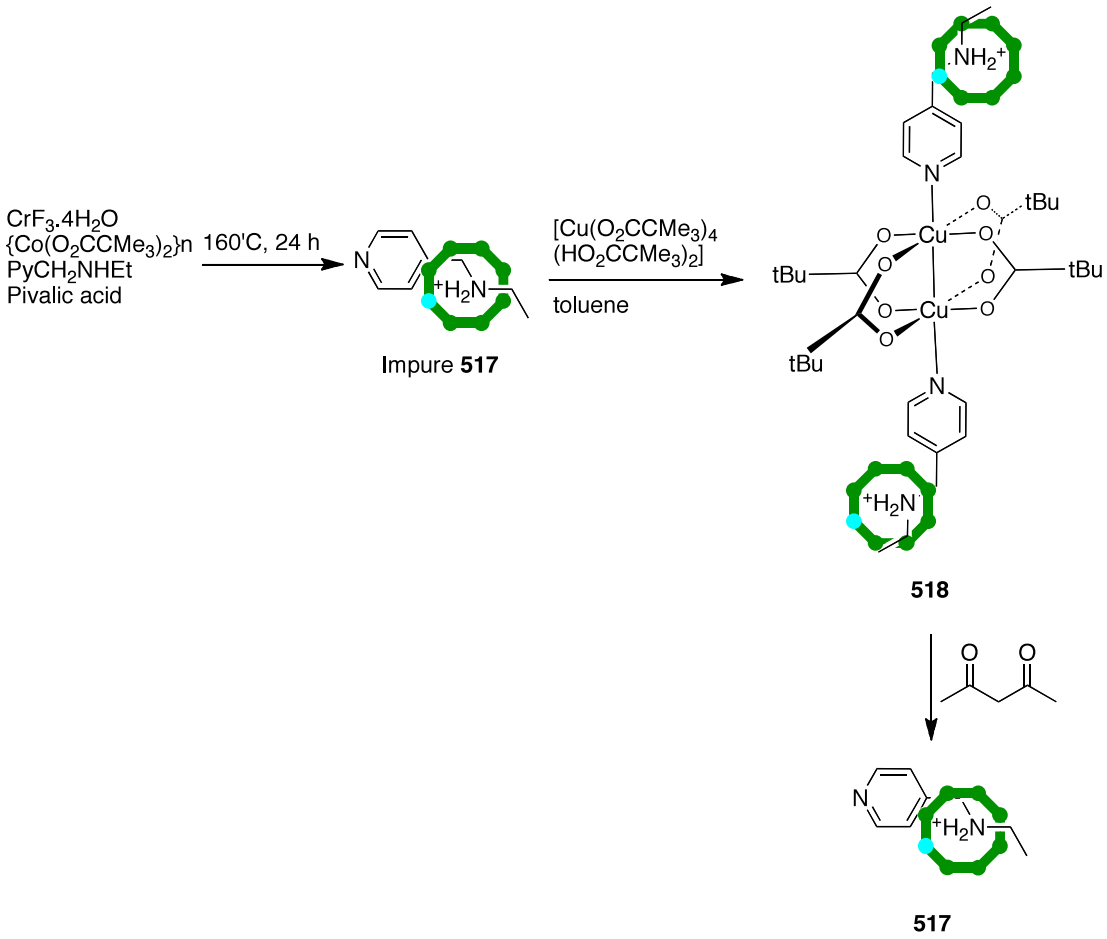

Scheme 34. Synthetic route to **517**.

5.3.1.5 Synthesis of a new "substitution molecule"

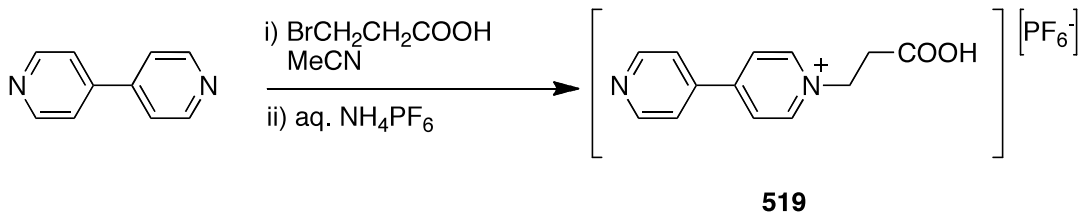

Scheme 35. Synthesis of a novel substitution molecule.

Based on preliminary studies with the two types of derivatised wheel, with the coordinating group in the template or substituted directly into the backbone of the wheel, it appears that the latter are the most useful. Besides iso-nicotinic acid, a series of other compounds have been identified as potential candidates for substitution into the wheel.

Compounds with extended structures may allow more space between a coordinated metal centre and the wheel, facilitating the preparation of more highly-substituted derivatives.

One compound synthesised for this purpose, but ultimately not further used is *N*-(3-carboxyethyl)-4,4′-bipyridine hexafluorophosphate, **519**. This was synthesised using a method identical to that used for **502**, but using 3-bromopropionic acid in place of 2-bromoethylamine hydrobromide (Scheme 35). The only other alteration was that purification was effected by metathesis to the PF_6^- salt by dissolving the bromide salt in a minimum amount of water and then adding aqueous ammonium hexafluorophosphate. This product has been characterised using ^{1}H NMR spectroscopy and elemental analysis. However, this compound was not further used because other avenues of investigation proved more attractive. **519** is a salt and it was decided to focus on charge-neutral species for substitution into the wheels as to use a charged carboxylic acid may have large and undesirable effects on the solubility of the resulting wheel-based pro-ligand.

5.3.2 Analysis of ^{1}H NMR Spectroscopy

The bromide salts of the three organic quaternised 4,4′-bipyridine derivatives were characterised by ^{1}H NMR spectroscopy in D_2O. The spectrum of **501** can be seen in Figure 87.

This compound is symmetric, so the spectrum shows only four signals relating to different environments, two associated with the ethylamine chain and two associated with the bipyridine. The two doublet signals associated with the bipyridine ring are shifted downfield due to quaternisation and appear between 8.5 and 9.2 ppm. No peak is observed for the terminal amine groups, which is to be expected as the protons attached to the nitrogen can undergo rapid exchange with the D_2O solvent.

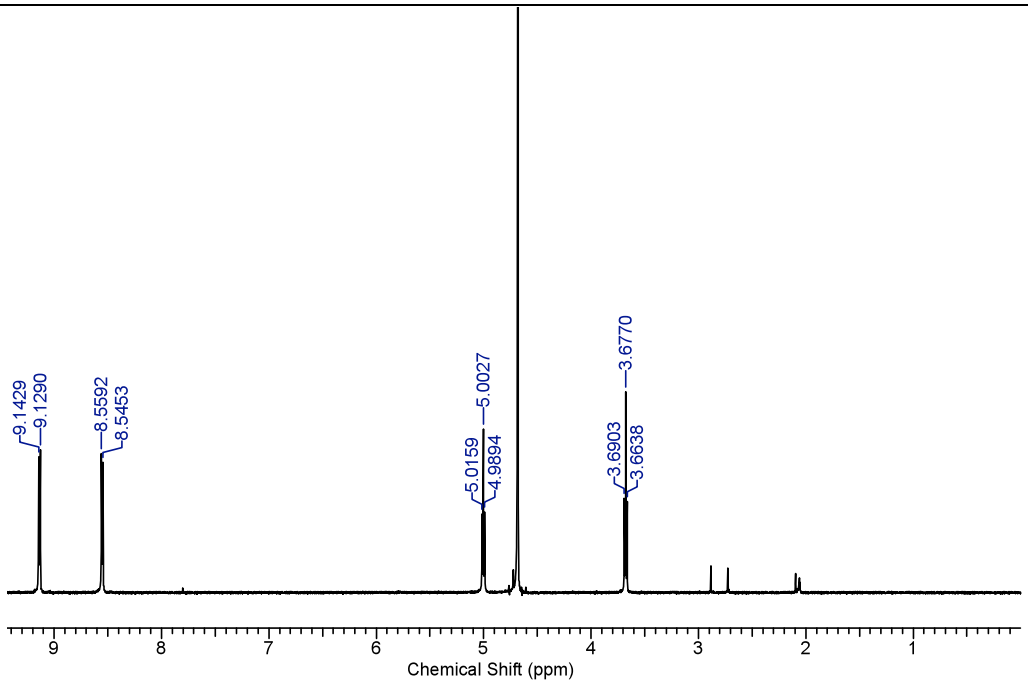

Figure 87. ^{1}H NMR spectrum of **501** in D_2O.

The ^{1}H NMR spectrum of the monoquaternised product, **502**, can be seen in Figure 88. The two triplet signals associated with the ethylamine chain are in positions virtually identical to those for **501**, but there are now four peaks in the aromatic region because the compound is no longer symmetrical. The most deshielded peak at 8.96 ppm can be assigned to the two protons on the carbon adjacent to the quaternised nitrogen. The spectrum for the monoquaternised bpe derivative **503** is very similar with the presence of two additional doublet signals at 7.66 and 7.47 ppm associated with the ethenylene unit, the coupling constant of 16.4 Hz confirming the *E*-geometry.

The ^{1}H NMR spectrum of **519** is as expected and very similar to that of the amine-based compound **502**, with two doublets assigned to the ethylene chain and four doublets assigned to the bpy fragment. As in **502** there is no peak associated with the terminal proton of the chain due to rapid exchange with the deuterium of the solvent.

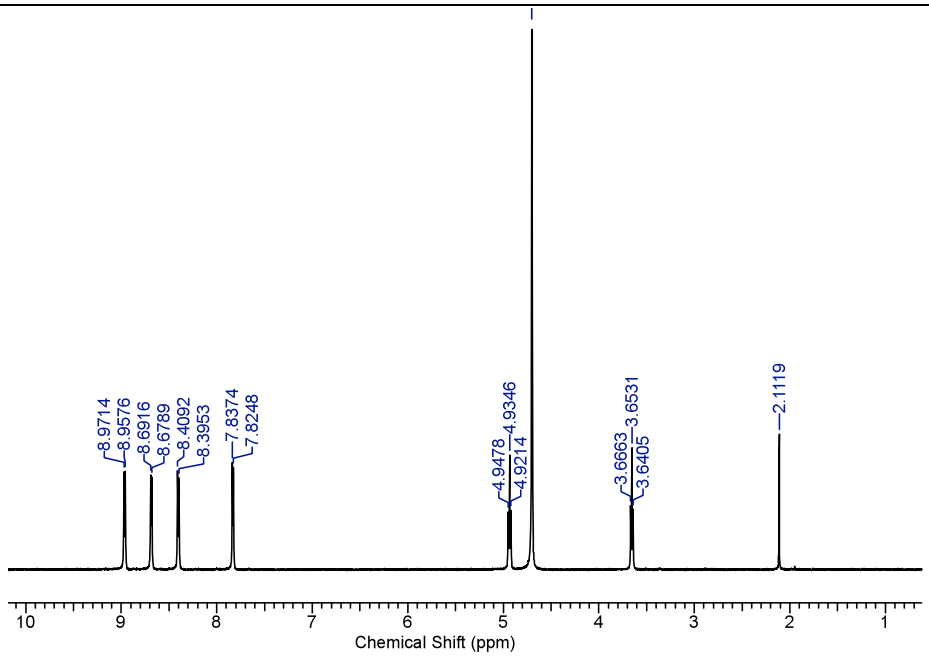

Figure 88. ^{1}H NMR Spectrum of **502** in D_2O.

The ^{1}H NMR spectrum of the pro-ligand **506** (Figure 89) was run in deuterated DMF due to solubility issues. A large singlet at 1.58 ppm arises from the 18 protons of the ^{t}Bu groups, and two triplets between 3.53 and 3.73 ppm are due to the two CH_2 groups. Two broad peaks at 7.15 and 9.25 ppm are attributable to the amide protons, that adjacent to the pyridyl rings being shifted well into the aromatic region. Three other peaks are observed in the aromatic region due to the pyridyl rings.

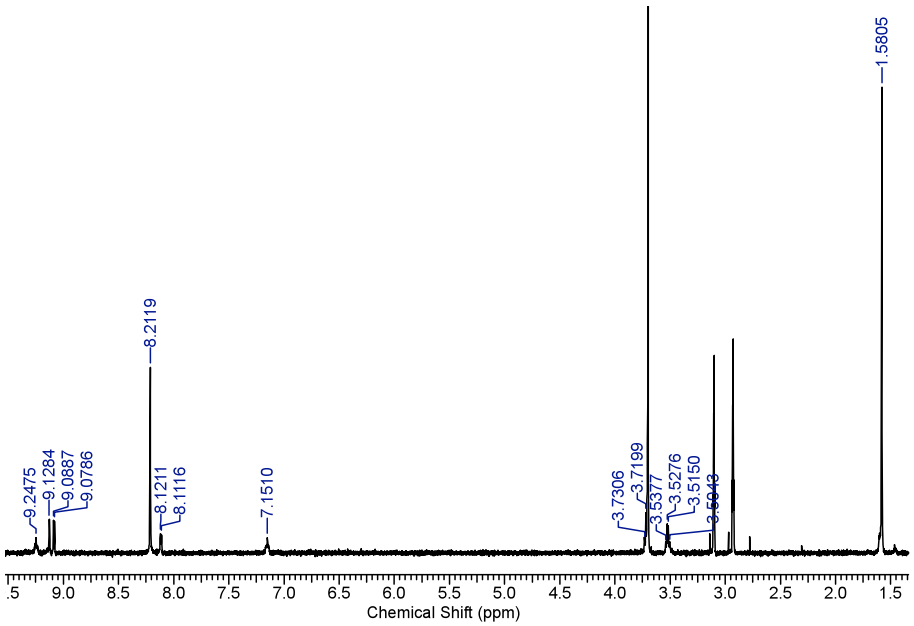

Figure 89. The ^{1}H NMR Spectrum of the pro-ligand **506** in d_6-DMF.

The spectrum of the Re complex **511** is very similar to that of **506**, but a direct comparison of the spectra in deuterated DMF shows that most of the signals for **511** are further deshielded when compared with those of **506**, especially the bpy signals which are deshielded by as much as 0.41 ppm. This observation can be attributed to the electron-withdrawing influence of the *fac*-$ReCl(CO)_3$ unit. The signal for the remote ^{t}Bu groups is predictably insensitive to complexation.

The ^{1}H proton NMR spectrum of **511** has also been run in deuterated acetone in order to allow comparisons with the spectrum of **508** (Figure 90). For the latter it is harder to assign particular peaks to the BOC protected ligand as the aromatic region is much more complicated. In general, however, it can be observed that once again the peaks associated with the Re complex **511** are more deshielded.

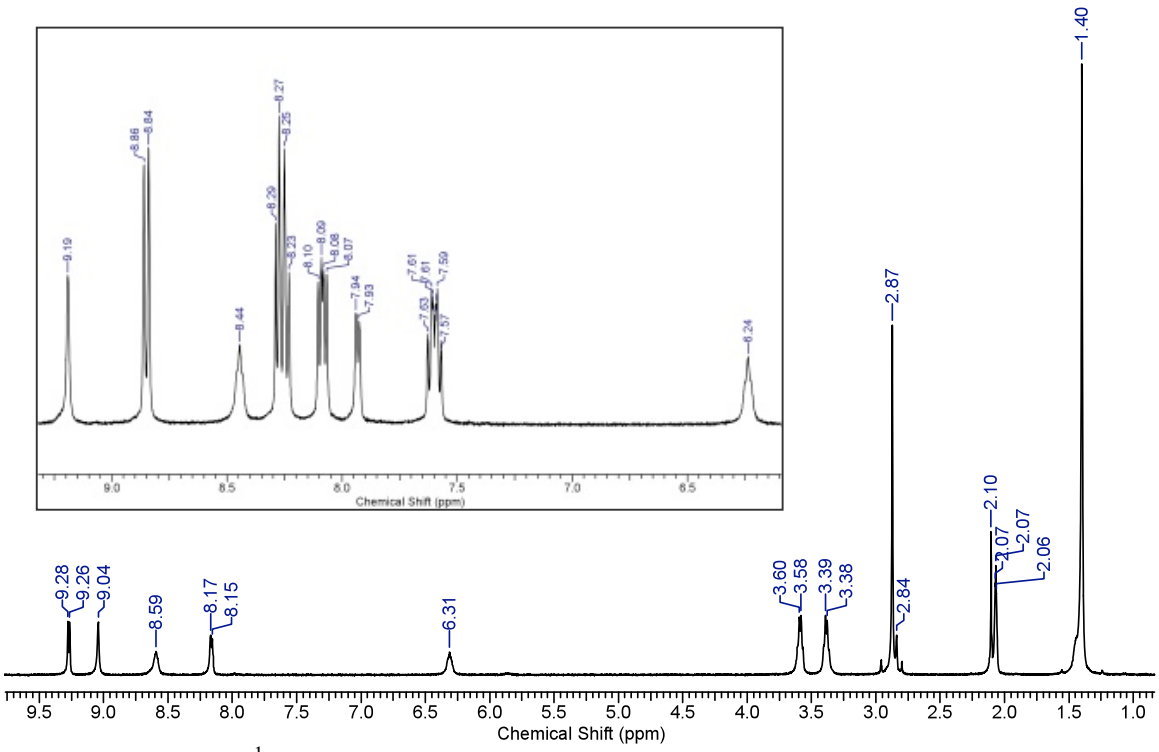

Figure 90. The ^{1}H NMR spectrum of **511** in acetone. Inset: The bpy region of the spectrum of **508**.

5.3.3 Paramagnetic NMR studies

Paramagnetic ^{1}H NMR studies are a potential diagnostic tool to identify wheel systems in the solution state when there is no crystal structure available. It may be possible to

identify how many wheels are attached to a metal centre by using the relative integrals in the spectrum. The two novel Cr_7Co systems described in this chapter have hence been studied using this technique. The full spectrum of **517** can be seen in Figure 91. The spectrum of **518** was too broad to yield any reasonable data due to the extra paramagnetism of the copper centres in the template, so it will not be discussed further.

The peaks are, as expected, broader than those normally seen in a ^{1}H NMR experiment and are spread over a far wider range than the typical 0–10 ppm, but the pivalate protons are five bonds away from the paramagnetic centres and therefore have signals sharp enough to be identified. Peaks assigned to the pivalates occur between 15 and –3 ppm and those assigned to the template lie between –5 and –35 ppm, showing that the template remains in the cavity in solution.

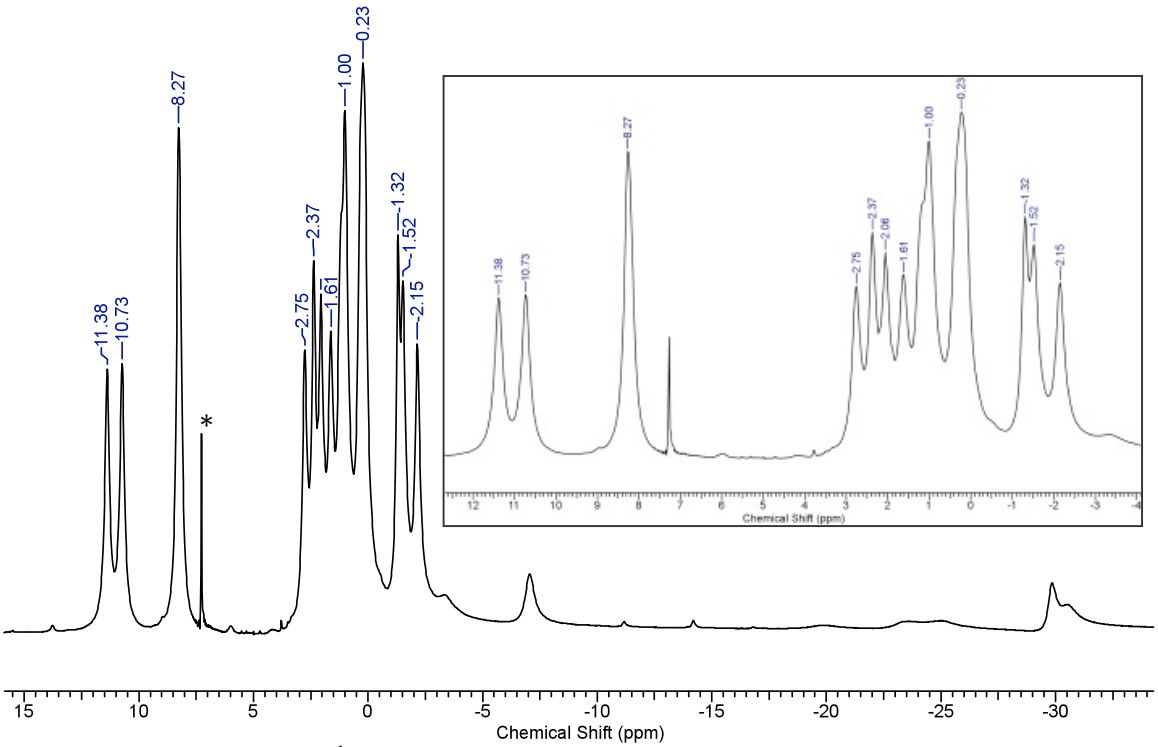

Figure 91. Paramagnetic ^{1}H NMR Spectrum of **517** in $CDCl_3$. Insert: expanded pivalate region.

As expected for wheels with asymmetric templates, this spectrum shows twelve peaks corresponding to the pivalate groups. Four of these peaks are assigned to the equatorial pivalates, each corresponding with two groups. This observation can be accounted for by

the fact that the equatorial pivalates do not feel any effect from the template and are only differentiated by their proximity to the hetero-metal. The other eight peaks can be assigned to the axial pivalates, each one different as they are affected by their location with respect to the hetero-metal *and* to the template. A small but sharp signal can be seen at 7.26 (*) corresponding to the solvent used, $CDCl_3$. The template region is very busy and hard to assign due to the number and size of the peaks.

5.3.4 IR Studies

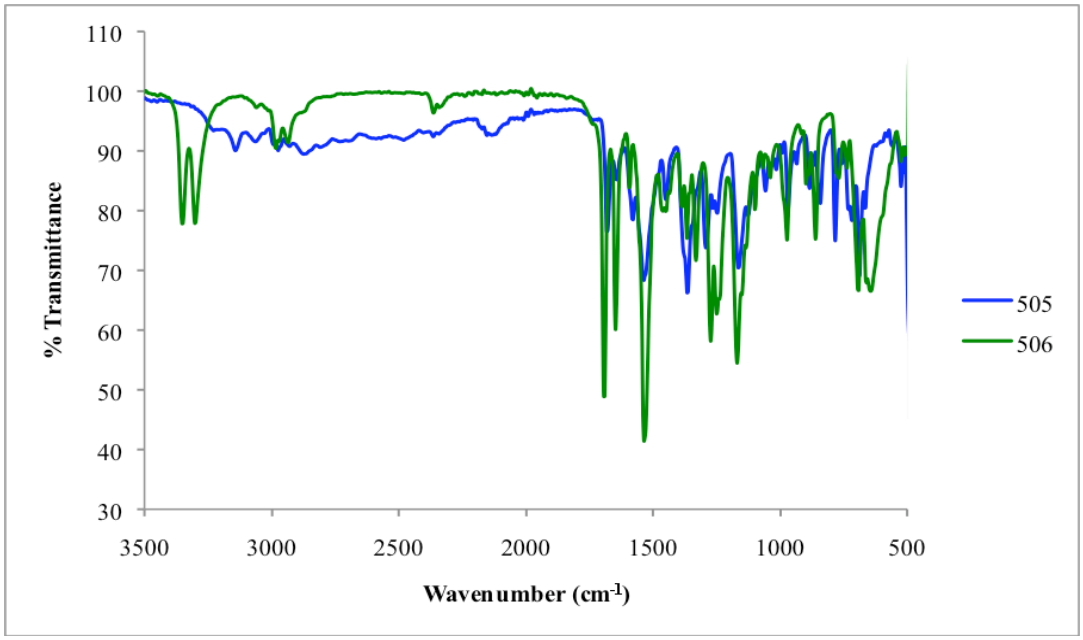

Figure 92. IR spectra of **505** and **506**.

While NMR spectroscopy shows no difference in structure between **505** and **506**, IR spectroscopy does allow these two compounds to be distinguished. A clear difference is seen in the N–H regions, with **506** showing two distinct bands at 3348 and 3298 cm^{-1} corresponding with the presence of two different secondary amide groups. The spectrum of **505** shows a shift to a lower wavenumber, as expected for an absorption caused by an amine instead of an amide N–H bond, and also a much broader absorption band in that region, which can be attributed to the increasing H-bonding ability of the primary protonated amine. Other differences are observed in the C=O (amide) stretching region, **506** showing two bands between 1690 and 1630 cm^{-1}, whereas **505** shows only one band

in this region and one band at 1560 cm^{-1} correlating to the carboxylate salt region. These differences in the spectra can be seen in Figure 92.

As can be seen in Figure 93, the IR spectrum of **511** shows three strong carbonyl stretching absorptions at 2026, 1919 and 1880 cm^{-1} which are characteristic of a *fac*-$\{Re^{I}(CO)_3\}^+$ unit. A broad peak corresponding to the two amide carbonyl groups in the ligand is also present at 1656 cm^{-1}, in contrast with the two sharp ν(C=O) peaks in the spectrum of the pro-ligand.

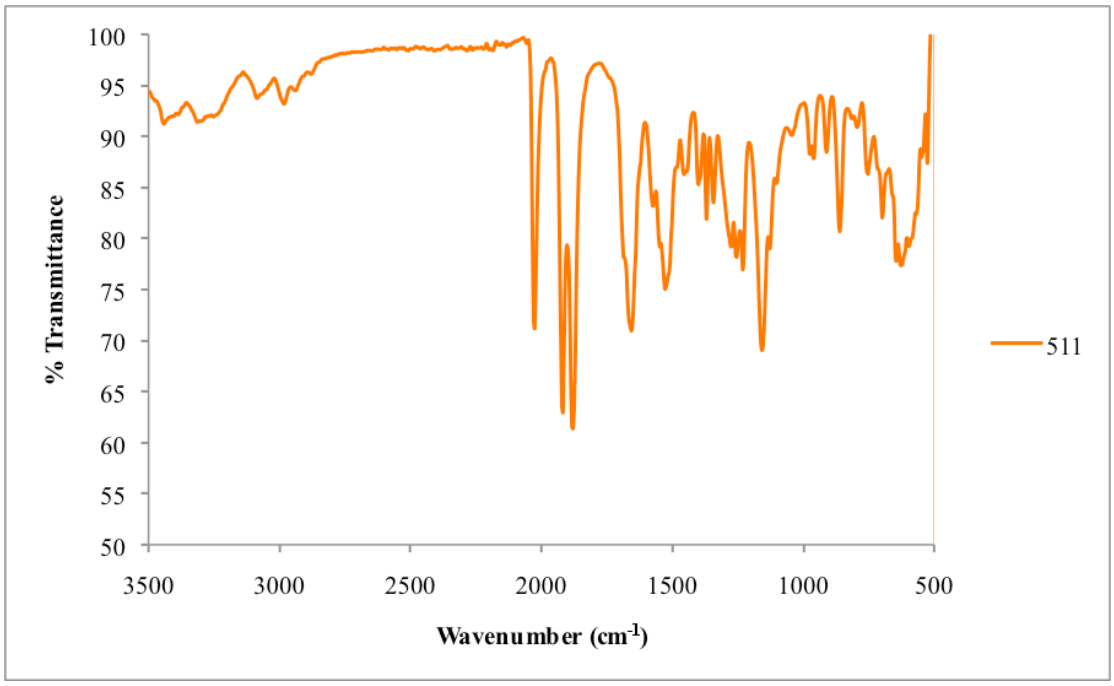

Figure 93. IR spectrum of **511**.

5.3.5 UV-VIS studies

The UV-VIS spectra of **509** and **511** are shown in Figure 94 and the corresponding data are collected in Table 9. As expected, broad bands due to MLCT transitions can be seen in the region of approximately 400–500 nm, and other bands are observed to higher energies, attributable primarily to intraligand π-π* transitions. These values do not differ greatly from the literature values obtained for the mono-armed Ru system.[118]

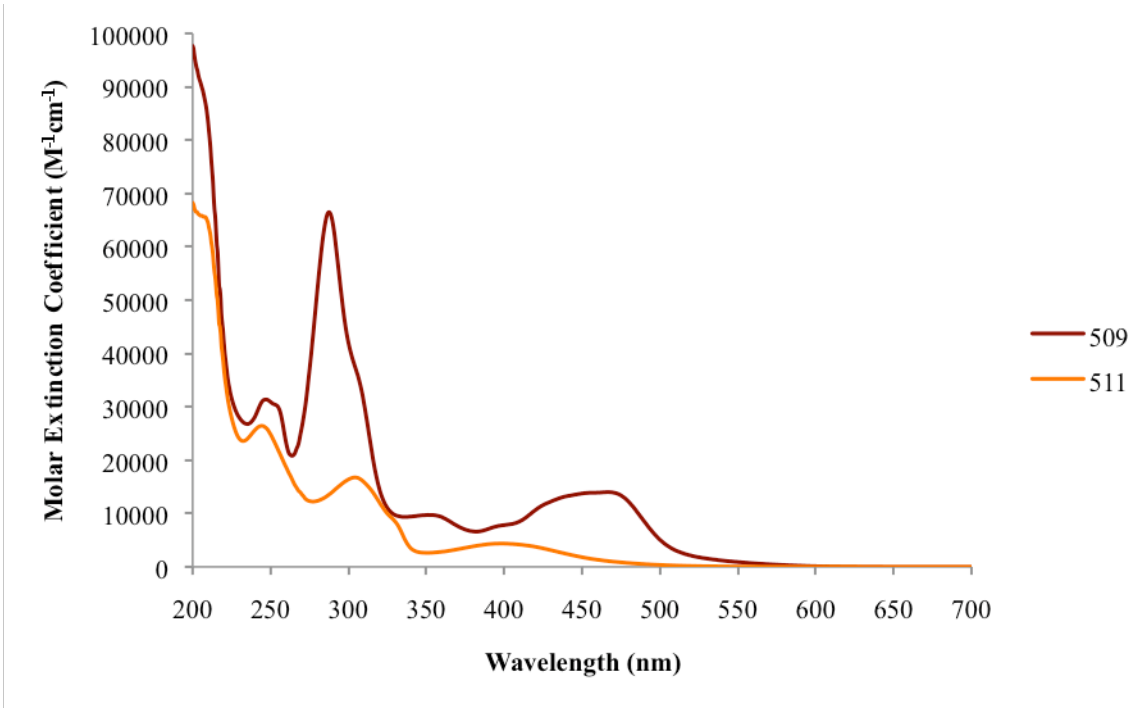

Figure 94. UV-VIS spectra of **509** and **511** in acetonitrile at 293 K.

Table 9. UV-VIS data for **509** and **511** in acetonitrile.

λ_{max} (nm)	ε (mol^{-1} dm^3 cm^{-1})	λ_{max} (nm)	ε (mol^{-1} dm^3 cm^{-1})
509	**509**	**511**	**511**
466	14 100	398	4 400
351	9 800	305	16 800
288	66 500	245	26 400
247	31 400		

5.3.6 Electrochemistry

The ruthenium complex **509** was studied using cyclic voltammetry in 0.1 M solution of $[NBu^n_4][PF_6]$ in acetonitrile. A representative voltammogram can be seen in Figure 95. A fully reversible process is observed at $E_{1/2}$ = 1.41 V vs. Ag–AgCl (ΔE_p = 60 mV), as expected for such complexes, relating to the $Ru^{III/II}$ oxidation. In addition, three quasireversible processes are observed for the bpy ligands at $E_{1/2}$ = –1.05 V, –1.42 V and –1.65 V (ΔE_p = 70 mV, 55 mV and 55 mV, respectively).

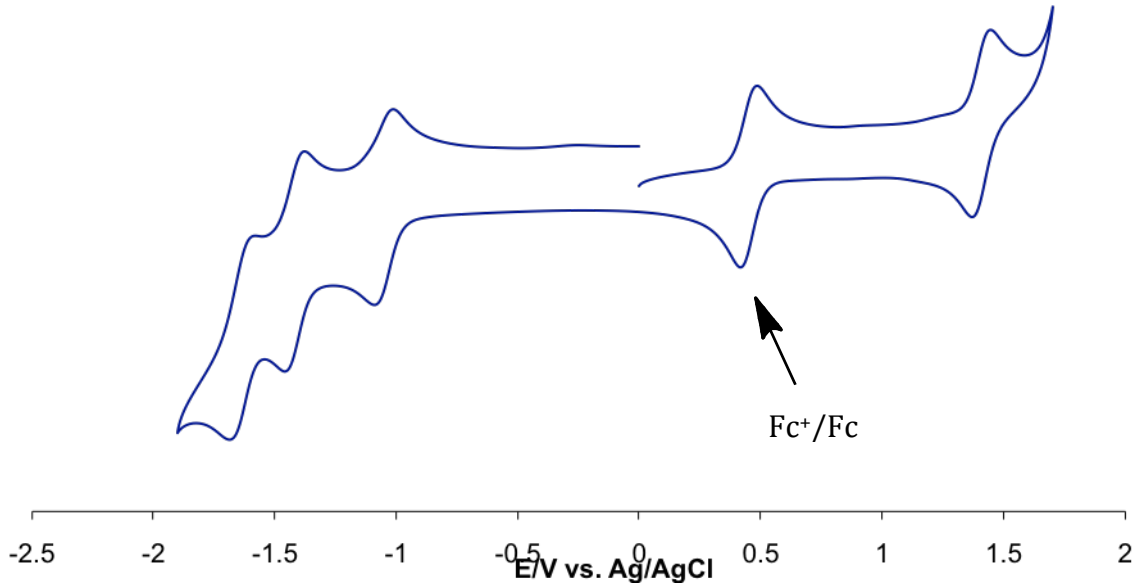

Figure 95. Cyclic voltammogram for **509**.

5.3.7 Crystal structure determination

5.3.7.1 Organic Molecules

Crystals of **505** were grown by vapour diffusion of diethyl ether into DMSO and a representation of the molecular structure can be seen in Figure 96. Only one cation is present in this representation, although there are two cations in the salt. The position of H13 has been refined so it is possible to calculate the distance between it and O2. This distance is relatively short and the angle between N2–H13….O2 is 166°, indicating that there is hydrogen bonding between the molecules. This is as is expected and helps to explain the crystal packing arrangement (Figure 97), as well as the broadened N–H peaks seen in the IR spectrum.

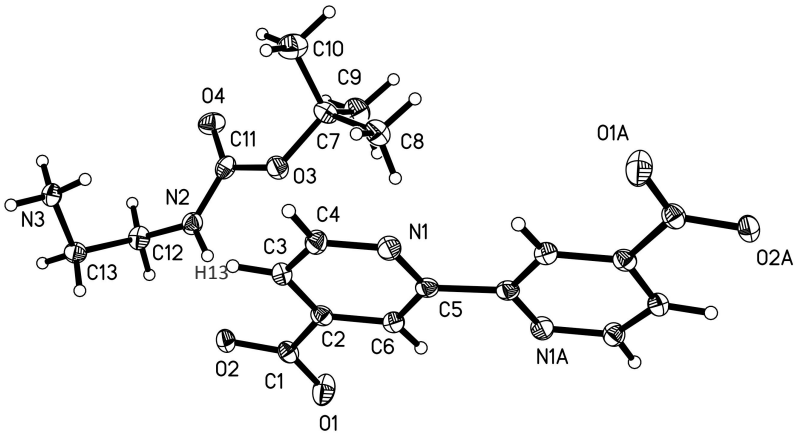

Figure 96. Representation of the molecular structure of **505**.

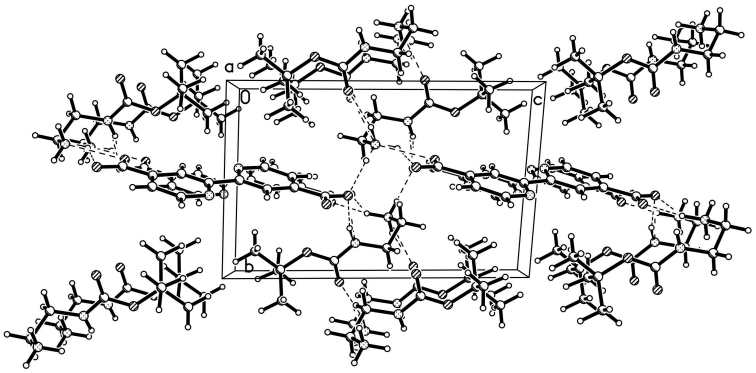

Figure 97. Crystal packing diagram of **505**.

Crystals of **502.$(PF_6)_2$** and **502.$(BPh_4)_2$** were grown by vapour diffusion of diethyl ether into acetone solutions at room temperature. Representations of the molecular structures can be seen in Figures 98 and 99 respectively. Interestingly, in both cases the product has reacted with the acetone solvent to form a Schiff base derivative. This observation is unexpected because it is believed that both terminal amine groups were protonated before crystallisation and therefore would not have had a free lone pair to donate in the Schiff base formation. A key difference between the two crystal structures is that the nitrogen atom of the imine group is still protonated in the crystal of the PF_6^- salt but no longer protonated in the crystal of the BPh_4^- salt.

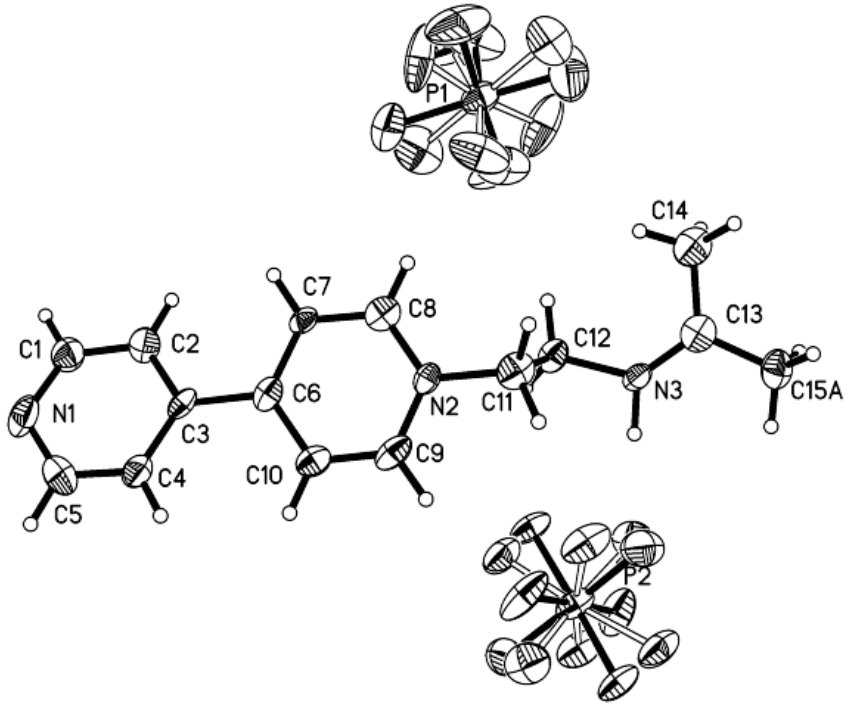

Figure 98. Representations of the molecular structures of **502.$(PF_6)_2$**.

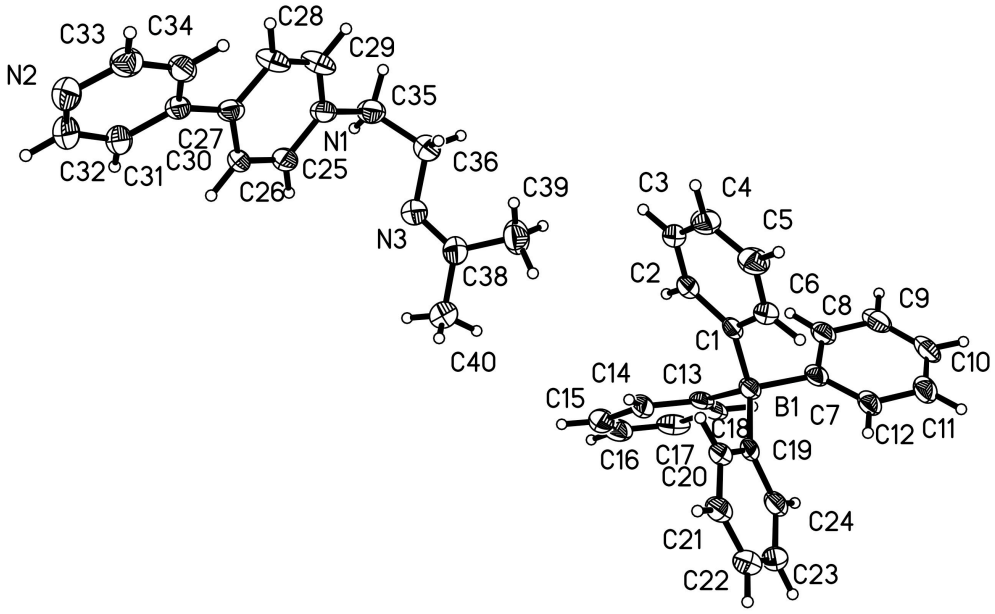

Figure 99. Representations of the molecular structures of **502.BPh_4**.

The counter-anion affects the crystallisation properties greatly, with the PF_6^- salt adopting the orthorhombic *Pca*2$_1$ space group and the BPh_4^- salt adopting the monoclinic

$P2_1/n$ space group. The counter-anion may also have determined whether the amine remained protonated following the condensation reaction with acetone. Other selected crystallisation data for the three salts can be seen in the Appendix.

5.3.7.2 Crystal structures of wheels and linked wheel systems

Crystals of **516** were obtained by evaporation of a 3:2 *n*-pentane/acetone solution at room temperature. The X-ray diffraction data were obtained at the University of Manchester by Dr Elizabeth Harper and Dr John Fielden. This crystal structure has not been finalised due to the severe disorder of the templating molecule, but the partially completed molecular structure can be seen in Figure 100.

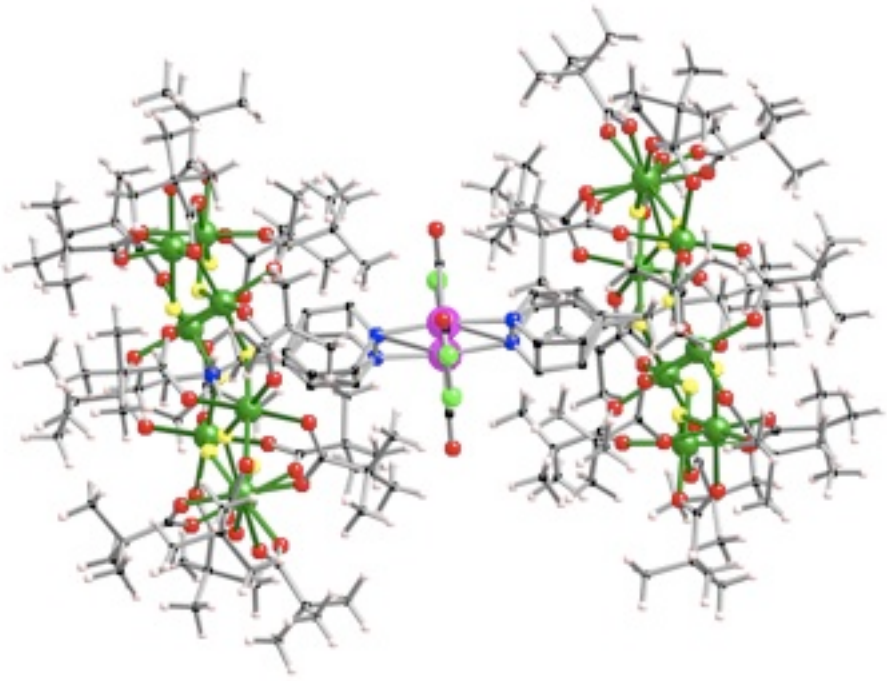

Figure 100. Unfinished Representation of the Molecular Structure of **516**.

This crystal structure clearly shows that the wheels are located trans to each other, meaning that the three carbonyl groups are coordinated in a meridional fashion around the rhenium centre. The rhenium itself, shown in pink, is disordered over two sites, meaning that the attached pyridyl units are also disordered. The chloride ligand is disordered over four sites, with each site having ¼ occupancy, and the carbonyl ligands

are disordered over four sites each having ¾ occupancy, giving a ratio of one chloride to three carbonyl ligands.

The crystal structures of **517** and **518**, both derived from data obtained at Daresbury, have not been fully solved as previous Cr7Ni analogous structures have already been finalised. From the raw data, it can be stated that the desired products have been synthesised. Both crystals were grown by evaporation of *n*-pentane/acetone solutions at room temperature.

5.4 CONCLUSIONS

A selection of purely organic molecules and metal complexes with potential applications as switchable linkers has been synthesised and characterised. However, attempts to use these as templates for the wheels, either in a direct synthetic method or in a template substitution reaction, have thus far proved unsuccessful. The direct synthesis method was unsuccessful mainly due to solubility factors; none of the templating molecules synthesised are soluble in pivalic acid, which was used as the reaction solvent. The template substitution reactions were unsuccessful, probably as a result of the wheels becoming detached from their templates.

While it has been proven that linking wheels directly through their backbones is much more effective, two novel indirectly-linked wheel systems have been synthesised, including a rare example of a *mer*-$ReCl(CO)_3(L)_2$ complex.

Ultimately it was concluded that linking wheels together through hydrogen bonds was not a particularly fruitful avenue of investigation and thus more effort was focused on linking the wheels together directly.

Conclusions

The primary aim of this project was to further develop the series of linked wheel systems. This has been achieved, on the whole, with great success but much further work is required on the study of these linked wheel systems to determine how interactions can be affected between the wheels and if it is possible to observe any magnetic switchable effects occurring with some of the MLCT/redox active links that were synthesised towards the end of the project.

A number of accomplishments have been achieved synthetically. It has been proven that selective substitution of functionalised carboxylates into the wheels is possible using a variety of carboxylates, **203 - 210**. These can then be used as ligands in complexation to metal centres. The series of first row transition metal complexes has been expanded using these novel wheel based ligands using facile crystallisation techniques (**211- 219**). These compounds are not expected to show switchable properties, but are anticipated to help understanding of how best to enable interaction between wheels. Certain complexes have been measured by EPR, however many more need to be studied in order to obtain a fuller picture on how best to interact the wheels.

The original wheel based ligand, containing an iso-nicotinate group has also been used as a bulky ligand in 2^{nd} and 3^{rd} row transition metal complexes, undergoing more harsh reaction conditions and column chromatography (**220** – **222**). Despite no crystallographic evidence, it is strongly believed that metal complex links between purple wheels have been achieved using the qpy, bbpe and pytpy ligands (**312** – **315**). While initial UV-VIS and cyclic voltammetry measurements have been used as characterisation techniques, there are suggestions that some of these complexes may demonstrate switchable properties. Further studies must be done to verify this, including time-resolved EPR spectroscopy to witness if the excited state is long lived enough to affect the interaction occurring between the wheels.

The series of organic linked wheel systems has been expanded, both by using organic linkers to join together two (or three) purple wheels (**301** – **304**). Organic links have also been utilised to form a novel series of mixed green-purple linked wheel systems, with variations being different carboxylate ligands acting as linkers and different divalent

metals being used in the purple wheel backbone (**401** – **414**). EPR studies have been undertaken on these systems showing some interesting results. There is evidence that the carboxylate affects the strength of interaction between the wheels, with the strongest interaction occurring using the iso-nicotinate ligand and the weakest using the 4-pyridazine carboxylate ligand, while use of a Cr_7Zn purple wheel effectively switches off interaction between the wheels.

Synthetically it has been proven that attempting to link wheels together indirectly is the most difficult method. The primary problem that arose during the attempts at direct synthesis of linked wheel systems was the lack of solubility of the templating molecules in the carboxylic acid solvent. When attempting to form linked wheel systems using a pre-made wheel containing a pendant pyridyl group, two difficulties became clear. The first was the bulk of the ligand, which was too great to enable any coordination cis to another wheel as displayed upon trans coordination to a Re^{I} metal centre, leaving the carbonyl ligands in a kinetically unfavourable *mer* arrangement (**516**). This meant the synthesis of any complex where the wheels needed to be in a *cis* arrangement, such as a $Ru^{II}(bpy)_2(L)_2$ type complex, became impossible. The second problem, was the ability of the wheel to "slip off" the template during more harsh reaction conditions, leaving the desired product minus the wheel. Given the lack of entanglement of wheels with these systems this is the least important avenue to be further investigated.

The areas of particular interest for future work are the potentially switchable systems, although it must first be established whether either the MLCT or redox activity in the previously synthesised systems do prove to alter any interaction between the wheels. Further suitable synthetic targets have been outlined at the end of each of the respective chapters, considering only Ru^{II} and Re^{I} complexes, however the possibilities of transition metal switchable systems are enormous, and should be considered should this project be moved forward.

Appendix

Table 10. Crystallographic data and refinement details of solved crystal structures.

	211	**213**	**215**	**217**	**219**
Formula	$C_{192}H_{344}Cr_{14}Cu_2F_{16}N_6Ni_2O_{72}$	$C_{219}H_{376}Cr_{14}Cu_2F_{16}N_4Ni_2O_{73}$	$C_{196}H_{350}Cr_{14}Cu_1F_{16}N_6Ni_2O_{76}$	$C_{182}H_{310}Cr_{14}F_{28}N_6Ni_3O_{68}$	$C_{311}H_{564}Cl_3Cr_{21}F_{24}Fe_3N_{12}Ni_4O_{112}$
M	5165.23	5509.74	5216.95	5106.49	8271.09
Crystal system	Monoclinic	Monoclinic	Triclinic	Orthorhombic	Triclinic
Space group	C_12/C_1	P_12_1/C_1	$P\bar{1}$	*Pccn*	$P\bar{1}$
a/Å	60.7106 (12)	31.2667 (15)	16.5140 (5)	55.0070 (14)	30.494 (2)
b/ Å	16.7468 (4)	17.5635 (9)	25.5460 (7)	17.2341 (4)	30.585 (2)
c/ Å	30.4987 (9)	30.8297 (15)	33.7510 (11)	30.5232 (8)	31.115 (2)
α/°	90	90	96.5040 (10)	90	65.113 (2)
β/°	103.9900	117.007 (2)	90.5440 (10)	90	64.782 (2)
γ/°	90	90	105.692 (2)	90	87.656 (2)
Volume/Å^3	30088.5 (13)	15084.0 (13)	13607.5 (7)	28935.9 (13)	23475 (3)
Z	4	2	2	4	2
T/K	100 (2)	100 (2)	100 (2)	100 (2)	100 (2)
Absorption Coefficient/mm^{-1}	0.815	0.817	0.828	0.773	0.756
Reflections collected	13885	21570	23425	15099	63579
Independent collections	5614	17314	14929	11390	47869
Goodness-of-fit on F^2	1.192	1.007	1.398	1.022	1.072
Final R1, wR2[I>2σ(I)]	0.0954, 0.2236	0.0702, 0.191	0.1789, 0.3418	0.0586, 0.1687	0.0639, 0.1887
(all data)	0.1747, 0.2494	0.0846, 0.206	0.2516, 0.3724	0.0781, 0.1871	0.0801, 0.1996

	220	**224**	**302**	**303**	**401**
Formula	$C_{178}H_{313}ClCr_{14}F_{16}N_4Ni_2O_{67}$	$C_{205}H_{340}Cr_{14}Cu_2F_{16}N_{10}Ni_2$	$C_{186}H_{314}Cr_{14}F_6N_4Ni_2O_{70}$	$C_{272}H_{468}Cr_{21}F_9N_7Ni_3O_{107}$	$C_{182}H_{328}Cr_{14}F_{11}N_3Ni_2O_{71}$
M	4966.4	5469.37	4683.28	6987.66	4748.89
Crystal system	Monoclinic	Monoclinic	Orthorhombic	Orthorhombic	Monoclinic
Space group	$P2_1/c$	$P2_1/n$	$C222_1$	$P22_12_1$	P_12_11
a/Å	30.477 (5)	16.9352 (6)	16.7843 (7)	16.698 (2)	24.7231 (4)
b/ Å	16.591 (3)	29.4007 (11)	36.8039 (14)	40.475 (5)	16.8366 (3)
c/ Å	53.880 (8)	29.4140 (13)	53.400 (2)	61.550 (8)	30.9698 (7)
α/°	90	90	90	90	90
β/°	99.480 (2)	90.834 (3)	90	90	94.2020 (10)
γ/°	90	90	90	90	90
Volume/Å^3	26872 (8)	14643.9 (10)	32987 (2)	41599 (9)	12856.6 (4)
Z	4	2	4	4	2
T/K	120 (2)	90 (2)	100 (2)	130 (2)	100 (2)
Absorption Coefficient/mm^{-1}	1.108	0.843	0.745	0.725	0.785
Reflections collected	10465	10465	21477	27068	14339
Independent collections	8195	8195	17813	19111	10433
Goodness-of-fit on F^2	1.107	1.107	1.021	0.881	1.292
Final R1, wR2[I>2σ(I)]	0.1426, 0.3067	0.1063, 0.2425	0.0538, 0.1387	0.0464, 0.0918	0.1055, 0.2418
(all data)	0.1865, 0.325	0.1231, 0.2526	0.0649, 0.1447	0.0678, 0.0976	0.1441, 0.2656

	402	**502.PF$_6$**	**502.BPh$_4$**	**505**
Formula	$C_{177}H_{316}Cr_{14}F_{11}N_3Ni_2O_{68}$	$C_{15}H_{19}F_{12}N_3P_2$	$C_{39}H_{38}BN_3$	$C_{26}H_{40}N_6O_8$
M	4634.18	531.27	559.53	564.64
Crystal system	Monoclinic	Orthorhombic	Monoclinic	Triclinic
Space group	P_12_11	$Pca2_1$	$P2_1/n$	$P\bar{1}$
a/Å	16.5405 (6)	8.0205 (14)	13.791 (3)	6.2675 (7)
b/ Å	30.8610 (11)	23.556 (4)	10.437 (2)	9.0154 (10)
c/ Å	24.8487 (10)	11.132 (2)	22.374 (5)	13.6027 (15)
α/°	90	90	90	91.703 (2)
β/°	101.805 (3)	90	104.783 (4)	93.908 (2)
γ/°	90	90	90	108.495 (2)
Volume/Å^3	12415.9 (8)	2103.1 (6)	3113.8 (12)	726.14 (14)
Z	2	4	4	1
T/K	100 (2)	100 (2)	100 (2)	100 (2)
Absorption Coefficient/mm^{-1}	0.763	0.320	0.069	0.097
Reflections collected	30422	30422	26261	4258
Independent collections	26107	26107	7410	2902
Goodness-of-fit on F^2	1.035	1.035	0.717	0.901
Final R1, wR2[I>2σ(I)]	0.0709, 0.1788	0.0523, 0.1057	0.0441, 0.0902	0.0358, 0.0764
(all data)	0.083, 0.1877	0.1083, 0.1210	0.1334, 0.1223	0.0512, 0.0806

References

1. http://www.computer50.org/mark1/contemporary.html

2. P. Ball, *Nature*, **2000**, *406*, 118

3. F. Meier, J. Levy, D. Loss, *Phys. Rev. Lett.* **2003**, *90*, 4, 047901-1

4. F. Meier, J. Levy, D. Loss, *Phys. Rev. B.* **2003**, *68*, 134417-1

5. F. K. Larsen, E. J. L. McInnes, H. El Mkami, J. Overgaard, S. Piligkos, G. Rajaraman, E. Rentschler, A. A. Smith, G. M. Smith, V. Boote, M. Jennings, G. A. Timco, R. E. P. Winpenny, *Angew. Chem. Int. Ed.*, **2003**, *42*, 1, 101

6. F. Troiani, A. Ghirri, M. Affronte, S. Carretta, P. Santini, G. Amoretti, S. Piligkos, G. Timco, R. E. P. Winpenny, *Phys. Rev. Lett.* **2005**, *94*, 207208-1

7. L. N. Mulay, E. A. Boudreaux, *Theory and Applications of Molecular Paramagnetism*, **1976**, Wiley-Interscience

8. P. Zeeman, *Nature*, **1987**, *55*, 347

9. P. W. Anderson, *Phys. Rev.* **1950**, *79*, 350

10. A. M. Ako, I. J. Hewitt, V. Mereacre, R. Clérac, W. Wernsdorfer, C. E. Anson, A. K. Powell, *Angew. Chem. Int. Ed.* **2006**, *45*, 30, 4926

11. A. Caneschi, D. Gatteschi, R. Sessoli, A. L. Barra, L. C. Brunel, M. Guillot, *J. Am. Chem. Soc.* **1991**, *113*, 15, 5873

12. T. Lis, *Acta Cryst.* **1980**, *B36*, 2042

13. E. M. Chudnovsky, *Science* **1996**, *274*, 938

14. G. Christou, *Polyhedron*, **2005**, *24*, 2065

15. H. Osio, N. Hoshino, T. Ito, *J. Am. Chem. Soc.* **2000**, *122*, 12602

16. C. Benelli, J. Cano, Y. Journeaux, R. Sessoli, G. A. Solan, R. E. P. Winpenny, *Inorg. Chem.* **2001**, *40*, 188

17. M. Murrie, S. J. Teat, H. Stoecklie-Evans, H. U. Güdel, *Angew. Chem. Int. Ed.* **2003**, *42*, 4653

18. Z. Sun, C. M. Grant, S. L. Castro, D. N. Hendrickson, G. Christou, *Chem. Commun.* **1998**, 721

19. J. J. Sokol, A. G. Hee, J. R. Long, *J. Am. Chem. Soc.* **2002**, *124*, 7656

20. S. Osa, T. Kido, N. Matsumoto, N. Re, A. Pochaba, J. Mrozinski, *J. Am. Chem. Soc.* **2004**, *126*, 420

21. P. H. Lin, T. J. Burchell, L. Ungur, L. F. Chibotaru, W. Wernsdorfer, M. Murugesu, *Angew. Chem. Int. Ed.* **2009**, *48*, 50, 9489

22. R. Feynman, *Simulating Physics with Computers* **1981**, Int. J. Theoretical Phys.

23. P. W. Shor, *Soc. Ind. Appl. Maths.* **1999**, *41*, 2, 303

24. L. K. Grover, *STOC* **1996**, 212

25. J. M. Kikkawa, I. P. Smorchkova, N. Samarath, D. D. Awschalom, *Science*, **1997**, *277*, 1284

26. D. Deutsch, *Proc. R. Soc. Lond. A.* **1989**, *425*, 73

27. K. L. Taft, C. D. Delfs, G. C. Papaefthymiou, S. Foner, D. Gatteschi and S. J. Lippard, *J. Am. Chem. Soc.*, **1994**, *116*, 823

28. T. C. Stamatatos, S. Mukherjee, K. A. Abboud, G. Christou, *Chem. Commun.* **2009**, 62

29. A. J. Tasiopoulos, A. Vinslava, W. Wernsdorfer, K. A. Abboud, G. Christou, *Angew. Chem. Int. Ed.* **2004**, *43*, 2117

30. A. Müller, J. Meyer, E. Krickemeyer, E. Diemann, *Angew. Chem. Int. Ed.* **1996**, *35*, 1206

31. A. Müller, E. Krickemeyer, H. Bögge, M. Schmidtmann, C. Beugholt, P. Kögerler, C. Lu, *Angew. Chem. Int. Ed.* **1998**, *37*, 1220

32. D. Fenske, A. Fischer, *Angew. Chem. Int. Ed.* **1995**, *34*, 307

33. M. Eshel, A. Bino, I. Felner, D. C. Johnston, M. Luban, L. L. Miller, *Inorg. Chem.* **2000**, *39*, 1376

34. H. Kumugai, S. Kitigawa, *Chem. Lett.* **1996**, *25*, 1860

35. E. C. Sanudo, A. A. Smith, P. V. Mason, M. Helliwell, G. Aromi, R. E. P. Winpenny, *Dalton Trans.* **2006**, 1981

36. V. B. Shur, I. A. Tikhonova, F. M. Dolgushin, A. I. Yanovsky, Y. T. Struchkov, A. Y. Volkonsky, E. V. Solodova, S. Y. Panov, P. V. Petrovskii, M. E. Vol'pin, *J. Organometallic Chem.* **1993**, *443*, C19

37. L. G. Westin, M. Kritikos, A. Caneschi, *Chem. Commun.* **2003**, 1012

38. A. L. Dearden, S. Parsons, R. E. P. Winpenny, *Angew. Chem. Int. Ed.* **2001**, *40*, 151

39. E. Rentchler, D. Gatteschi, A. Cornia, A. C. Fabretti, A.-L. Barra, O. I. Shchegolikhina, A. A. Zhdanov, *Inorg. Chem.* **1996**, *35*, 4427

40. E. K. Brechin, O. Cador, A. Caneschi, C. Cadiou, S. G. Harris, S. Parsons, M. Vonci, R. E. P. Winpenny, *Chem. Commun.* **2002**, 45

41. T. Kemmitt, N.I. Al-Salim, G. J. Gainsford, *Eur. J. Inorg. Chem.* **1999**, 1847

42. V. B. Shur, I. A. Tikhonova, F. M. Dolgushin, A. I. Yanovsky, Y. T. Struchkov, A. Y. Volkonsky, E. V. Solodova, S. Y. Panov, P. V. Petrovskii, M. E. Vol'pin, *J. Organometallic Chem.* **1993**, *443*, C19

43. H. C. Yoa, J. J. Wang, Y. S. Ma, O. Waldmann, W. X. Du, Y. Song, Y. Z. Li, L. M. Zheng, S. Decurtins, X. Q. Xin, *Chem. Commun.* **2006**, 1745

44. Z. H. Ni, L. F. Zhang, V. Tangoulls, W. Wernsdorfer, A. L. Cul, O. Sato, H. Z. Kou, *Inorg. Chem.* **2007**, *46*, 15, 6029

45. M. Li, A. M. Ako, Y. Lan, W. Wernsdorfer, G. Buth, C. E. Anson, A. K. Powell, Z. Wang, S. Gao, *Dalton Trans.* **2010**, *39*, 3375

46. M. Murugesu, W. Wernsdorfer, K. A. Abboud, G. Christou, *Angew. Chem. Int. Ed.* **2005**, *44*, 892

47. C. Cadiou, M. Murrie, C. Paulsen, V. Villar, W. Wernsdorfer, R. E. P. Winpenny, *Chem. Commun.* **2001**, 2666

48. N. V Gerbeleu, A. S. Batasnov, G. A. Timco, Yu. T. Struchkov, K. M. Indricham, G. A. Popovich, *Pat. SU*, 1299116, **1985**

49. J. Overgaard, B. B. Iverson, S. P. Palii, G. A. Timco, N. V. Gerbeleu, F. K. Larsen, *Chem. Eur. J.*, **2002**, *8*, 12, 1775

50. J. van Slageren, R. Sessoli, D. Gatteschi, A. A. Smith, M. Helliwell, R. E. P. Winpenny, A. Cornia, A-L. Barra, A. G. M. Jansen, E. Rentschler, G. A. Timco, *Chem. Eur. J.*, **2002**, *8*, 1, 277

51. D. Loss, D. P. DiVincenzo, *Phys. Rev. A* **1998**, *57*, 120

52. R. H. Laye, F. K. Larsen, J. Overgaard, C. A. Muryn, E. J. L. McInnes, E. Rentschler, V. Sanchez, S. J. Teat, H. U. Güdel, O. Waldmann, G. A. Timco, R. E. P. Winpenny, *Chem. Commun.*, **2005**, 1125

53. E. C. Sañudo, C. Muryn, M. A. Helliwell, G. A. Timco, W. Wernsdorfer, R. E. P. Winpenny, *Chem. Commun.*, **2007**, 801

54. M. Affronte, A. Ghirri, S. Carretta, G. Amoretti, S. Piligkos, G. A. Timco, R. E. P. Winpenny, *Appl. Phys. Lett.* **2004**, *84*, 18, 3468

55. E. C. Sañudo, T. B. Faust, C. Muryn, R. Pritchard, G. A. Timco, R. E. P. Winpenny, *Inorg. Chem.*, **2009**, *48*, 9811

56. O. Cardor, D. Gatteschi, R. Sessoli, F. K. Larsen, J. Overgaard, A. L. Barra, S. J. Teat, G. A. Timco, R. E. P. Winpenny, *Angew. Chem. Int. Ed*., **2004**, *43*, 5196

57. G. A. Timco, A. S. Batsanov, F. K. Larsen, C. A. Muryn, J. Overgaard, S. J. Teat, R. E. P. Winpenny, *Chem. Commun*., **2005**, 3649

58. S. L. Heath, R. H. Laye, C. A. Muryn, N. Lima, R. Sessoli, R. Shaw, S. J. Teat, G. A. Timco, R. E. P. Winpenny, *Angew. Chem. Int. Ed.*, **2004**, *43*, 6132

59. P. Christian, G. Rajaraman, A. Harrison, J. J. W. McDouall, J. T. Raferty, R. E. P. Winpenny, *Dalton Trans*, **2004**, 1511

60. G. A. Timco, E. J. L. McInnes, R G. Pritchard, F. Tuna, R. E. P. Winpenny, *Angew. Chem. Int. Ed.*, **2008**, *47*, 9681

61. F. K. Larsen, J. Overgaard, S. Parsons, E. Rentschler, A. A. Smith, G. A. Timco, R. E. P. Winpenny, *Angew. Chem. Int. Ed.*, **2003**, *42*, 5978

62. M. Affronte, I. Casson, M. Evangelisti, A. Candini, S. Carretta, C. A. Muryn, S. J. Teat, G. A. Timco, W. Wernsdorfer, R. E. P. Winpenny, *Angew. Chem. Int. Ed*., **2005**, *44*, 6496

63. M. Affronte, F. Troiani, A. Ghirri, S. Carretta, P. Santini, R. Schuecker, G. Timco, R. E. P. Winpenny, *J. Magnetism and Magnetic Materials* **2007**, *310*, e501

64. M. Affronte, F. Troiani, A. Ghirri, S. Carretta, P. Santini, V. Corradini, R. Schuecker, C. Muryn, G. Timco, R. E. P. Winpenny, *Dalton Trans.* **2006**, 2810

65. G. A. Timco, S. Carretta, F. Troiani, F. Tuna, R. J. Pritchard, C. A. Muryn, E. J. L. McInnes, A. Ghirri, A. Candini, P. Santini, G. Amoretti, M. Affronte, R. E. P. Winpenny, *Nature Nano.* **2009**, *4*, 173

66. V. Milway, G. A. Timco, *unpublished results*

67. A. Cornia, A. C. Fabretti, M. Pacchioni, L. Zobbi, D. Bonacchi, A. Caneschi, D. Gatteschi, R. Biagi, U. del Pennino, V. de Renzi, L. Gurevich, H. S. J. van der Zant, *Angew. Chem. Int. Ed.*, **2003**, *42*, 1645

68. V. Corradini, R. Biagi, U. del Pennino, V. de Renzl, A. Gambardella, M. Affronte, C. A. Muryn, G. A. Timco, R. E. P. Winpenny, *Inorg. Chem.*, **2007**, *46*, 4937

69. V. Corradini, A. Ghirri, U. del Pennino, R. Biagi, V. A. Milway, G. A. Timco, F. Tuna, R. E. P. Winpenny, M. Affronte, *Dalton Trans.* **2010**, *39*, 4928

70. V. Corradini, F. Moro, R. Biagi, V. De Renzi, U. del Pennino, V. Bellini, S. Carretta, P. Santini, V. A. Milway, G. Timco, R. E. P. Winpenny, M. Affronte, *Phys. Rev. B* **2009**, *79*, 144419

71. A. Ghirri, V. Corradini, C. Cervetti, A. Candini, U. del Pennino, G. Timco, R. J. Pritchard, C. A. Muryn, R. E. P. Winpenny, M. Affronte, *Adv. Funct. Mater.* **2010**, *20*, 1552

72. Y. L. Zhao, W. R. Dichtel, A. Trabolsi, S. Saha, I. Aprahamian, J. F. Stoddart, *J. Am. Chem. Soc.* **2008**, *130*, 11294

73. F. Vögtle, W. M. Müller, U. Müller, M. Bauer, K. Rissanen, *Angew. Chem. Int. Ed.* **1993**, *32*, 1295

74. M. Von Delius, E. M. Geertsema, D. A. Leigh, *Nature Chem.* **2010**, *2*, 96

75. B. Kolaric, M. Sliwa, M. Brucale, R. A. L. Vallée, G. Zuccheri, B. Samoni, J. Hofkens, F. C. Dde Schryver, *Photochem. Photobiol. Sci.* **2007**, *6*, 614

76. M. L. Boillot, C. Roux, J. P. Audière, A. Dausse, J. Zarembowitch, *Inorg. Chem.* **1996**, *35*, 3975

77. Y. L. Zhao, W. R. Dichtel, A. Trabolsi, S. Saha, I. Aprahamian, J. F. Stoddart, *J. Am. Chem. Soc.* **2008**, *130*, 11294

78. K. Matsuda, M. Irie, *J. Am. Chem. Soc.* **2000**, *122*, 7195

79. L. Michaelis, *Chem. Rev.* **1935**, *16*, 243

80. P. M. S. Monk, *The Viologens: Physiochemical Properties, Synthesis and Applications of the Salts of 4,4′-Bipyridine*, **1998**, J. Wiley

81. D. I. Gittens, D. Bethell, D. J. Schiffrin, R. J. Nicholls, *Nature* **2000**, *408*, 67

82. A. Juris, V. Balzani, F. Barrigelletti, S. Campagna, P. Belser, A. Von Zelewsky, *Coord. Chem. Rev.* **1988**, *84*, 85

83. N. Sutin, C. Creutz, *Inorganic and Organometallic Photochemistry* **1978**, *Am. Chem. Soc.*, Ch. 1, 1

84. L. A. Worl, R. Duesing, P. Chen, L. D. Ciana, T. J. Meyer, *J. Chem. Soc. Dalton Trans.* **1991**, 849

85. G. Aromí, A. S. Batsanov, P. Christian, M. Helliwell, A. Parkin, S. Parsons, A. A. Smith, G. A. Timco, R. E. P. Winpenny, *Chem. Eur. J.* **2003**, *9*, 5142

86. M. K. Nazeeruddin, M. Gratzel, *Inorg. Syntheses 33*, 185

87. E. G. Il'ina, N. A. Santalova, K. M. Dunaeva, *Zh. Neorg. Khim.* **1991**, *36*, 2301

88. F. Izumi, R. Kurosawa, H. Kawamoto, H. Akaiwa, *Bul. Chem. Soc. Jap.* **1975**, *48*, 11, 3188

89. R. D. Cannon, R. P. White, *Inorg. Chem*. **1988**, *36*, 195

90. T. Otieno, S. J. Rettig, R. C. Thompson, J. Trotter, *Acta. Cryst.* **1993**, *C49*, 2067

91. M. Wrighton, D. L. Morse, *J. Am. Chem. Soc.* **1974**, 998

92. A-M. A. La Pensée, J. Bickley, S. J. Higgins, M. Marcaccio, F. Paolucci, S. Roffia J. M. Charnock, *J. Chem. Soc. Dalton Trans.* **2002**, 4095

93. M. S. Wrighton, D. L. Morse, L. Pdungsap, *J. Am. Chem. Soc.* **1975**, *97*, 2073

94. S. R. Stoyanov, J. M. Villegas, A. J. Cruz, L L. Lockyear, J. H. Reibenspies, D. P. Rillema, *J. Chem. Theory Comput.* **2005**, *1*, 95

95. A. Vlcek Jr, *Top. Organomet. Chem.*, **2010**, *29*, 73

96. B. Durham, J. L. Walsh, C. L. Carter, T. J. Meyer, *Inorg. Chem.* **1980**, *19*, 860

97. J. L. Walsh, B. Durham, *Inorg. Chem.* **1982**, *21*, 1, 329

98. G. A. Timco, *unpublished results*

99. S-S. Sun, A. J. Lees, *J. Am. Chem. Soc.* **2000**, *122*, 8956

100. S. Woitellier, J. P. Launay, C. W. Spangler, *Inorg, Chem.* **1989**, *28*, 758

101. A. J. Amoroso, A. M. W. Cargill Thompson, J. P. Maher, J. A. McCleverty, M. D. Ward, *Inorg. Chem.* **1995**, *34*, 4828

102. B. J. Coe, J. A. Harris, L. A. Jones, B. S. Brunschwig, K. Song, K. Clays, J. Garin, J. Orduna, S. J. Coles, M. B. Hursthouse, *J. Am. Chem. Soc.*, **2005**, *127*, 4845

103. A. Shi, M. R. Pokhrel, S. H. Bossman, *Synthesis* **2007**, *4*, 505

104. B. J. Coe, J. Fielden, S. P. Foxon, B. S. Brunschwig, I. Asselberghs, K. Clays, A. Samoc, M. Samoc, *J. Am. Chem. Soc.* **2010**, *132*, 3496

105. E. C. Constable, A. M. W. Cargill Thompson, *J. Chem. Soc. Dalton Trans.* **1992**, 2947

106. E. C. Constable, A. M. W. Cargill Thompson, *J. Chem. Soc. Dalton Trans.* **1994**, 1409

107. M. A. Hayes, C. Meckel, E. Schatz, M. D. Ward, *J. Chem. Soc. Dalton Trans.* **1992**, 703

108. P. de Wolf, S. L. Heath, J. A. Thomas, *Inorg. Chim. Acta*. **2003**, 280

109. J-J. Jin, T. Uchida, T. Kuwabara, M. Hirai, M. Nanasawa, *J. Photochem. Photobiol. A: Chem.* **1999**, *123*, 87

110. M. N. Collomb, A. Deronzier, K. Gorgy, J-C. Leprêtre, *New J. Chem.* **2000**, *24*, 455

111. K. Bierig, R. J. Morgan, S. Tysoe, H. D. Gafney, T. C. Strekas, A. D. Baker, *Inorg. Chem.* **1991**, *30*, 4898

112. N. Hirota, S. Yamauchi, *Journal of Photochemistry and Photobiology C: Photochemistry Reviews 4*, **2003**, 109

113. M. Yagi, S. Yamaguchi, M. Noda, K. Seki, *Appl. Magn. Reson.* **2000**, *18*, 385

114. C. J. Kleverlaan, D. M. Martino, H. van Wiligen, D. J. Stufkens, A. Oskam, *J. Phys. Chem.* **1996**, *100*, 18607

115. S. Cradock, C. Purves, D. W. H. Rankin, *J. Molecular Structure* **1990**, *220*, 193

116. W. W. Porter III, T. P. Vaid, A. L. Rheingold, *J. Am. Chem. Soc.* **2005**, *127*, 16559

117. G. Mezei, J. W. Kampf, V. L. Pecoraro, *New J. Chem.*, **2007**, *31*, 439

118. S. J. A. Pope, B. J. Coe, S. Faulkner, R. H. Laye, *Dalton Trans*. **2005**, 1482

119. M. S. Vickers, K. S. Martindale, P. D. Beer, *J. Mater. Chem.* **2005**, *15*, 2784

120. C. L. Donnici, *J. Braz. Chem. Soc.* **1998**, *9*, 5, 455

121. M. Catteneo, F. Fagalde, N. E. Katz, *Inorg. Chem.* **2006**, *45*, 6884

122. R. G. Lin, Y. G. Fu, C. P. Brock, T. F. Guarr, *Inorg. Chem.* **1992**, *31*, 4346

123. L. Sheeney-Haj-Ichia, J. Wasserman, I. Willner, *Adv. Mater.* **2002**, *14*, 18, 1323

124. S. P. Gromov, A. I. Verdernikov, E. N. Ushakov, N. A. Lobova, A. A. Botsmanova, L. G. Kuz′mina, A. V. Churakov, Y. A. Strelenko, M. V. Alfimov, J. A. K. Howard, D. Johnels, U. G. Edlund, *New J. Chem.* **2005**, *29*, 881

125. B. Buschhaus, A. Hirsch, F. Alexander, *Eur. J. of Org. Chem.* **2005**, *6*, 1148

126. T. Hasegawa, T. Yonemura, K. Matsuura, K. Kobayashi, *Bioconjugate Chem.* **2003**, *14*, 4, 728

127. B. J. Coe, N. R. M. Curati, E. C. Fitzgerald, S. J. Coles, P. N. Horton, M. E. Light, M. B. Hursthouse, *Organometallics* **2007**, *26*, 2318

128. A. M. Bond, R. Colton, M. E. McDonald, *Inorg. Chem.* **1978**, *17*, 10, 2843

129. R. Carballo, S. Garcia-Fontan, E. M. Vazquez-Lopez, P. Losada-Gonzalez, P. Rodriguez-Seoane, *Zeitschrift für Kristallographie* **1998**, *213* (2), 379

130. U. Floerke, H. J. Haupt, *Zeitschrift für Kristallographie*, **1993**, *204* (2), 316

131. F. L. Thorp-Greenwood, M. P. Coogan, A. J. Hallett, R. H. Laye, S. J. A. Pope, *J. Organometallic Chem.* **2009**, *694*, 1400

132. A. J. Hallett, P. Christian, J. E. Jones, S. J. A. Pope, *Chem. Commun.* **2009**, 4278

133. J. V. Caspar, T. J. Meyer, *J. Phys. Chem.* **1983**, *87*, 952